An in-shoe laser Doppler sensor for assessing plantar blood flow in the diabetic foot.

Jonathan Edwin Cobb

A thesis submitted in partial fulfilment of the requirements of Bournemouth University for the degree of Doctor of Philosophy

May 2000

Bournemouth University

Abstract

An in-shoe laser Doppler sensor for assessing plantar blood flow in the diabetic foot.

Jonathan Edwin Cobb

Plantar ulceration is a complication of the diabetic foot prevalent in adults with type II diabetes mellitus. Although neuropathy, microvascular disease and biomechanical factors are all implicated, the mechanism by which the tissue becomes pre-disposed to damage remains unclear. Recent theories suggest that the nutritional supply to the tissue is compromised, either by increased flow through the arteriovenous anastomoses ('capillary steal' theory) or through changes in the microvasculature (haemodynamic hypothesis). Clinical data to support these ideas has been limited to assessment of the unclad foot under rest conditions. A limitation of previous studies has been the exclusion of static and dynamic tissue loading, despite extensive evidence that these biomechanical factors are essential in the development of plantar ulceration. The present study has overcome these problems by allowing assessment of plantar blood flow, in-shoe, during standing and walking.

The system comprises a laser Doppler blood flux sensor operating at 780nm, load sensor, measurement shoe, instrumentation, and analysis software. In-vitro calibration was performed using standard techniques. An in-vivo study of a small group of diabetic subjects indicated differences in the blood flux response between diabetic neuropaths, diabetics with vascular complications and a control group. For example, following a loading period of 120s, relative increases in response from rest to peak were: Control (150% to 259%), Vascular (-70% to 242%), Neuropathic (109%-174%) and recovery times to 50% of the peak response were: Control (33s to 45s), Vascular (43s to >120s), Neuropathic (>120s). Dynamic re-perfusion rates (arbitrary units per millisecond) obtained for the swing phase of gait were: Control (6.1 a.u/ms to 7.9 a.u/ms), Vascular (4 a.u/ms to 6.2 a.u/ms), Neuropathic (2.3 a.u/ms to 4.5 a.u/ms).

List of contents

CHAPTER 2 THEORETICAL BACKGROUND

CHAPTER 3 LITERATURE REVIEW

CHAPTER 4 DEVELOPMENT OF A PLANTAR MONITORING SYSTEM

CHAPTER 5 IN VITRO RESULTS

CHAPTER 6 IN VIVO RESULTS

CHAPTER 7 CONCLUSIONS

List of illustrations and tables.

Figures (continued) **Page**

Photographs. **Page**

Tables. **Page**

List of accompanying material

Acknowledgements

The study presented in this thesis was achieved with the help and kindness of many people for which I am very grateful. I would like to give special thanks to:

All of the patients and control subjects who volunteered for the study.

Colleagues:

- Professor Denzil Claremont for supervision, encouragement and advice.
- Dr Mike Lunt for general help and assistance with calibration.
- Dr David Kerr for providing the patients for the study.
- Dr Claire Doody for many useful discussions and continued encouragement.
- Nurse June Murphy for assistance with the clinical measurements.
- Mr Robert Hedges for advice and help with instrumentation.

Family:

- My parents for their continuous love, guidance and support.
- Vicky, Quincy and Tom, Teresa and Rachel for their love and help.

Declaration

This thesis contains the original work of the author except where otherwise indicated.

Abbreviations

Abbreviations used throughout the thesis are defined at first usage and listed below, where possible in their standard form.

^{o}C	Temperature degrees Celsius.
Hz	Hertz
kHz	Kilo Hertz
RBC	Red blood cell
mm	Millimeter (10^{-3}) meter
ms	milli-seconds (10^{-3}) seconds
MPa	Mega Pascal (10^{6}) Pascal
FSR	Force sensing resistor
DC	Direct current
λ	Wavelength
p-p	Peak to Peak
mV	millivolts
ml	milli-litres (10^{-3}) litres
mW	milli-watts (10^{-3}) Watts

μW	micro-watts (10^{-6}) Watts
μm	micro-metres (10^{-6}) metres
mA	milli-amps (10^{-3}) Amps
APC	Automatic power control
SNR	Signal to Noise ratio
dB	decibel
opamp	Operational amplifier
PCB	Printed circuit board
SMD	Surface mount device
BPM	Beats per minute
LDF	Laser Doppler flowmetry
a.u	Arbitrary units

Chapter 1 Introduction

1.0 Introduction

This thesis documents a research project to develop and characterise a system capable of monitoring pressure and blood flow, at the plantar surface of the human foot, within a shoe.

1.1 Rationale

Plantar ulceration in the diabetic foot is a serious complication of diabetes mellitus, which can result in gangrene and may require amputation of the affected limb. In 1989, the St Vincent declaration (World Health Organisation 1990 – Appendix A) included a five year target for Europe to reduce the rate of limb amputations arising from diabetes mellitus by 50% (Campbell and Lebovitz 1996). Despite improvements in the prevention and treatment of diabetic foot complications, the incidence remains unacceptably high. Williams (1994) estimates that of approximately 750,000 people in the United Kingdom diagnosed with diabetes 4% (30,000) have already undergone amputation of all or part of the limb and 6% (45,000) have plantar ulcers.

Microvascular and neuropathic factors have been proposed as the principal factors in the pathogenesis of plantar ulceration (Flynn and Tooke 1995, Netten et al. 1996, Vigilance et al. 1997, Shaw and Boulton 1997). There is also considerable evidence that abnormal plantar pressures occur in the diabetic foot (Boulton et al. 1983, Lord et al. 1986, Stess et al. 1997). Plantar ulcers do not normally occur in the absence of pressure and a reduction in pressure is the normal pre-requisite for healing (Cavanagh and Ulbrecht 1994). Consequently, plantar pressure is an important contributory factor in the development of ulceration (Ulbrecht et al. 1988, Brand 1990, Grunfeld 1992).

The precise role of pressure in the development of plantar ulceration is unknown. It has been suggested that the mechanical properties of skin may be altered in the diabetic (Elkeles and Wolfe 1991, Nikkels-Tassoudji et al. 1996). Abnormally high plantar pressures may affect skin blood flow in plantar tissue. Although pressure does have a significant affect on skin blood flow in normal tissue (Daly et al. 1976, Tsay 1991, Kabagambe et al. 1994) a temporary reduction in blood flow is compensated for by the

hyperaemic response. However, in the diabetic, this response is frequently impaired (Rayman et al. 1986b, Flynn and Tooke 1995).

To the author's knowledge, there has not been a clinical study of the affect of plantar pressure on microcirculatory blood flow in the diabetic foot, at typical sites of ulceration. This is in part due to the difficulty of making non-invasive, skin blood flow measurements, particularly in-shoe. The recent availability of low cost, miniature laser diodes together with photodiodes and thin film pressure sensors, provides the basic technology for an in-shoe sensor to give a simultaneous indication of plantar skin blood flow and plantar pressure. The realisation of this type of sensor could be of use to the clinician seeking to further understanding of ulceration in the diabetic foot.

1.2 Diabetes Mellitus

1.2.1 Introduction

Diabetes Mellitus is a chronic, incurable disease of man arising from various metabolic disorders; each having the common feature of elevated blood glucose levels (hyperglycaemia). Variations occur in the aetiology, presentation and complications of the various forms of the disease. In order to distinguish between these, a standardised classification has been promoted by the World Health Organisation. The two most prevalent sub-classes, which occur in developed countries, are:

1. Type I (Insulin-dependent diabetes mellitus).
2. Type II (Non-insulin dependent diabetes mellitus).

Type I diabetes mellitus occurs primarily in Caucasian children. The peak onset age range is 10 to 13 years (Kelleher 1988). It is a consequence of the destruction of Beta cells in the islets of Langerhans, generally considered an autoimmune reaction, and triggered by environmental factors in those genetically predisposed to the disease. Treatment is by regular injection of insulin to restore blood glucose back to normal levels.

Type II diabetes mellitus is the most common form of the disease accounting for about 80 per cent of all cases of diabetes (Campbell and Lebovitz 1996). This form typically affects those in middle to old age, and the incidence increases with age. The causative

mechanisms are not well understood although increased insulin resistance and reduced Beta cell function are widely implicated (Corbett and McDaniel 1995, Sinagra et al. 1997). Treatment is typically by diet and orally administered anti-hyperglycaemic medication.

1.2.2 Epidemiology and outlook

In the west, the number of people with diabetes mellitus is typically estimated at 2-6% of the population. However, the prevalence for those over the age of 65 is typically 10-20% of the population (Cambell and Lebovitz 1996).

The 1998 estimate of 143 million diabetics world wide, is expected to double by 2025, as life styles in developing countries become similar to those in the west (International Diabetes Federation 1998).

The use of insulin and anti-hyperglycaemic treatments has greatly improved the life expectancy of the diabetic. However, the disease pre-disposes the long-term diabetic to a number of acute and chronic complications, which reduce the life expectancy of the diabetic by about ten years for both, type I and type II. The insidious nature of type II diabetes mellitus often results in complications being present at the time of diagnosis. The nature of these complications is often severe, leading to a reduced quality of life for the individual and imposing high costs on the health care service.

1.2.3 Complications

Chronic complications of diabetes mellitus affecting the microvascular system are retinopathy, nephropathy and neuropathy. These complications are specific to the disease. Complications affecting the macrovascular system are cardiovascular, cerebrovascular and peripheral vascular disease. These macrovascular conditions also occur in non-diabetic groups, although are more likely to coexist and exhibit accelerated development in the diabetic. With respect to the diabetic foot, the most important complications of diabetes are neuropathy and peripheral vascular disease.

Diabetic neuropathy is thought to occur as a result of demyelination due to metabolic change, or ischaemia due to haemodynamic change (Ellenberg 1990). In chronic peripheral neuropathy, sensory function is particularly affected, and the loss of

sensation frequently results in ulceration of the foot due to repeated unrecognised trauma. Peripheral vascular disease is up to six times more common in the diabetic than in the non-diabetic population (Levin and O'Neal 1988). Peripheral vascular disease can impair the nutritional supply to and within the foot, often resulting in ulceration which, if untreated may become gangrenous.

1.3 The Diabetic foot

1.3.1 Introduction

Complications, assessment techniques and methods of treatment of the diabetic foot are summarised.

1.3.2 Symptoms and complications of the diabetic foot

The term 'diabetic foot' refers to complications of the foot specific to the diabetic, as distinct from those that occur in the diabetic because of peripheral vascular disease. In the latter case the foot is very painful, ischaemic and exhibits patches of gangrenous tissue typically on the dorsum of the foot. This condition is rare under sixty years of age. However, the incidence increases with age because of accelerated atherosclerosis. In contrast the true diabetic foot appears distended, is warm to the touch and appears well perfused. Tissue damage frequently affects the plantar aspect of the foot and is particularly prevalent under the heads of the metatarsal bones (Lord et al. 1986, McKeown 1994). The incidence increases above forty years of age to reach a peak of 14% in the eighty plus age group (Connor 1994). The most important distinguishing feature is the absence of pain accompanying these symptoms, due to sensory neuropathy. Photograph 1(a,b) shows two examples of plantar ulceration in the neuropathic diabetic foot.

(a)

(b)

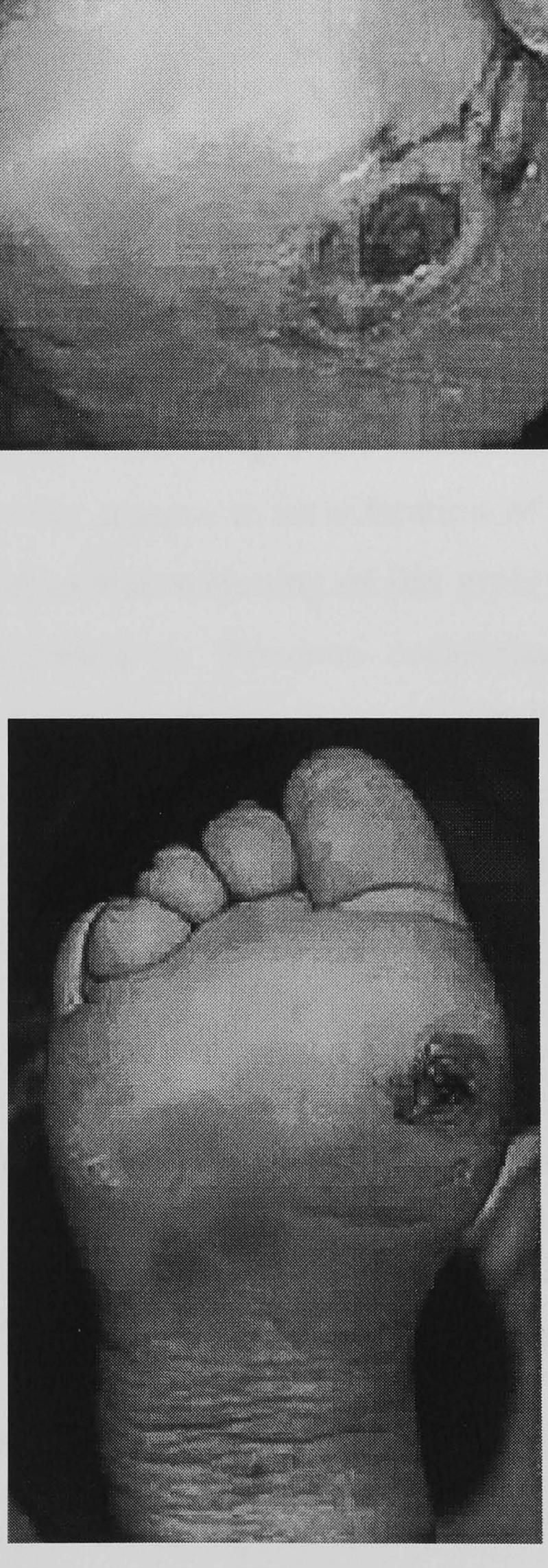

Photograph 1 Plantar neuropathic ulceration in type II diabetes mellitus.

(a) Under 4th metatarsal head in 65 year old male,

(b) Under 1st Metatarsal head, in 53 year old female.

Sensory neuropathy, affecting the foot of the diabetic, increases the risk of further tissue damage, as the absence of pain can prevent the subject from seeking treatment. For this reason, diabetic clinics advocate that patients adopt a policy of regular inspection of their feet. However, the foot surface may exhibit only superficial damage during the early phases of ulceration, whilst considerable damage is occurring in deeper tissue (Levin 1988, Elkeles and Wolfe 1991). If the condition continues to progress, gangrene can spread within the foot and the skin eventually ruptures, leading to an increased risk of infection. This process typically occurs over a period of several weeks to several months, and results in a build up of toxins, leading to a rapid deterioration in health, which can be fatal. In the past, the standard treatment for the advanced diabetic foot was amputation of foot or lower limb. Following the St Vincent declaration (Appendix A), considerable effort has been applied to reduce the number of amputations resulting from diabetic foot disease. The most important factor in preventing the severest complications of diabetic foot disease is identification of those most at risk, together with regular inspection and routine screening of this group. The risk factors leading to ulceration have been identified as: Previous occurrence, age, peripheral vascular disease, neuropathy and structural deformity (Connor 1994). The most important step to prevent further ulceration and allow healing is to reduce or remove the biomechanical forces acting on the affected region (Levin 1988, Cavanagh and Ulbrecht 1994). Methods of assessment and treatment of the diabetic foot are considered in more detail in the following sections.

1.3.3 Assessment techniques for complications of the diabetic foot

A number of techniques have been applied to screening and monitoring of the diabetic foot and these are routinely employed in diabetic clinics and in hospitals.

During a routine inspection, an initial manual assessment is made of the whole foot. Symptoms of swelling, increased temperature, ischaemia, reduced sensitivity, the formation of callus, dry fissured skin and changes in the structure of the foot, are all signs of a deterioration in foot status (Hill 1987, Connor 1994) and should be monitored. It is recommended that plantar callus be removed (McInnes 1994, Steed et al. 1996) as this is known to increase pressure within plantar tissue (Young et al. 1992, Murray et al. 1996). If a patient has a history of ulceration, sites of previous ulceration

should be carefully assessed, as recurrence is common (Grunfeld 1992, Apelqvist et al. 1993). If possible the insole of the patients shoes should be inspected for signs of excessive wear as this indicates a localised increase in pressure. The shoes should be checked for embedded objects such as stones and the adequacy of fit checked, as these are frequent causes of damage to the insensitive diabetic foot.

Non-manual techniques are also used to assess the diabetic foot. Plantar pressures can be monitored using one of the several commercially available systems (Cobb and Claremont 1995 – Appendix E). Increases in pressure or the duration for which pressure is applied, as well as changes in the overall pressure distribution, require careful evaluation and preventative measures to reduce the risk of ulceration. Assessment of the progression of sensory neuropathy can be achieved using sensory stimulators (Grunfeld 1992), for example, the Semmes-Wienstein monofilaments, Biothesiometer or thermal probe. The patients perception of the applied stimuli provides an indication of the extent of sensory neuropathy (Brand 1990, Lavery et al. 1998) and can be useful as part of the overall assessment of the risk of ulceration. The presence and extent of peripheral vascular disease can be assessed using Doppler ultrasound (Hill 1987, Williams et al. 1993), plethysmography (Levin 1988) or laser Doppler flowmetry (Stevens et al. 1993), to determine systolic pressure at the ankle or great toe respectively.

Where a routine assessment of the diabetic foot gives an indication of ulceration, structural changes in the foot, inadequate blood supply or infection the patient can be referred for radiological assessment (Dyet 1994). Application of magnetic resonance imaging is increasing (Patton 1991, Weinstien et al. 1993, Edelman et al. 1997), as the technique is capable of resolving between skin, soft tissues, blood vessels and bone, and has proved useful in identifying areas of oedema and infection (Cook et al. 1996).

1.3.4 Methods of prevention and treatment of diabetic foot complications

Regular inspection by the informed patient and attendance at a diabetic foot clinic are important in reducing the risk of developing complications of the diabetic foot.

There are several preventative measures that the diabetic patient can employ to reduce the risk of complications of the foot. Some clinics advise patients adopt a routine of soaking of the feet (Grunfeld 1992) together with application of moisturising creams, to

prevent dry skin. Prescription treatments rather than commercial treatments are required for fungal infections such as Athlete's feet, due to the increased risk of secondary infection in the diabetic. Similarly, corn plasters should not be used, as there is a risk of increased pressure. Regular cutting of toenails is necessary to avoid ingrown toenails, which are a particular hazard for the insensitive foot. Minor cuts and abrasions should be carefully cleansed, treated with an antiseptic, and monitored until fully healed.

Correct choice of footwear is important (Cavanagh et al. 1996, Mueller 1997) and in many cases, orthopaedic shoes and insoles are prescribed for the diabetic patient. These may reduce the risk of ulceration by reducing peak plantar pressures (Schaff and Cavanagh 1990). In the design of orthopaedic shoes for the diabetic, an indication of the plantar pressure distribution needs to be obtained, so that an insole can be designed to reduce pressure in regions prone to ulceration. Fitting by a specialist is required to ensure that a safe pressure distribution has been achieved under the whole foot.

Unfortunately, despite the benefits of regular care many diabetic patients, through a lack of awareness or inclination, fail to adopt simple preventative measures to protect their feet (Knowles and Boulton 1996, McCabe et al. 1998). This factor coupled with the presence of sensory neuropathy, often results in the symptomatic diabetic foot being ignored prior to ulceration (Brand 1990). The undesirable consequence is that treatment must be started immediately to stem progress of the ulcer and this may require hospitalisation.

The first step in the treatment of the ulcerated diabetic foot is to assess sufficiency of the vascular supply to the foot (Edmonds and Foster 1994). If this is found to be inadequate the ulcer can fail to respond to treatment, and furthermore, the trauma of surgical intervention can lead to permanent tissue damage and gangrene. To avoid such complications, the patient can be referred for vessel revascularisation using procedures such as arterial reconstruction (Stonebridge and Murie 1993) or angioplasty (Faglia et al. 1996).

Treatment of a neuropathic plantar ulcer commences with removal of the protective callus to allow underlying necrotic tissue to be excised (McInnes 1994). A sample of the tissue is analysed by the pathology lab and if the foot is infected, an appropriate antibiotic administered (Jeffcoate and Finch 1994). A suitable dressing is applied to the

wound and progress routinely monitored. Mobilisation of the patient typically requires immobilising the foot to avoid loading of the ulcerated region. For example, Brand (1990) describes the application of a total contact plaster cast with a rocker base, which covers the foot and lower limb, extending to below the knee. A limitation of this approach arises from the difficulty of assessing the progress of healing. This problem has been solved by the introduction of orthopaedic footwear, which performs an equivalent reduction of loading under the site of ulceration, for example the Darco healing shoe (Orthopaedic Systems Ltd, Widnes, Cheshire).

Following successful healing, the location in which the ulcer occurred should be routinely assessed to reduce the risk of recurrence.

1.4 Summary

The most important consequences of the diabetic foot are the risk of amputation to the patient and the high cost of treatment to the health service. Early detection of risk factors is important in preventing the development of ulceration. Current methods for assessment of vascular, neuropathic and biomechanical complications of the diabetic foot are limited by difficulty of application and of clinical interpretation. The highest incidence of plantar ulceration occurs in type II diabetics with sensory neuropathy. In these subjects, it is reasonably straightforward to quantify the degree of neuropathy and plantar pressures but threshold levels for ulceration are not well defined. The basic problem in stating threshold levels for ulceration is the difficulty of assessing the affects of increased plantar pressures on plantar skin tissue. However, it is generally considered that the nutritional supply to the tissue is impaired. In the majority of cases, this is made worse by additional vascular complications, which may include macrovascular and microvascular disease and autonomic neuropathy. Assessment of plantar vascular status in the diabetic foot is complicated by the problem of obtaining data during normal conditions of loading i.e. for standing and walking. The objective of this research is therefore to enable such measurements to be made in order to gain further insight into the underlying mechanisms of ulceration. It is hoped that this will provide a basis for improving the accuracy with which ulceration in the diabetic foot can be predicted. Consequently, the aims of the project are now stated.

1.5 Aims

The aim of this research is to design and evaluate a sensor for assessment of plantar blood flow in-shoe, during standing and walking.

Chapter 2 Theoretical background

2.0 Aims and introduction

The aim of this chapter is to review the general background and relevant theory. In the first section, the osteology and angiology of the foot are described, with emphasis on the plantar and metatarsal regions of the foot. The second section considers the structure of the skin and the effects on the cutaneous microcirculation of compression and shear. Risk factors in the development of pressure sores are stated. The final section considers the theory of laser Doppler flowmetry and shows the basis for obtaining an estimate of blood flux from measurements of the optical field, backscattered from the skin.

2.1 The foot

The foot comprises 26 bones and 11 muscles, which together with various ligaments and tendons support the body weight and provide leverage during walking (Palastanga et al. 1994).

2.1.1 Anatomy of the plantar aspect of the foot

The skeletal structure of the foot includes the posterior tarsus (hindfoot), central metatarsus (midfoot) and anterior phalanges (forefoot), (Whittle 1991). Figure 1 illustrates the skeletal structure of the foot.

2.1.2 Osteology

Two bones of the hindfoot provide the structural link between the foot and the bones of the lower leg. The largest is the oblong calcaneous, which projects rearward to form the heel. A large number of ligments form a strong connection between the calcaneous and the bones of the midfoot and forefoot. Body weight is transmitted downward through the calcaneous to the ground. To protect the calcaneous against these forces, the plantar surface of the bone is covered with the fibrous cushioning tissue of the heel pad. The internal structure of the bone is also adapted for weight bearing. The anterior surface articulates with the cuboid bone of the midfoot. The second hindfoot bone, the talus, lies above the calcaneous. It is angled slightly forward and medially, providing a

coupling of force between the tibia and the calcaneous. The anterior aspect of the talus connects to the navicular bone of the midfoot.

The cuboid and navicular bones, together with three anterior cuneiform bones form the structural midfoot. The navicular articulates with the talus and the three cuneiform bones. The cuboid is located inferior and lateral of the navicular and cuneiforms. The anterior surface articulates with the two minor metatarsals of the forefoot. Both long and short plantar ligaments connect to the cuboid. The largest of the cuneiforms, the anterior medial cuneiform, articulates the first metatarsal bone. The second and third metatarsals are articulated by the anterior of the intermediate cuneiform and lateral cuneiform, respectively.

The forefoot of each foot has five metatarsal bones, which articulate at their basal end with the bones of the hindfoot and through a cylindrical shaft to a head, which connects to the phalanx of the associated toe. The metatarsal heads are convex in both the lateral and transverse planes. To the rear on either side are a tubercle and a small depression to which ligments attach. The phalanges of the forefoot form the toes.

2.1.3 Arthrology

At the rear of the foot, the ankle joint acts as a hinge allowing dorsiflexion and plantarflexion of the foot, as well as limited lateral sway. Seven joints form the intertarsal group, which support movement of the foot including inversion, eversion and some rotary movement and contribute to weight bearing. The tarsometatarsal and intermetatarsal joints determine movement of the metatarsals, which is limited by bounding tendons, except for the first metatarsal, which can exhibit considerable freedom of movement. The metatarsophalangeal joints occur at the interface between the metatarsal heads and the posterior phalanges. Considerable transverse movement is possible, whereas, lateral movement of only a few degrees is normal. Movement of the phalanges is determined by the digitorum brevis muscle (Van De Graff and Fox 1992), situated in the dorsum of the foot. Movement of the rest of the foot is determined by various plantar muscles, active at different times during the gait cycle. These muscles provide propulsion, balance and maintain the arches of the foot.

2.1.4 Arches of the foot

The arches of the foot arise from the curved nature of the ligaments and tendons, binding the bones of the foot. The resulting structure provides a spring like suspension mechanism, that results in the transmission of body weight primarily through the calcaneous and metatarsal bones (Lord 1986). The medial and lateral arches reach from the calcaneous to the heads of the metatarsals, reducing the transmission of body weight through the midfoot region. Load bearing capability is increased by a transverse arch across the base of the metatarsals.

2.1.5 Angiology

The arterial supply to the foot is provided by posterior and anterior tibial arteries (Sarrafian 1993). The posterior tibial artery joins the foot at the medial mid-heel and divides into the medial and lateral plantar arteries, close to the heel. The lateral plantar artery continues, proximal with the centre line of the foot, to the midfoot, where it branches into the four plantar metatarsal arteries. This branching segment forms the deep arterial plantar arc, which continues transversally across the foot to meet the continuation of the medial plantar artery. The first plantar metatarsal arteries extend to form arterial loops. For example, the junction of the deep arterial plantar arc and the medial plantar artery, branches medially, as a continuation of the first plantar metatarsal artery and transversally, as the common digital artery. These branches are joined at the beginning of the great toe by the transverse hallucal anastomotic branch. The lateral and medial plantar arteries supply the extensive vessels of the plantar skin tissue, the Planta pedis. The plantar surface can be divided into four arterial regions of which the region under the metatarsal heads is referred to as the distal region. In this region, perforating arteries arise from the plantar metatarsal and digital arteries, which are situated above the plantar fascia. They pass vertically through the plantar fascia to reach the subdermal plexus. Figure 2 illustrates the distribution of the plantar arteries.

The venous network of the Planta pedis forms an extensive mesh of vessels over the entire superficial surface of the foot. This mesh extends through the subdermal plexus and into the dermis. The superficial venous system converges into the medial and lateral veins of the dorsal venous system. These plantar veins do not have valves and the direction of blood flow in the foot is determined by the veins of the dorsum.

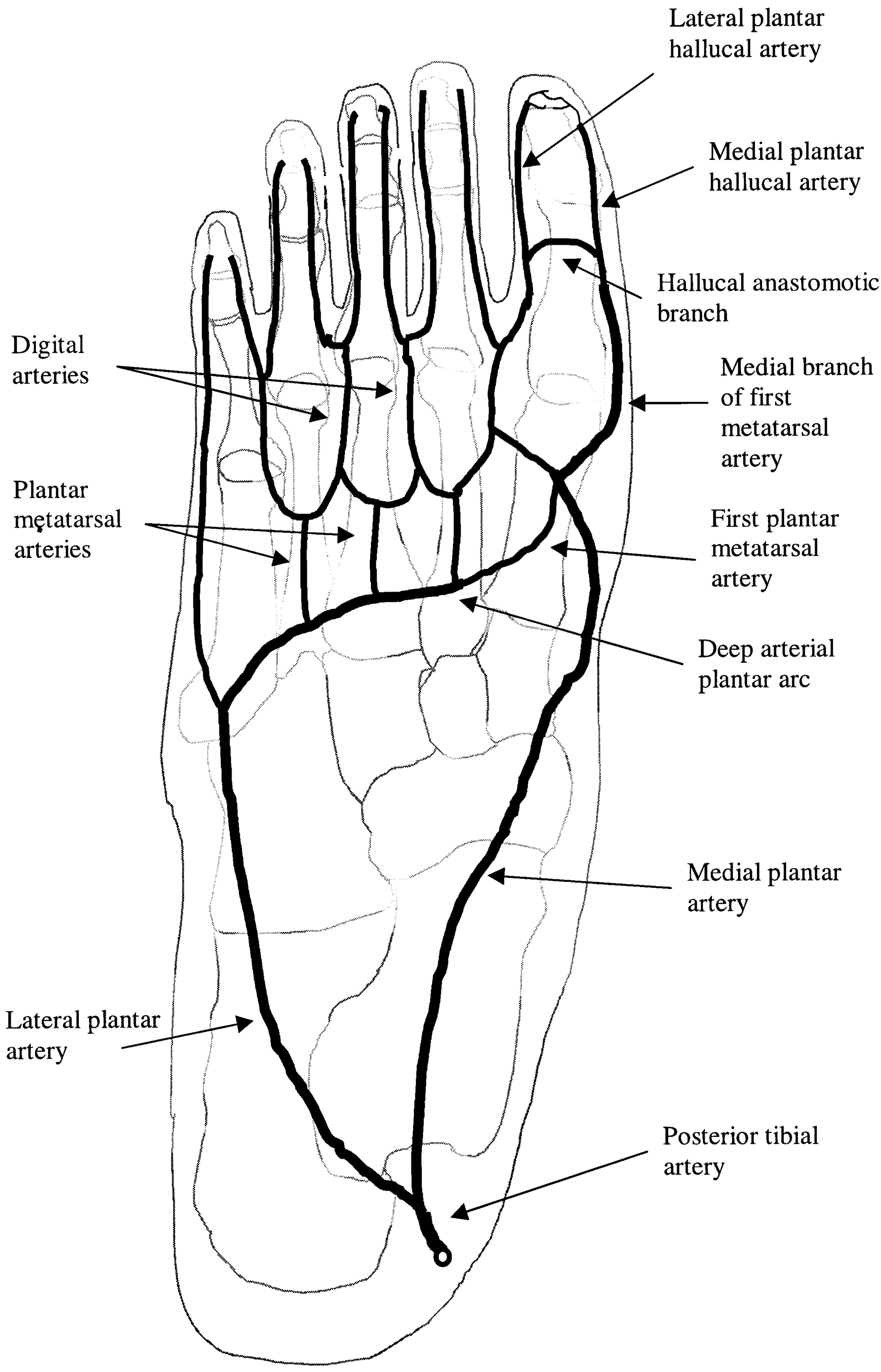

Figure 2 Distribution of the plantar arteries.

2.1.6 Anatomy of the metatarsal head region

Although the skin under the metatarsal region is relatively thick, the metatarsal heads are easily felt through the skin. Between the skin and the bone are adipose cushions that provide protection from external forces. Similar fat bodies occur in the separations between each metatarsal bone. These oblong fat bodies are retained by layers of collagenous sheet, the plantar aponeurosis, located in the inter-metatarsal head regions and subcutaneously. The lower bands connect intermediately with the dermis forming a strong bond, consequently, the skin in this region exhibits little movement.

The sub-metatarsal adipose bodies, directly under the metatarsal heads contain collagenous fibres, which extend from the plantar aponeurosis, and local tendons and ligaments. The superficial plantar arteries and plantar nerves traverse only those sub-metatarsal adipose bodies located between the metatarsal heads. The plantar arteries are located deep within the fat body and are well protected. Figure 3 illustrates the anatomy of the metatarsal head region.

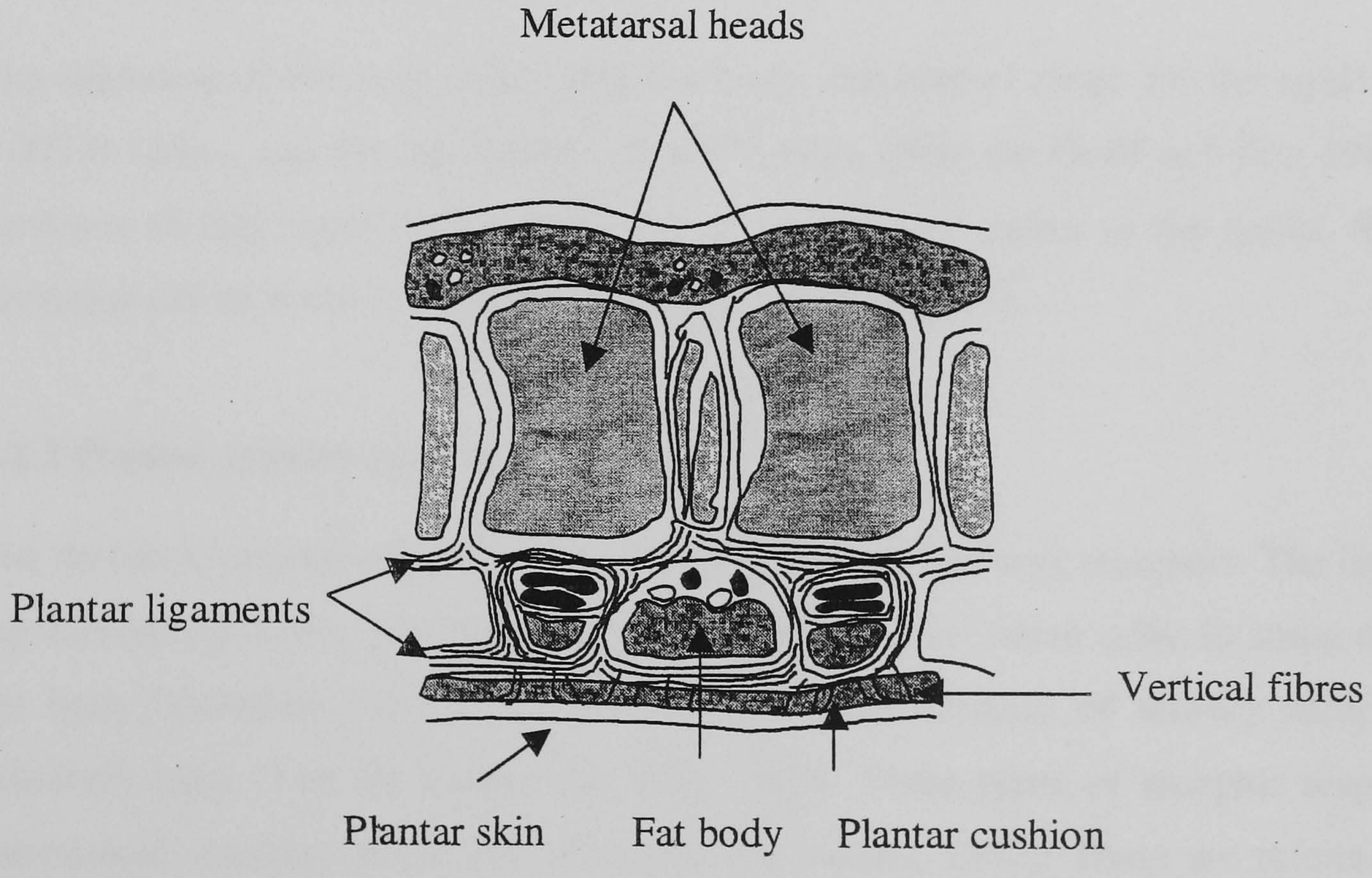

Figure 3 Anatomy of metatarsal head region.

2.2 The skin

2.2.1 General structure

The skin is the largest organ of the human body, accounting for 7% of body weight. The two main layers are the epidermis and dermis. Figure 4 illustrates the structure of the skin and microvasculature. The surface of the epidermis, the stratum corneum, is composed of dead keratinised cells, which protect the body from the environment. This layer is continually produced by keratinocytes in the lower epidermal, stratum basale layer. Macrophages within the epidermis provide protection from ingress of bacteria and debris.

The dermal or corium layer below the epidermis contains a network of vessels, supporting fibres and nerves. As well as performing localised functions, the dermis is important in regulating body temperature and blood pressure.

Lying below the dermis is the hypodermis or subcutaneous tissue, which binds the skin to underlying structures. There is a high proportion of lipid storing adipose cells in this region, providing thermal insulation for the body.

The thickness of the skin varies over the body, the normal range for the epidermis is 0.007-0.12mm, and for the dermis 1-2 millimetres, (Van De Graff and Fox 1985). At locations of high wear such as the soles of the feet and palms of the hands, the skin thickness can increase to about 6mm (Palastanga et al. 1994).

2.2.2 Plantar sensory system

The dermis is extensively innervated with effectors and sensory receptors. The latter are represented by tactile, pressure, thermal or pain sensitive, nerve cells. In some areas of the body, including the soles of the feet, the concentration of sensory receptors is relatively high (Van De Graaff and Fox, 1985). Three types of receptor respond to mechanical stimulus of the skin (Schmidt and Thews, 1987). These are referred to as slowly adapting (SA), rapidly adapting (RA) and very rapidly adapting. The SA fibres in the sole of the foot are sensitive to the intensity of plantar pressure. Both types of rapidly adapting receptors only respond to dynamic changes in plantar pressure. Dynamic pressure changes, due to tissue deforming with constant velocity, are sensed

by the RA fibres. Tissue deformations with increasing velocity (acceleration) are sensed by the very rapidly adapting receptors. Each of the receptors relays signals to the central nervous system, which continually alters stance and gait, to optimise the distribution of body weight. Response times of these receptors are are typically within 50 to 500ms (Schmidt and Thews 1989).

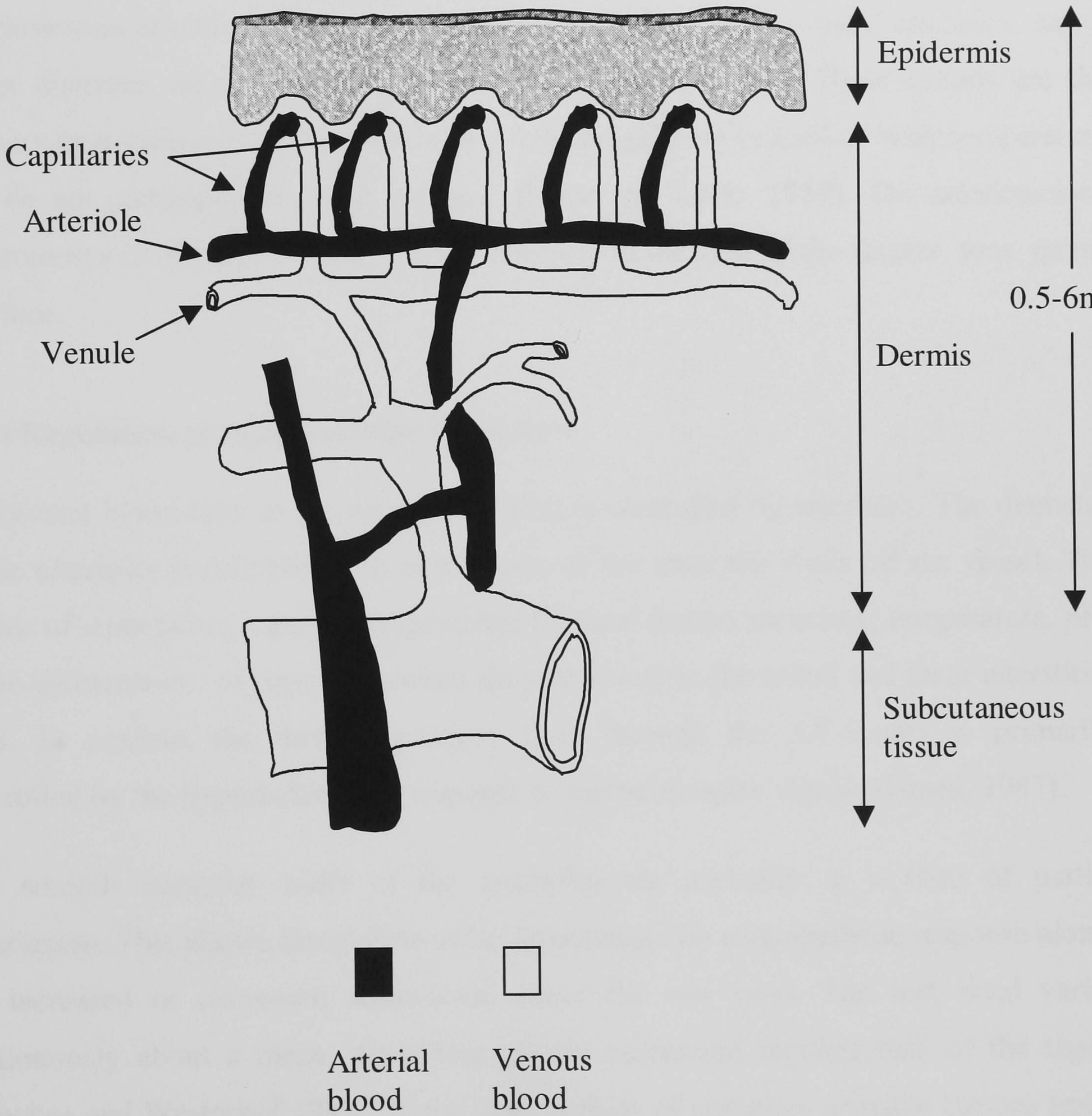

Figure 4 Structure of the skin and microvasculature.

2.2.3 Structure of the cutaneous microcirculation

The arterioles that supply the microcirculation terminate in meta-arterioles and capillaries, which are thin walled vessels with diameters of less than 100µm. The meta-arterioles form a link between arteriole and venule. The capillaries are looping structures that extend orthogonal from the meta-arterioles, to perfuse tissue, before entering a draining venule. Each meta-arteriole supports several capillaries. Each capillary is a single layer of endothelial cells supported by a thin basement membrane. Nutrients pass through intracellular channels in the capillary wall and diffuse into local tissue cells. At some sites on the body arteriole-venule linking structures, the arteriovenous anastomoses are observed. These differ from the meta-arterioles, being larger diameter vessels with prominent, smooth muscle walls. These vessels are the primary heat exchange mechanism in the thermoregulatory control of body temperature and do not participate in tissue nutrition (Little and Little, 1989). The arteriovenous anastomoses (AV-shunts) occur in large numbers in the skin of the fingers, toes, palms and face.

2.2.4 Regulation of microvascular blood flow

Nutritional blood flow in the microcirculation is controlled by arterioles. The diameter of the arterioles is determined by stimulation of the muscular walls off the vessel. The degree of stimulation is primarily governed by local factors including; temperature, pH, tissue deformation, oxygen and carbon dioxide levels in the blood and local interstitial fluid. In contrast the thermoregulatory flow through the AV-shunts is primarily controlled by the hypothalamus in response to thermoreceptor signals (Green, 1987).

The smooth muscular walls of the arterioles are normally in a state of partial contraction. This allows blood flow to be determined, via a sympathetic response alone, via increased or decreased stimulation about the rest level. The rest level varies continuously about a mean, depending on the nutritional requirements of the tissue (Strackee and Westerhof 1993). In the skin, periods of complete arteriole closure and a consequent cessation of capillary blood flow are observed (Little and Little 1989). This periodic variation in flow is termed vasomotion and has a typical frequency in skin of 5-6 times per minute (Fagrell et al. 1977).

Increased tissue activity leads to a rise in the by-products of metabolism, many of which are vasoactive substances (Guyton 1992). These act as a trigger, resulting in vasodilation of arterioles. The heightened blood flow satisfies the additional nutritional demands of the tissue and diminishes the concentration of by-products, thus reducing the stimulus for further vasodilation. The same autoregulatory mechanism also helps to isolate local blood flow from changes in main arterial blood pressure, so that a relatively constant perfusion pressure is maintained throughout the capillary bed.

The transient phase of this autoregulatory, blood flow mechanism is termed hyperaemia. If blood flow to skin tissue is occluded for a short time, the build up of vasoactive substances can trigger a period of full arteriole vasodilation, termed reactive hyperaemia (Michel and Gillott 1990). This also occurs in response to abnormal tissue deformation, induced for example, by shear forces and following skin trauma, such as a sting. In the case of abnormal forces, the trigger mechanism is the stretching of the muscular walls of the arterioles, whereas for trauma, the trigger is the release of a vasoactive compound, such as histamine (Guyton, 1992).

Localised control of nutritional blood flow by metabolic factors is dominant for skin surface temperatures of 25-30^{o}C (Scott, 1986). Below this range, cellular activity in skin tissue falls considerably and the degree of centralised control of microcirculatory blood flow is increased to avoid a reduction in core temperature. Above this range, thermoreceptors in the skin activate a parasympathetic triggering of sweat glands, which release the vasodilator bradykinin. The increased microcirculatory blood flow helps to radiate heat from the body in addition to that lost via the AV-shunts. This mechanism is necessary, as the AV-shunts do not exhibit autoregulatory behaviour in response to local physical or metabolic factors.

2.2.5 Nutritional exchange between blood and tissue

The junction between arteriole and capillary is termed the pre-capillary sphincter. When fully dilated the cross sectional area of the orifice is only 0.2mm^2. For this reason, blood flow in the capillaries is by singular or small chains of red blood cells (RBC), which are separated by pockets of plasma. Capillaries typically vary in length from 0.4-0.7mm (Schmidt and Thews 1989) and have a typical diameter of 0.008mm (Van De Graff and Fox 1992).

The parallel structure of the capillary network reduces perfusion pressures to relatively low levels, with mean RBC velocities in the range of 0.07-2mm.s^{-1} (Nilsson and Tenland 1980). These conditions are adequate for the exchange of nutrients between RBC, and plasma and the interstitial space. Cellular by-products also diffuse into the vessels. Nutrients in the interstitial space quickly reach active cells because the mean distance from a capillary is only 20µm (Little and Little, 1989). The rate of diffusion is high due to the large surface area of capillaries. The skin as a whole receives between 150ml and 500ml of blood per minute (Green 1987) with each capillary supplying from 0.04 to 0.27mm^2 of the dermis (Nilsson et al. 1980).

The anatomical structure of the microcirculation exhibits considerable variation at different body sites and between individuals (Ryan 1985).

2.2.6 Biomechanics of the skin

Skin is one of the most complex soft tissues of the body. The layers of the epidermis and dermis are interconnected meshes of collagen, elastin, blood, nerve and lymphatic vessels surrounded by interstitial fluid. The thick keratinised stratum corneum of the upper superficial epidermis is important in determining the mechanical strength of the skin of the palms and soles. In general however, the mechanical strength of the skin is determined by collagen, elastin and the properties of the subcutaneous tissue to which these fibres attach (Scales 1990).

The mechanical strength of the skin can be assessed in vivo by application of vertical stress to tension the skin. These tests indicate a nearly exponential increase in extension with applied force. If the skin is relaxed and re-tensioned, the extension is increased, indicating a significant time-rate dependence or creep (Kennedi, 1980). The particular results obtained also depend on the orientation of the skin in tension, so that the mechanical properties of the skin are anisotropic.

Forces acting on the skin can occur as result of external loading or from internal loading by bony prominences. In general, a load will act over a definite area, and the ratio of the magnitude of load to area is termed pressure. The effect of pressure on skin is to induce stresses within the skin tissues (Bader 1990). These induced stresses depend on the

direction in which load is applied. Compressive stress results from the application of a perpendicular load and shear stresses from horizontal loading.

2.2.7 Development of pressure sores

The effect of applying relatively low level forces to the skin is a reduction in perfusion, evidenced by a visual paling termed blanching. This type of response requires the collapse of capillaries, suggesting that the external force is greater than the normal capillary pressure of 30-32mmHg (Kabagambe et al. 1994). If excessive pressures are applied for long periods, there is inadequate tissue nutrition, and the result is a pressure sore or, more properly, a decubitus ulcer (Huether 1998). Pressure sores predominate in those over seventy years of age (Pfeffer 1991) and this may be as a result of the altered mechanical properties of the skin in the elderly, for example reduced collagen synthesis (Phillips 1997).

Pressure sores tend to occur in specific regions of the body and these correspond to positions with bony prominences near to the skin. In particular the lower back (sacrum), the medial and lateral upper thigh, the rear and lateral heel, are all prevalent sites (Barton and Barton 1981).

Loss of nutritional blood flow, with pressure, normally occurs in the capillaries of the dermal layer, which extend upward from subcutaneous tissue. The looped structure of these capillaries makes them susceptible to collapse (Pfeffer 1991). This problem is compounded by shear forces, which cause the skin to move laterally over the subcutaneous tissue. This tissue is composed mainly of fatty adipose tissue, which distributes applied load over a larger area, reducing pressure. The amount of fatty tissue depends on the body location and upon the individual. Thus, the cushioning effect is variable.

The start of pressure sore formation is normally indicated by a region of under perfused, blanched tissue that fails to reperfuse following removal of external pressure (Simpson et al. 1996). Biopsies of this tissue indicate substantial structural damage to vessels including capillary haemorrhaging (Reddy 1990). The consequent loss of nutrition can result in tissue necrosis, occurring typically within 24 hours (Daniel et al. 1981). If the necrotic tissue becomes infected rapid breakdown of tissue can occur, spreading

through subcutaneous tissue and resulting in destruction of muscle and bone (Sandeman and Shearman 1999).

Although the magnitude and duration of applied pressures are important indicators of the risk of a pressure sore, the actual values required for ulceration, depend largely on the distribution of forces within the tissue. In general, the microcirculation of the skin does not exhibit ordered structure and individual vessels are, therefore, susceptible to varying levels of compressive and shear force, depending on their location and orientation. For this reason, both types of force are considered to contribute to pressure sore formation (Pfeffer 1991).

2.2.8 Pressure sore risk factors

Several other factors can contribute to the development of a pressure sore. The normal composition of the bulk tissue space of skin is a slightly gelatinous semi-fluid, which provides some structural strength (Kenedi 1980). In many pathological conditions excess water collects in skin tissue resulting in oedema. Pockets of fluid within the skin may increase the risk of ulceration by lowering resistance to pressure (Robertson et al. 1990). The presence of oedema is also thought to modify tissue nutrition (Mani et al. 1995).

The metabolic demands of skin tissue vary considerably with temperature. Small increases in temperature result in a rapid increase in the nutritional demands of the tissue (Scott 1986). For this reason, the duration for which an excessive pressure can be tolerated reduces with increasing temperature because the tissue becomes hypoxic at a faster rate. At lower temperatures, the metabolic demands of tissue are reduced. However, if pressure induced ischaemia occurs, the required hyperaemic response can be offset by the reduced blood flow arising from thermal vasoconstriction.

The malnourished and the obese are at greater risk of developing pressure sores. If body fat reserves are low, the regions of skin under the bony prominences are not well protected by a cushioning layer of fat, leading to increased pressures. In the obese, the higher incidence of cardiovascular complications is thought to be associated with the higher incidence of pressure sores in this group (Simpson et al. 1996).

In some types of injury or disease, the risk of pressure sore formation is increased by absent or reduced sensitivity, for example spinal cord injuries (Basel 1991) and diabetic neuropathy (Sandeman and Shearman 1999). In these cases, pain associated with ischaemic tissue is not present, and shifting of body weight to relieve the affected region, does not occur. Pressure sores in diabetics are particularly serious, as there is an increased risk of infection, inflammation of adjacent tissue and septicaemia (Huether 1998).

2.2.9 Assessment of skin pressure

Quantification and analysis of pressure distribution and the effects of pressure on skin are important in developing understanding of pressure sore formation. Compressive stresses under bony prominences have been shown (Tsay 1991) to act vertically from the point of load application, through tissue to bone. Shear forces affect deep tissue (Simpson et al. 1996), particularly where high-pressure gradients occur, for example at tissue-bone and tissue-muscle interfaces.

Measurement of compressive loads on tissue is relatively straightforward if the transducer can be applied to a nominally flat region of skin. Measurement of pressures over curved surfaces and of shear stresses is normally impractical, due to the difficulty of designing suitable transducers. Determination of the distribution of stresses within tissue is complicated by the difficulty of measurement and specification of reliable models because of the structural complexity of skin tissue. Some data has been provided by using phantoms or through invasive animal studies (Tsay 1991).

The basic equation for determining pressure at the skin surface is P = F / A where *F* is the force in Newtons and *A* is the area in square metres, resulting in normal SI units for pressure of N/m^2. The SI name for the unit of pressure is the Pascal (Pa).

In the literature, the large pressures acting under the foot are generally quantified in units of kPa – MPa, or in terms of static loading by the body weight, in units of Kg/m^2.

Useful conversion factors for these quantities are (Sykes et al. 1981):

$1000N/m^2 = 101.9Kg/m^2 = 1kPa = 7.501mmHg.$

The preceding values are only valid for static loading. In dynamic studies, the additional acceleration of the foot under motion requires consideration (Whittle 1991).

The use of force sensors to measure skin pressure requires careful consideration of several factors: reducing sensor size is important to avoid altering the pressure distribution in the region (Ferguson-Pell 1980), the area of the sensor over which the force is applied should remain constant, and the sensor should respond only to compression or to shear, so that each force can be independently quantified (Laing et al. 1992).

2.2.10 Methods of assessing skin pressure

Measurement of pressure at the body-support interface can be achieved using null-type pressure sensors normally based on an air bladder, or by deflection type sensors based on the principle of deformation of a material. The null-type of sensor is normally considered more accurate than the deflection type (Morris 1993).

A typical application of a bladder pressure sensor is in measurement of interface pressure between the skin and a support cushion. The principle of operation is inflation of a bladder until electrical connections on the upper and lower surfaces become open circuit, at which point the bladder pressure is determined from a connected air gage. Zhou (1991) states the main advantages of this type of sensor as: good compliance with curvature of soft tissues, good repeatability and insensitive to shear forces and temperature variations.

For some clinical measurements including in-shoe measurement of plantar pressures, a bladder pressure sensor is unsuitable. It is then necessary to use or adapt a conventional deflection type of sensor for interface pressure measurement. An important constraint is that the device should have a thickness of less than 0.5mm (Ferguson-Pell 1980) to avoid redistribution of pressure. Sensors for measuring skin pressure are characterised by a number of standard parameters: linearity, hysterisis, accuracy, frequency response, range, creep and repeatability. Additionally factors such as temperature, humidity and fatigue are often important. Cobb and Claremont (1995) have reviewed the sensor technologies for determination of skin pressure with particular emphasis on foot

pressure measurement (Refer to Appendix E). The basic types of deformable sensor are summarised in the following paragraphs.

Semiconductor and metal strain gages mounted on a metallic diaphragm offer the highest levels of performance in terms of repeatability, linearity and hysterisis. However these devices require thermal compensation and produce incorrect responses for off-axis loading.

Capacitive pressure sensors, based on a change in capacitance between two or more electrodes in parallel, with deformation of an elastomer dielectric offer good measurement performance and some compliance over curved surfaces. However, they are difficult to use because the small changes in capacitance (~100pF) are difficult to measure and the connection leads provide additional stray capacitance. Capacitive pressure sensors for plantar measurement, have been described by Kothari et al. (1988) and Zhu and Spronck (1992).

Piezoelectric transducers based on polyvinylidene flouride (PVdF) film can provide accurate measurement of skin pressures and are easily scaled to suit a specific area or constructed into arrays. The different axes of the material respond to either vertical or horizontal loads and it is therefore feasible to simultaneously measure both perpendicular and shear stress (Akhlagi and Pepper 1996). Such sensors can be difficult to use because of the difficulty of electrical connection to the polymer film and the generation of additional charge with temperature. Furthermore, the technique is only responsive to dynamic loading and is therefore unsuitable for static assessment. A complete plantar monitoring system based on this technology has been described by Nevill (1991).

For reasons of cost, size and ease of use, the pressure sensor used in the plantar monitoring system is a Force Sensing Resistor. This device is discussed in detail in the following section.

2.2.11 The Force Sensing Resistor

Transducers based on Force Sensing Resistor (FSR) technology are routinely used in foot pressure measurement (Cavanagh et al. 1992). These are thin, 0.25mm – 0.7mm, circular devices with diameters from 10-30mm. They are capable of measuring orthogonal pressures over a range of 0-4MPa. This range includes the maximum pressures observed under the diabetic foot of 3MPa (Whittle 1991). The FSR has the advantage of being insensitive to shear forces in the typical range for skin, has measurement repeatability per device of 2% and a frequency response to 1 kHz over the full measurement range. Previous studies (Lord et al. 1992, Akhlaghi and Pepper 1996) indicate that a frequency response extending to 200Hz is sufficient to track the dynamic forces under the foot during walking.

Disadvantages of the FSR are:

A logarithmic response – giving reduced sensitivity at high loads.
A response, temperature dependence of 0.1% per Kg^{-1}. ^{o}C.
A device to device repeatability of +/-15% for loads above 1MPa.

These limitations can be overcome by compensation circuitry or software. However, this requires individual calibration of each sensor over the full load and temperature ranges. Calibration of the Force Sensing Resistor used in the plantar monitoring system is discussed in Chapter 5.

2.2.12 Assessing the affects of pressure on the microcirculation

It is difficult to determine the effect on tissue blood flow of compressive and shear stresses induced by external loading. The ^{133}Xenon-clearance technique (Chittenden and Shami 1993) is a reliable but invasive method that can be used to determine blood flow during external loading (Daly et al. 1976). Using this method Daly et al. (1976) found blood flow to reduce rapidly for pressures up to 10mmHg and then at a slower rate until cessation at systolic pressure. More recently, non-invasive techniques have been investigated in clinical studies, including Transcutaneous oxygen tension (Kabagambe et al. 1994) and laser Doppler flowmetry (Castronuovo et al. 1987).

2.2.13 Methods of measuring skin blood flow

Techniques for assessment of the skin microcirculation are either invasive or non-invasive.

Invasive methods allow accurate measurement of flow based on clearance of radioisotope isotopes or of tissue perfusion based on fluorescent dyes. The application of these methods usually results in a degree of trauma at the measurement site. Detection of isotope clearance is made using a scintillation detector; distribution of fluorescent dye can be studied under ultraviolet illumination. None of these techniques is suitable for continuous monitoring (Obied 1989).

Non-invasive techniques support qualitative assessment through capillaroscopy or absolute or comparative measurement using thermal techniques (skin thermometry and thermal clearance), evaluation of pressure (Skin perfusion pressure and transcutaneous oxygen tension) and optical methods (Photoplethysmography and laser Doppler flowmetry) (Fronek 1989).

In static capillarosopy, the microcirculation is viewed directly using a microscope, which is usually connected to a television camera to allow recording. Dynamic capillaroscopy extends this technique to include electronic synchronisation and processing of the image to allow quantification of red blood cell velocities (Fagrell et al. 1977). System size restricts application to easily assessable regions of the skin.

Thermal techniques employ thermistors or thermocouple probes to measure the clearance or conductance of heat in the skin, which is related to cutaneous blood flow (Challoner 1975). Careful control of ambient temperature is required and the response is slow (~<1Hz).

Skin perfusion pressures provide an indication of the volume of blood in tissue and therefore provide an indirect assessment of the adequacy of blood flow to the region. Sensitive plethsymographic sensors based on strain gage, capacitive or electrical impedance techniques are used in this application (Fronek 1989).

Determination of transcutaneous oxygen tension ($tcPo_2$) is a quantifiable method of assessing skin blood flow (Romanelli and Falanga 1999). A Clark-type platinum electrode provides a current proportional to Po_2 (oxygen tension) at the skin surface. At

normal skin temperature Po_2 at the skin surface is close to zero mmHg. Heating of the skin usually in the range of 37-45°C results in an increase in blood flow and a consequent increase in Po_2 at the skin surface to measurable levels (50-120mmHg dorsal forearm).

Optical methods are increasingly used for assessment of the microcirculation because of the ease of use and fast response. Photoplethsymography relates changes in intensity to changes in blood volume (pulsatile) in the sample tissue (Challoner 1979). Both transmissive and reflective modes of operation are possible. The dependence of the response on the optical geometry of the sensor and uncertainty regarding the physiological origin of the photplethysmographic signal are important limitations (Lindberg et al. 1991). Laser Doppler flowmetry provides a response that increases linearly with changes in both mean red blood cell velocity and red blood cell concentration in a sample of tissue. The response is not quantifiable and the technique is sensitive to movement artefact. Despite these limitations it has been widely used to study the microcirculation and has previously been used to demonstrate microcirculatory abnormalities on the dorsum of the neuropathic diabetic foot (Stevens et al. 1993).

Justification for the use of laser Doppler in the present study is discussed in section 3.8 and a detailed discussion of the technique is presented in the following sections.

2.3 Determination of skin blood flow by laser Doppler flowmetry

2.3.1 Haemodynamics of the microcirculation

Determination of blood flow is complicated by the non-homogenous composition of blood and the pulsatile nature of flow. The viscosity of blood is dependent on the shear forces, exerted on the fluid at it moves (Evans et al. 1989). This dependence is most significant in small vessels of less than 100 microns, which includes the arterioles and capillaries of the microcirculation. In terms of flow, the fluid in these vessels is considered as non-Newtonian (Francis 1976). The evaluation of this type of flow requires a complex model incorporating details of shear rate, blood viscosity and non-linear flow effects such as plasma skimming (Little and Little 1989). An estimate of blood flow rate can be obtained using a simplistic model that ignores these effects

(Strackee and Westerhof 1993). Empirical studies (Slaaf et al. 1993) indicate that this approach can overestimate flow rate by up to 25%. However, equations (1) to (4) given below are useful for obtaining approximate values for the red blood cell velocity range in small vessels.

In the case of vessels for which mean particle velocities are low, and particle size is small, relative to vessel diameter, laminar flow is predominant (Marion and Hornyak 1985). Steady flow is defined by constant velocity and pressure conditions at each point, within a vessel, and with respect to time. Arteriole flow is intermittent but during active periods, the flow is laminar at a rate proportional to the metabolic demands of the tissue. In this situation, the velocity profile across the vessel becomes parabolic, so that blood in the centre is moving with maximum velocity and is stationary at the vessel walls. This is referred to as Poiseuille flow and the velocity of any particle within the vessel can be determined from (Evans et al. 1989):

$$v(r) = v_{Max}(1 - r^2 / R^2) \qquad (1)$$

Where, $v(r)$ is the velocity of a particle, at distance r from the centre of the vessel.
v_{Max} is the maximum particle velocity in the vessel, which is the centre velocity.
R is the radius of the vessel.

The volumetric flow Q of blood within the vessel is then defined as the number of particles passing through a cross section of the vessel, in a given time, and thus is dependent on mean particle velocity:

$$Q = \bar{v} \cdot A \qquad (2)$$

Where Q is the volumetric flow in m^3/s.
A is the cross sectional area of the vessel $A=\pi R^2$.

Determination of the mean particle velocity, requires integration of the velocities of each particle at each radial position r, for all r, averaged over the cross sectional area A.

$$\bar{v} = 1/\pi R^2 \cdot \int_{r=0}^{R} v_{Max}(1 - r^2/R^2) \cdot 2\pi r \quad dr \tag{3}$$

$$= 1/\pi R^2 \cdot 2\pi v_{Max} \int_{r=0}^{R} r - (r^3/R^2) \quad dr$$

$$= 1/\pi R^2 \cdot 2\pi v_{Max} \left[\int_{r=0}^{R} r - \frac{1}{R^2} \int_{r=0}^{R} r^3 \right] \quad dr$$

$$= \frac{1}{\pi R^2} \cdot 2\pi v_{Max} \cdot \left[\frac{R^2}{2} \right] - \frac{1}{R^4} \cdot 2\pi v_{Max} \cdot \left[\frac{R^4}{4} \right] \quad = \frac{v_{Max}}{2} \tag{4}$$

The preceding equations are particularly useful for estimating the particle velocities that occur in an idealised vessel such as a blood flow phantom. The half-maximum value for the mean velocity is a consequence of the uniform distribution of velocities that occur in an idealised vessel, for laminar flow.

2.3.2 Optical properties of the skin and blood

Colouration of the skin is largely determined by the pigments melanin and carotene, and by haemoglobin (Matcher and Cooper 1994). The concentration of the two pigments is determined by exposure to sunlight and varies around the world. Absorption by skin pigments occurs mainly below 600nm, above this wavelength scattering processes dominate (Duck 1990).

If light is incident on the skin, 4-7% is diffusely scattered directly from the surface, due to the change in refractive index, from unity in air, to 1.55 in the stratum corneum (Van der Zee 1993). This process is independent of wavelength and pigmentation levels (Anderson and Parrish 1981).

The remainder of the light penetrates into the epidermis and dermis, to a depth dependent on wavelength and pigmentation (Gush and King 1991). In studies of the skin, wavelengths in the visible and near infrared regions are normally used (Schmitt et al. 1986).

The transmittance and scattering of light by blood depends significantly on the erythrocyte concentration (Fronek 1989). In large arteries, red blood cell concentrations can reach 45% by volume, compared to around 4.5% in small vessels, such as the arterioles of the skin (Bonner and Nossal 1990). The penetration depths achieved at wavelengths of 500nm and 1000nm are, 50μm and 400μm for the larger vessels and 500μm and 2500μm for the smaller vessels (Duck 1990). These figures are based on an oxygen saturation of 100% and increase slightly at reduced oxygenation levels.

2.3.3 Optical scattering in skin tissue

Anderson and Parrish (1981) found that the scattering processes in the dermis were mainly determined by erythrocytes, blood vessels, and structural fibres such as collagen. The size and topology of non-erythrocyte cells ensures that light is scattered in all directions within the tissue (Cheong 1990). For this reason, the instantaneous distribution of light within tissue does not correlate with structural order in the tissue.

The scattering process itself occurs as a result of a change in direction of a photon, following interaction with matter. With elastic scattering there is no change of energy. With inelastic scattering a change of energy occurs, which results in a change in the wavelength of the photon (Weidner and Sells 1980). The scattering of near infrared electromagnetic waves by tissue, including red blood cells, is generally considered an elastic scattering process (Bonner and Nossal 1990). This provides the basis for measurement of blood flow by laser Doppler techniques. The direction of propagation of a scattered wave depends on the shape of the scattering particle. For non-spherical particles, including red blood cells, the scattering direction can be estimated using the Rayleigh-Gans method (Van der Zee 1993). Using this method, Bonner and Nossal (1981) estimated a mean value for the scattering angle from erythrocytes of 5.4^{o}, in the forward direction. This low scattering angle reduces the probability of scattering from multiple erythrocytes, which improves accuracy of the laser Doppler technique.

2.3.4 Physical basis of the Doppler shift of light in tissue

If the light from a single mode, monochromatic source illuminates skin tissue, penetration into the tissue will occur, if the wavelength is within the therapeutic window of 600-1200nm (Duck 1990). If the wavelength of the source is greater than about 600nm, absorption by chromophores in the tissue is relatively low, and scattering processes will dominate. Absorption spectra for the skin are given in figure 5. The structure and composition of skin tissue results in a very high coefficient of scattering (Van der Zee 1993) with a mean distance between scattering events, termed the scattering length of ~100μm (Bonner and Nossal 1981). Consequently, light is scattered diffusely within the tissue forming a scattered field. If the incident radiation is spatially and temporally coherent, then the scattered field will resonate with the incident field and exhibit spatial and temporal coherence (Bonner and Nossal 1990). These conditions give rise to electromagnetic waves of the same frequency as the incident radiation. Conversely, if a moving particle, such as a red blood cell traverses a coherent field, electromagnetic waves scattered by the particle will exhibit a shift in frequency, due to the Doppler effect (Drain 1980).

Some of the electromagnetic waves scattered in the tissue will be backscattered to the skin surface and can be detected using a photodetector. Response times of practical photodetectors prevent direct measurement of optical frequencies. However, optical beating occurs between those electromagnetic waves scattered solely from static structures and the waves scattered by moving particles within the tissue. For the range of red blood cell velocities that occur in skin tissue, the corresponding optical beat frequencies have a typical range of 20Hz-12kHz (Barnett et al. 1990) and are easily detected as intensity fluctuations in the optical field incident on the detector.

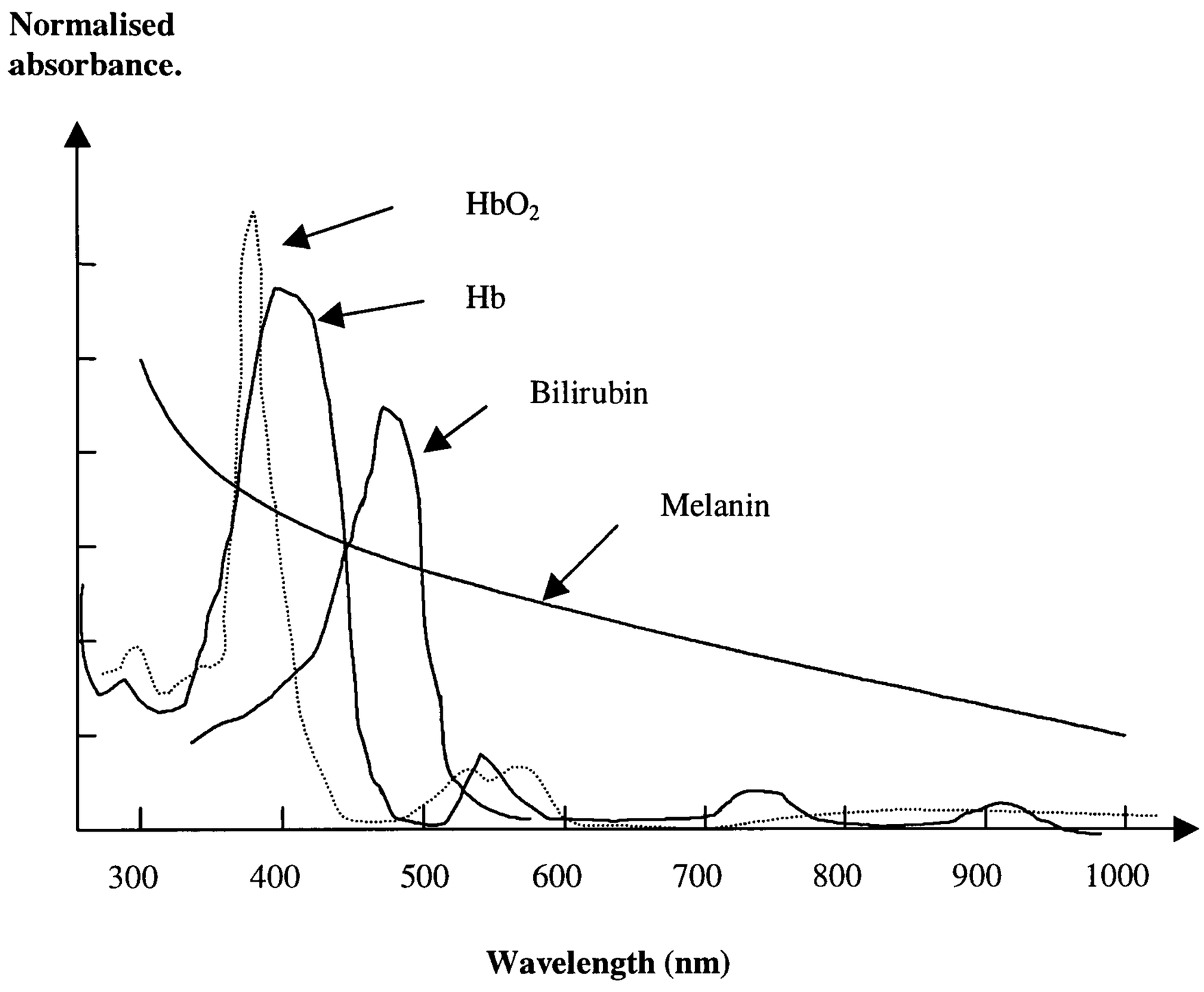

Figure 5 Optical absorbance spectra of the skin.

2.3.4 Derivation of the photocurrent for light scattered from skin tissue

The output from a single, longitudinal mode laser is an electromagnetic wave:

$$E(t) = \tilde{E}_A(t) \cdot e^{-j\omega t}$$

Where:

$\tilde{E}_A$ is the mean amplitude of the wave over one cycle. If the laser output is stabilised, the mean amplitude is constant and is denoted by E_A.

ω is the angular frequency of the wave.

If this field is incident upon the skin and the wavelength is within the therapeutic window photon scattering will occur within the tissue. A small proportion (<1%) of the scattered photons will be detectable at the surface of the skin.

The backscattered optical field comprises of waves scattered from static tissue structures and from moving particles within tissue, predominantly red blood cells (Bonner and Nossal 1980).

The field scattered from static tissue incident on a photodetector at a position *u* and at time *t* is:

$$E_{\mathrm{Re}f}(t,u) = E_{A\mathrm{Re}f}(t,u) \cdot e^{-j\omega_{\mathrm{Re}f}t} \qquad (5)$$

For this case, there is no frequency shift due to the Doppler effect and the field oscillates at the same frequency as the incident wave:

$$\omega_{\mathrm{Re}f} = \omega$$

The field backscattered from moving structures within the tissue is:

$$E_{AShift}(t,u) = E_{AShift}(t,u) \cdot e^{-j\omega_{Scat}t} \qquad (6)$$

For this case, a frequency shift occurs as a result of interactions with moving red blood cells within the tissue.

By the principle of superposition, the total field, $E_{Total,}$ is the algebraic sum of the individual fields (Wilson and Hawkes 1989), thus combining equation (5) and equation (6) gives:

$$E_{Total}(t,u) = E_{ARef}(t,u)\cdot e^{-j\omega_{Ref}t} + E_{AShift}(t,u)\cdot e^{-j\omega_{Scat}t} \qquad (7)$$

The slow response times of standard photodetectors prevent direct measurement of the frequencies in an optical field such as E_{Total}. In practical terms, a photodetector integrates the optical field over many cycles so that the photocurrent is dependent upon the intensity of the incident light. Intensity is proportional to the square of the optical field and for a complex field such as E_{Total}, the resultant photocurrent can be determined from:

$$i(t,u) = E_{Total}(t,u)\cdot E^{*}_{Total}(t,u) \qquad (8)$$

Where the * operator denotes the complex conjugate.

Substitution of equation (7) in equation (8) yields an expression for the photocurrent in terms of the frequency unshifted and frequency shifted fields.

$$i(t,u) = (E_{ARef}(t,u)\cdot e^{-j\omega_{Ref}t} + E_{AShift}(t,u)\cdot e^{-j\omega_{Shift}t})\cdot(E^{*}_{ARef}(t,u)\cdot e^{j\omega_{Ref}t} + E^{*}_{AShift}(t,u)\cdot e^{j\omega_{Shift}t})$$

Expanding this equation and simplifying yields:

$$\begin{aligned} i(t,u) &= E_{ARef}(t,u)\cdot E^{*}_{ARef}(t,u) + \\ &E_{AShift}(t,u)\cdot E^{*}_{AShift}(t,u) + \\ &(E_{AShift}(t,u)\cdot E^{*}_{ARef}(t,u)\cdot e^{j(\omega_{Ref}-\omega_{Shift})t} + E^{*}_{AShift}(t,u)\cdot E_{ARef}(t,u)\cdot e^{-j(\omega_{Ref}-\omega_{Shift})t}) \end{aligned} \qquad (9)$$

In equation (9), the first term represents the contribution to the photocurrent due to backscatter from static tissue structures. The second term represents the contribution to the photocurrent due to homodyne mixing of waves backscattered solely from red blood cells in motion. In the capillary layer of cutaneous tissue the volume of red blood cells per unit volume of tissue is <0.5% (Nilsson and Tenland 1980) and the homodyne term

can be neglected (Bonner and Nossal 1990). The third term in equation (9) represents the heterodyning (optical beating) of the field backscattered from static tissue structures with the field backscattered from red blood cells in motion. By application of Euler's relation the complex exponentials in the third term of equation (9) can be written in terms of sinusoids:

$$\Re\{e^{-j(\omega_{\mathrm{Re}\,f}-\omega_{Shift})t} = \cos(\omega_{\mathrm{Re}\,f}+\omega_{Shift})t$$

$$\Re\{e^{j(\omega_{\mathrm{Re}\,f}-\omega_{Shift})t} = \cos(\omega_{\mathrm{Re}\,f}-\omega_{Shift})t$$

If the first term is removed with a low pass filter, the shift in frequency due to the Doppler effect is obtained:

$$\Delta\omega = \omega_{\mathrm{Re}\,f}-\omega_{Shift}$$

To find the total photocurrent due to the intensity at each position u within the photosensitive area of the detector requires integration of equation (9). It is also necessary to include a factor, η, to represent the differences in the phase at each point, u, of the optical field, due to differences in the optical pathlength traversed by each photon. These phase differences result in variations in the spatial coherence of the field, over the detector, and result in a reduction in the efficiency of the heterodyning process. A further factor, β, is incorporated to account for the quantum efficiency of the photodetector.

$$i_{Total}(t) = i_{\mathrm{Re}\,f}(t) + i_{Scat}(t) + \beta\cdot\eta\cdot(E_{AScat}(t)\cdot E^{*}_{A\mathrm{Re}\,f}(t) + E^{*}_{AScat}(t)\cdot E_{A\mathrm{Re}\,f}(t)) \qquad (10)$$

where:

β Is the quantum efficiency of the photodetector.

$0 \le \eta \le 1$ Represents the efficiency of the heterodyning process (Nilsson et al. 1980)

2.3.5 Determination of blood flux from Doppler photocurrent

In cutaneous tissue the erythrocyte concentration typically accounts for 4.5% of the total tissue volume (Anderson and Parrish 1981). The erythrocytes are non-uniformly distributed in tissue due to vessel containment. Consequently, the contribution made by the homodyne term in (10) is very small (<0.01%). The heterodyne term makes a more significant contribution to the total signal current (~1%). Bonner and Nossal (1990) investigated how the spectral information of the scattered field, encoded in the heterodyne term, was affected by the mean number of photon scattering events and the mean speed of the red blood cells. They found that provided the mean number of scattering events is low, as is the case for skin tissue, the effects of multiple scattering were small. The fluctuations in the width of the optical spectrum of the scattered field were proportional to mean RBC speed and could be used to determine blood flow. As the distribution of RBC velocities is assumed a Gaussian (Nilsson and Tenland 1980), the width of the optical spectrum of the scattered light will vary randomly in time. It is therefore necessary to obtain a mean value, which for a random variable is given by the first moment $<\omega>$ of the power spectrum (O'Flynn 1982). As the power spectrum is obtained over a finite measurement time, the number of scattering events encountered for a given RBC depends on the transit time through the illuminated tissue. Therefore, higher speed RBC will undergo fewer scattering events, contributing less to the power spectrum, and blood flow will be underestimated. To compensate for this low frequency bias, the power spectrum is weighted by the frequency ω, (Obied 1993).

In terms of the weighted power spectrum, of the fluctuating portion of the photocurrent, the first moment can be expressed as:

$$<\omega>=\int_{\omega_L}^{\omega_H}\omega p(\omega)d\omega \qquad (11)$$

In equation (11), the lower limit represents the cut-off frequency of a low pass filter used to discriminate against motion artefact, arising from tissue and probe motion. The upper limit represents the cut-off frequency of a high pass filter used to reject any frequencies above the maximum Doppler shift expected for a given tissue type or particular study. In commercial systems these parameters are typically 20Hz and

12kHz, respectively (Barnett et al. 1990). The maximum flow rates obtained in the microvascular correspond to frequency shifts of a few kHz, and for studies of the microcirculation, the upper cut-off frequency is typically 4kHz (Obeid 1993).

2.3.6 Normalisation of blood flux

Several other factors require consideration before equation (11) can be applied to real measurements. The blood flow parameter $<\omega>$ is dependent on the RBC concentration in the illuminated tissue sample (Fronek 1989). As the precise concentration is normally unknown the actual output obtained is a product of both mean RBC velocity and RBC concentration, and is termed Blood flux. To correctly interpret mean flow values, careful consideration must be given to RBC concentrations. This limits comparison to similar tissue types and may require equal tissue temperatures to allow for variations due to thermoregulatory arteriovenous shunting. For comparable RBC concentrations, blood flux is proportional to blood flow, minus a constant term, $V_{Noise,}$ representing the shot and dark noise sources of the photodetector, determined by calibration. The intensity of the photocurrent can vary between tissue types and individuals, due to variations in pigmentation. To account for these variations the blood flux value is normalised through scaling by the mean photocurrent, $<i_{Ref}>^2$. The RBC flux for the microcirculation is then fully expressed by:

$$V_{RBCFlux} = \frac{\int_{20Hz}^{4kHz} \omega p(\omega) d\omega - V_{Noise}}{< i_{\mathrm{Re}\, f} >^2} \qquad (12)$$

A theoretical study of Doppler scattering in the microcirculation by (Bonner and Nossal 1990), showed that the algorithm of equation (12) provides a linear response to blood flow for low RBC concentrations, such as those found in the microcirculation. This was verified empirically by Nilsson et al. (1980) and Obied (1993).

2.4 Summary

The foot is well adapted to load bearing with an anatomical structure that results in the transmission of the body weight through the calcaneous and metatarsal heads. Consequently the plantar surface of these bones is protected by a cushioning layer of relatively thick (~5mm) skin tissue. The integrity of the tissue in these regions is essential to protect the underlying bone. Changes in plantar pressure distribution, trauma or an impaired vascular supply would normally result in compensatory changes in loading and perfusion of the tissue. However, sensory and autonomic neuropathy in the diabetic foot can result in continued loading and impaired regulation of blood flow, respectively. A frequent consequence is a breakdown of the tissue followed by infection, which may spread within the foot.

Previous studies have demonstrated impaired autoregulation of blood flow in the skin of diabetics evidenced by a reduced or absent hyperaemic response following a short period of occlusion e.g 4 minutes. Although this type of impairment has been demonstrated on the dorsum of the diabetic foot, it has not previously been demonstrated at prevalent sites of neuropathic ulceration. This is because of the difficulty of measuring plantar blood flow, particularly during the normal loading conditions of standing and walking with the foot in-shoe. In order to assess the adequacy of the blood supply to tissue during functional loading it is necessary to simultaneously determine blood flow through and the magnitude of the load upon the tissue. This is complicated by necessary limitations on the maximum size of the sensor, even when located in the insole of a measurement shoe, that ensure normal gait. The specification of the load sensor can be simplified by restricting assessment of blood flow to conditions of zero and full loading which allows a thin film passive sensor such as a Force Sensing Resistor to be employed. The techniques available for determination of plantar blood flow are limited by the requirement of small size and for continuous and non-invasive assessment of rapid changes in blood flow. A review of the available techniques suggests that laser Doppler is the only method that can satisfy all of these criteria.

In vivo calibration of laser Doppler systems is not feasible due to the difficulty of making simultaneous measurements of the same tissue sample using a quantifiable

method such as isotope clearance. This requires an in vitro calibration method based upon a model of the skin microcirculation. Representation of the vascular dynamics of the microvessels is complicated and approximations based upon Poiseuille flow, provide a basis for the design of a calibration flow rig and a basis for specifying the design parameters for the laser Doppler system. Further design parameters can be established from knowledge of the optical properties of the skin. The high coefficient of optical absorption below 600nm and the increase in the depth of penetration with wavelength suggest operation at visible / near-infrared wavelengths. A further factor arises from the variation in response with differences in optical absorption between oxygenated and deoxygenated haemoglobin. This can be overcome by operating at the isobestic wavelength of 805nm where the spectra for the two states of haemoglobin are equal. In practice, the nearest wavelength for which laser diodes are widely available is 780nm.

Specification of the operational laser Doppler wavelength combined with calculations of velocities in the microcirculation provides a basis for estimating frequency shifts due to Doppler scattering by red blood cells. Optical heterodyning between the shifted frequencies and incident frequency result in intensity variations with a spectrum in the audio band which can be detected by a photodiode. The power spectrum of the resultant photocurrent contains equivalent information regarding the distribution of red blood cell velocities. Previous studies have demonstrated that the first moment of the power spectral density of the photocurrent scales linearly with particle velocity and concentration for the typical ranges found in the microcirculation. With suitable scaling and normalisation, a parameter termed 'blood flux' can be calculated which allows relative comparison between subjects. The dependence of this term on both velocity and concentration results in arbitrary units, which prevent a quantifiable measurement.

Chapter 3 Literature Review

3.0 Introduction

Plantar ulceration in the neuropathic diabetic foot and assessment of blood flow in the cutaneous microvasculature are central to this project. In the first half of this literature review, factors implicated in the development of ulceration in the diabetic foot are considered. The second half focuses on the development of the laser Doppler technique as a tool for assessing blood flow in the skin.

3.1 Introduction to the diabetic foot

Evidence linking structural change, microvascular disease, neuropathy and haemorheological changes to ulceration in the neuropathic diabetic foot is reviewed. Two recent theories on the pathogenesis of ulceration in the neuropathic diabetic foot are discussed.

3.2 Structural change and undetected trauma in the neuropathic foot

3.2.1 Plantar pressure changes in the diabetic foot

During the last two decades clinical studies employing pressure transducers have provided substantial evidence to suggest that diabetic plantar ulceration occurs as a result of changes in plantar pressure distribution. The difficulties associated with this type of measurement and the development of the technology have been reviewed in the literature (Lord 1981, Alexander et al. 1990, Cobb and Claremont 1995). A detailed review of clinical findings is given in Lord et al. (1986). These studies have demonstrated that vertical force, anterioposterior shear and mediolateral shear, are important in the development of plantar ulceration, particularly when sensation is reduced by neuropathy. More evidence is available to support the role of vertical forces in the development of plantar ulceration, as shear forces are inherently more difficult to measure. There is however, little agreement on the vertical pressure thresholds that result in ulceration at specific locations under the foot. By considering the findings from several clinical studies, Cavanagh and Ulbrecht (1992) have suggested several factors that may affect the pressure thresholds for plantar tissue breakdown: variation between

different plantar sites; adequacy of the vascular supply, and tissue perfusion; glycosylation of the tissues; the presence of scar tissue; the duration for which pressure is applied rather than peak pressure.

Boulton et al. (1983) first concluded plantar pressure in the diabetic could increase with time. This is supported by the findings of Veves et al. (1992) who measured plantar pressure in three subject types over a thirty-month period. They found average peak plantar pressure increased by 21% in a neuropathic diabetic group, 20% in a non-neuropathic diabetic group and by 2.5% in a non-diabetic control group. Both diabetic groups included subjects with type I and type II diabetes mellitus. In these tests, changes in body mass were ruled out, as a previous independent study Cavanagh et al. (1991) had demonstrated this factor to be unimportant in relation to changes in plantar pressure distribution. The conclusion drawn was that increases in localised pressure levels occur as a result of changes in plantar anatomy. Findings from other studies (Ulbrecht et al. 1988, Grunfeld 1992) lend support to this conclusion. For example, in a random radiographic study of neuropathic diabetic feet (Ulbrecht et al. 1988), 22% of subjects with a history of ulceration were found to have evidence of traumatic fracture in the foot. In many cases this had not been previously diagnosed, due to neuropathy. This incidence was significantly higher than for a nondiabetic control group, a diabetic control group without neuropathy, and a diabetic control group with neuropathy but without history of ulceration. In a study by Grunfeld (1992) of 92 diabetic subjects (20% type I, 80% type II) 68% of patients with a history of ulceration had structural abnormalities and in many cases multiple deformations were observed. These studies suggest that changes in bone structure due to trauma are important in the redistribution of plantar pressure. Trauma induced structural changes in the insensitive neuropathic foot may, therefore, lead to localised pressure points without compensatory changes in gait. Consequently, plantar tissues would be exposed to increases in average peak pressure and/or the duration for which load is applied.

3.2.2 Plantar soft tissue changes in the diabetic foot

Structural changes in musculoskeletal and soft tissue mechanics occur in diabetes mellitus, which can increase plantar pressure and reduce tolerance to biomechanical stress (Brash et al. 1999). The majority of plantar ulcers, accounting for around 80% of

hospitalised cases, occur in superficial soft tissues i.e. the epidermis and dermis (Norton et al. 1975). The remaining 20% occur in subcutaneous tissue and may extend to affect tendon and bone. Neuropathy affecting the muscles of the foot can transfer load bearing from the toes to the metatarsals resulting in the toe claw deformity (Elkeles and Wolfe 1991). Ulbrecht et al. (1988) suggests that the toe claw deformity may result in displacement of the soft tissue that normally protects the metatarsal heads. A reduction in tissue thickness under the metatarsal heads has been demonstrated in diabetics (Young et al. 1995).

Altered structure and function of soft tissue has been demonstrated in diabetes mellitus (Brash et al. 1999). Normally, soft tissues subjected to mechanical forces are able to resist distortion by distributing the forces over the network of skeletal proteins that bind the soft tissues of the skin to deeper tissue and bone (Ryan 1990). Studies (Brownlee et al. 1988, Marova et al. 1995) have shown that several skin proteins are impaired by nonenzymatic glycosylation (NEG). The elasticity of the skin tissues appears to be reduced by NEG and this may affect the ability to redistribute plantar pressure effectively during walking. Delbridge et al. (1985) demonstrated that the keratin in the stratum corneum of the foot is glycosylated in comparison to the skin of the non-diabetic. Both collagen and keratin are known to become stiffer when glycosylated (Brownlee et al. 1984, Delbridge and Ctercteko 1985) and this is probably detrimental to the mechanical properties of the skin. Metabolic changes may also affect the healing rate of ulceration. Glycosylated tissues reduce the activity of leucocytes and macrophages producing insufficient fibroblasts to synthesise collagen and other proteins (Elkeles and Wolfe 1991). When healing eventually occurs the reduced compliance of scar tissue may be a factor in the high incidence of recurrent ulcers.

Plantar soft tissue damage is also linked to the increased risk of keratosis associated with neuropathy (Sage 1987) and evidenced by the build up of callus frequently observed in the diabetic foot. A study of 92 diabetic subjects (20% type I, 80% type II) by Grunfeld (1992) found evidence of callus formation in 51% of patients with a history of ulceration. The presence of callus often results in the formation of a fluid filled cavity, which if infected may result in rapid tissue necrosis (Hill 1987). The risk of infection is increased by autonomic neuropathy, which may prevent the foot from

perspiring (Brand 1990); consequently, the skin becomes dry and fissured, presenting ideal conditions for infection (Levin 1988).

3.3 The role of microvascular disease in the diabetic foot

Peripheral vascular disease affecting the blood supply to the foot may occur at any level within the hierarchy of vessels supplying the pedal tissues (Levin and O'Neal 1988). There is an increased incidence of small vessel disease in the diabetic, which often results in a more distal impairment of the blood supply than in the non-diabetic (Vermillon 1986). As the rate of progression of atherosclerosis varies, throughout the peripheral vascular tree, both macrovascular and microvascular disease can exist at different levels of development (Levin 1988). Consequently, an adequate dorsalis pedis or posterior tibial pulse is a poor indicator of the adequacy of the vessels within the foot (Stevens et al. 1993). The prevalence of microvascular disease differs between type I and type II diabetics and it has been suggested that the pathogenesis of microvascular disease in the two forms is different (Jaap and Tooke 1995). However, in both type I and type II diabetes mellitus the complications that occur as a result of microvascular disease are similar, there is however a particularly high prevalence of foot ulceration in type II (Jaap and Tooke 1995).

A thickened capillary basement membrane (microangiopathy) is indicative of diabetic microvascular disease, becoming more pronounced with age and the duration of diabetes and is common in subjects with a history of ulceration (Grunfeld 1992). The mechanisms involved in this change are not well understood, although several contributory factors have been identified: endothelial cell damage (Hilsted and Christensen 1992), increased platelet adhesions (Manduteanu et al. 1992), migration of atypical cells to the site of injury and accumulation of cholesterol and fats (Sargent 1988). Impaired microvasculature regulatory mechanisms are also implicated in the development of microangiopathy (Flynn and Tooke 1995). The high incidence of microangiopathy in diabetic subjects is thought to be an important factor in some of the complications observed in the diabetic foot. The permeability of the membrane is increased and it has been suggested that this may account for some of the oedema commonly observed (Levin and O'Neal 1988). Flynn and Tooke (1995) agree with this suggestion, for the earlier stages of diabetes, however they point out that oedema is rare

in the advanced neuropathic foot. Furthermore, they argue that oedema is due to a reduction in fluid filtration across the capillary membrane that deteriorates with the duration of diabetes.

3.4 Neuropathy and the regulation of blood flow in the diabetic foot

In addition to microvascular disease, several studies have identified neuropathy as important in the impairment of blood flow in the diabetic foot (Rayman et al. 1986b, Flynn et al. 1988). In these studies, type I diabetic subjects with neuropathy and without clinically detectable peripheral vascular disease exhibit increased blood flow in the foot. Flynn et al. (1988) also demonstrated increased blood flow in some subjects apparently free of neuropathy, giving support to previous suggestions that peripheral denervation may occur before neuropathy is clinically detectable (Watkins and Edmonds 1983). The importance of neuropathy in the pathogenesis of diabetic plantar ulceration is emphasised by the findings of the study by Grunfeld (1992) and other studies, which provide estimates indicating: 60-70% diabetic foot ulcers are purely neuropathic; 15-20% are purely vascular lesions; 15-20% are mixed lesions. However, the same study indicated a higher incidence of peripheral vascular disease and neuropathy in subjects with a history of ulceration. Although the rate of progression of each of these factors may vary with individuals Flynn and Tooke (1995) have argued that both vascular and neuropathic disease are interdependent. They suggest that a detrimental cycle may persist in which changes in the microcirculation affect the regulatory mechanisms controlling blood flow, leading to further changes in the microcirculation. It is, therefore, appropriate to consider the affect of neuropathy on regulation of blood flow, in the foot.

Neuropathy affects both peripheral and autonomic nerves, which regulate the non-nutritive, thermoregulatory flow of the arteriovenous anastomoses and the nutritional flow of the cutaneous capillaries, respectively. Both neuropathies are implicated in the development of plantar ulceration (Flynn and Tooke 1995). In a study, by Flynn et al. (1988) of 39 neuropathic, type I, diabetic subjects free of peripheral vascular disease, nutritive capillary blood flow under the toe pulp was assessed. In comparison to control subjects, it was found that diabetics with peripheral and autonomic neuropathy exhibited substantially increased blood flow. A further link between vascular and

neurogenic factors is suggested by changes in vasomotion observed in diabetic subjects with neuropathy (Flynn and Tooke 1995). These changes can result from reduced vessel elasticity, microangiopathy, or neuropathy affecting the vasomotor nerves, all of which would have a significant effect on regulation of local tissue perfusion and fluid exchange. This may explain the non-uniformity of tissue perfusion observed in diabetic subjects (Flynn and Tooke 1995) and commonly presented by an impaired hyperaemic response (Vigilance et al. 1997). This impairment has been investigated by Rayman et al. (1986b), in a study of 23 type I diabetic subjects with no evidence of peripheral vascular disease, who were exposed to minor thermal injury on the skin of the foot. The response of the microvasculature was assessed using laser Doppler flowmetry and compared to that from a control group of 21 healthy subjects. The response to thermal injury was significantly reduced in the diabetic group and was independent of skin capillary density and diabetic control. It was concluded that an impaired hyperaemic response is significant in the development of ulceration following minor trauma.

3.5 Haemorheological changes in diabetes mellitus

Haemorheological changes in the blood supply are a widely observed complication of diabetes mellitus (Levin 1988). It is unclear whether these changes are a consequence of vascular disease, or result in accelerated microvascular disease e.g. microangiopathy (Sargent 1988). Several factors have been identified as being contributory to increased plasma viscosity and hence reducing blood flow. In pre-capillary vessels, increases in red blood cell concentration occur due to high levels of blood clotting factors such as fibrinogen (Elkhawand et al. 1993, Giansanti et al. 1996). This finding is important because changes in blood viscosity are known to result in a substantial reduction in blood flow (Muller 1981), due to the formation of roleux. Within the capillaries, blood flow is largely determined by deformability of red blood cells, which change shape to reduce their effective diameter from 7.4μm to 4-5μm to match the capillary diameter (Chien 1967). The ability of the red blood cell to deform is controlled by the cell membrane. Changes in: pH (Goodman and Shiffer 1983), red blood cell adenosine triphosphate content (Marchesi 1983), concentrations of metabolic end products (Shohet and Lux 1984) and nonenzymatic glycosylation of the erythrocyte membrane (Watala 1992), all affect the ability of the red blood cell to deform.

3.6 The pathogenesis of ulceration in the neuropathic diabetic foot

It is widely agreed in the literature that microvascular disease and neuropathy are the underlying complications that pre-dispose the diabetic foot to ulceration and slow healing (Tooke and Brash 1996, Shaw and Boulton 1997). However, ulceration is always preceded by some form of trauma, such as minor injury to the surface of the foot. For the particular case of the plantar ulcer, there is considerable evidence that abnormal pressure is the initiating factor. However, the primary reason for ulceration is that the metabolic demands of tissue are not satisfied. The most recent theories developed to explain the link between these complications and ulceration are the 'capillary steal' theory (Leslie et al. 1986) and the haemodynamic hypothesis (Jaap and Tooke 1994).

3.6.1 The capillary steal theory

In the 'capillary steal' theory, it is postulated that blood bypasses the nutritive capillaries and instead flows almost entirely through the arteriovenous anastomoses, due to neuropathic impairment of regulatory mechanisms (Uccioli et al. 1992). Furthermore, it has been suggested that this might occur as a normal thermoregulatory response to the increased temperature frequently observed in the neuropathic foot (Leslie et al. 1986). However, these ideas are in contradiction to findings from other studies (Stevens et al. 1993, Netten et al. 1996) that have demonstrated normal or elevated perfusion in nutritional capillaries.

3.6.2 The haemodynamic hypothesis

In contrast, the haemodynamic hypothesis (Jaap and Tooke 1994) suggests that anatomical and functional changes within vessels are important. Chittenden and Shami (1991) identify these changes as, vessel wall thickening, proliferation of vessels, capillary basement membrane thickening, changes in vessel permeability and, reduced elasticity of the vessel wall. Recent studies support this hypothesis; for example Rayman et al. (1995) assessed microvascular structure using electron microscopy and identified structural abnormalities in superficial capillaries. Comparison with pre-biopsy, in vivo measurement of blood flow, using laser Doppler flowmetry confirmed that blood flow was reduced during reactive hyperaemia in the tissue.

Netten et al. (1996) used laser Doppler flowmetry to investigate if increased flow through thermoregulatory vessels resulted in decreased or increased flow in nutritional capillaries. They concluded that nutritional capillaries were overperfused, a finding in contradiction to the 'capillary steal' hypothesis. Although changes in blood rheology could explain changes in blood flow and perfusion, it is thought that haemodynamic abnormalities precede changes in microvascular rheology (Japp and Tooke 1994).

3.6.3 Importance of changes in the capillary wall

Evidence for increased nutritive flow does not invalidate the idea that the metabolic demands of plantar tissue are unsatisfied because changes in the capillary wall membrane could impair the diffusion of nutrients into tissue. The high incidence of microangiopathy, the frequently observed abnormal perfusion and an impaired hyperaemic response are all indicative of an impaired capillary membrane (Chittenden and Shami 1991). An important factor implicated in this impairment is the increased adherence of diabetic platelets to endothelial cells (Manduteanu et al. 1992). Furthermore, with an increased blood flow rate, the diffusion of oxygen could be reduced, due to the flow dependency of oxygen exchange (Rayman et al. 1986a). However, in a recent study, of type I diabetic subjects, with minimal evidence of microangiopathy, the mean capillary filtration coefficient was significantly increased (Jaap et al. 1993). Insulin has been demonstrated to have acute effects on capillary permeability, the exact mechanism is unknown, although thought to be linked to changes in endothelial cell morphology (Hilsted and Christensen 1992). An increased capillary filtration coefficient suggests, that the metabolic demands of supplied tissue can be met and, there is a possibly increased risk of oedema (Rayman et al. 1994).

Currently, endothelial dysfunction is emerging as one of the most important areas of research in diabetic microvascular disease (Pham et al. 1998). With improved understanding in this area, a full explanation of the pathogenesis of ulceration in the neuropathic diabetic foot may become possible.

3.7 Introduction (laser Doppler)

In section 3.8 common techniques for assessing the microvasculature are identified and arguments given for the use of laser Doppler flowmetry in the present study. In section 3.9, the development of laser Doppler flowmetry is summarised. Sections 3.10 to 3.12 review the important issues of calibration, sampling depth and the affects of external loading of the skin.

3.8 Justification for use of laser Doppler in the present study

Various methods of studying cutaneous blood flow were considered for the present study. Invasive techniques, for example clearance of isotopes and radioactive microspheres were considered inappropriate, as they are not suitable for continuous monitoring. Non-invasive microscopy techniques tend to be limited to directly observable blood vessels and are not well suited to miniaturisation. The very slow response time of the thermal clearance method was considered unsuitable for assessment of rapid changes in blood flow that occur during post occlusive reactive hyperaemia. All of these methods are well documented in the literature and are not considered further.

The measurement of partial pressures of oxygen ($tcPO_2$) as been successfully applied to assessing microvasculature status of the dorsum of the diabetic foot (Romanelli and Falanga 1999) and the rate of healing of ulceration is known to be correlated with local $tcPO_2$ (Japp and Tooke 1994, Mani and White 1988). An important advantage of this method compared to laser Doppler flowmetry is that results are quantifiable. This technique was considered inappropriate for the present study because although suitable for post occlusive reactive hyperaemia study, typical response times of 10s to 50s (Fronek 1989) were considered too slow to track the rapid changes in tissue perfusion, during walking.

In the present study a prototype reflective mode Photoplethysmograph (PPG), based on a modified probe from a pulse oximeter (Nellcor type D-20) was developed and evaluated by the author. The construction of this type of sensor is relatively simple compared to the laser Doppler technique.

Although the techniques are not directly comparable, the Photoplethysmograph signal had, in general, a much lower sensitivity to intensity variations in plantar skin than the laser Doppler signal. Although this problem may have been overcome by developing a laser based photoplethysmograph, the PPG signal has greater dependence on the optical properties of the probe and is difficult to interpret in comparison to the laser Doppler flux signal (Lindberg et al. 1991). Furthermore, laser Doppler flowmetry has been used successfully in numerous studies of blood flow in the skin of the diabetic.

3.9 Evolution of laser Doppler systems for blood flow measurement

3.9.1 Early development of laser Doppler flowmetry

The application of laser Doppler techniques to the measurement of blood flow in the cutaneous microvasculature was first proposed by Stern (1975). By illuminating the skin with a Helium-Neon laser and monitoring the back-scattered signal, it was possible to demonstrate differences in the frequency spectrum at rest and during occlusion of the brachial artery. This original system was unsuitable for clinical study due to incorporation of fixed optics and the use of a photomultiplier tube as the detector. Subsequently a portable, laser Doppler system suitable for clinical application was developed by Holloway and Watkins (1977) using optical fibres and an integrated photodetector. Evaluation of this and another similar system (Nilsson and Tenland 1980) revealed two important problems, excessive laser noise and poor correlation with existing techniques. The use of a He-Ne laser resulted in interference of multiple output modes producing beat frequencies in the same band as the blood flow signal. A comparative study with the ^{133}Xe-clearance technique demonstrated the difficulty of obtaining measurements at the same site, furthermore, the laser Doppler response also depended on the red blood cell concentration. These issues were addressed by Nilsson et al. (1980) who introduced a dual detection system capable of rejecting laser and other sources of common mode noise via a differential amplifier. To evaluate this technique in vitro models of fluid flow in the skin were developed to allow independent calibration. These developments motivated further refinement and clinical application of the technique.

3.9.2 Evolution of laser Doppler signal processing algorithms

The signal processing algorithms used in these early systems were based on empirical studies of different in vitro models. Subsequently, the results obtained for identical measurement conditions were found to differ from one system to another. To overcome this problem a theoretical model of light scattering in tissue was developed by Bonner and Nossal (1981). This work resulted in an algorithm that produced a single output parameter 'blood flux' that scaled linearly with red blood cell velocity and concentration over a limited range. The blood flux value was determined by calculation of the first moment of the power spectral density of the Doppler signal. The validity of this approach depends on the contribution made by each back-scattered photon to the power spectral density, which is dependent on the number of red blood cell scattering events and the type of mixing at the photodetector surface. For red blood cell tissue concentrations of less than 0.2%, the model predicts single scattering will dominate and in this situation wave mixing at the photodetector surface is primarily heterodyne in nature (Nilsson et al. 1980). At higher concentrations, the probability of multiple scattering increases and homodyne mixing occurs at the detector surface resulting in a non-linear flux response. Nilsson (1984) extended the linear operating range of the Bonner and Nossal algorithm by correcting the transfer function to match the idealised response. It was then possible to demonstrate a linear response for high flow rates and for red blood cell concentrations to 0.6% of tissue volume. This approach is used in the Perimed laser Doppler flowmeter, which has found widespread clinical application.

3.9.3 The problem of movement artefact

An important limitation of the use of laser Doppler flowmetry in the clinical environment is the need for static measuring conditions to reduce movement artefact. This problem arises from intensity fluctuations due to optical fibre or tissue movement that results in the addition of considerable noise to the blood related Doppler spectrum. One approach to overcoming this problem is to eliminate the fibre optic delivery and detection optics and use a direct contact probe. In order to implement such a system the relatively large Helium-Neon laser has to be replaced by a laser diode source. This was achieved by De Mul et al. (1984) who reported a compact integrated probe containing a visible laser diode and two photodiodes. This solution has not been widely adopted in commercial systems, primarily because the use of fibre optics allows the use of

interchangeable probe heads that are optimised for particular sites on the body. Therefore, considerable effort has been applied to overcoming the problem of fibre movement artefact by other means. For example, Gush and King (1987) investigated how optical fibre size, probe geometry and fibre cladding could be varied to reduce artefact. They suggest that the probe geometry should be designed to prevent overlap of the optical fields of the source and detection fibres, at the skin surface. The use of mechanical dampening of the fibres by application of a suitable cladding material is also recommended by the authors. Small diameter optical fibres support less transmission modes, which has been shown to reduce motion artefact Newson et al. (1986). However, precise optical alignment is necessary to ensure adequate coupling into these small fibres. Furthermore, the smaller tissue sampling volume decreases the probability of a scattering event and thus the signal to noise ratio is reduced. It is possible to identify fibre movement artefact within the signal processing subsystem and this is used in the Perimed PF2 commercial system to control the output. In this author's experience, artefact elimination using a differential amplifier is not possible due to the lack of a common noise component in each fibre. Simple filtering is not a viable solution because the artefact noise and blood flow signals occupy the same bandwidth.

3.9.4 Current status

With the fundamental design issues of laser Doppler flowmetry resolved by the late eighties a number of second generation commercial systems were available, for example, Perimed's Periflux PF2b (Nilsson 1990) and TSI's Laserflo system (Borgos 1990). Several operational problems remained to be solved, which prompted continued research into development of the technique in addition to applied clinical studies. Some of these issues are considered in the following sections.

A relatively recent and important advancement of laser Doppler flowmetry is the development of Laser Doppler Imaging (Mani 1999). This technique allows non-contact imaging of blood flow over large areas of skin, through use of raster scanned source and detector optics.

3.10 Calibration methods

There is no 'gold standard' for quantifying continuous blood flow in tissue (Oberg 1990), therefore calibration of any measurement technique for this application is normally achieved by absolute or comparative methods. For laser Doppler flowmetry, absolute calibration in vivo cannot be achieved unless a section of skin can be isolated, for which total blood flow can be determined. Comparative calibration, with microscopy and clearance methods requires simultaneous measurement on the same tissue sample, which is difficult to achieve. Often, for the laser Doppler technique, the only viable solution is the use of an in vitro calibration phantom. This approach, however, raises a number of questions regarding construction and accuracy of the model.

The basic requirements for a calibration model are: an interface that mimics the optical scattering of the epidermis; a scattering media to represent red blood cells; and a method of varying the velocity of the scattering particles.

Static scattering ensures that the angles of incidence of the photons entering the vascular part of the model have random directions as in real tissue. Furthermore, some of the incident photons are scattered back directly to the photodetectors providing the unshifted reference beam. A block of polyacetal (Bogett et al. 1986) is typically used to meet this requirement.

3.10.1 Scattering media for calibration

The scattering media used to represent red blood cells can be whole blood, treated to prevent coagulation. However, this can be difficult to obtain, requires special safety precautions and remains prone to aggregation. Alternatives include whole milk and particles in suspension; for example, graded latex microspheres are routinely used by manufacturers including Perimed and Moor Instruments. The scattering particles should have dimensions close to those of red blood cells to ensure that the scattering angle is highly directional (Bonner and Nossal 1981). If this condition is not met, the proportion of incident light scattered from moving particles can be much greater than for the in vivo case. An important issue regarding scattering media in suspension is the difficulty of maintaining a stable and homogeneous solution over a long period. One approach to

overcoming this problem is the use of particles such as aluminium oxide (Oberg 1990) dispersed evenly within a moulded acrylic block. In any of these methods, it is usual to predetermine the concentration of scattering particles at the time of preparation of the medium.

3.10.2 Methods of obtaining particle velocities for calibration

To simulate the flow of blood in vessels, one or more plastic tubes are normally used, through which the scattering medium is pumped (Barnett et al. 1990, Liebert et al. 1998). The flow rate is normally controlled using a syringe pump or via a gravity fed valve arrangement. As Borgos (1990) points out, the use of tubes with diameters greater than 20μm is likely to result in an overestimate of blood flux due to the increased probability of multiple scattering. Conversely, Obied (1993) suggests that the Doppler signal obtained from large tubes is predominately due to scattering from slower particles close to the tube wall, so that multiple scattering is not a problem in practice. If the scattering system is implemented as a solid block with embedded particles, a rotational or linear actuator is required to provide motion. For example, Mito (1992) used a simple rotating turntable to obtain a Doppler signal, whereas Cai et al. (1996) employed a complex linear drive table. A major benefit of using a rotational scattering block is the ease of reproducibility and control of particle velocity. This approach, therefore, seems to be the most suitable for realising a standardised method of calibrating laser Doppler systems.

3.11 Determination of sampling depth

3.11.1 Operating wavelength

From a clinical perspective, determination of sampling depth is an important factor in interpreting laser Doppler blood flux. A flux value that reflects conditions in the superficial vessels alone may be useful in estimating the extent of microvascular disease. Selective sampling is not easily attainable because the standard available wavelengths of 632.8nm for He-Ne and 780nm for near infrared are capable of penetrating deep into the dermal and possibly into the sub-dermal layers (Anderson and Parish 1981). Obied et al. (1988), investigated the use of a green He-Ne laser with a wavelength of 543nm and obtained results that were consistent with a sampling depth restricted to the capillary beds of the skin. The problem with adopting a green He-Ne laser for general use is the lower power available, and the increased absorption by skin pigments, which result in a poor signal to noise ratio. Furthermore, laser diodes operating at this wavelength and with sufficient power are not widely available. In a study by Gush and King (1991), a photomultiplier tube was used to amplify the Doppler signal from a low power Green He-Ne laser. The authors then implemented a signal-processing algorithm based on the intensity autocorrelation technique, which was able to resolve between blood flow in capillaries and larger microvascular vessels.

3.11.2 Geometry of delivery and sensing optics

A second factor that affects sampling depth is the geometry of the optics used to guide light to and from tissue. Mito (1992) compared three commercial systems with differing optical arrangements and found large differences in the minimum and maximum sampling depth of each system. In this study, a wedge section of tissue with depth ranging from zero to 6mm was perfused from a reservoir of heparinised blood. The author suggests that depth of penetration increases with distance between the emitting and detecting optics and may depend on numerical aperture. In a study by Jakobsson and Nilsson (1993), a Monte Carlo simulation was developed to predict photon-sampling depth. The results of this study also indicated that sampling depth was increased if the separation, in their case of optical fibres, was increased. The authors point out that a greater source to detector distance also increases the probability of

multiple scattering which tends to reduce the linearity of the response. A more comprehensive investigation of this problem has been achieved by the recent development of a multiple depth flow model and multi-channel probe (Liebert et al. 1998). In this system, detection fibres were located at multiples of 200μm from an emitting fibre. The more distant fibres were sensitive to deeper flows in the model, and in vivo the maximum hyperaemic response and the biological zero were dependent on fibre spacing.

3.12 Effects of external pressure on response

Typical laser Doppler probes, have small contact areas, which combined with the force required to maintain the probe in position can result in pressures that affect skin blood flow (Obied 1990). For general measurements, this undesirable effect can be reduced by increasing probe area and ensuring the applied force is small. However, in several clinical applications it is useful to be able to assess the affects of applied pressure on blood flow. Castronuovo et al. (1987) used laser Doppler to compare the skin perfusion pressures (blood flux) in the lower limbs of non-diabetic subjects and diabetics with complications including rest pain, ulceration and amputation wounds. In this study, blood flow was controlled by applying a blood pressure cuff around the limb at the measurement site and inflating to 200mmHg for two minutes. Using this approach, the author reported differences in skin perfusion pressures between ischaemic and normal limbs, which were particularly significant at the dorsal and plantar toe. The results of this study should be treated with some caution, however, because of the difficulty of specifying a reliable flux baseline that equates to the biological zero flow condition. Sacks et al. (1988) recorded flux at 30 percent above the instrument baseline, for an applied cuff pressure of 300mmHg. The same problem was also observed by Kabagambe et al. (1994) who concluded that laser Doppler measurement is not applicable to assessing skin blood flow during application of external pressure. More recently Zhong et al. (1998) performed a mathematical analysis of this problem and suggested a method of correction that was shown to provide reliable flux values at low flow rates.

3.13 Summary

Previous studies have demonstrated average increases in plantar pressure of around 20% in diabetic subjects independent of diabetic complications. Although the mechanisms for these increases are not well established, the consequences are most important in the insensitive neuropathic foot because of the risk of ulceration resulting from failure to redistribute the load. The protective tissues under points of plantar loading normally adapt to withstand increases in pressure, however in the diabetic structural changes can occur in soft tissues that are detrimental to this process. Furthermore, changes can occur in the microcirculation of diabetics, which further reduces tolerance of these tissues to pressure. These changes can be physical including microangiopathy or functional for example impaired regulation due to autonomic neuropathy. Evidence for both physical and functional changes in the microcirculation of the diabetic are well documented in the literature. A further factor, generally considered a consequence of these changes, are haemorheological abnormalities resulting in increased blood viscosity and reduced blood cell deformability, which compound the problem. Clinical evidence has led to the formation of theories to explain the development of ulceration in the neuropathic foot. The most successful of these is the haemodynamic hypothesis, which identifies physical changes in the microcirculation as the basis for a failure to satisfy the metabolic demands of tissue. This in turn affects nutrition of the autonomic nerves and consequently leads to impaired regulation of the microcirculation.

Laser Doppler flowmetry has been used previously to demonstrate changes in the microcirculation of the diabetic. Techniques have been developed to reduce the significance of the inherently poor signal to noise ratio and problem of movement artefact. Various in vitro calibration techniques have been proposed to validate the linearity of the system response in relation to changes in velocity and concentration of scattering particles. The simplest approach involves comparison with absolute measurement of the scattering medium collected over time for different concentrations of scattering particles. For in-vivo studies, interpretation of the response is complicated by the difficulty of ascertaining the depth of sampling in tissue and of specifying a biological zero level.

Chapter 4 Development of a plantar monitoring system

4.0 Introduction

The development of a plantar monitoring system for determining plantar blood flow is described. The system comprises a laser Doppler and load sensor, a measurement shoe, instrumentation and software. Section 4.1 discusses the initial work used to establish the design constraints. Development of the sensor and instrumentation is described in sections 4.2 and 4.3. The approach adopted to realise a complete measurement system, including system software, is detailed in sections 4.4 and 4.5. In section 4.6, the techniques used to calibrate the system are described.

4.1 Pre-development work

4.1.1 Design of initial prototype system

Two commercial systems (Moor Instruments model MBF3 and Perimed model PF3) were assessed for the intended application and were found unsuitable because:

They were not sufficiently portable to allow measurement during walking.
They were sensitive to motion artefact, requiring the subject to be static.
The probe heads were not suitable for in-shoe measurement.
The cost was prohibitive within available budget constraints.

To evaluate the feasibility of producing a custom sensor an evaluation rig was developed, figure 6. This comprised a simple probe head, constructed by arranging eight plastic optical fibres concentric about a central fibre. To contain the fibres in the correct geometric orientation an outer sleeve of silicone rubber tubing of length 30mm and internal diameter of 2.8mm was used. The tubing was expanded to allowing insertion of the fibres. The fibres extended 5mm from the end of the tube and this section was inserted into a 3mm hole in a piece of 3mm thick polycarbonate sheet of dimensions 25mm^2. The fibres were bonded into position using epoxy adhesive. After curing, the exposed section of the fibres was made flush with the surface of the block using an abrasive, and polished using a mandril. The instrumentation end of the fibres were terminated at a length of 500mm and polished. Eight 1mm-diameter holes were drilled through a block of 6mm thick polycarbonate sheet and a circular recess of depth

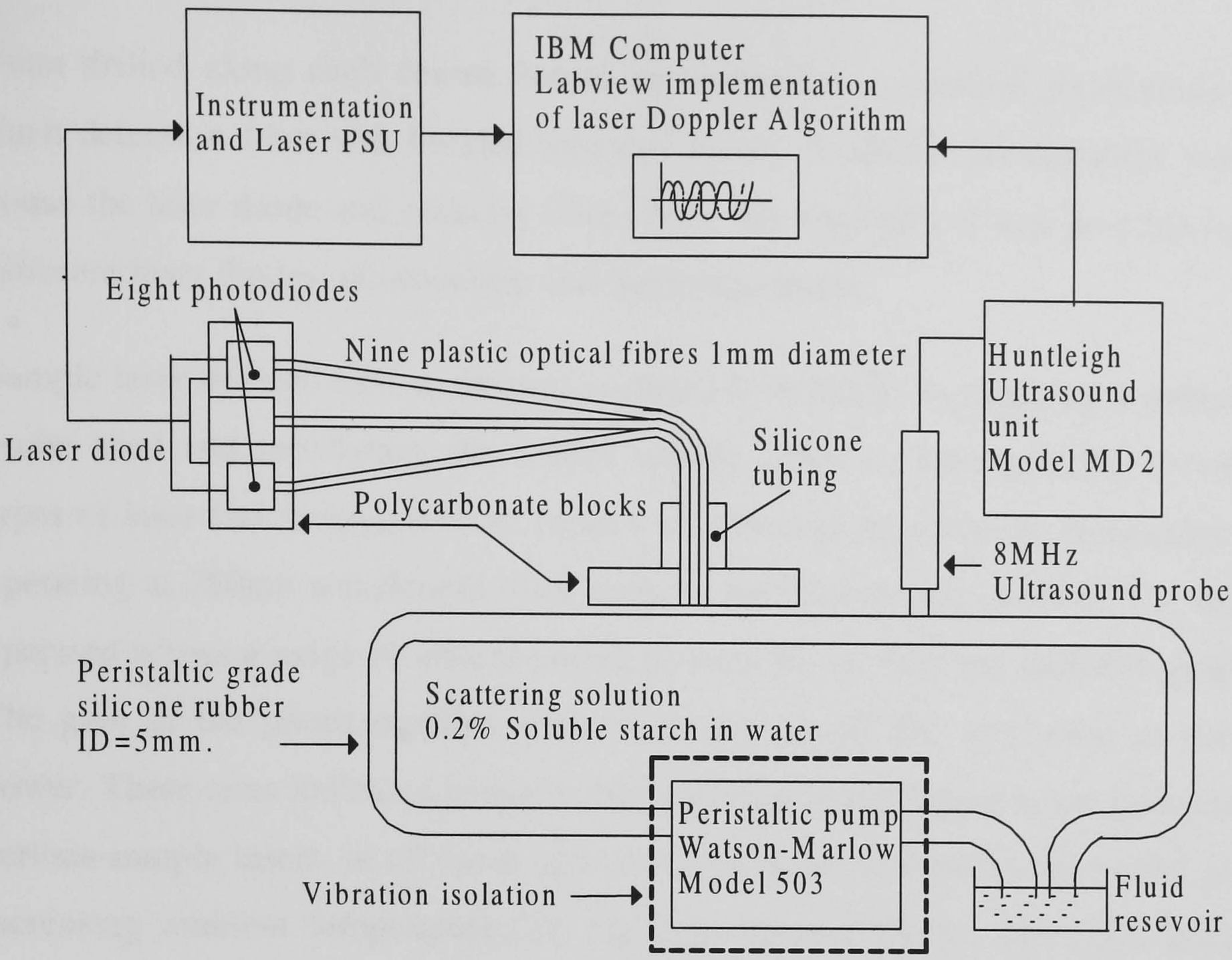

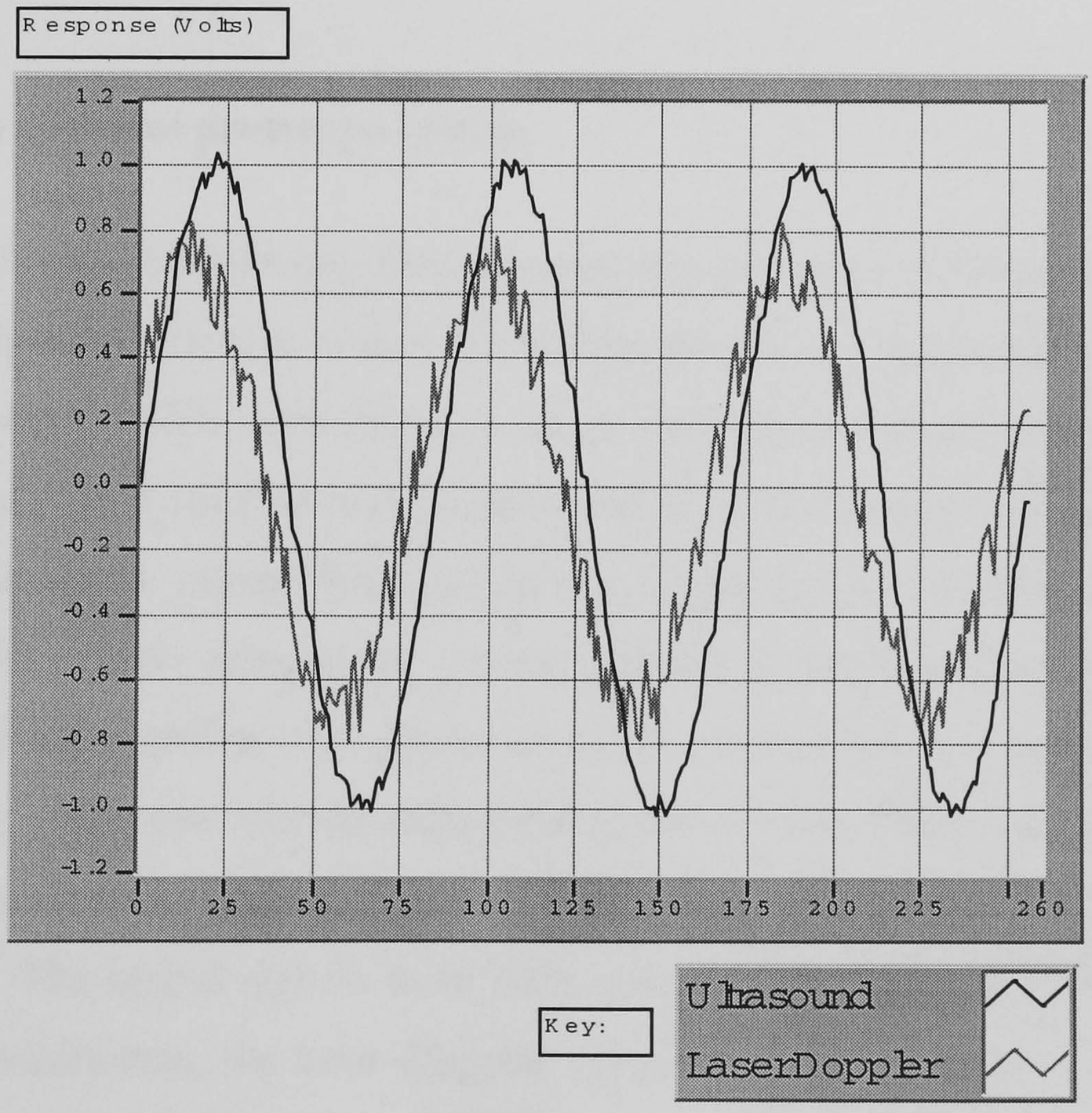

Figure 6 Block diagram of early evaluation system and comparison of response with Doppler ultrasound. The pump rate is 100 RPM giving an output waveform with a frequency of ~80us corresponding to a Doppler shift of ~12.5KHz. The laser Doppler signal is shown before signal processing.

3mm drilled along each centre line to accommodate a standard photodiode package. Each detection fibre was bonded into this block. A similar arrangement was used to house the laser diode and emitting fibre. With this approach, it was possible to evaluate different laser diodes, photodiodes and instrumentation.

Sample laser devices were evaluated in closed loop mode, by applying a reflector to the probe head and monitoring the output voltage from a photoamplifier. Details of the types of laser and measured noise figures are given in Appendix F. Near-infrared lasers operating at 780nm wavelength were used, as for commercial systems. The lasers were operated across a range of optical output powers and at different ambient temperatures. The gain of the photoamplifier was adjusted to avoid DC saturation at each output power. These tests indicated considerable variation in the output noise generated by the various sample lasers, in all cases optical output noise increased with output power and increasing ambient temperature. Of the nine devices tested, the three lowest noise devices were retained for further evaluation.

4.1.2 Evaluation of initial prototype system

To test the effectiveness of detecting flow, a scattering medium was made by dissolving soluble starch (Sigma-Aldrich) in water. Pre-boiling the water was essential to drive out dissolved air bubbles, which were found to cause intensity variations that affected the output signal. The cooled solution was pumped around a closed loop of silicone rubber tubing, using a peristaltic pump (Watson-Marlow, model 503). A venting system was introduced and the system pumped for several minutes to force out residual air. The output from the photoamplifier was connected to an oscilloscope and audio amplifier. The laser Doppler probe was located orthogonal to the silicone tubing and the probe of a Doppler ultrasound unit (Huntleigh, model MD2) was placed onto the tubing at an adjacent position. The output signals from both systems were compared. Both outputs were sinusoidal waveforms, the laser Doppler signal had a phase lead of 30 degrees compared to the ultrasound Doppler signal. This was the first real indication that the system was responding to flow due to Doppler scattering, as opposed to changes in optical intensity. One of the laser devices failed to provide a suitable response at this stage and this was attributed to the multiple mode output characteristics. The remaining

two devices were single longitudinal mode output types and it was concluded that this was an essential characteristic for this application.

It was noted that the whole probe assembly had to be isolated from vibration. The cause of this sensitivity was identified as the optical coupling fibres. Various methods proposed by Gush (1987) for reducing fibre sensitivity to movement artefact were evaluated. Although these techniques are useful for static measurements, the same techniques were ineffective for the levels of tissue movement that occurred during walking. Elimination of movement artefact noise by electronic means was only possible if the optical fibres were matched and this required several hours to achieve. The use of single-mode glass fibres was discarded as a possible solution, due to the difficulty of construction. Furthermore, the risk of exposure of tissue to glass fibre under sensor loading was unacceptable. It was concluded that fibre optic connection between the sensing site and detection system was not feasible. This imposed considerable constraints on the design of the system specifically it required that the laser diode and detection system be situated adjacent to the foot to allow direct optical coupling between the laser, tissue and detector.

The evaluation rig was modified to eliminate free moving optical fibres and an initial in vivo evaluation made by applying the probe to the underside tip of the index finger. To comply with safety standards the optical output power at the tip of the emitting fibre was adjusted to 1mW, using an optical power meter (Melles Griot, model Pocket power meter). The presence of a Doppler signal could be easily established if monitored with an audio amplifier capacitively coupled to the laser Doppler output signal. The same signal viewed on an oscilloscope exhibited no discernible features. Once a reliable audio signal had been obtained, a spectrum analyser (Hewlett Packard, model E4411B) was used to assess the characteristics of the signal. It was evident that the signal to noise ratio of the system was reduced compared to that observed in vitro. In the flow rig a minimum of two detection fibres, equivalent to a detection area of $2mm^2$, were required for an acceptable signal to noise ratio. However, in vivo four fibres were required to obtain a comparable signal to noise ratio. This was attributed to a reduction in power due to scattering, attenuation in the skin and the non-homogenous distribution of the vessels within the sampled volume. This last factor is thought to result from a lower scattering rate per unit volume, whereas, in the flow rig the distribution of scatterers is

uniform. It was possible to demonstrate the detection of blood flow in cutaneous tissue under the first metatarsal head using the same approach.

4.1.3 Determination of the maximum dimensions of the sensor

To establish an acceptable upper limit for sensor area, tests were carried out using acrylic models of the sensor housing. These were affixed in-shoe under the first metatarsal head using double-sided surgical tape. Ten adult male subjects were asked to comment subjectively on the effect of the insert after several minutes of walking. It was concluded that the maximum lateral dimension allowing normal flexing of the foot was 30mm (range 10-50mm), for both circular and square inserts. The acceptable height range of the insert was 2-3mm, with lower values fracturing and higher values uncomfortable.

Using the same study group, the size of the first metatarsal head and movement of the bone during walking was evaluated. The bone was identified by palpation (Nevill et al. 1995) and the centre and circumference marked. The mean diameter was estimated as 18mm (range 14-22mm). A piece of white gloss card was cut to fit the subjects shoe. The metatarsal circumference line and centre marks were inked and the subject carefully placed their foot in-shoe and walked a number of steps. A maxim lateral deviation of 5mm occurred, which was biased toward the rear of the foot. This value is in reasonable agreement with a published value for metatarsal head movement of 7mm (Maalej et al. 1989).

Based on these findings, a maximum sensor dimension of 30mm was considered the optimum value to maintain normal gait and support the metatarsal head during maximal deviation. This was important to prevent shear between the edge of the sensor and tissue under the metatarsal head.

4.1.4 Selection of pressure sensor

Two proprietary pressure sensors were identified as suitable for measuring plantar pressure in-shoe and for compatibility with the sensor housing. The Entran EFL1000-26 is a linear, silicon based bridge sensor with a measurement accuracy of 1%. The device was considered too costly for the present study (£320) and produces erroneous readings

for off axis loads. The height of 3mm was also a limiting factor. By contrast, the Force-Sensing Resistor (Steadlands International, type FSR174NS) is a thin film logarithmic device with accuracy of 10%. The benefits are low cost (<£10) and a thickness of 0.7mm.

The Force Sensing Resistor (FSR) was found to exhibit thermal dependence and hysterisis. Instrumentation was developed to compensate for these deficiencies and to translate the logarithmic characteristic to a linear function. Despite these improvements, the device proved unsuitable due to poor measurement repeatability. For this reason, and FSR device was used only as an indicator of zero and full load.

4.2 Sensor development

An attempt was made to construct a thin sensor that could be located within normal footwear. This was complicated by the problem of accommodating a laser diode within the required thickness of 3mm. Although unpackaged laser diodes are available, they require special bonding, hermetic sealing and mechanical stress relief, making them unsuitable for the present requirement.

This problem was overcome by development of a measurement shoe, in which the sensor could be mounted within the insole. This allowed the height of the sensor to be increased allowing standard components to be used. The draw back of this approach was the requirement to construct a measurement shoe for each test subject.

4.2.1 Development and evaluation of first prototype sensor

The first prototype sensor contained a 5.6mm diameter laser diode (Hitachi, type HG7806G), four photodiodes with integral daylight filter (Siemens, type SFH203PFA), a Peltier heat pump (Radio Spares, rating 5.3Watt), integrated thermal sensor (Radio Spares, type LM35) and a strain gauge (Radio Spares, 2mm aluminium foil), within a cylindrical aluminium housing. A drawing of the first prototype is given in figure 7.

In order to simplify fabrication of the sensor housing, the machine shop scaled the diameter up from 30mm to 36mm. The total sensor height of 18mm was determined by the aluminium housing, an integral instrumentation printed circuit board and two end caps.

The Peltier heat pump and integrated thermal sensor provide a mechanism for regulation of the laser diode temperature. These three components were mounted in an integral chamber, which was filled with a ceramic powder, to provide thermal insulation between the hot and cold faces of the Peltier device. The strain gauge bonded to the inner wall of the housing allowed evaluation of sensor compression. The laser Doppler signal path was coupled from tissue by four short segments of 1mm diameter, plastic optical fibre (Edmund Scientific Ltd), spaced regularly about a central emitting fibre. These collimate light to and from the sample tissue. All fibre segments were bonded to the sensor housing using epoxy to eliminate the problem of movement artefact. Each photodetector was aligned with the corresponding detecting fibre via a milled recess within the housing. The photodetector leads were then connected to a small PCB, resident on the sensor, which contained a single transimpedance stage, with the four photodiodes connected in parallel to the input. The photoamplifier stage was implemented using surface mount components. The PCB was mounted on the sensor to reduce electrical noise pickup. Three sensor units were fabricated and evaluated in vitro.

It was apparent that the hot and cold faces of the Peltier heat pump could not be efficiently isolated within the small dimensions of the housing. At the maximum operating current of two amps, a temperature reduction of only seven degrees below ambient was achievable, which had an insignificant affect on laser noise. It was possible, however, to use the heat pump to maintain a constant laser operating temperature. This was important as the laser wavelength varied as a function of temperature and small variations in wavelength appeared as noise in the Doppler signal. However, the thermal dependence of the wavelength was a non-linear series of discrete steps. The laser diode selected for the sensor exhibited wavelength stability over the range of 26°C to 34°C. This encompasses the optimum measurement temperature of 30°C for which thermoregulatory blood flow is minimal, for normal nutritional flow (Scott 1986).

Experiments were made to determine if a constant temperature could be maintained for a reasonable measurement period without the use of thermal regulation. It was found that a foot pre-warmed in water could be maintained at a temperature of 30+/-3°C, if placed on an insulating surface of neoprene. For static measurements, the target temperature could be maintained for in excess of forty minutes. During walking

however, the target temperature could only be reliable maintained for about ten minutes. Given the findings it was decided to eliminate the Peltier device from further prototypes, the temperature sensor was retained however for monitoring of skin temperature.

A standard strain gauge amplifier (Radio Spares No. 846-171) was connected to the sensor and the signal recorded during static and dynamic loading. Compressive distortion of the housing was immeasurably small.

The prototype sensor was evaluated in vivo on the underside of the fingertip. To obtain an acceptable signal level an increase in the laser operating power to 3mW was required. It was also noted that the mean photoamplifier output level increased with tissue loading. Both of these factors necessitated a reduction in the value of the transimpedance stage gain to avoid amplifier saturation. The increase in the laser output power was undesirable for reasons of safety. Furthermore, the increased power dissipation of the laser heated the sensor housing to an extent that could affect the measurement, by invoking a thermoregulatory increase in blood flow.

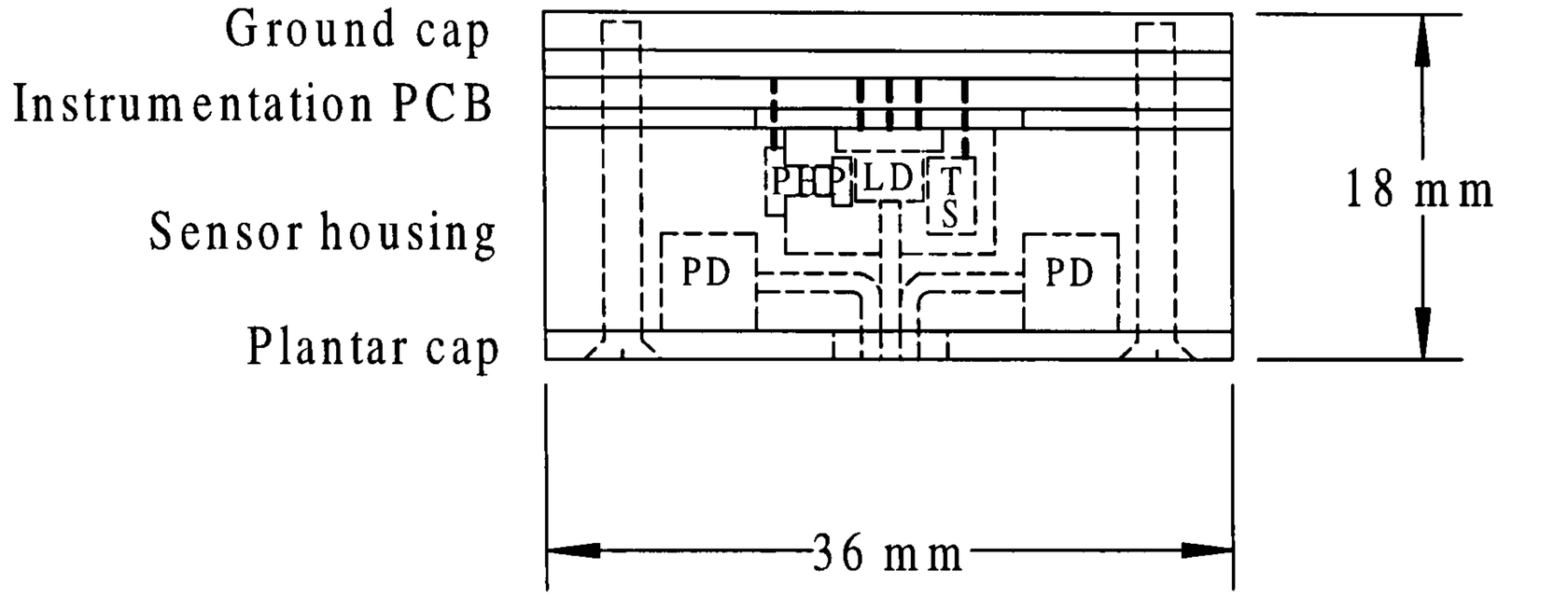

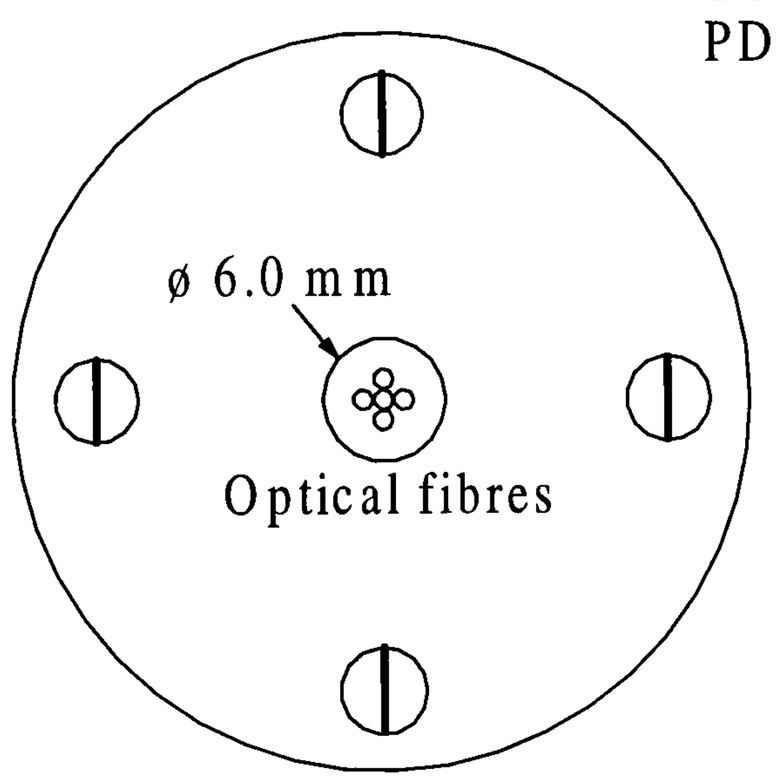

Figure 7 Cross sectional and plan views (plantar) of first prototype.

4.2.2 Development and evaluation of second prototype sensor

An improved device was designed to overcome the problems of the first sensor. By increasing the number of detection fibres to eight, the Doppler channel gain was improved. This allowed the laser output power to be reduced to 1mW. In isolation, this measure is counterproductive, as the increase in intensity requires a concomitant decrease in the stage gain to avoid saturation. To solve this problem a differential stage was used to amplify the output of two transimpedance stages, each of which was coupled to four photodiodes. By ensuring uniform illumination of the sample tissue and matched transimpedance stages, the DC intensity signal was rejected. This allowed a substantial increase in Doppler signal gain whilst also rejecting power line interference. However, the level of improvement depended on matching of the optical path and transimpedance stages. To simplify fabrication the differential gain was set to a relatively low value of five, allowing an input DC imbalance up to a hundred millivolts before output saturation.

Despite the addition of four extra photodiodes, the overall size of the sensor housing was reduced by eliminating the Peltier heat pump and thermal isolation chamber. The laser diode also became available in a smaller, 3mm package. The height of the sensor was reduced by making the instrumentation remote from the sensor although the PCB was retained for electrical connection. The connection PCB also supported a temperature sensor to allow monitoring of skin temperature. The dimensions of the second housing were 30mm diameter by 12.5 mm. Figure 8 is a drawing of the second prototype sensor. Photograph 2, is an exploded view of the sensor. Technical drawings for the second prototype are given in Appendix C.

The depth of the sensor was selected to match the orthopaedic insoles (Orthopaedic Systems, type 2013N-MXL) used to construct the measurement shoe. By running the laser diode at low power, the thermal dissipation was negligible and alternative materials to aluminium were evaluated for the housing to simplify component bonding and reduce sensor weight. Acrylic was prone to cracking and nylon-66 had poor dimensional stability with deformation after several hundred loading cycles. Silica doped nylon (Radio Spares, type Glass filled nylon-66) was found to be the optimum material with good strength, dimensional stability, resistance to thermal shock, low

moisture absorption and ease of bonding. The disadvantage of this material was the requirement for hardened machine tools for processing. A moulded housing was considered, however the tooling cost was prohibitive for the small number of units required. The change of material and the decrease in sensor size, resulted in a 50% reduction in sensor weight down to 15g. The strength of the sensor was maintained by incorporating eight 8BA stainless steel securing bolts. There was a slight increase in the material cost of the housing. The fabrication time increased significantly, requiring around twenty hours, over several days, to allow curing at successive bonding stages.

Five devices were constructed and electrical connections were made to three leads. To reduce noise, the two signal leads were isolated and shielded from the laser supply connection. In vivo evaluation of the second prototype indicated two problems. First, an acceptable signal to noise ratio could not be achieved if the signal connections were longer than 500mm, due to external interference. This problem was solved by moving the instrumentation from the waist to a unit strapped above the heel as shown in photograph 3. The second problem was coupling of interference directly into the photodiode leads, from the subject. This was not observed in the first prototype due to the integral instrumentation and the signal shielding afforded by the grounded metal housing. To overcome this problem an insulated metal sleeve was fabricated to fit the outside circumference of the sensor housing. The sleeve was grounded to act as a shield and a subject lead was introduced to ground the subject via a self-adhesive electrode worn on the dorsum of the foot.

Five devices were evaluated extensively in vitro and in vivo. The repeatability of the sensors over time was within 10%. However, device to device repeatability was poor with response variations approaching 25%. This was attributed to the difficulty of matching and alignment of the fibre optic segments within the sensor housing.

Despite these limitations, the second prototype sensor was used to obtain some initial data from five non-diabetic subjects, for a range of test procedures. A real-time signal processor was developed based upon a standard laser Doppler algorithm (Bonner and Nossal 1981) and evaluated in vitro. Using the processor it was possible to demonstrate that the sensors responded as expected, for example, tracking blood flow reduction during inflation of a pressure cuff.

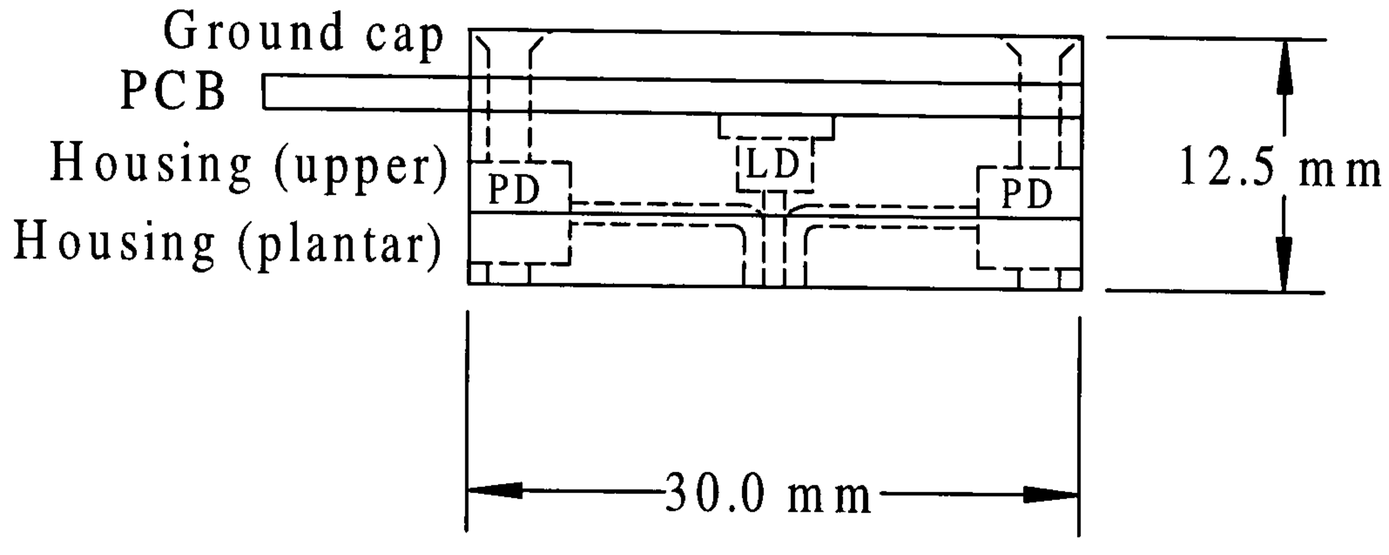

Figure 8 Cross sectional and plan views (plantar) of second prototype.

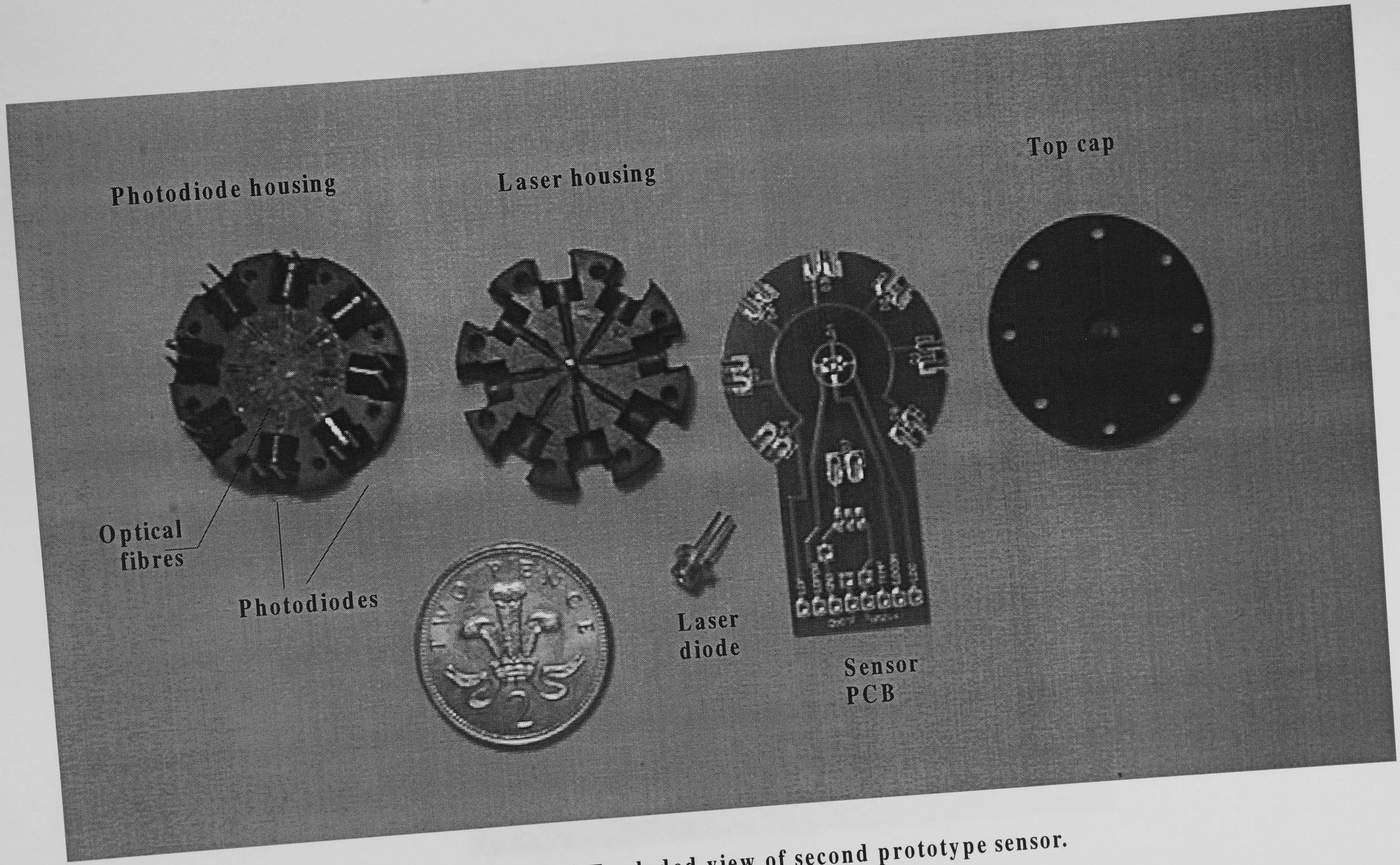

Photograph 2 Exploded view of second prototype sensor.

Photograph 3 Heel mounted instrumentation unit for second prototype sensor.

4.2.3 Development and evaluation of final prototype sensor

To improve device to device repeatability a third prototype was designed. This eliminated the use of fibre optics entirely by employing large area surface mount photodiodes (Siemens BPW34S) directly adjacent to plantar tissue. These photodiodes comprised a photosensitive area surrounded by a small border region. They were abutted and a 1mm hole drilled at the centre point, through the border to avoid exposing the active area to moisture. By incorporating the photoamplifier within the sensor the signal to noise ratio was improved sufficiently to eliminate the heel instrumentation unit. Connections were then made directly to an interface unit worn at waist level. With this approach, it was possible to obtain a level of performance equal to that of the concentric fibre technique. Additionally a device to device repeatability of better than 10% was achieved.

The third (final) prototype was fabricated in a square geometry from copper clad fibreglass board and acrylic sheet, using the artwork shown in Appendix D. The length was maintained at 30mm and height set to 12.5mm to match the measurement shoe insole depth. The plantar end-cap implemented a copper electrode for direct tissue connection, eliminating the requirement for a separate subject ground. This approach reduced the construction time and cost of the sensor and the modular design made the sensor serviceable. The on board instrumentation was realised using surface mount technology. The FSR device was bonded to the ground end-cap as in the previous prototypes. Figure 9 illustrates the third prototype device. Photographs 4 and 5 show exploded views of the final prototype sensor.

To simplify the system and increase portability the real time signal processor was eliminated and data was recorded directly to an instrumentation recorder (Sony, model PC208A). Data was downloaded off-line for processing, allowing different signal processing approaches to be evaluated.

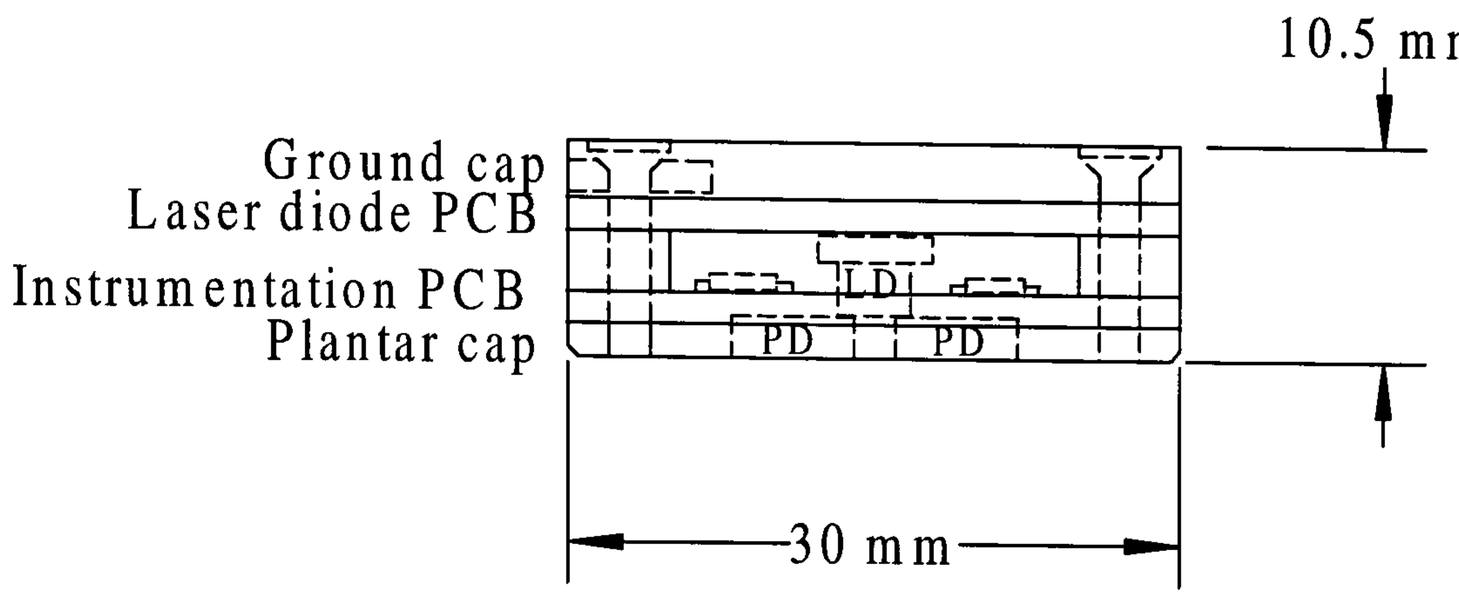

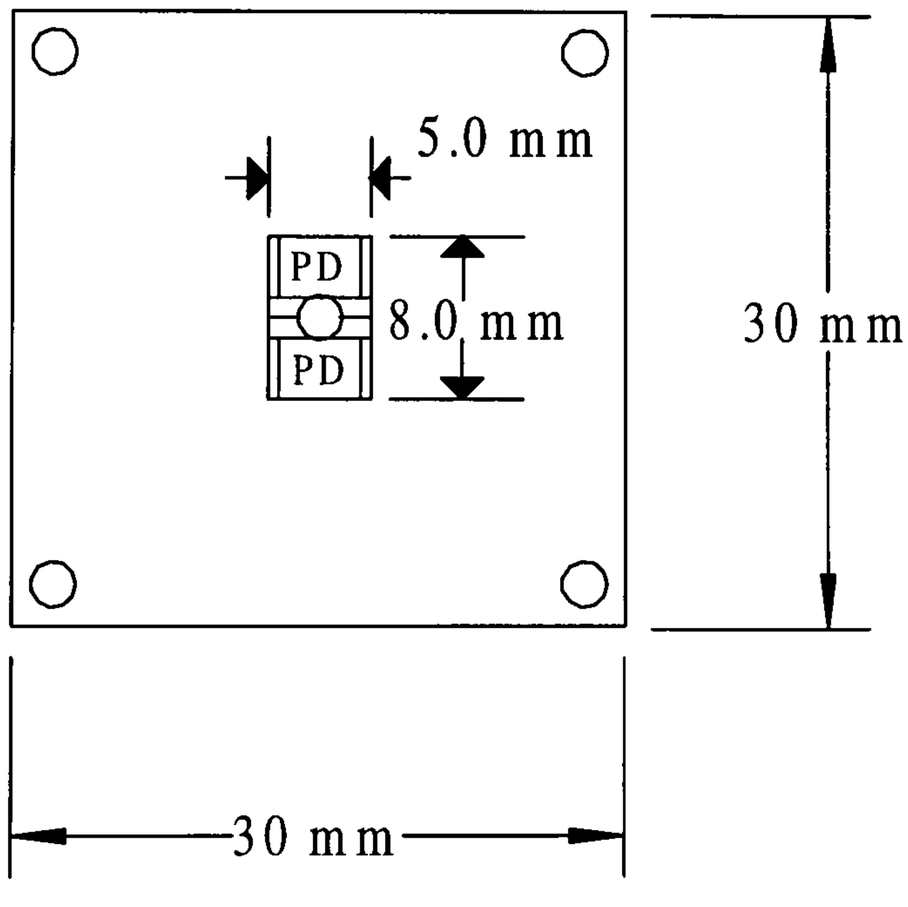

Figure 9 Cross sectional and plan views (plantar) of final prototype.

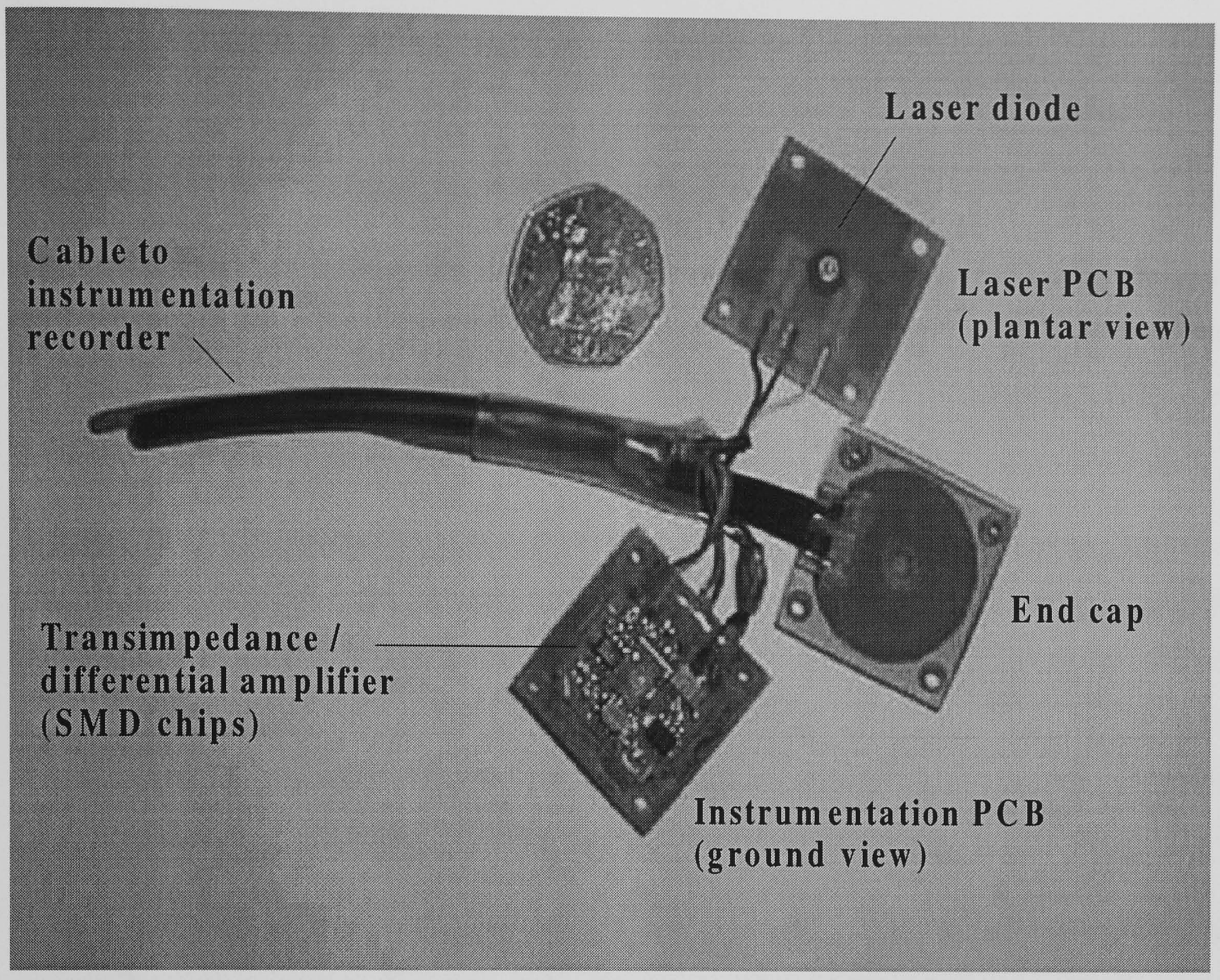

Photograph 4 Exploded view of final prototype sensor (internal view)

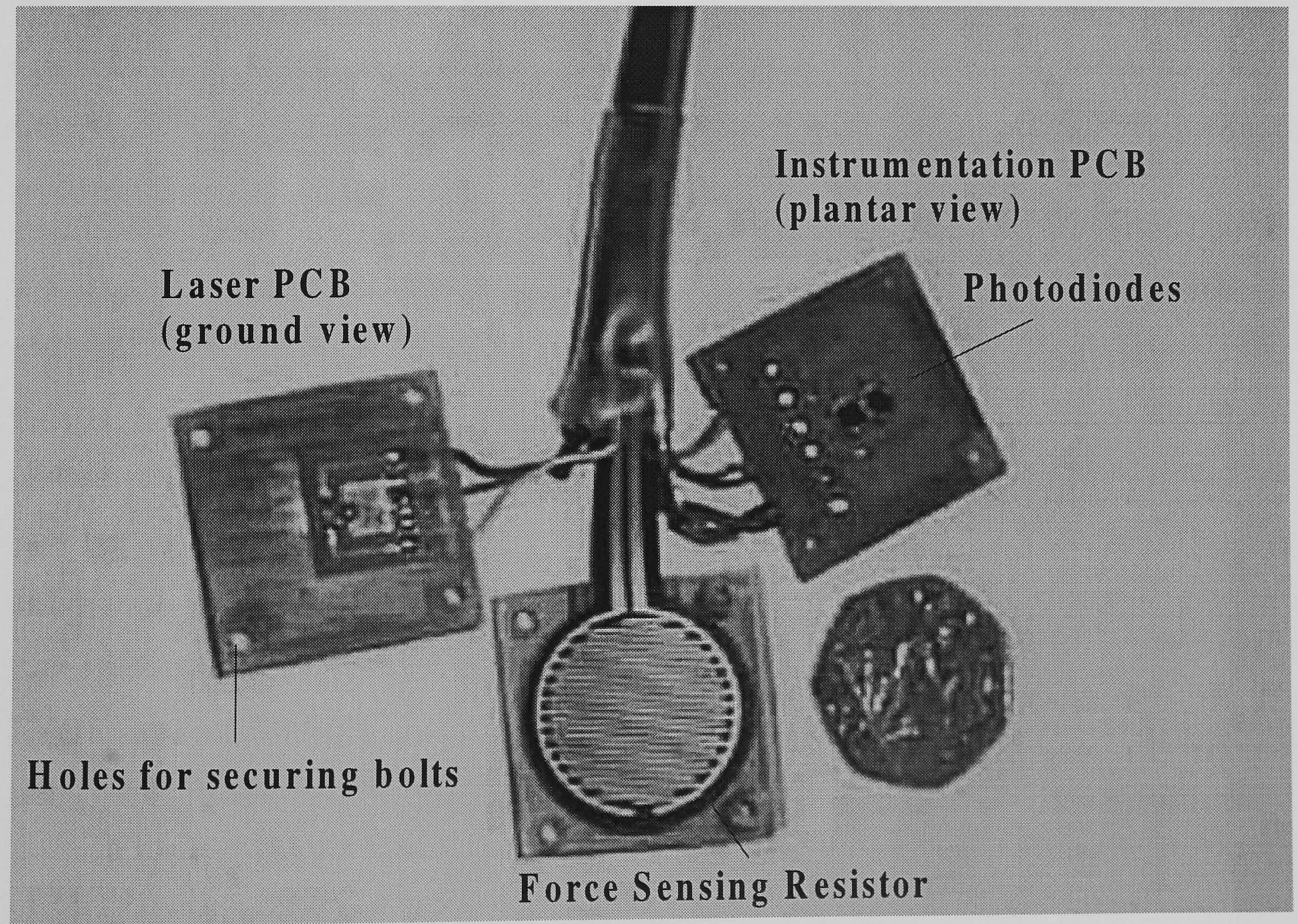

Photograph 5 Exploded view of final prototype sensor (external view)

4.3 Development of sensor instrumentation

4.3.1 Signal to noise ratio of the laser Doppler channel

Achievable signal to noise ratios in laser Doppler flowmetry systems are inherently low (Drain 1980, Oberg 1990), De Mul (1984) for example, states a SNR power ratio of 10. To obtain reliable estimates of blood flux, instrumentation and signal processing was designed to optimise this parameter.

In theory the signal to noise ratio can be improved by repeated signal averaging over time (Tagare 1993) to realise an improvement of $N^{1/2}$ where N is the number of sets of samples averaged. In practice, the number of samples that can be averaged is dependent on the desired update rate of the output signal, in this case the blood flux value. This value depends on the nature of the flow being observed, with typical rates in the range of 100 milliseconds (Borgos 1990) to 1.5 seconds (Dryden et al. 1992).

In the present study, blood flux was evaluated over a Doppler signal bandwidth compatible with the range found in commercial systems of 20Hz to 4KHz (Obied 1990) for studies of the microcirculation. However, the upper frequency limit of the system was extended to 20KHz to allow for the possibility of a wider signal bandwidth resulting from increased flow during reactive hyperaemia. This upper frequency was limited by the maximum 40kHz per channel sampling rate of the instrumentation recorder.

To resolve frequency components down to 20Hz requires a minimum of 50ms of sampling time, thus for a blood flux update rate of 100ms, two sets of samples could be obtained and averaged, giving an SNR improvement factor of root two. By reducing the update rate to once per second, twenty sets of samples were averaged giving an SNR improvement factor approaching five. However, for the required application, fast changes in flow due to post occlusive reactive hyperaemia were expected. It was therefore necessary to design the instrumentation without relying on an improvement in SNR by means of averaging. Thus, a low-noise transimpedance stage was developed to implement the photometric amplifier. The circuit employed is shown in figure 10.

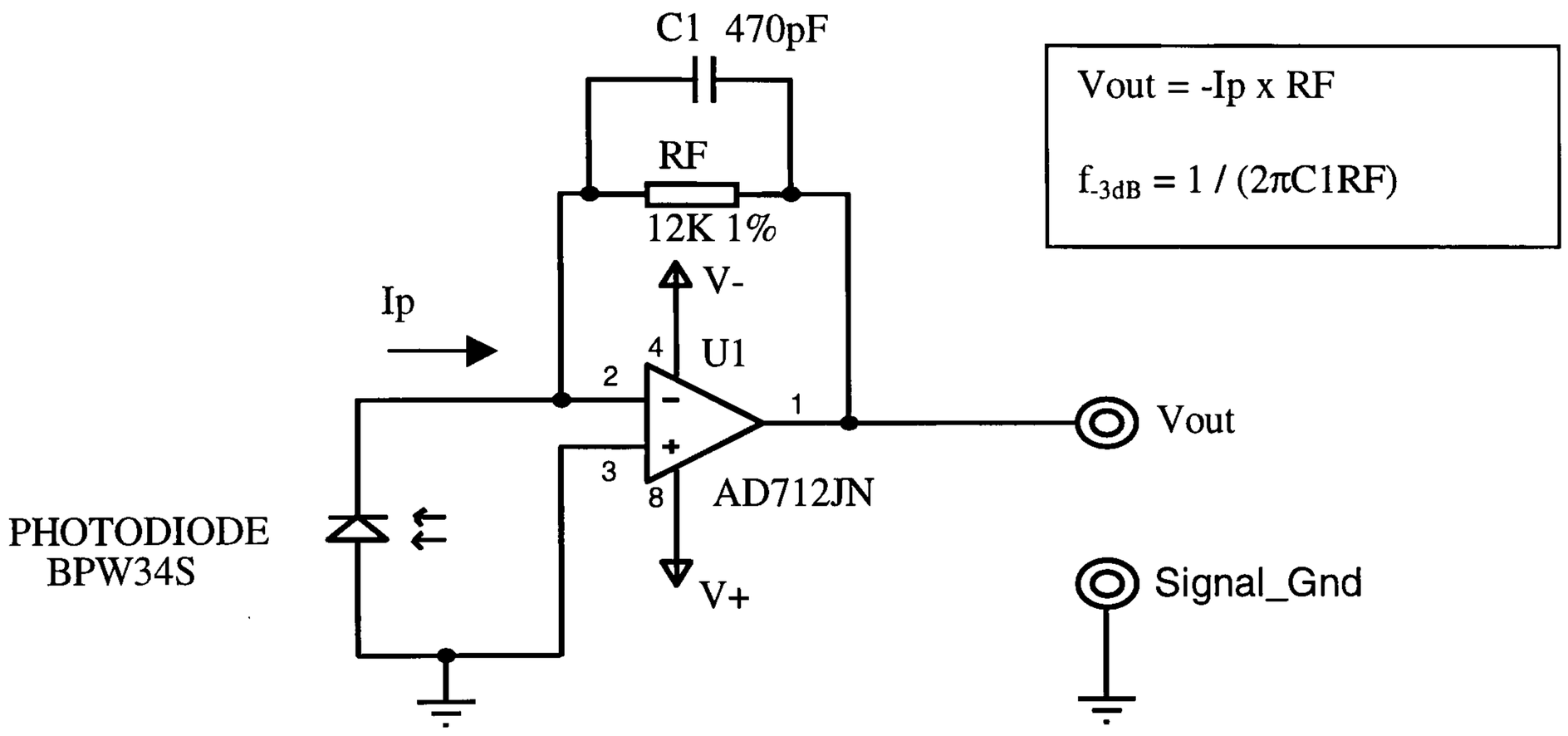

Figure 10 Schematic diagram of transimpedance amplifier.

The photodiode generated a photocurrent in response to incident light, which was converted to an output voltage proportional to the product of the photocurrent and feedback resistance. The feedback capacitor provided first order low pass filtering, f_{-3db} = 28.2kHz, to reduce the signal bandwidth.

4.3.2 Design of low noise photocurrent amplifier and the laser power supply

The main criteria in the design and implementation of the transimpedance stage were low noise and availability in surface mount technology. The BPW34S (Siemens) photodiode was selected, as this device could be abutted to form an almost continuous detection region. A low-noise, dual opamp AD712 (Analog Devices) was used for the current to voltage conversion. An estimate of the noise performance of the transimpedance stage was obtained as follows. An output level of 2.8 volts, representing the mean intensity across a sample of subjects with varying skin pigmentation was determined. The corresponding photocurrent, Ip was V_{mean} / Rf = $233x10^{-6}$ A. For the selected photodiode, the conversion factor S, at 780nm was 0.4 A/W, so that an estimated total optical power incident on the photodiode was Ip / S = $582x10^{-6}$ Watts.

A typical estimate for the fraction of the total backscattered light that has been Doppler shifted is <0.1% (Bonner and Nossal 1981), corresponding to $582x10^{-9}$ Watts for the present case and generating a photocurrent of 1.45uA. The output signal level from the transimpedance stage is then I_{signal} x Rf = 17.5 mV.

Intrinsic noise sources within the signal path were found to originate from the laser diode, photodiode and transimpedance amplifier. The principle noise sources of the laser diode were variations in optical output power due to injection current noise and wavelength drift with temperature, which can result in heterodyne mixing of output modes (Nilsson and Tenland 1980). To quantify these noise sources, the output of the laser was passed through a collimating lens and focused onto a large area photodiode (Sharp 1997), (Radio Spares, type OSD15-5T). The photodiode was cooled using a Peltier heat pump and operated in photocurrent mode to minimise photodiode noise (Wilson and Hawkes 1989). The photocurrent was converted to a signal voltage using a low noise, wide bandwidth opamp OP471G (Analog Devices) configured as a transimpedance amplifier. The laser diode operated in continuous wave mode with a

small (~100mV) sinusoidal signal coupled into the DC bias to modulate the output, about a mean value of 1mW. The laser was mounted in a thermally insulated chamber and the ambient temperature adjusted via a heating resistor adjacent to the device. The power spectrum of the output signal was monitored on a spectrum analyser over a frequency band from DC to 100kHz with a resolution of 10Hz.

Figure 11 shows the measured power spectrum and demonstrates the bias signal at 1kHz and the laser noise, which is reasonably uniform across the band. A worst case signal to noise ratio of –42dB was established using this method. To improve performance an automatic power control (APC) circuit was introduced and the laser was operated in a constant temperature chamber at 30+/-0.5^{o}C. The resulting spectrum is shown in figure 12.

The APC circuit is based on a standard design modified for use with the ML40123N laser diode (Mitsubishi) and has the benefit of battery operation to reduce injection current noise. The design was implemented in surface mount technology to improve portability. The circuit diagram of the APC circuit is given in Figure 13. The internal monitoring photodiode of the laser is used as a feedback element to the input of the opamp, which varies the bias across the laser diode to maintain constant output power. The remaining components provide supply filtering, and surge protection for the laser. Optical output power is set manually via the potentiometer.

With these improvements, the SNR as measured by the preceding technique was improved to a value of –88dB. Further improvement would have required a more complicated controller with expensive low noise components (Libbrecht and Hall 1993). Further improvement could have been obtained using an opamp with a lower noise figure, however the NE532 (National semiconductor) was retained for the advantages of single supply operation and low drain current.

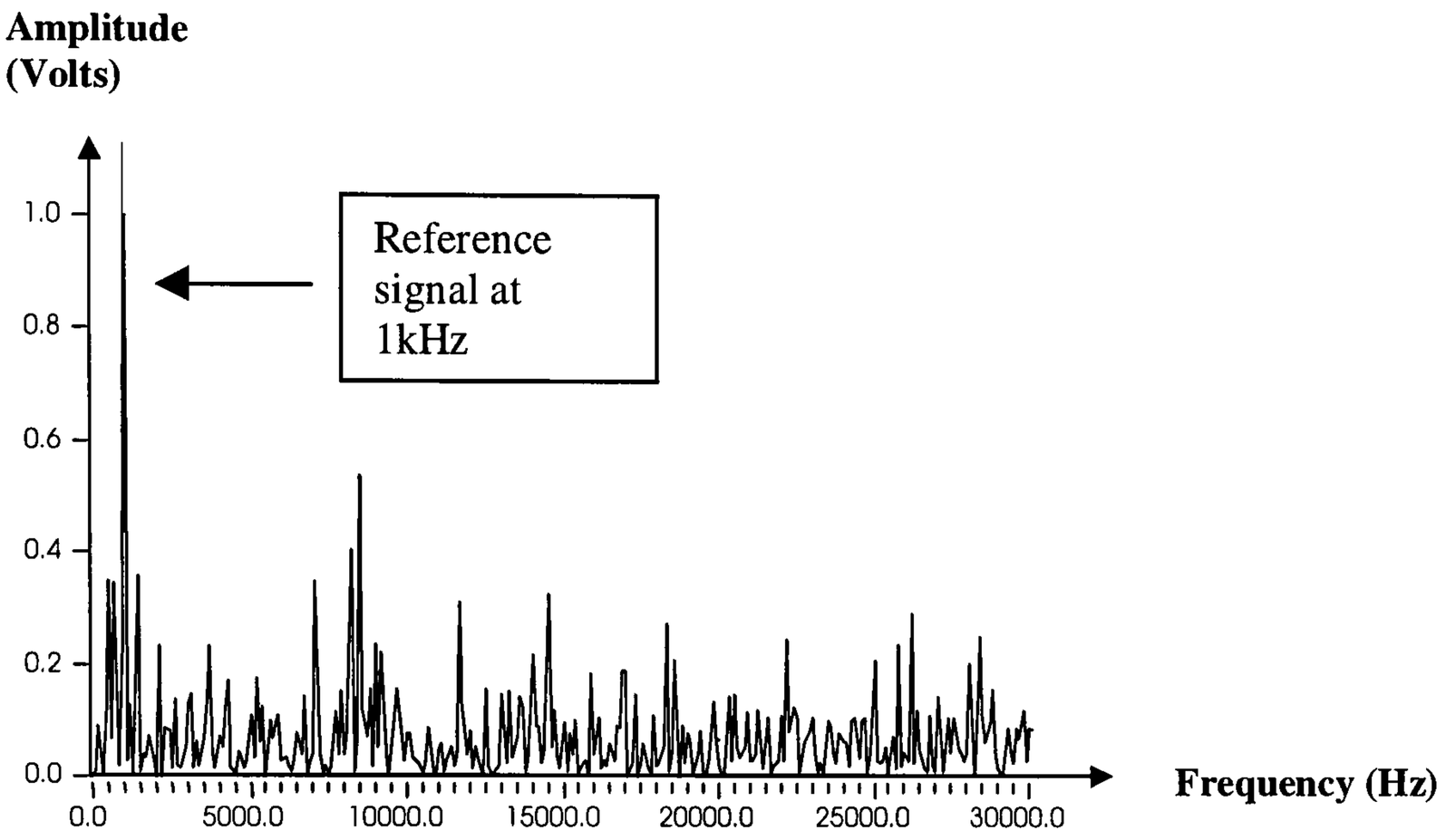

Figure 11 Laser diode noise spectrum without stabilisation.

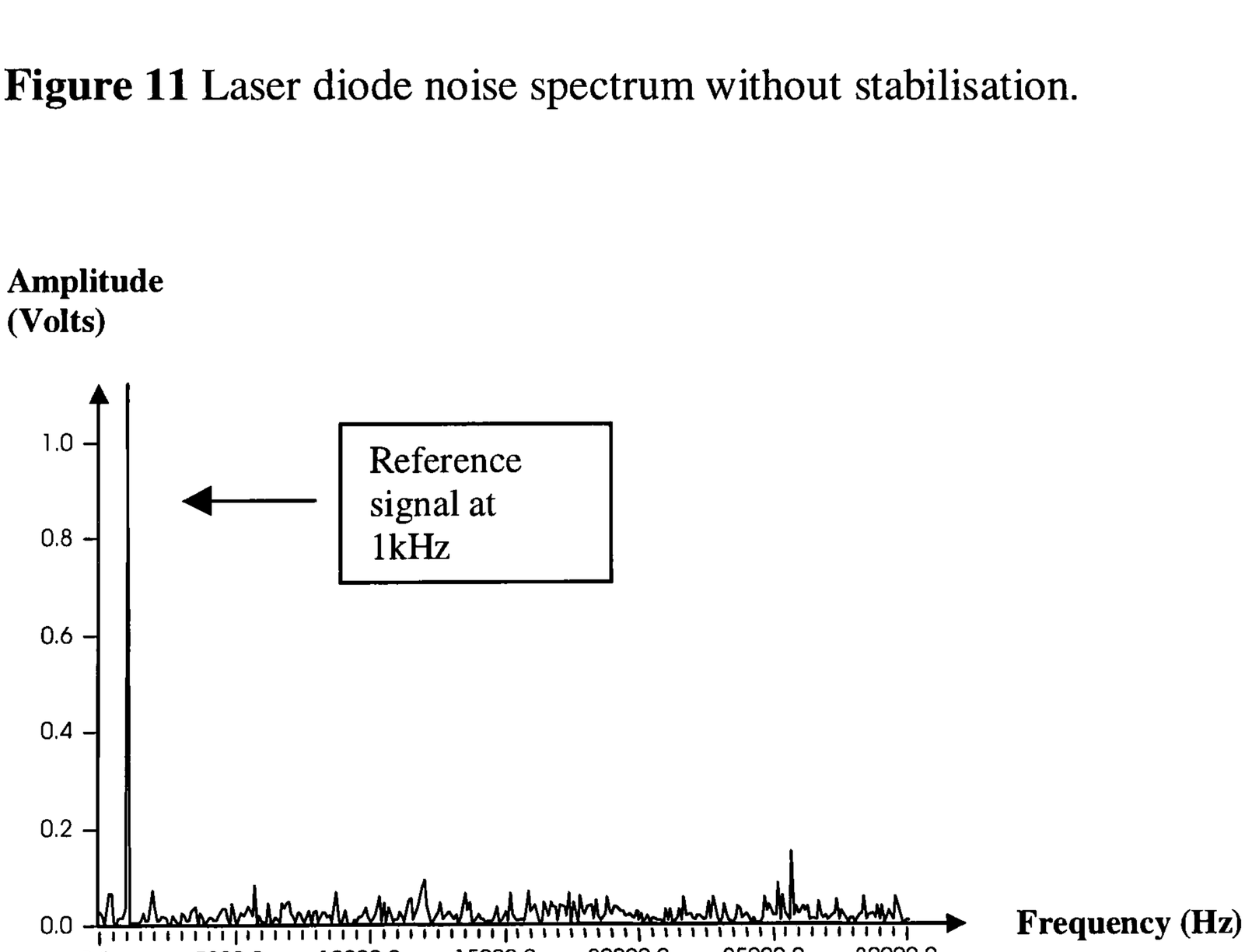

Figure 12 Laser diode noise spectrum with thermal and power stabilisation.

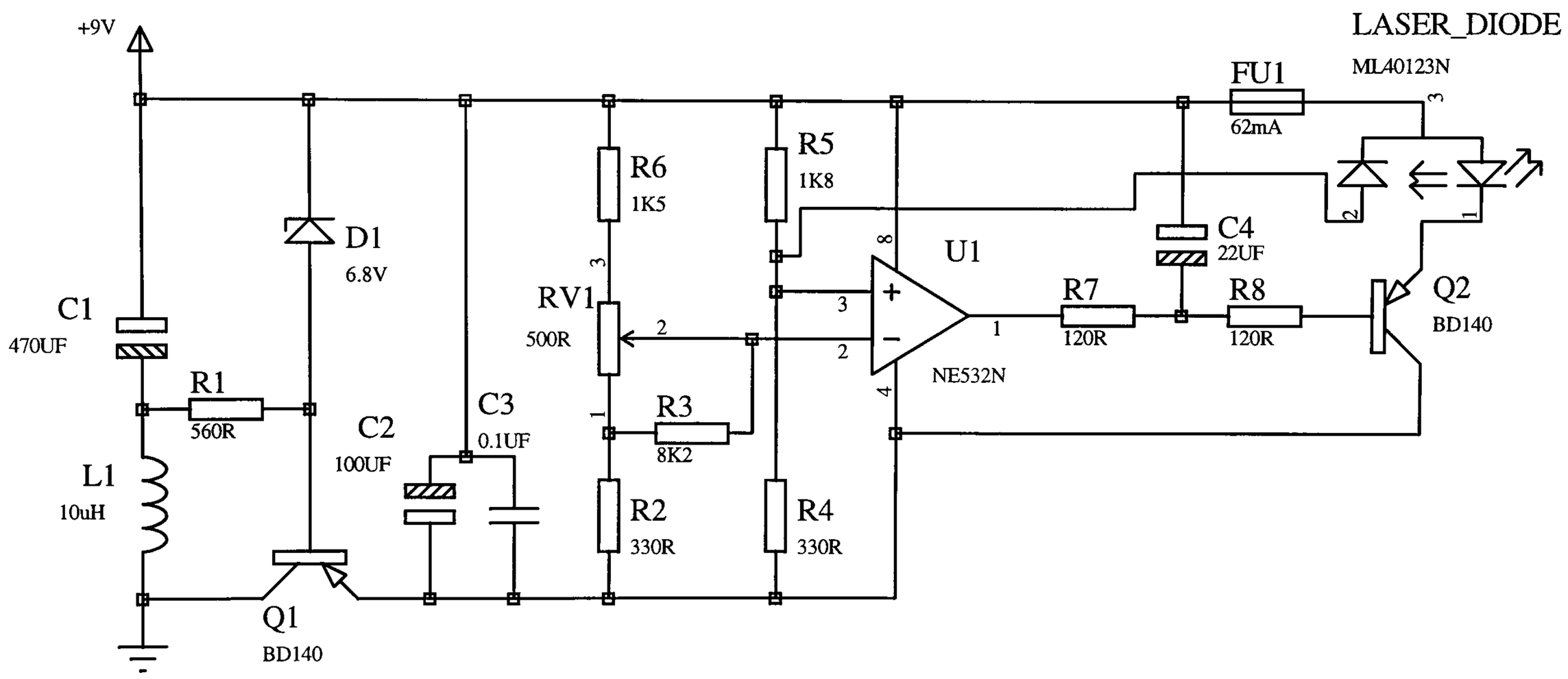

Figure 13 Laser diode power controller.

The optical output noise power (P) for the measured signal to noise ratio (dB), was determined from (Sharp 1997):

$$SNR = 10\log\left(\frac{\delta P}{P}\right)^2 \tag{13}$$

Where δP is the fluctuation in the optical power output.

Resulting in a value of 40nW, a corresponding noise current of 16nA and contributing 192uV of noise to the output signal.

For the detection system the total noise current is given by (Bertone and Webb 1998):

$$i_{n(Total)} = \sqrt{\left\langle i_{n(Diode)} \right\rangle^2 + \left\langle i_{n(Rfeedback)} \right\rangle^2 + \left\langle i_{n(Opamp)} \right\rangle^2} \quad Amps/\sqrt{Hz} \tag{14}$$

The operating configuration for the photodiodes used in the sensor was photocurrent, which resulted in superior noise performance at signal frequencies below 100kHz (EG&G Optoelectronics 1998). In this mode, the equivalent noise generated by the device was due to intrinsic shunt resistance. Therefore, both the photodiode noise and the noise generated by the feedback resistor have a Johnson spectrum with a flat characteristic from DC to the cut-off frequency. For this type of source the noise current is given by (Horowitz and Hill 1984):

$$i_{n(Johnson)} = \sqrt{\frac{4KT\Delta f}{R}} \quad Amps/\sqrt{Hz} \tag{15}$$

Where:

K is Boltzmann's constant (1.38×10^{-23} Joules/°K).

T is absolute temperature in degrees Kelvin.

Δf is the bandwidth in Hz.

R is the resistance in Ohms (12K Ohms)

For operation at 30°C over a signal bandwidth of 30kHz equation (15) yields a value of: 11.2nA/Hz$^{1/2}$ for the photodiode and 204.5nA/Hz$^{1/2}$ for the feedback resistor.

The noise generated by the operational amplifier was given by (Jung 1989):

$$i_{n(Opamp)} = \sqrt{\left\langle i_{(Leakage)} \right\rangle^2 + \left\langle V_{(Noise)} \omega C_{(Total)} \right\rangle^2} \quad Amps/\sqrt{Hz} \qquad (16)$$

For the AD712 opamp, used for the transimpedance stage the input leakage current $i_{(Leakage)}$ is 0.01pA/Hz$^{1/2}$ and the input noise voltage, $V_{(Noise)}$ is 45nV/Hz$^{1/2}$. The total input capacitance $C_{(Total)}$ at the input of the amplifier is dominated by the junction capacitance of the photodiode which has a total value of 72pF at 25°C. Using these values, and for a bandwidth of 30KHz, equation (16) gives a value of 10fA/Hz$^{1/2}$.

From the values obtained for the noise sources of the transimpedance stage, it was evident that the photodiode noise current dominated the other sources. The total noise estimated for the contribution by the detector and transimpedance stage was 45nA/Hz$^{1/2}$, which corresponds to a noise power of 112.5nW.

4.3.3 Optimisation of the laser Doppler instrumentation

Using the preceding figures for signal and noise power, the estimated SNR was +7dB. However, when the SNR was evaluated in vitro, using a calibration rig, and in vivo, it was impossible to distinguish the Doppler signal from background noise. The spectrum also included significant components at the supply frequency and harmonics. A number of design modifications were made to improve performance. Guard electrodes were introduced around the photodiode and opamp input junction to reduce leakage current into the opamp (Jung 1989). The single-ended evaluation circuit was converted to a differential stage by introducing a second photodiode and transimpedance stage and an instrumentation amplifier. The instrumentation amplifier provided rejection of common mode noise sources from the laser diode and external line interference. In practice, the 50Hz component of the power line was not fully rejected by the instrumentation amplifier due to strong coupling directly from the subject. It was therefore necessary to incorporate an electrode to ground the subject. The improved detection circuit is shown in figure 14.

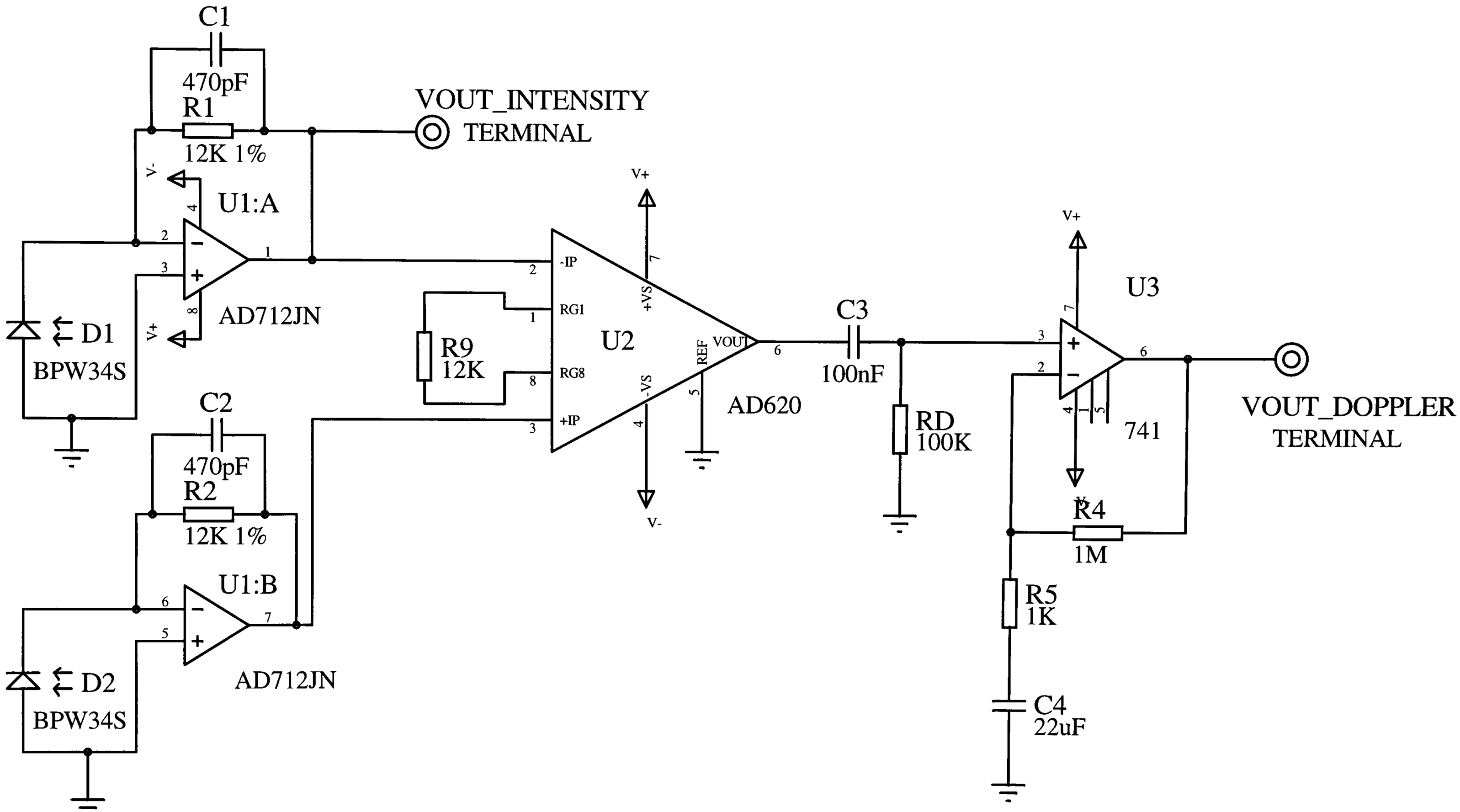

Figure 14 Differential detector.

The output of the instrumentation amplifier was band pass filtered f_{-3dB} = 16Hz - 20kHz, to separate the signal component, which was subsequently amplified to produce a signal with maximum swing (+/-4.5V p-p), within the supply rails. To prevent signal clipping the gain of the instrumentation amplifier was adjusted empirically during calibration. It was noted that clipping occurred during movement artefact and this was exploited in the signal processor, by rejecting data for short, isolated periods of clipping.

With these modifications, it was possible to observe a laser Doppler signal amplitude of 20mV p-p above the 5mV p-p of background noise, at the instrumentation amplifier output. Application of the laser Doppler algorithm to this signal provided a blood flux value that tracked changes in flow. However, the blood flux graphs obtained for constant flow and concentration test conditions were considered too noisy for clinical interpretation, figure 15. It was possible, to demonstrate that the transient changes in blood flow during reactive hyperaemia, occurred on a scale of seconds. Given this observation and the difficulty of improving the instrumentation without substantially increasing the sensor size, the blood flux update rate was reduced to one second. Signal averaging was then introduced to improve the signal to noise ratio. The resulting improvement in the graphs was of an acceptable quality to allow clinical assessment of blood flux, 16.

Photograph 6 shows the implementation of the instrumentation unit used with the second prototype sensor. Location of the transimpedance stage remote from the sensor simplified sensor construction. However, the instrumentation unit had to be situated at the heel to obtain an acceptable signal to noise ratio. By including the front-end amplification within the final prototype sensor, a simplified instrumentation unit, photograph 7, was achieved that could be worn at waist level.

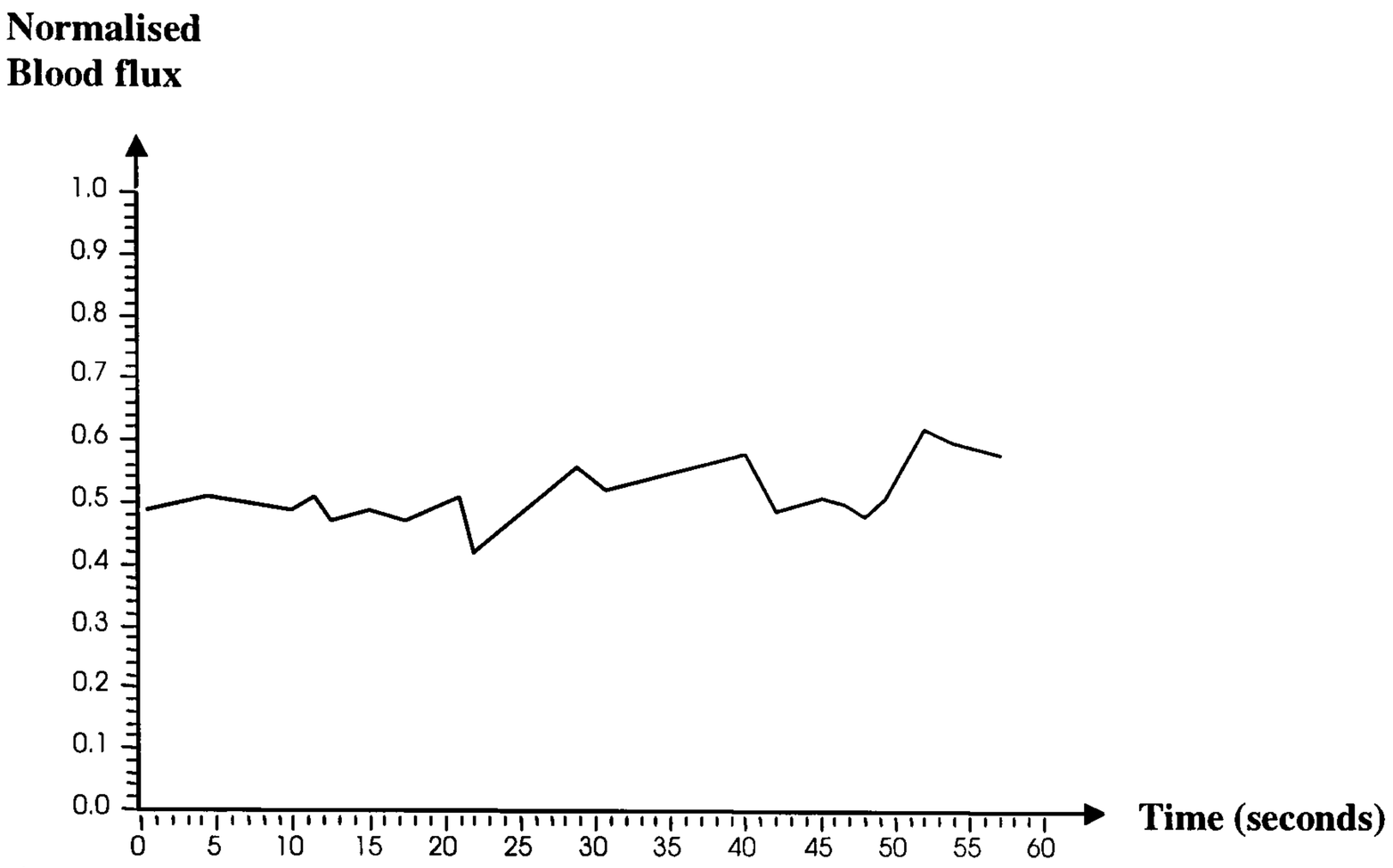

Figure 15 Graph of flux obtained from Doppler signal (without averaging), in vitro at a mean velocity of 2mm.s^{-1} and concentration of 0.2%.

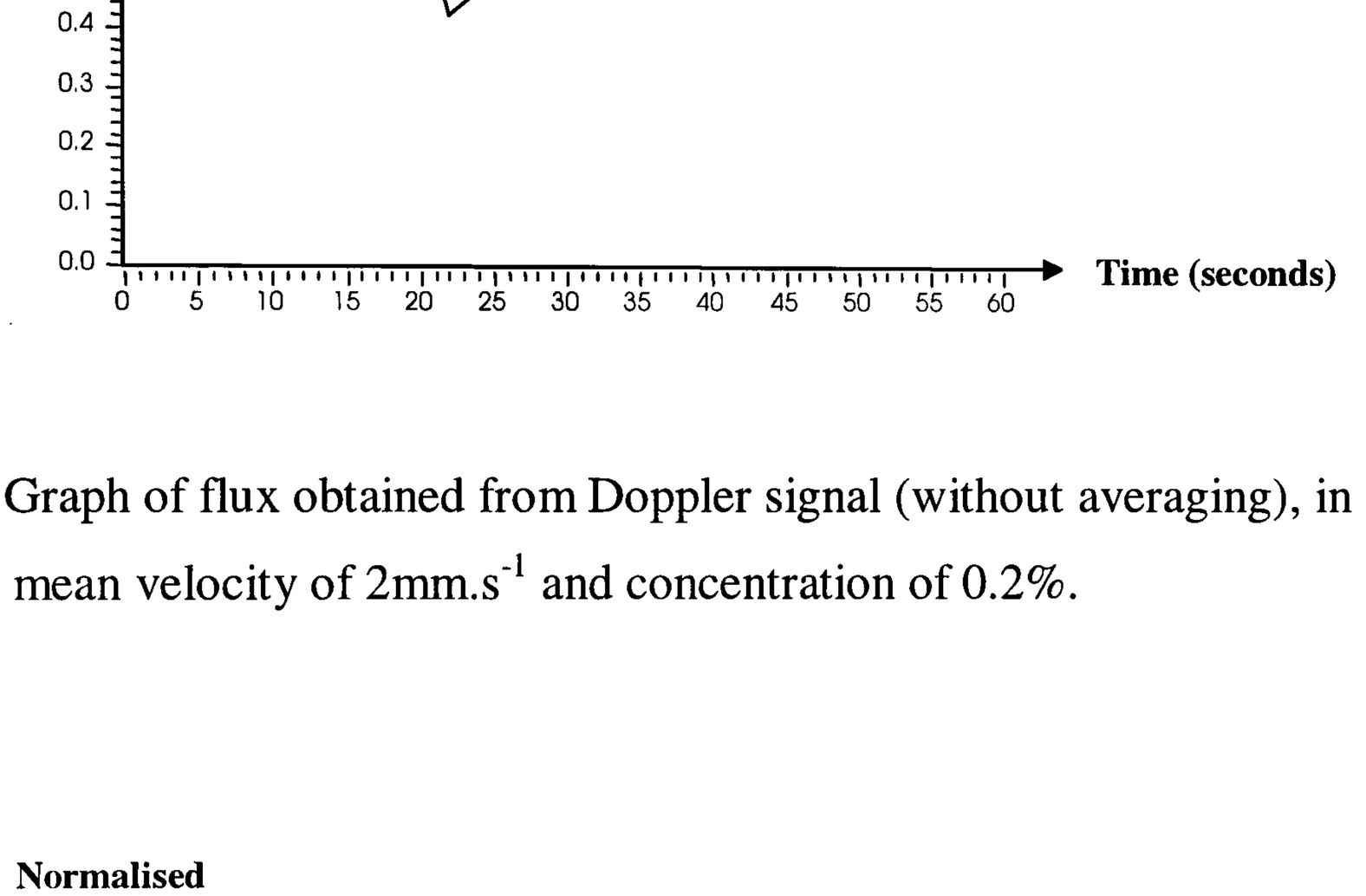

Figure 16 Graph of flux obtained by averaging 20 sample sets of Doppler data obtained for identical conditions to those stated for figure 15.

BOURNEMOUTH
UNIVERSITY
LIBRARY

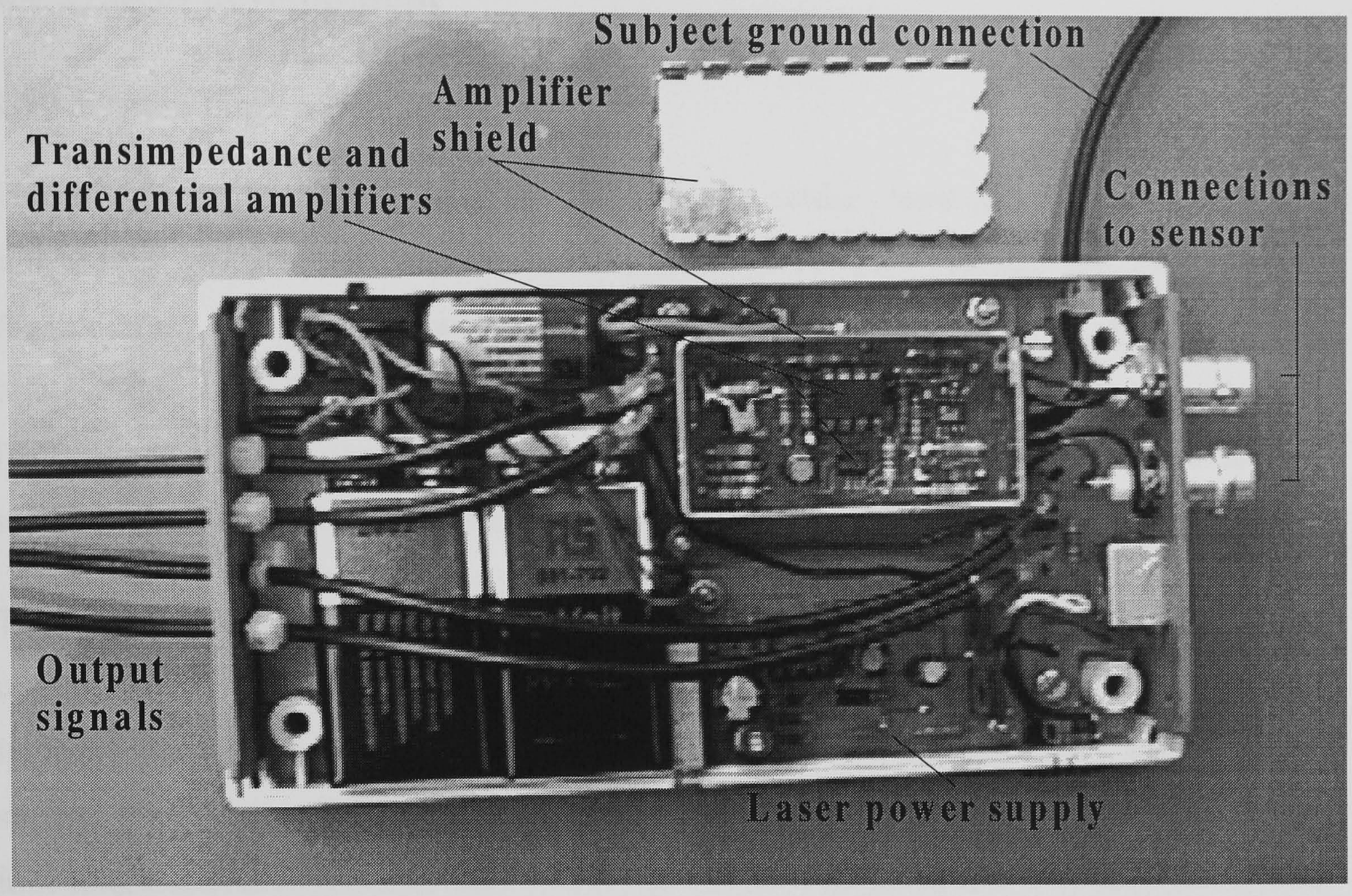

Photograph 6 Heel instrumentation unit used with second prototype sensor

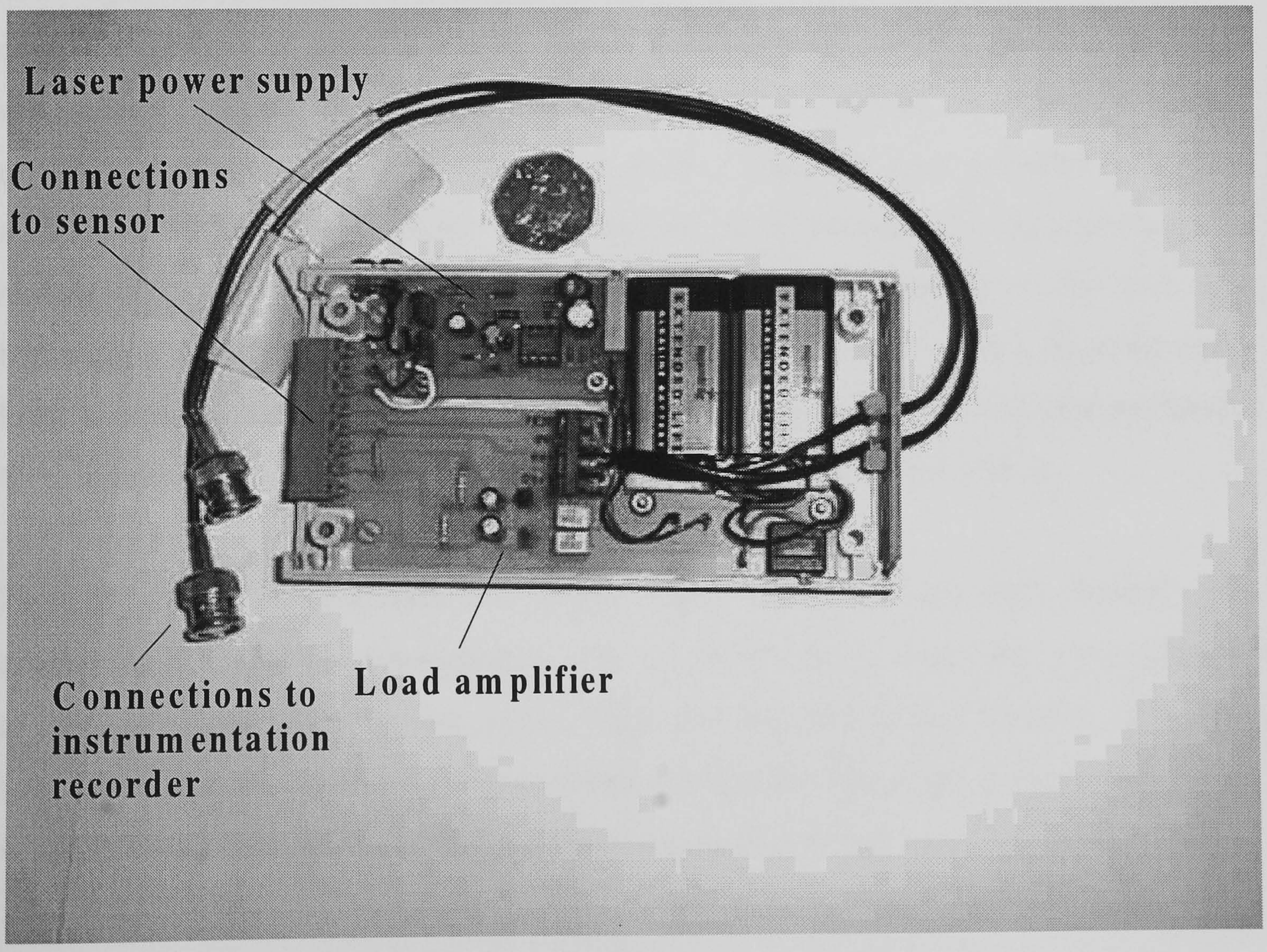

Photograph 7 Waist instrumentation unit used with final prototype sensor

4.4 System development

4.4.1 System implementation

The full plantar monitoring system consisted of a sensor, measurement shoe, interface and power supply unit and an instrumentation recorder carried by the subject. Additionally, a data acquisition system and software were used to download and process the data. Figure 17 is a block diagram of the plantar monitoring system. Photographs 8 and 9 shows the implementation of the basic system and the method of securing the foot in the measurement shoe.

The load signal was amplified in the instrumentation unit mounted at waist level. This unit provided an interface to the instrumentation recorder for the laser Doppler and intensity signals, together with a load amplifier and a regulated laser diode power supply. Two high capacity 9-volt alkaline batteries powered the unit, providing up to four hours of continuous use.

The instrumentation recorder (Sony, model PC208A) was configured to sample the three signals at a rate of 40 K/samples per channel. An input gain factor of two on all channels provided additional gain, and each channel was calibrated prior to measurement using an autocalibration function. An integral rechargeable battery afforded continuous recording for 50 minutes. The data was recorded to digital audiotape (BASF, type 4D-90M) with a capacity of 90 minutes. During recording, the signals were monitored using the audio output and visual displays on the unit. The lightweight instrumentation recorder was carried by the subject using a shoulder strap. Prior to measurement, trailing connection leads between the sensor and instrumentation were located at the rear of the leg and adjusted in length to suit the subject.

Recorded data was download to computer using a high speed, multi-channel, data acquisition card (National Instruments, type AT-MIO-16F-5). This card was configured to re-sample the three signals output from the instrumentation recorder. The data acquisition also incorporated programmable antialiasing filters and a large data buffer, which allowed continuous, asynchronous downloading of data.

4.4.2 Construction of the measurement shoe

The measurement shoe was developed around a standard orthopaedic insole made of plastazote foam (Orthopaedic systems, Widnes, Cheshire). The insole was encapsulated, using contact adhesive, between two sheets of neoprene rubber of thickness 1.5mm. The whole assembly was flexible eliminating abnormal bending stresses on the foot, during walking. The ground side neoprene layer protected against foreign matter such as grit penetrating the insole. The plantar side neoprene layer provided thermal insulation for the foot during the measurement period and prevented the normally permanent compression of the plastazote with time. The measurement shoe was fixed to the foot using neoprene straps laced through a plastic buckle. The straps were fixed to the walls of the plastazote insole using blunted self-tapping screws that were bonded into the material using a cycroanylate adhesive. A piece of neoprene rubber was mounted at the rear of the measurement shoe onto which an ankle strap was bonded and fixed using a press-stud. Photograph 10 shows the method of locating the sensor within the insole of the measurement shoe.

Software was developed using National instruments Labview version 5.0 development system. The plantar monitoring system required a fast access hard disk, with capacity of 500 Mbytes per hour of measurement time. A Pentium 200MHz processor and 32Mbytes of RAM were required for data acquisition and signal processing.

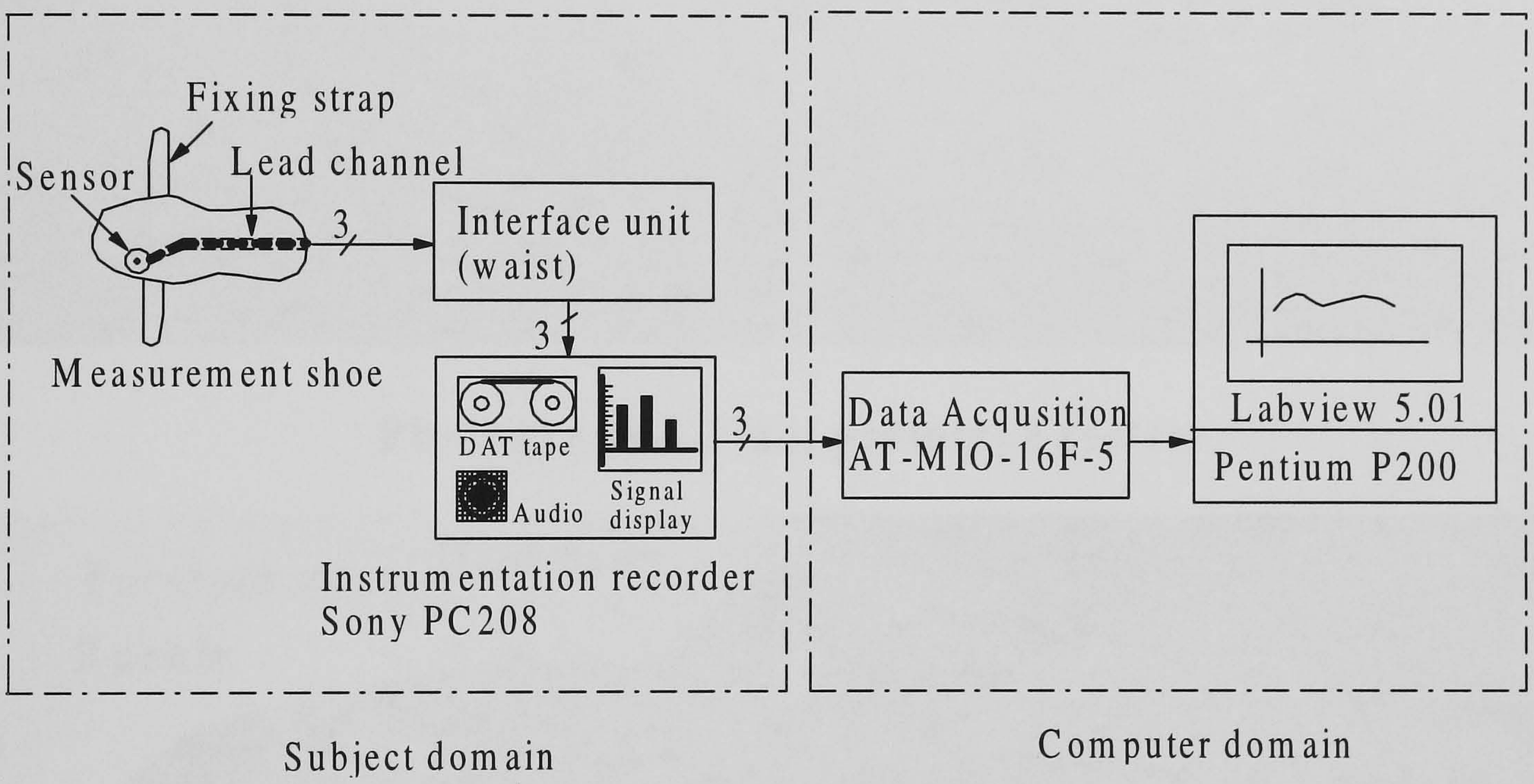

Figure 17 Block diagram of plantar monitoring system.

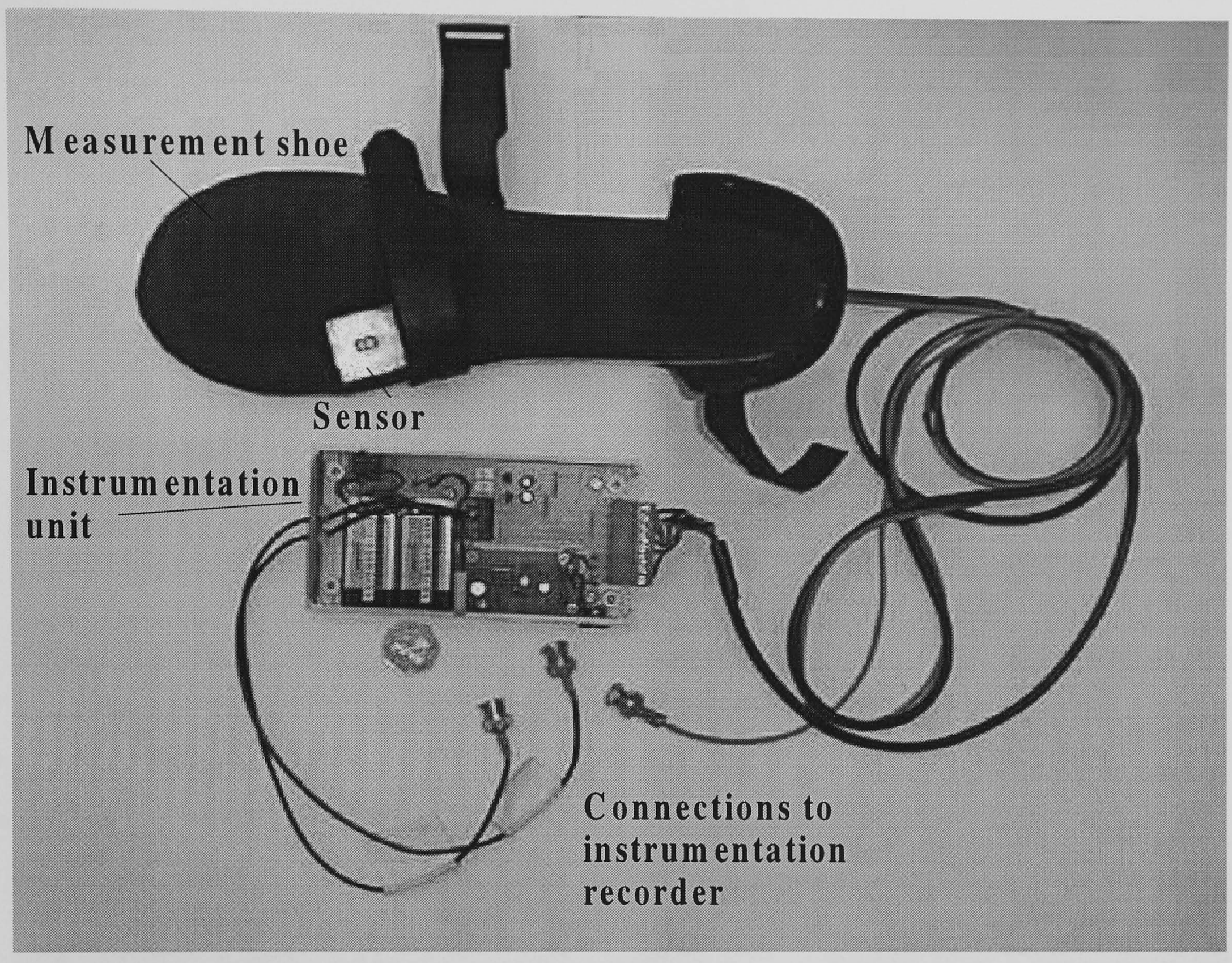

Photograph 8 Final prototype system.

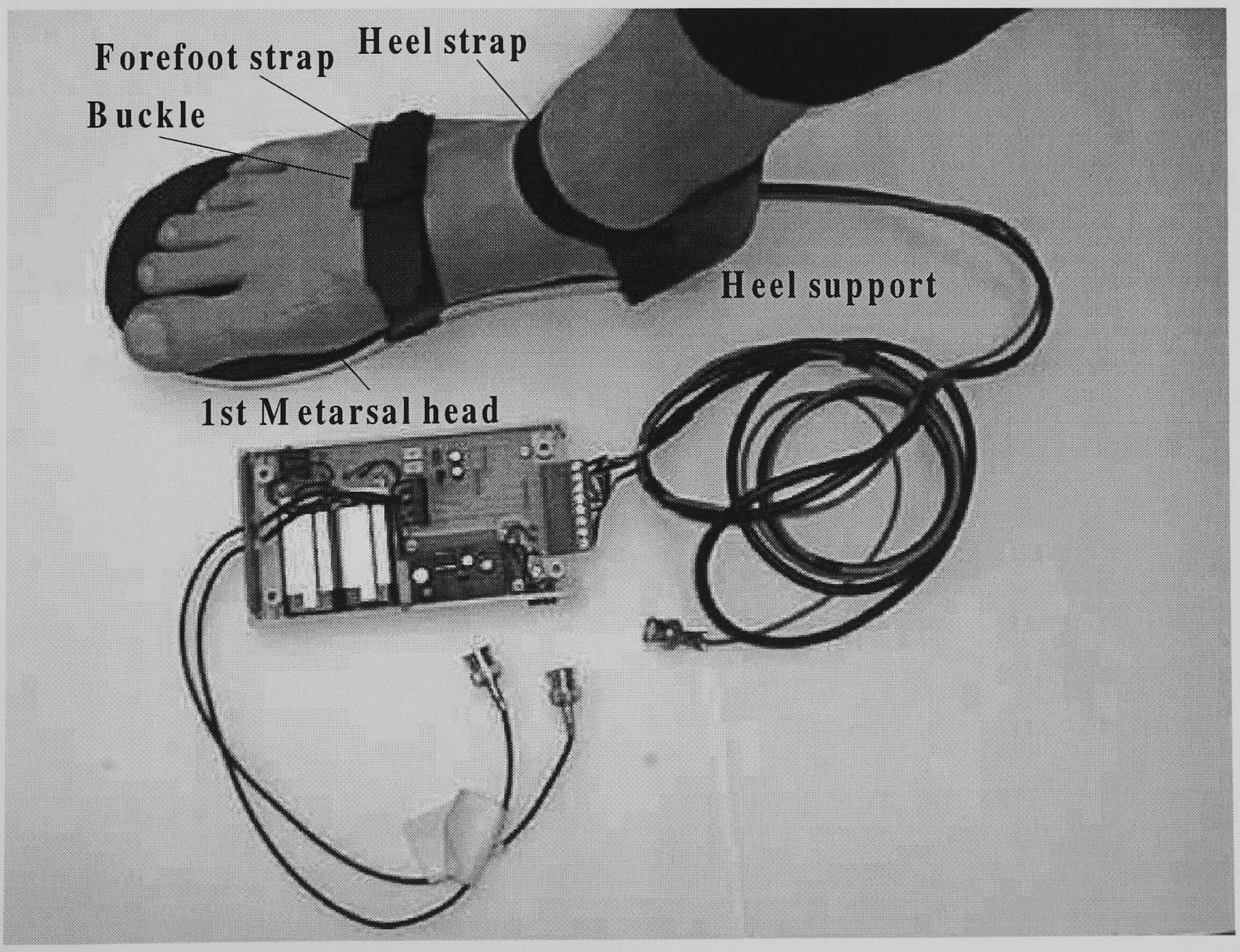

Photograph 9 Method of fixing for measurement shoe.

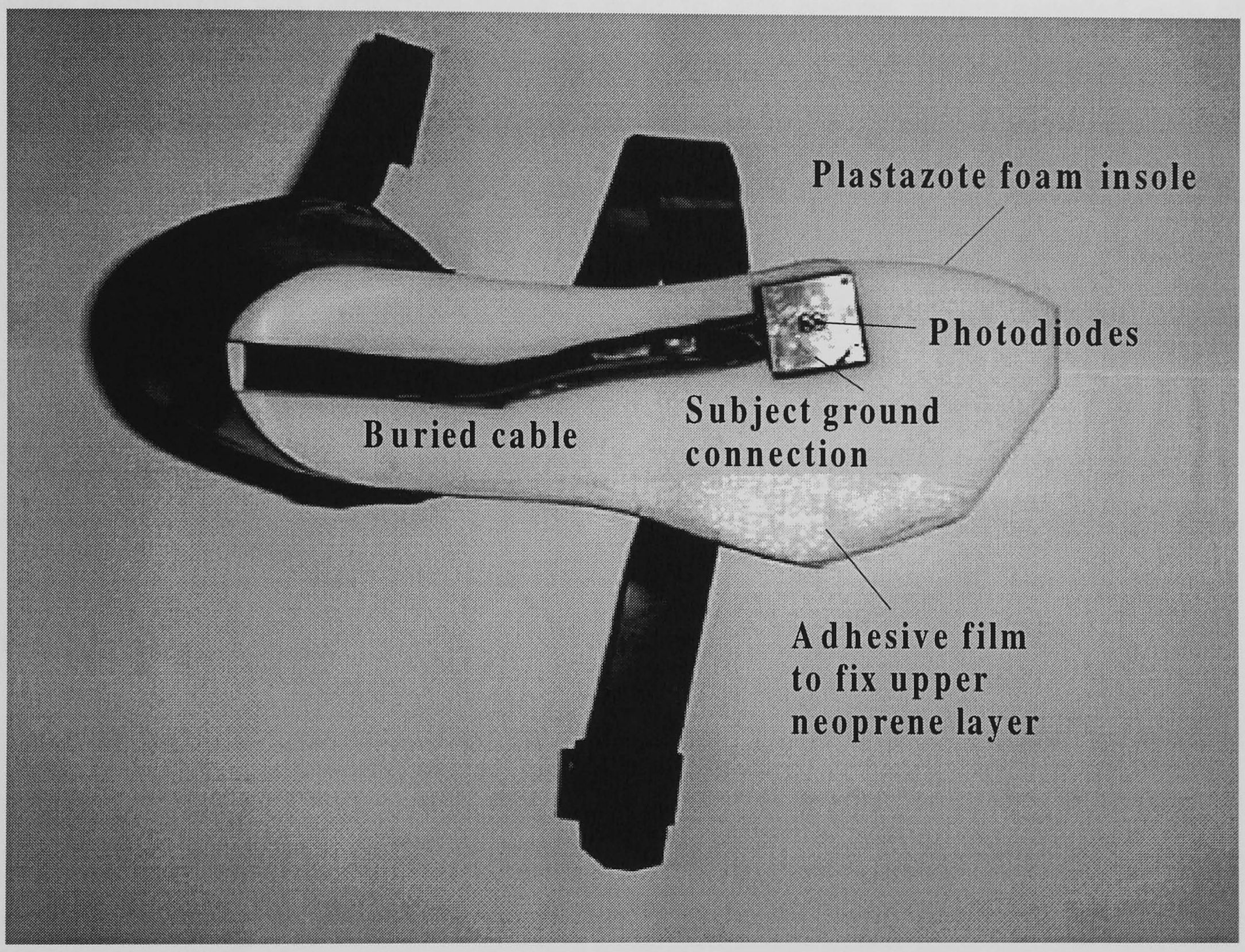

Photograph 10 Method of locating sensor in measurement shoe.

4.5 Software

4.5.1 Data acquisition and pre-processing

Software developed for the plantar monitoring system realised acquisition, processing and analysis of Doppler and load signals obtained from the sensor. Different approaches were required to deal with static and dynamic data.

Data acquisition was performed using a spool_to_disk routine, which sampled each of the three analog to digital channels sequentially and stored all of the data in a single file. This approach was required to prevent overflow of the data input buffer during disk write cycles. Additionally, the buffer memory on the acquisition card was expanded to 1Mbyte and time critical elements were achieved through assembly level, hardware calls. These methods allowed real time storage of up to 2Gbytes (68 minutes) of test data onto a pre-formatted hard disk without loss of data.

The raw data file, tagged as test_number.dat, was separated using a channel_separator routine to extract the Doppler, intensity and pressure signals. The raw data for each signal was stored in three files: test_number.lac, test_number.ldc and test_number.lod, respectively.

Each of the raw data files was processed using a verification routine to identify segments of dropout in the data. For the Doppler and intensity signals, the maximum permissible dropout for which the signal remained at 0 volts was set to 1ms. Tolerance of longer dropout segments resulted in significant under estimation of blood flux. For the load signal, the permissible duration at minimum value depended on the time taken for the swing phase of the step, which was proportional to walking speed. A value of two seconds was used. The Doppler signal was also assessed for saturation by thresholding the data at five volts. During development, signal dropout was found to occur during occlusion of the optical path and for loss of contact between foot and sensor. Both problems were overcome by using double-sided surgical tape to retain the foot in contact with the sensor. Saturation of the Doppler signal occurred at transient points of loading and unloading, due to movement artefact induced by tissue compression during dynamic studies. To overcome this problem, blood flux was only determined using data recorded during the swing phase of gait, when the signal was stable. As the duration of these periods was inversely proportional to the speed of

walking, the averaging period and hence the signal to noise ratio, decreased with walking speed. For this reason, dynamic studies were restricted to walking rates below 80 steps per minute.

4.5.2 Determination of blood flux

Computation of blood flux was based on the standard theoretically derived algorithm of Bonner and Nossal (1981). A diagram of the algorithm is given in figure 18.

Doppler data was processed by a Hanning window to reduce spectral leakage and filtered to match the required bandwidth. Each Doppler sample was normalised through division by the instantaneous, intensity value. This corrected for fluctuations in the laser output power and for variations in total backscattered light due to differences in skin pigmentation.

Filtered data was grouped into sets, each containing 2000 samples, and representing 50 milliseconds of real measurement time. The corresponding minimum frequency resolution was 20Hz. The power spectrums, of twenty successive samples sets, were averaged to achieve a signal to noise improvement factor of 4.5 . The averaged power spectrum was amplitude weighted by frequency to compensate for the inherent low frequency bias.

The weighted power spectrum was integrated over the frequency range, to provide a single blood flux value. This value overestimated flow to an extent dependent on noise generated by the detector and instrumentation. As it was not practical to determine the noise contribution during the measurement period, look up tables were used to store mean noise reference levels obtained for a range of temperatures. The measurement temperature was entered manually prior to processing, to allow the correct compensation value to be subtracted from the blood flux value. Processed data was displayed on a graph depicting blood flow versus time. To allow the load signal to be superimposed on the blood flow graph a mean value was obtained, for each second of raw load data. This approach supported observation of the relationship between changes in load and corresponding changes in blood flow.

The coding of the blood flux algorithm is given in Appendix B.

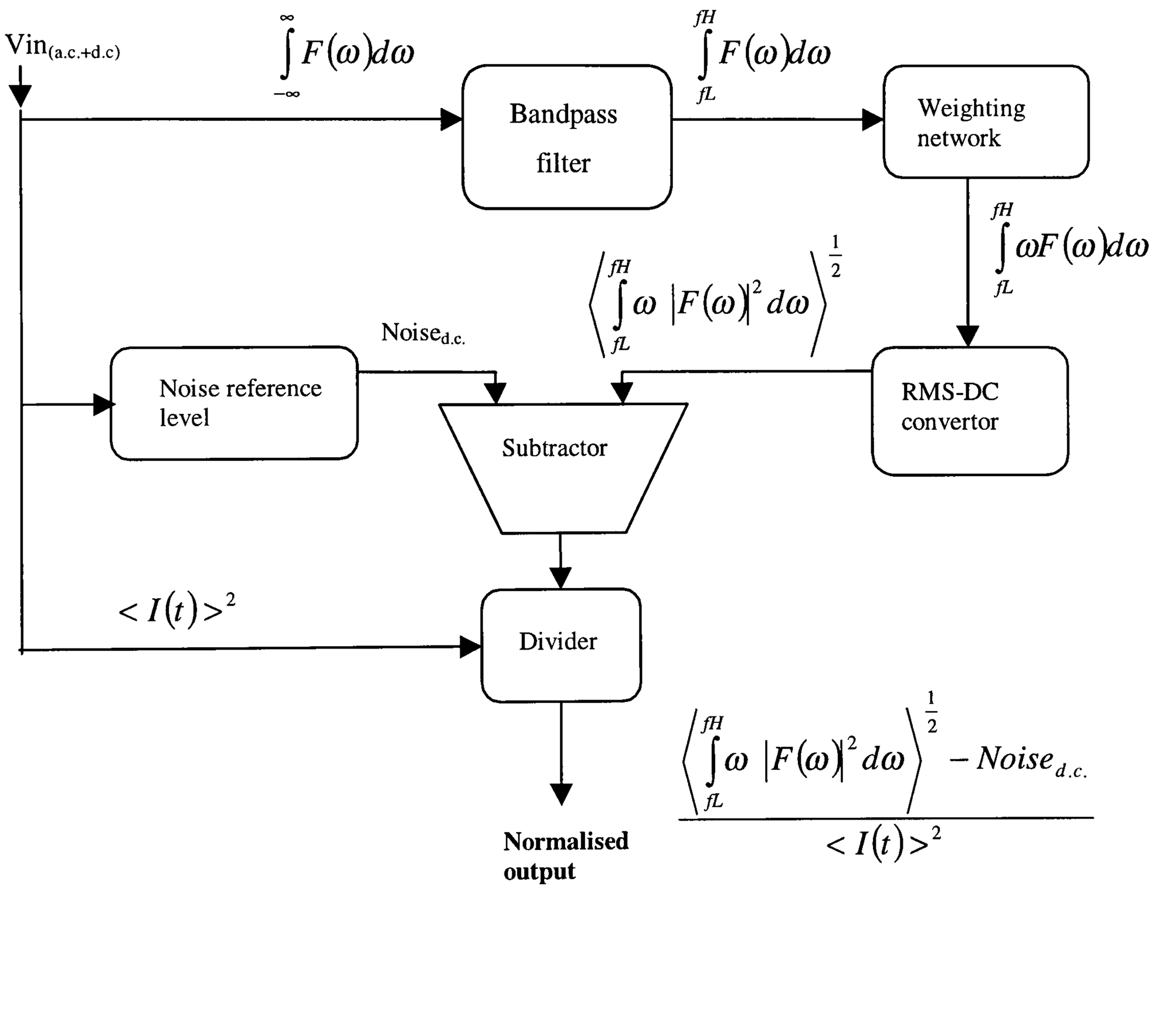

Figure 18 Block diagram of the laser Doppler processing algorithm.

4.6 Calibration

The main objective of calibrating a laser Doppler flowmetry system is to demonstrate a linear response across the physiological range of flow rates for the target tissue. This requirement is complicated by the lack of a standard reference technique for determination of cutaneous blood flow and by the difficulty of developing reliable in vitro models. Such models are generally realised at scales much greater than physiological tissue dimensions and using substitute scatterers with differing sizes and geometries to those of red blood cells (Borgos 1990). However, as these techniques are widely used in commercial systems, similar techniques were used in the present study.

4.6.1 Construction of calibration flow rig

In the following descriptions, the scattering solution is soluble starch (Merck Ltd) dissolved in boiling water by stirring for one minute. Concentrations by weight of 0.1%, 1%, 5% and 8% were prepared in 250ml of water. Solutions were stored in a refrigerator and allowed to warm to room temperature before use. A solution of 8% was the highest concentration that could be achieved without congealing. For reasons of safety, real blood was not used for in vitro assessment. Full fat milk was evaluated, however it has a limited lifetime compared to the starch solutions, which could be maintained for up to two weeks with the addition of sodium citrate as a preservative.

The initial flow rig comprised a 50ml glass syringe (Sigma-Aldrich, Perfektum glass syringe), a precision valve assembly (Merck Ltd, type stainless Luer lock valve) and a 500mm column of capillary tubing (Merck Ltd, type PEEK tubing). A low friction platform supporting a 1Kg weight was used to drive the syringe piston at a constant rate, determined manually by a valve. Various flow ranges were afforded by using tubing of different diameters from 170μm to 1mm. For higher flow rates, an absolute flow calibration was obtained by measuring collected fluid in a finely calibrated measurement cylinder over a known duration. At low rates, where droplet flow occurred, the mean droplet mass was established using an electronic balance, followed by droplet counting.

The probe assembly was located at the mid-point of the tubing column in an opaque chamber to eliminate interference from external light sources. A small square of

polyacetal sheet (Tufnol Ltd, Birmingham, England) was placed in the optical path to act as an analog for the optical diffusion that occurs in the epidermis (Liebert et al. 1998). The probe assembly was carefully aligned with the tube and the end located in the collecting receptacle. The signal level was increased by addition of a mirror at the opposing side of the tubing.

An important limitation of the flow rig was the relatively short period during which consistent flow rates could be achieved. It was observed that the flow varied in the syringe due to start and end effects, which required the first and final 10ml of flow to be ignored. This resulted in flow periods of between 20s and 180s, depending on flow rate. It was however possible to demonstrate flow rates and calculate mean particle velocities with a range close to those found in the microvasculature of 0.04-7.5mm.s^{-1} (Barnett et al. 1990). This was limited at the low end by the difficulty of obtaining a consistent flow and the measurement range for calibration was limited to 0.5mm.s^{-1} to 10mm.s^{-1}. To simplify adjustment, a graduated scale plate was added to the valve assembly. To overcome the problem of short measurement duration the flow rig was modified to include a pump and fluid reservoir to replace the syringe, figure 19.

The reservoir was designed to ensure a head pressure equivalent to that obtained by the weight in the syringe model and the output from the reservoir was controlled by the same valve assembly. With careful adjustment of the pumping rate it was possible to balance the reservoir level and hence obtain consistent flow at a rate set by the control valve. In practice, it was essential to isolate the laser Doppler probe from vibrations induced by the fluid pump and to eliminate air bubbles by purging the system. Using this technique three minutes of data was obtained over the full range of flow rates and for different scatterer concentrations. The procedure was repeated on three separate days and variations in temperature in the probe chamber were investigated. The recorded data was processed and a graph of response versus flow rate obtained.

4.6.2 Alternate methods of calibration

Although the preceding method of calibration was useful for validating the linearity of the system, an obvious drawback is the total time required to perform the procedure. For this reason, a simple method was developed for routine checking of the probe response. A calibration kit was obtained from a commercial laser Doppler company (Moor

instruments Ltd, type PFS). This comprised solutions of graded latex microspheres at specific concentrations. The microspheres exhibit Brownian motion determined precisely by temperature. Thus given a specific set of conditions a singular response of the laser Doppler system could be determined and compared to the corresponding point obtained during full calibration. The equivalence of one or preferably several such points (obtained by altering temperature) was taken as an indication that the system remained in calibration.

The single point type assessment was unsuitable for evaluating the prototype sensors because of the lower manufacturing tolerance compared to commercial systems, requiring each sensor to be fully calibrated prior to application. To reduce the calibration time to an acceptable level whilst allowing a range of particle velocities and concentrations, an alternative calibration rig was required. Syringe pumps and linear actuators have been used for calibration (Cai et al. 1995) and were evaluated but were considered too costly and difficult to construct, respectively. The system developed in this study was a simple, low cost approach using a motor to rotate a platter, onto which the scattering solution was mounted, figure 20. The scattering solution was contained in a tubular ring constructed by bonding the ends of a segment of silicone rubber tubing. This material was self-sealing following injection of the scattering solution by syringe. Care was taken to avoid introducing air bubbles and the tube was completely filled to prevent lateral movement of the solution. A polyacetal disk was placed above the tube to act as an optical diffuser.

The mean particle velocity was determined by the rotational speed of the platter, which was controlled by the DC excitation of the motor. A motor speed controller was essential to obtain consistent revolution rates at low speed. The period of revolution was determined via a frequency counter coupled to a photodiode (D) that was illuminated by an LED (E), via a reflector on the underside of the platter. To perform routine calibration of each sensor, following fabrication, and prior to in vivo measurements the response to ten velocities over the range 1-10mm.s^{-1} were obtained. The total time to perform the procedure, process the data and obtain a calibration graph was reduced from around three hours to 30 minutes.

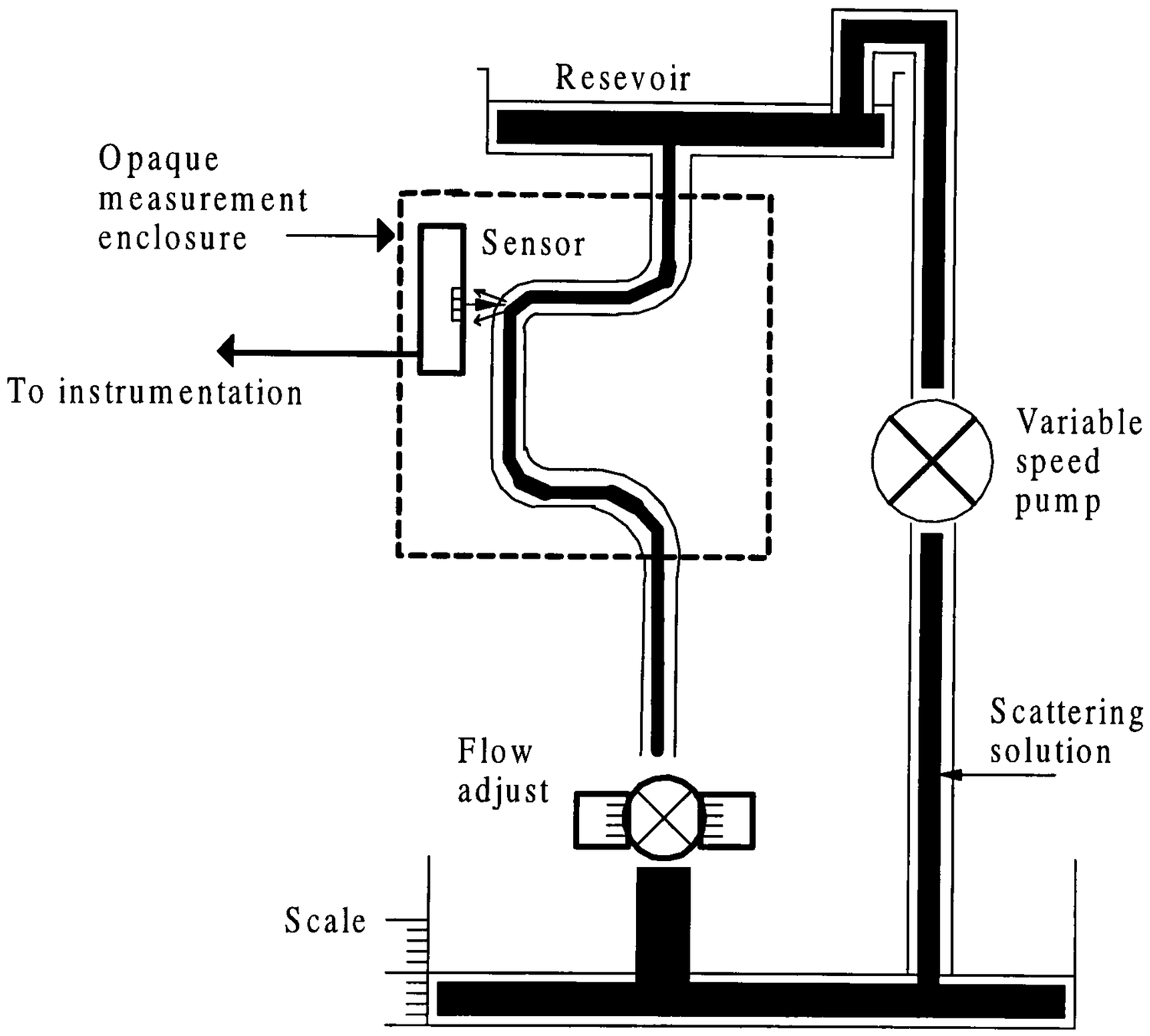

Figure 19 Calibration flow rig with sensor positioned to give maximum Doppler signal.

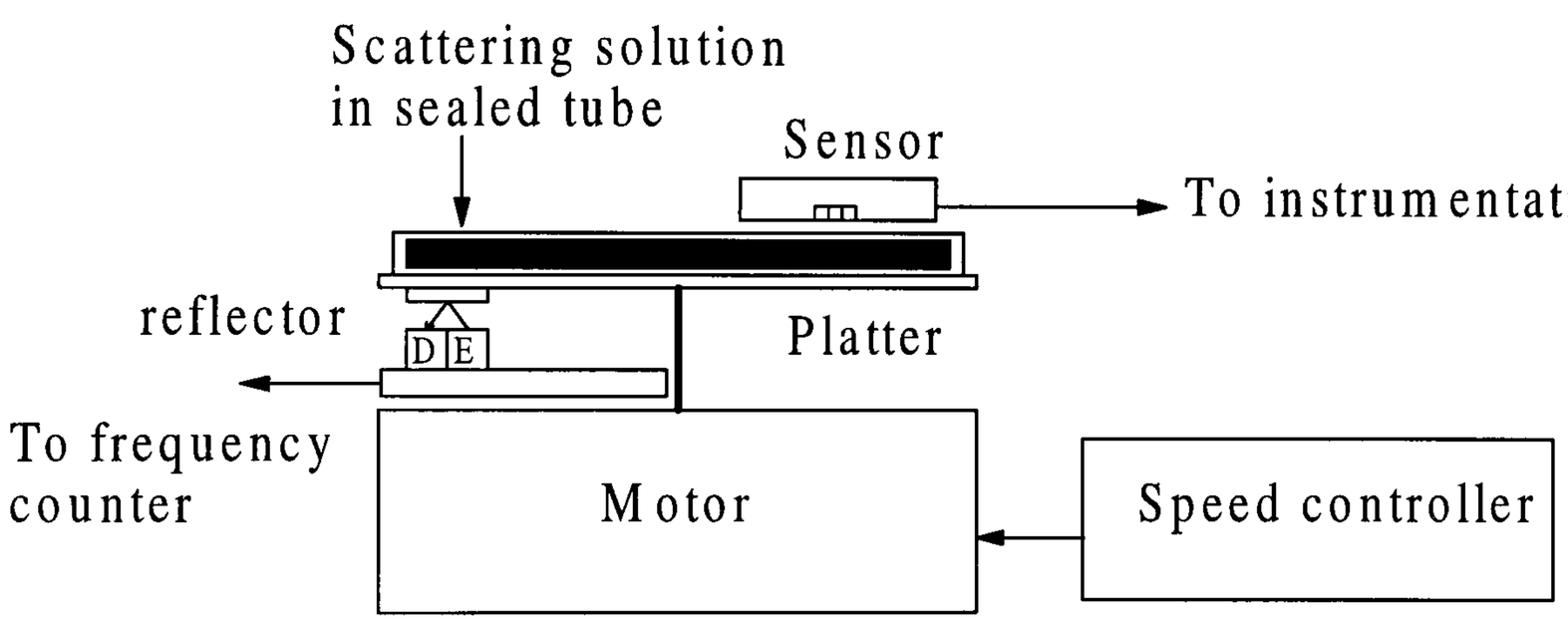

Figure 20 Rotational platter calibration unit.

4.6.3 Comparison with Doppler ultrasound

In most clinical situations, laser Doppler systems are not required to track continuously changing flow rates, whereas for the intended application this situation could arise during walking. As it was not feasible to simulate a continuously varying change using the calibration systems previously discussed, an alternative approach was developed. A peristaltic pump (Watson Marlow, model 503) was used to drive scattering solution around a closed loop of silicone rubber tubing, of differing diameters, depending on the required flow rate. To obtain a comparative reference signal a Doppler ultrasound probe (Huntleigh, model MD2) was placed adjacent to the sensor on the tubing. To prevent coupling of mechanical vibrations from the pump into the optical path, the monitored section of tubing was isolated and clamped to a second bench. The unfiltered laser Doppler flux signal was compared to the analog output waveform obtained from the ultrasound unit, using an oscilloscope. Using this approach, it was possible to demonstrate that the laser Doppler system could track pulsatile flow at different flow rates without distortion, refer to figure 6 on page 75.

4.7 Summary

Existing laser Doppler systems were found unsuitable for the proposed study and a new system was developed to allow in-shoe assessment of plantar blood flow during walking. The laser Doppler sensor was specifically designed for location under the first metatarsal head because of the high incidence of diabetic plantar ulceration in this region. Optimum signal to noise ratio was achieved using eight segments of optical fibre, which collimated light from tissue onto eight photodiodes. However, the difficulty of matching the optical characteristics of the fibres resulted in a device to device repeatability approaching 25%. To overcome this problem the optical fibres were eliminated and photodiodes were mounted adjacent to tissue. This resulted in a device to device repeatability of better than 10%. However, to obtain a comparable signal to noise ratio amplifiers had to be mounted within the sensor. Consequently, it was not possible to reduce the size of the device for incorporation in normal footwear and a custom-made measurement shoe was required for each subject. The design of the measurement shoe was complicated by the requirement to achieve relatively constant

temperature of the plantar skin and of maintaining the sensor in contact with the foot whilst allowing normal flexion during walking. The design of the instrumentation integral to the sensor was based on the standard laser Doppler differential amplification scheme. Compromises were required in order to mount the instrumentation within the sensor and signal averaging techniques were required in software to achieve an acceptable signal to noise ratio. The system also included a small power supply for the sensor and an instrumentation recorder mounted at waist level. Battery operation allowed data to be collected during walking and provided electrical isolation. Doppler, optical intensity and load signals were recorded onto the instrumentation recorded and download off-line to computer for analysis. Software was developed for the acquisition and processing of the data to extract the blood flux parameter.

In vitro calibration was achieved by developing a flow rig to allow the system response to be obtained for a range of particle velocities and concentrations. Graded latex microspheres or soluble starch dissolved in water were suitable substitutes for blood as the calibration scattering medium.

Chapter 5 In vitro results

5.0 Introduction

Results of in vitro evaluation and calibration of the plantar monitoring system are presented.

The primary objective in determining operational performance was to allow reliable in vivo estimates of blood flow to be obtained and compared. An exhaustive in vitro study was not practical; however, sufficient data was acquired to ensure representation of systematic and random errors.

Calibration of the Force Sensing Resistor is also discussed.

5.1 Sensor calibration

5.1.1 Methodology

Laser Doppler systems are difficult to calibrate in vivo (Oberg 1990), consequently a number of in vitro techniques have been developed (Mito 1992, Cai et al. 1996, Liebert et al. 1998). These models do not reflect the scale, complexity or variability of skin tissue, site to site or subject to subject. However, they are routinely used to assess the response to changes in flow rate and concentration (Barnett et al. 1990). A simple flow rig of the type described in chapter four was used to calibrate the plantar monitoring system. To facilitate comparison with published data, flow and concentration variables were matched to those used by Obied (1993), in evaluation of the signal processing algorithm of Bonner and Nossal (1981). The same frequency weighted algorithm is used for calculating the flux response in the present system.

A polyacetal disk with a thickness of 400μm was used to simulate the optical scattering of the epidermis (Boggett et al. 1986). One side of the disk was attached to the contact face of the sensor and the other abutted to a polythene tube (internal diameter = 3.0mm, wall thickness = 0.5mm) in the flow rig. The flow rate was determined by a pre-calibrated in-line control valve. This arrangement allowed the mean particle velocity to

be adjusted from 0-10mm.s^{-1}, in steps of 0.5mm.s^{-1}. A homogeneous solution of latex microspheres or dissolved starch was pumped through the flow rig. The scattering medium was diluted with pre-boiled water to achieve concentrations from 0%-0.5% by volume in steps of 0.05%. This range corresponds to the maximum haematocrit value encountered in the microvasculature (Barnett et al. 1990). To exclude ambient light effects, and allow localised control of temperature and humidity, the sensor and sampled segment of the flow tube were enclosed in an opaque plastic chamber. Within the chamber the flow tube was bent, to form a u-shape with the sensor perpendicular to the right angled bend. This arrangement placed the optical path in line with the direction of flow to maximise the Doppler scattering angle, providing the maximum frequency shift of the Doppler signal.

5.1.2 Estimation of maximum frequency shift

General characteristics of the Doppler signal were identified by averaging the frequency spectra of 100 sets of data, for each test. During calibration, the Doppler signal was monitored on a spectrum analyser. The signal was continuous and decayed with an exponential type profile, to the background noise level. Bandwidth and amplitude varied with flow rate and scattering particle concentration, respectively. The baseline of the analyser was adjusted to exceed the noise floor and the maximum frequency determined for each test.

For comparison, estimates of the frequency shift were calculated using the general Doppler equation (Barnett et al. 1990):

$$\Delta f = (2nv / \lambda) \cos\theta \qquad (17)$$

Where: n = Refractive index of scattering medium (Approx. 1.4 in tissue).

v = Velocity of the scattering particle.

λ = Wavelength of incident photon (780nm +/- 10nm at 25°C).

θ = Angle between incident photon and scattering particle (~0°).

The value of θ can be estimated by geometric consideration of the optical path and the maximum penetration depth, which for near infrared is 1-2mm (Johnson 1990). The

optical arrangement of the sensor allows detection for values of θ close to 0°. Thus $\cos\theta$ tends to unity and the maximum frequency shift predicted by equation (17), is possible for real measurements.

Estimates of the maximum frequency shift, Δf, at the minimum and maximum flow rates, achievable in the calibration rig, were:

For a mean particle velocity of $0.5 mm.s^{-1}$,

$$\Delta f = (2 \times 1.4 \times 0.5 \times 10^{-3}) / 780 \times 10^{-9} \approx 1.8 kHz$$

For a mean particle velocity of $10 mm.s^{-1}$,

$$\Delta f = (2 \times 1.4 \times 10 \times 10^{-3}) / 780 \times 10^{-9} \approx 35.9 kHz$$

Measured values of Δf were consistently higher than the estimated values, by 2% at the lower flow rate and 4% at the higher flow rate. These differences remained after the estimates were refined to include the refractive index of the polyacetal disc. When a flow regulator was substituted for the flow control valve, the difference at the higher flow rate was reduced to <2%. The original error was attributed to the difficulty of calibrating the flow control valve. However, using a set of flow regulators was impracticable, due to the difficulty of construction for lower flow rates. Furthermore, substitution of a regulator substantially increased the set-up time for each test.

The sensor instrumentation has an upper cut-off frequency of 28.2kHz, which can be shown, by equation (17), to limit the maximum resolvable particle velocity to a value of $8 mm.s^{-1}$. This value encompasses the range of red blood cell velocities found in the capillaries of the skin, which extends to $3.5 mm.s^{-1}$ (Barnett et al. 1990) for rest conditions.

5.1.3 Linearity of blood flux response versus mean particle velocity

Figure 21 shows the system response versus flow rate, for a particle concentration of 0.2% by volume, determined over the range of 0-10mm.s^{-1}. The sensor response is linear for mean particle velocities of 0.5mm.s^{-1} to 6mm.s^{-1}, above which the response is limited by the bandwidth of the instrumentation. For a bandwidth of 100kHz, the same blood flux algorithm has been demonstrated to be linear for mean particle velocities up to 14mm.s^{-1} (Obied 1993). The maximum non-linearity for any sensor, defined as the maximum deviation from the best straight-line fit, was 3.7%. At zero flow, an offset was present, which varied with the scattering media and test conditions. The magnitude of this offset suggests a contribution due to random agitation of scattering particles in addition to instrumentation noise.

Latex microspheres (Moor Instruments) of diameter 10μm were used in the experiment to approximate red blood cell dimensions. It was not possible to use this scattering medium for all of the calibration work due to the high cost. The experiment was repeated using soluble starch (Sigma-Aldrich) with an estimated particle size range of 50-300μm. The responses for the two types of media were equivalent within +/-10% over the full working range, which justifies the use of soluble starch as a scattering medium for calibration.

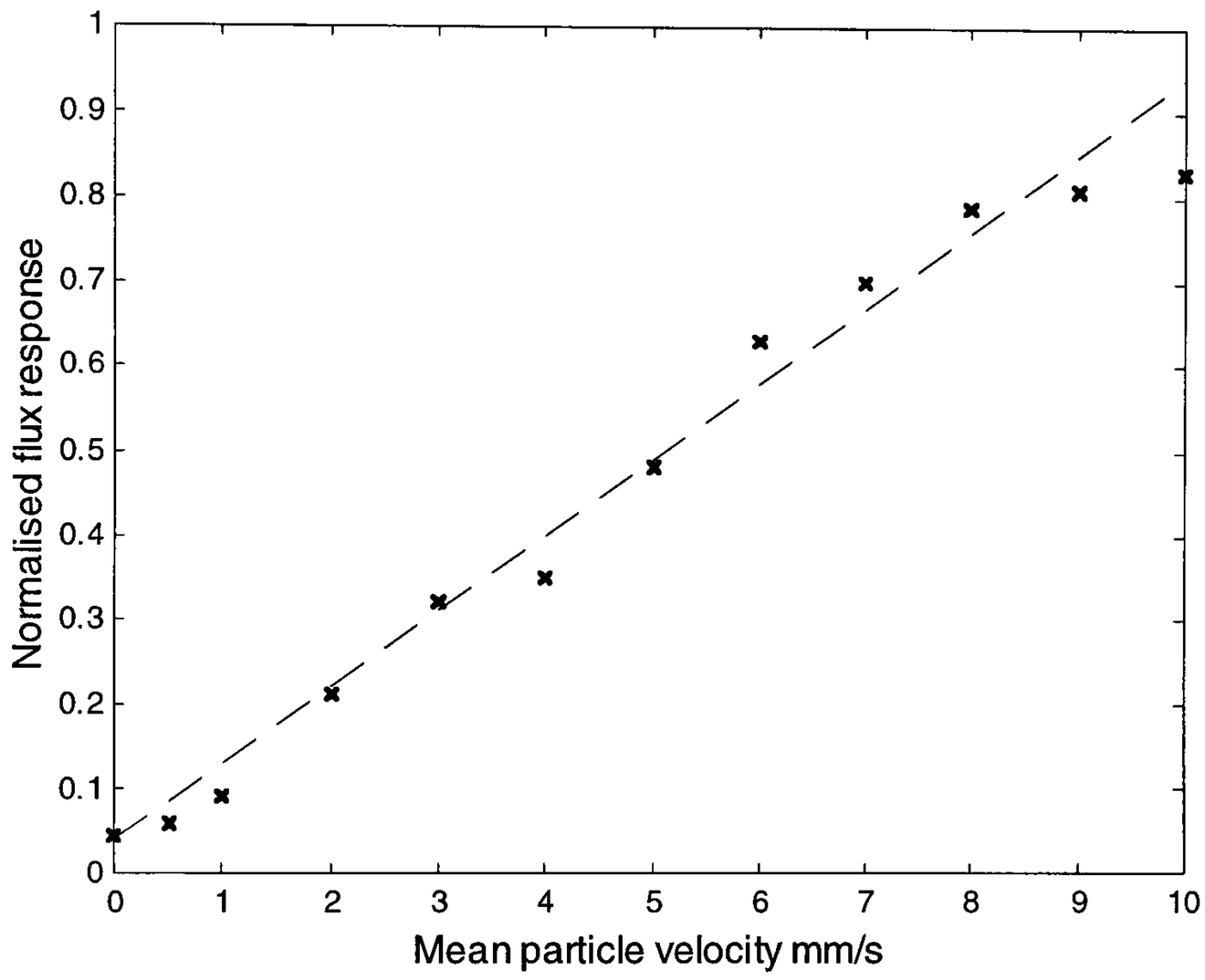

Figure 21 Graph of normalised flux response (flux / $flux_{(max)}$) for a scattering solution of 0.2% by volume, of latex microspheres. The best straight-line fit, is described by $y = 0.09x+0.04$.

5.1.4 Linearity of the blood flux response versus particle concentration

In the preceding tests, the minimum deviation from the ideal best straight-line fit occurred at a mean particle velocity of 2mm.s^{-1}. This flow rate was used to assess the system response for different particle concentrations. Figure 22 shows the corresponding normalised flux response. Figure 22 indicates a linear response for particle concentrations comparable with those expected in the capillary beds of the skin (Nilsson 1990). A best straight-line fit is superimposed for concentrations $\leq 0.2\%$ by volume. At higher values, particle concentration is increasingly underestimated due to the inherent nonlinearity of the processing algorithm (Obeid 1993). This type of response is in good agreement with the findings of similar studies (Nilsson et al. 1980, Nilsson 1984, and Obied 1993). No attempt was made to increase the linear range of the concentration response, because the in vivo requirement was limited to assessing flow in superficial vessels, where concentrations are normally within the linear range of the system.

Figure 23 shows normalised flux response versus mean particle velocity for different particle concentrations. This graph verifies that the flux increases linearly, with scattering particle velocity and concentration, over the required range for the microvasculature. Outside of this range, a non-ideal response is obtained due to under-estimation of particle concentration and instrumentation bandwidth limitations.

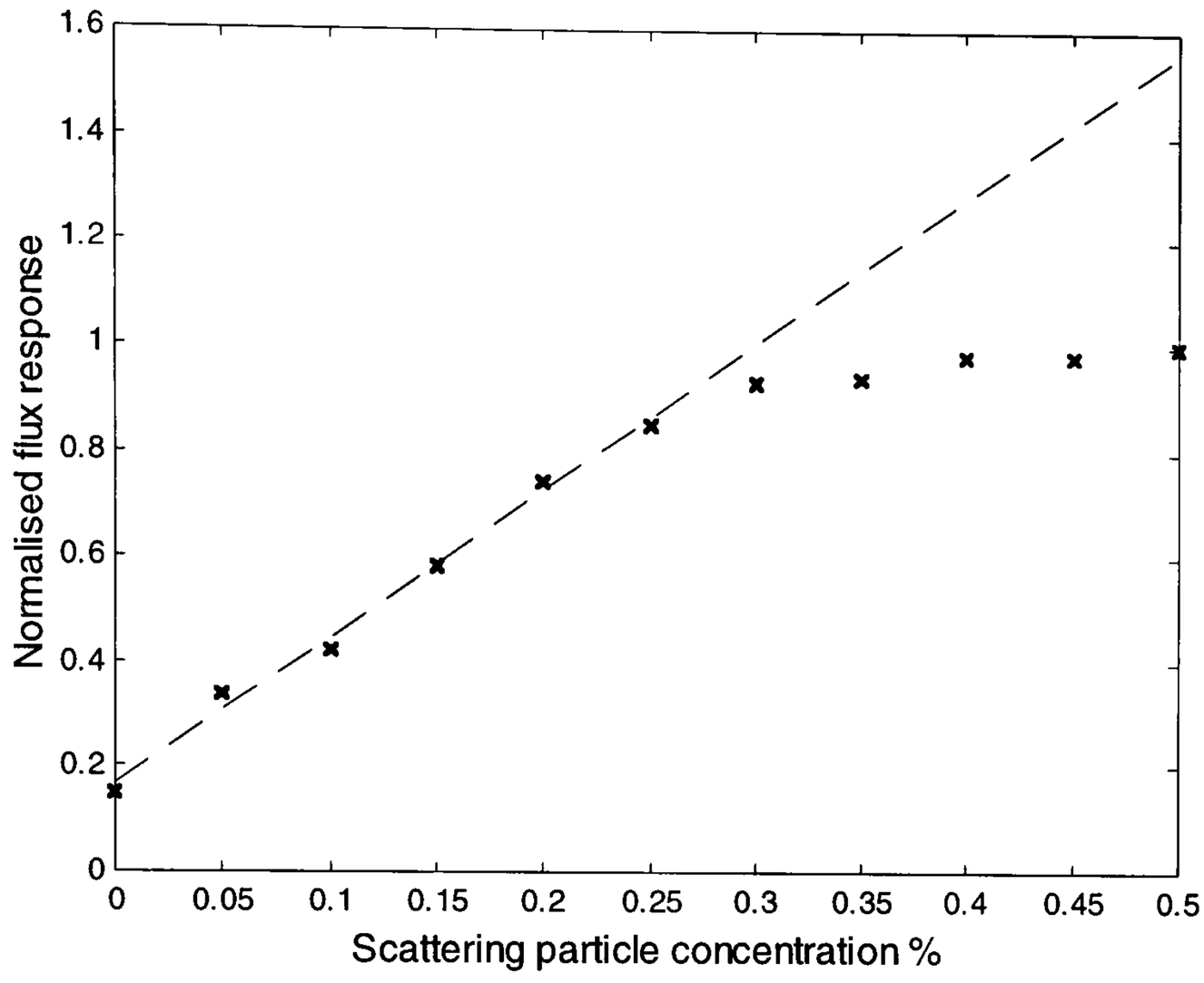

Figure 22 Graph of normalised response (flux / $flux_{(max)}$) versus scattering particle concentration percentage by volume. The best straight-line fit for the normal cutaneous microvasculature range of 0 to 0.25% is given by y=2.78x+0.17.

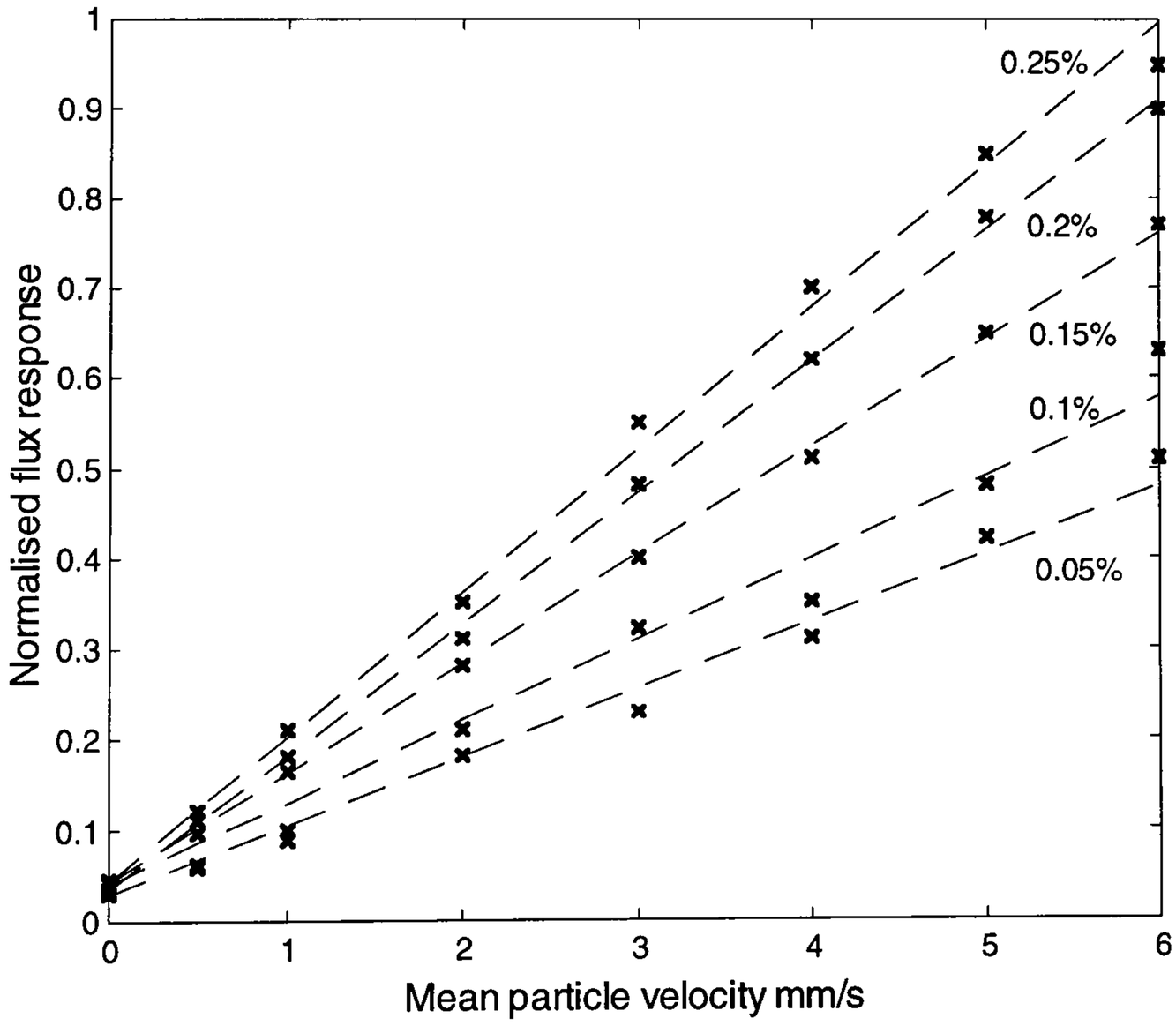

Figure 23 Graph of normalised response (flux / $flux_{(max)}$) versus mean particle velocity, at various particle concentrations.

5.1.5 Operating region and hysterisis

Several commercial systems quote a general scale factor for quantification of in vivo measurements (Borgos 1990). However, this approach is considered unreliable in the literature (Oberg 1990) as significant site to site and subject to subject variations occur in skin. For the linear region of the present system, it was possible to estimate a scale factor of 20mV per $mm.s^{-1}$, for each gram of starch dissolved in 250ml of water, this conversion proved useful for checking in vitro measurements.

The calibration data indicated a full-scale output of 3.8 volts over the full calibration range. For the limited range representing the velocities and concentrations found in skin, a maximum output of two volts was adequate, this value is subsequently referred to as the full-scale working range.

In the calibration experiments, flux responses were evaluated for both increasing and decreasing flow. When compared, the graphs exhibited small systematic differences due to hysterisis. Values for increasing flow produced a flux response up to 170mV greater than for decreasing flow, at the corresponding mean particle velocity. This important error is equivalent to 8.5% of the working range. To evaluate this problem further, a microsphere motility standard (Moor Instruments type PFS) was placed in a test chamber, and the temperature increased from 22°C to 35°C in steps of 1°C, followed by cooling. The flux response was recorded at corresponding values for both directions of the thermal cycle. Results from this experiment exhibited negligible hysterisis. It was concluded that the hysterisis error was inherent in the flow rig valve.

5.1.6 Calibration of the Force Sensing Resistor

The Force Sensing Resistor (FSR) used in the plantar monitoring was calibrated to allow blood flow to be assessed over a continuous range of plantar pressure between zero and full static loading during standing. The FSR174NS is a circular FSR with an outer diameter of 28mm which provides the closest match to the laser Doppler sensor housing diameter of 30mm. The resistance of the device varied over a range of 11.4MΩ at zero load to 4.2kΩ at maximum load. An amplifier was used to buffer the

device and provide a useful output voltage signal with a range of 0-5V. The circuit is shown in figure 24.

For calibration, metal weights and water filled containers (1L=1Kg) were used to load the device via a platform, supported by a wooden pole of diameter 30mm, incident on the device. A total load range of 0 to 100Kg corresponding to a pressure of 0-1600kPa was used. The response was obtained at ambient temperatures of 22°C and 30°C. The response is shown in figure 25, which includes both unloading and loading cycles.

The response of the sensor was logarithmic with a sensitivity range of 40mV/kPa at low load (10kPa) increasing to 0.1mV/kPa at high load (1000kPa). It was straightforward to compensate for this non-linear response using lookup-tables implemented in Labview software. However, for accuracy simultaneous measurement of temperature using an LM35 sensor (Radio Spares) proximal to the FSR was required because of an estimated temperature related drift of 1%/°C. Measurement repeatability was assessed over five loading cycles and was within 5% of full-scale. The sensor response exhibited a maximum hysterisis of 6% of full-scale at 30°C.

Off-axis loading was not assessed as the FSR is bonded to the laser Doppler sensor housing in the plantar monitoring system.

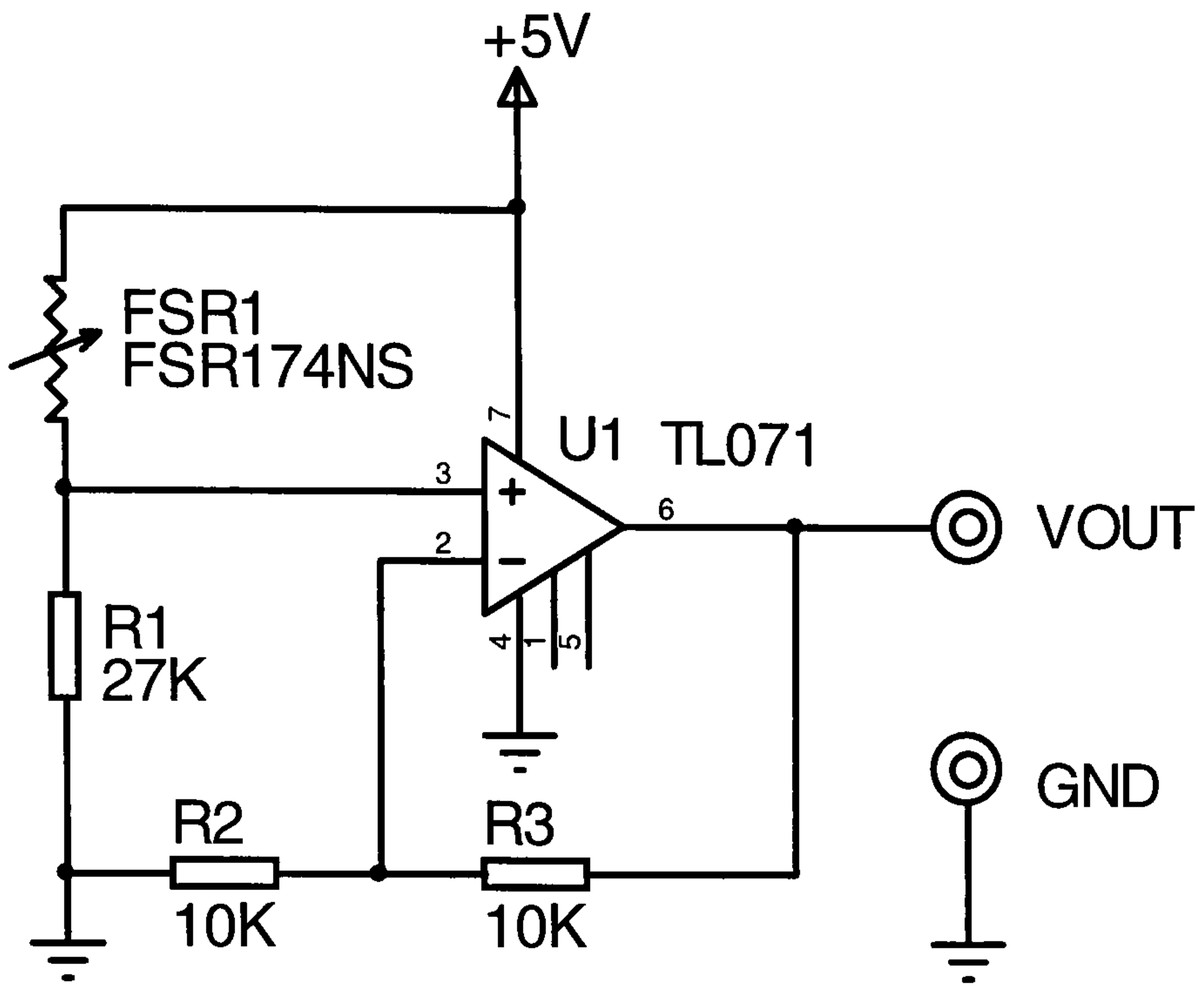

Figure 24 Buffer circuit for calibration of Force Sensing Resistor.

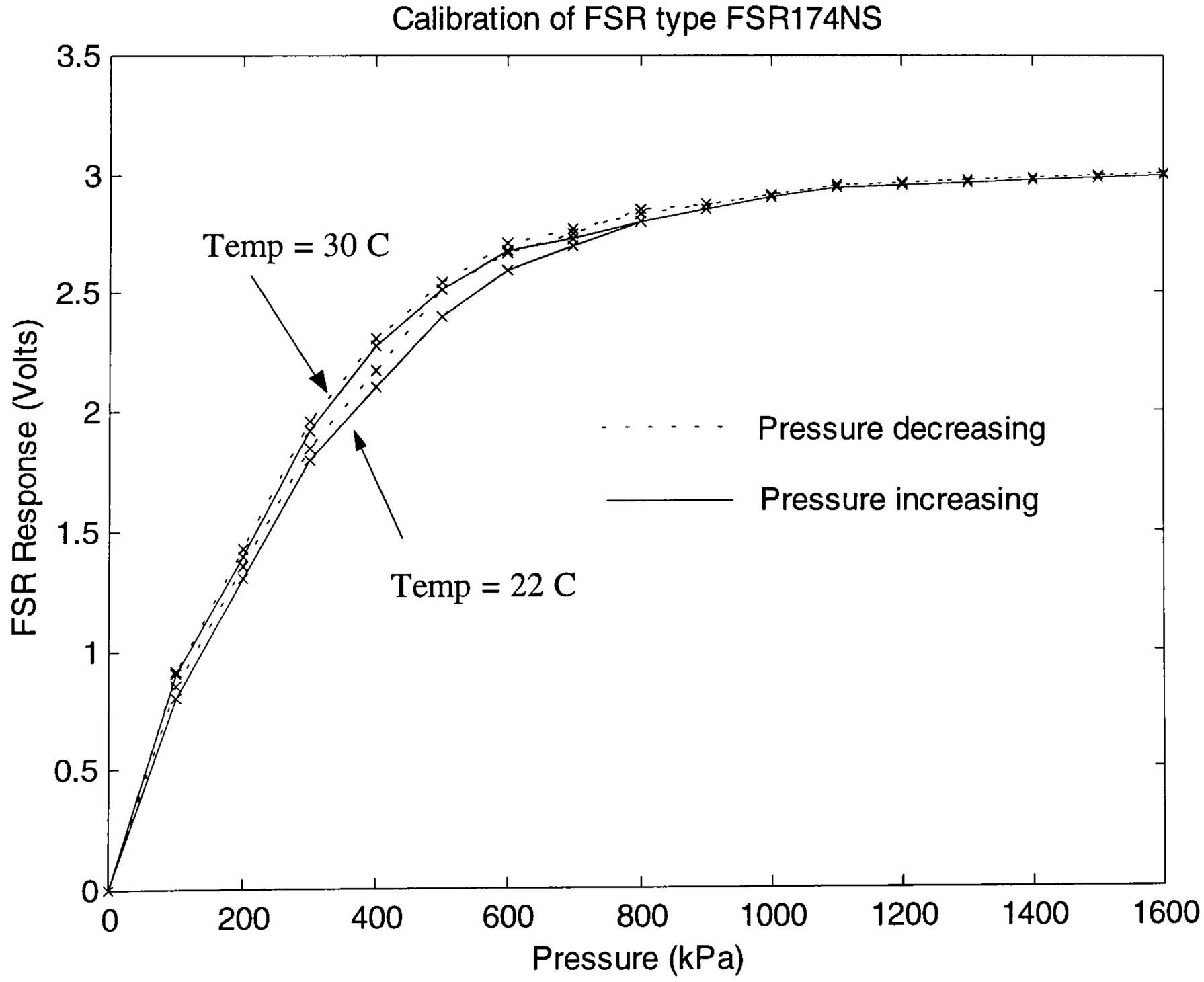

Figure 25 Calibration graph for Force Sensing Resistor type FSR174NS.

5.2 Sensor resolution

To establish the sensitivity of the system to changes in mean particle velocity, the flow control valve in the calibration rig was replaced by fixed aperture flow regulators. These were constructed from plastic pipette tips (Merck Ltd, PK series) and calibrated to provide mean particle velocities in steps of 0.1mm.s^{-1} over the range from 3 to 4mm.s^{-1}. Lower flow rates could not be achieved with precision due to the difficulty of obtaining small diameters accurately. At tested particle concentrations of 0.1% and 0.5% the incremental changes were resolvable, giving step increases in flux of 50mV± 15mV. This is equivalent to an increase of 2.5% of the full-scale range. At the lowest test concentration of 0.05%, the resolution was reduced, requiring increments of 0.2-0.3mm.s^{-1}, to produce the same change in output as for the higher concentration.

The capability of the system to resolve changes in particle concentration was evaluated by preparing concentrations of scattering medium in steps of 0.01% (100µl) by volume, over the ranges from 0-0.05% (0-500µl) and 0.15%-0.2% (1.5ml-20ml). These small concentrations were prepared by introducing saturated solutions of the scattering media into 1000ml volumes of cooled, pre-boiled water using calibrated fixed volume micro-pipettes (Merk Ltd, type 4900). For example, a concentration of 0.01% by volume required use of a 100µl micro-pipette.

The lower range was included to investigate the reduced particle velocity resolution, at low particle concentrations. It was not possible to resolve concentration changes of less than 0.05% for mean particle velocities of less than 1mm.s^{-1}. For the higher concentration range, incremental changes of 0.01% were resolved over a range of particle velocities from 1mm.s^{-1} to 4mm.s^{-1}. The corresponding increase in output flux voltage was 67mV± 5mV per increment. A satisfactory explanation for the reduced sensitivity at small values of particle velocity or concentration has not been established.

5.3 Sensor repeatability

During calibration, sensor to sensor measurement repeatability was assessed for five prototype sensors. The limited size of the measurement enclosure and problems of optical cross-talk, prevented sensors from being mounted in parallel. It was however, straightforward to substitute each sensor without affecting flow conditions in the rig. Only the excitation voltage required readjustment. A worst case difference of 220mV occurred across the five sensors, corresponding to an error of 11% of the full-scale working range. This error could not be reduced in the prototype devices without improving manufacturing tolerance or modifying instrumentation, to allow the gain of each sensor to be adjusted. For the studies detailed here, the effect of this error was reduced by compensation, in software, on a per sensor basis.

Sensor measurement repeatability over time was evaluated for a six month period at intervals of zero, three and six months. Calibration conditions were identical to those used to assess sensor to sensor repeatability. As exact conditions were difficult to recreate, a method of isolating changes in the sensor from those in the calibration rig was devised. A sinusoidal signal from a frequency generator (Thandar, model IGC2230) was injected into the anode of the laser diode. The magnitude of this signal was made adjustable, to provide a variation in optical output power of 1-50μW about the mean output power of 1mW. The laser output was reflected backward into the photodetection path, via glossed white card, located at a suitable distance to avoid detector saturation. The transfer function for each sensor was plotted manually by sweeping the output frequency of the signal generator from DC to 40kHz. Use of internally compensated operational amplifiers at moderate gain resulted in a flat response in the passband with a gradual roll-off imposed by the single pole filters of the front-end stage. With this approach, a total drift in stage gain, equivalent to an increase in flux response of 20mV (1% of full scale), was established for the six month period. This compared to values obtained using the calibration rig, of +60mV (3% of full-scale) for the zero to three-month period and +100mV (5% of full-scale) for the three to six month period.

5.4 Sensor response time

Red blood cell velocities greater than those observed in the skin at rest were expected following the end of a period of cessation of blood flow. To ensure that the sensor could respond to the increased Doppler frequency bandwidth, evaluation of response time was required. This was achieved by injecting a pulsatile signal into the anode of the laser diode and monitoring the signal, reflected from white card. A value of 40μs was established, which is consistent with the bandwidth of the instrumentation. This experiment independently confirmed, by manipulation of equation (17), that the sensor was capable of responding to mean particle velocities up to $8mm.s^{-1}$.

The maximum in vivo red blood cell velocities were expected to occur at the peak of the hyperaemic response. Measurements were made during this period under the first metatarsal head of five non-diabetic test subjects (Mean age 28 years, range 25-35 years). Tissue ischaemia was induced by standing for periods of two, four, six, eight and ten minutes. The results from this experiment indicated that flux response during hyperaemia increased in proportion to duration of loading. However, within the group, flux responses exceeded the full-scale working range of the system for mean loading periods of 6.5 minutes (range 6-8 minutes). This is an important result as it sets an upper limit on the duration for which static loading can be applied in vivo. In practice, a maximum load period of five minutes was specified to ensure that the flux response remained within the linear operating region.

5.5 Environmental factors

To evaluate the affect of temperature on response, calibration experiments were repeated, with the addition of a sealed thermostatically controlled heating element, introduced into the measurement chamber. The flux responses at the limits of the operating range (26-34°C) were compared and a mean difference of 8.4% noted. As the photodiodes are exposed at the contact face of the sensor, it is likely that this variation arises from the thermal dependence of the response of these devices. Within the range, the flux response was observed to increase non-linearly with temperature. To reduce this error, correction factors were calculated for each 1°C step, over the operating range and encoded in system software. It therefore became essential to record the ambient or

skin temperature, during in vitro and in vivo measurement, respectively. In practice, skin temperature measurements were recorded manually at the start and end of each test. The mean of the two values was used to determine the required compensation factor. This approach does not account for changes, which occur during a test, for example the increase in skin temperature during the hyperaemic response (Kabagambe et al. 1994). It is for this reason that the initial sensor specification included a requirement for continuous temperature measurement.

For in-shoe measurement, the sensor must operate in an environment with a high relative humidity (Nevill 1991). When water vapour was introduced into the measurement chamber, the output from the laser diode eventually became intermittent. This problem was resolved by sealing the connection port to the instrumentation, with epoxy resin.

5.6 Measurement uncertainty

An estimate of measurement uncertainty was made using the 'square root of the sum of squares' method (Fraden 1997). This estimate was limited to the main uncertainty components as identified in table 1 and calculated using equation (18).

$$Uc = \sqrt{u_1^2 + u_2^2 + \cdots u_i^2 + \cdots + u_n^2} \qquad (18)$$

Where Uc is the combined standard uncertainty and U_n is the standard deviation from the mean for the nth source of uncertainty.

For calibration purposes, measurement uncertainty is 8.7% of the full scale working range. With the uncertainty associated with setting the calibration flow rate excluded, the measurement uncertainty for a single sensor, is reduced to 6.3%. For comparative studies, the sensor to sensor variability increases the measurement uncertainty to 12.5%. This figure is interpreted as the typical variation in flux response across the five prototype sensors, for identical in vivo flow conditions. The value is slightly higher than the original aim of 10% of the full scale working range.

Source of uncertainty	**Calibration** Standard uncertainty (Millivolts)	**Single sensor** Standard uncertainty (Millivolts)	**Multiple sensor** Standard uncertainty (Millivolts)
Setting flow rate	120	N/A	N/A
Non-linearity	74	74	74
Sensor repeatability	N/A	N/A	220
Concentration sensitivity	100	100	100
Sensor noise	20	20	20
Combined uncertainty (% of full-scale)	174 (8.7%)	126 (6.3%)	253 (12.6%)

Table 1 Estimated measurement uncertainty for calibration, single and multiple sensor measurements.

5.7 Effects of other physical parameters

Although particle velocity and concentration are the primary factors that determine the response of a laser Doppler system, several other factors require consideration. The most important being movement artefact, sampling depth and blood oxygen levels.

5.7.1 Movement artefact

Three forms of movement artefact can arise during measurement of skin blood flow, by laser Doppler flowmetry. The first, is associated with use of optical fibres, an approach not employed in the final prototype sensor. The second mechanism arises from lateral movement of the sensor, relative to sample tissue. In the present system, the measurement shoe incorporates a sensor recess, elasticated straps and an adhesive tape, to restrain the position of the foot relative to the sensor. The effectiveness of the approach was assessed by monitoring the Doppler signal on an oscilloscope. Compared to the relatively low-level and continuous blood flow signal, noise due to lateral movement artefact tended to occur in discrete bursts, with much greater amplitude, typically limited by the supply rails. It was therefore, possible to identify periods of lateral artefact noise. Furthermore, the characteristics of this noise could be analysed in isolation, by loading the foot to reduce blood flow, and inducing relative movement between the foot and sensor. For poor sensor-fit, omission of adhesive tape, or low strap tension, the Doppler signal was swamped by movement artefact noise. At moderate strap tension, this noise was reduced to a low level, of typically ten millivolts. Thus, by ensuring that the sensor and sample tissue remained in good alignment the error in the flux response, due to lateral movement artefact, was limited to around 0.5% of full scale.

The third type of movement artefact noise arises from movement within the tissue sample volume during external mechanical loading or internal anatomical movement. For the majority of clinical applications this error can be minimised by ensuring measurements are made on subjects at rest, and with minimal probe pressure applied. During walking, substantial artefact noise can be expected during tissue loading transients. Analysis of the transient signal indicated that the blood flow and noise signals were not easily distinguished. It was therefore, evident, that a reliable estimate of blood flux could not be achieved, continuously, throughout the full gait cycle. The

solution to this problem was to restrict analysis to the unloaded, swing phase of the gait cycle. The period of the total swing phase during which valid measurements could be achieved was limited by an initial unloading transient. Extraction of a segment of the Doppler signal about the centre point of the swing phase was used to exclude the unloading transient.

5.7.2 Simulation of dynamic loading using a pressure cuff

An alternative method of obtaining dynamic data, by simulated loading, was investigated as a possible method of eliminating movement artefact noise. The technique used by Castronuovo (1987) of applying load at a measurement site using a pressure cuff was evaluated. The plantar sensor was affixed under the first metatarsal head using a double-sided adhesive ring and a pressure cuff wrapped around the foot, enclosed the sensor. Cuff pressure was increased in increments of 20mmHg, at intervals of one minute, up to the cessation level of 200mmHg (Sacks et al. 1988). Continuous recording of the Doppler signal was made for the duration of the experiment and flux responses were subsequently calculated for each of three test subjects. The response began to reduce at a mean pressure, for these subjects, of 55mmHg and fell rapidly to a minimum value. This suggests that relatively small increases in skin pressure are sufficient to stop skin blood flow - a finding compatible with results previously published in the literature, for other measurement sites (Obied 1990). This technique proved useful, for comparing some characteristics of walking response with an artefact free response. However, several problems were identified, that limited the clinical validity of the results obtained using this method. For example, the effect of the pressure cuff on overall blood flow in the foot could not be established. It was also difficult to maintain a constant load, necessitating continuous adjustment of cuff pressure. Furthermore, latency associated with inflating and deflating the cuff reduced the dynamic range of the simulated loading.

5.7.3 Sampling depth

Depth of optical penetration into tissue also alters the characteristics of the Doppler spectrum. As the sampling depth increases, a greater contribution is made by red blood cells from deeper, larger vessels, which exhibit higher mean particle velocities

compared to superficial vessels. As blood flux is normally interpreted as representing conditions in the capillary bed, significant contribution from deep vessels result in an overestimate, for this region. The magnitude of this error is dependent on skin thickness at the measurement site. Some control of the sampling depth can be achieved by: Operating at a suitable source wavelength (Gush and King 1991); excluding Doppler frequencies above those normally found in the cutaneous microvasculature (Borgos 1990); increasing source to detector separation (Jakobsson and Nilsson 1993). In the present study, the thickness of the epidermal and dermal layers under the metatarsal heads was expected to prevent significant contribution from subcutaneous vessels. This was supported by the observation that the maximum Doppler frequencies obtained in vivo were well below 12.5kHz, the upper limit of red blood cell velocity in the capillaries.

5.8 Summary

In vitro calibration of the plantar monitoring system was made using a simple variable flow rate rig with different pre-determined concentrations of scattering particle. The response to changes in mean particle velocities over a range of 0.5mm.s^{-1} to 6mm.s^{-1} was linear to within 3.7% of the best straight line fit for a particle concentration of 0.2%. The response to changes in particle concentration over the range of 0 to 0.25% was linear to within 2% of the best straight line fit for a mean particle velocity of 2mm.s^{-1}. The drift in these values over a six- month period was 1% of the full scale working range. The stated linear operating range of the sensor includes the range of red blood cell velocities and concentrations typically found in the microcirculation of the skin. Outside of this range, the response becomes increasingly non-linear due to the effects of multiple scattering. At particle concentrations of 0.1% to 0.5% changes in mean particle velocity of 0.1mm.s^{-1} were resolved. At lower concentrations, the resolution reduced to 0.3mm.s^{-1}. Sensor response time is limited by the components of the transimpedance stage, which impose an operational bandwidth of 28.2kHz. This limited resolvable mean particle velocity to less than 8mm.s^{-1}. Consequently, a maximum occlusion time of 6.5 minutes was required to prevent saturation during reactive hyperaemia. The variation in response over the operational temperature range of 26-34^{o}C was 8.4% this required ambient and skin temperature measurements to be recorded to allow for compensation in software. Measurement uncertainty was

estimated as 6.3% for a single sensor increasing to 12.6% across five devices. The use of double-sided tape to attach the sensor to the skin and correct tensioning of the restraining straps of the measurement shoe was required to minimise artefact arising from lateral movement of the foot relative to the sensor. Movement artefact due to tissue compression/decompression prevented assessment of blood flux during dynamic loading/unloading and restricted analysis to the swing phase of gait.

Chapter 6 In vivo results

6.0 Introduction

This chapter is divided into two main sections. Section 6.1 discusses pre-clinical in vivo assessment of the system. Section 6.2 describes the clinical measurement protocol and presents results from a clinical evaluation of the plantar monitoring system.

6.1 Effect of physiological factors on blood flux

A pre-clinical in vivo assessment of the system was performed, to evaluate sensitivity to physiological factors, including the effects of load, skin temperature and heart rate. These tests were performed on a group of five, non-diabetic male subjects (Mean age 28 years, range 25-35 years).

6.1.1 Relationship between blood flux and load

The Doppler signal was recorded under the first metatarsal head, for a period of ten minutes, at 0% and 50%±10% of the static load value during standing. The half load value was maintained manually by the subject via feedback from the load signal indicator on the instrumentation recorder. The mean Doppler spectrum for each load was obtained by averaging five hundred spectra. An example for a single test subject is shown in figure 26. Similar results were obtained from other subjects.

The frequency response range extended to 4-6kHz at 0% of full load, falling to 3-4kHz at 50% of full load, for the group. This was interpreted as a reduction in blood flow with tissue loading. The reduced amplitude at the higher load is consistent with a reduction in the number of blood cells in the sample volume due to loading of tissue. The amplitude of the DC component, however, increased with load - a proposed explanation is that total light reflected from skin tissue is inversely proportional to the number of red blood cells present. This finding has important consequences for the DC scaling required for subject to subject comparison, and suggests a need for compensation, that takes into account the subject specific dependency, of intensity on load. For the present study, this difficulty was overcome by restricting comparison between subjects to zero and full load. At zero-load, tissue perfusion must be independent of load. By

considering body weight, the size of the foot and the area of the sensor it was estimated that the external vertical load at the measurement site during standing exceeded a value of 35mmHg for each subject. This value is sufficient to cause closure of skin capillaries (Pfeffer 1991). The results obtained for all subjects during static loading have a blood flux level within a few percent of the instrument baseline. Therefore, it was considered that at full load, blood flow was minimal and valid comparison could be made between subjects. Under these conditions the mean intensity will be determined by skin pigmentation and the standard method of compensation - scaling by the mean intensity, remains valid.

6.1.2 Relationship between blood flux and skin temperature

Bircher (1993) states that 'Exercise has a considerable effect on cutaneous blood flux' and 'Undoubtedly among the important factors which influence cutaneous blood flux is skin temperature'. In clinical laser Doppler studies, these influences are controlled by making measurements on subjects at rest and at stable ambient temperatures, typically in the range of 25-30^{o}C, for which thermoregulatory flow is low. For these stable conditions, variations in blood flux can be considered as due predominately, to changes in nutritional flow - the normal parameter of interest. Although this approach is applicable to static measurements in plantar tissue, there are obvious difficulties in interpreting flux values acquired during walking. Consequently, an in vivo evaluation of the effects of exercise and skin temperature on blood flux during walking was made.

The effect of skin temperature on response was assessed by cooling and warming of the foot, in water, for ten minutes, which resulted in measured, mean skin temperatures of 12.5°C and 41.2°C across the group. Measurements were made at a constant ambient temperature of 23^{o}C. The dried foot was placed in the measurement shoe, for thermal insulation, and a mean Doppler spectrum averaged over five minutes, calculated as shown in figure 27. The experiment was performed on other test subjects under similar conditions. For all subjects, the individual responses demonstrated a clear dependence on skin temperature. The increased amplitude and bandwidth of the spectrum at the higher skin temperature can be explained by normal thermoregulatory mechanisms of the skin. Specifically, total cutaneous blood flow increases with temperature, and due to arteriovenous shunt flow, the concentration of red blood cells within the sample volume

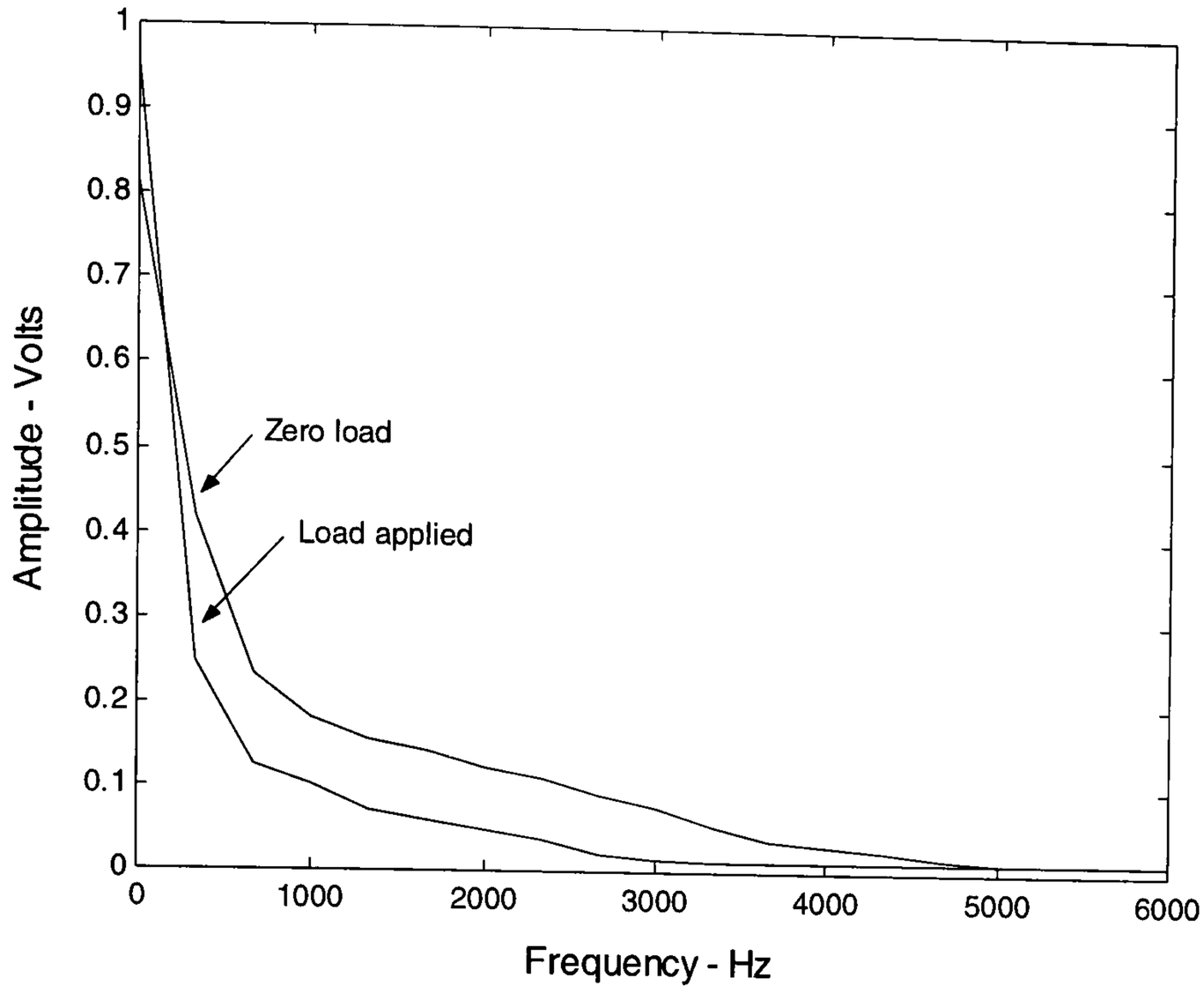

Figure 26 Characteristics of the Doppler spectrum acquired from under the first metatarsal head, at 0% and 50%(+/- 10%) of the full load value for the subject.

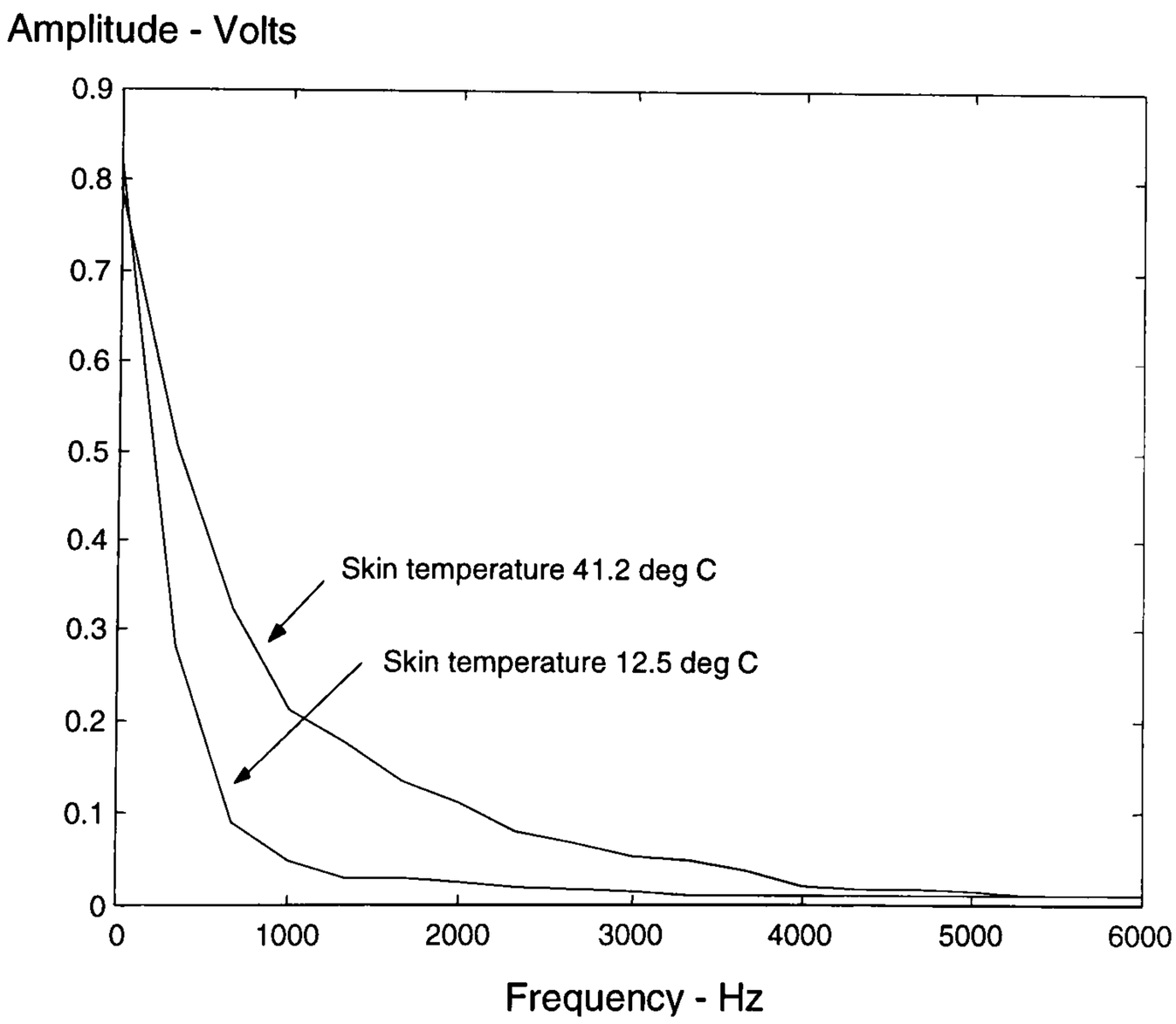

Figure 27 The mean Doppler spectrum obtained from the Doppler signal acquired under the first metatarsal head, over a period of five minutes, at measured skin temperatures (mean) of 12.5°C and 41.2°C.

is likely to increase. The result of this experiment confirmed the need for close matching of skin temperature between test subjects.

6.1.3 Relationship between blood flux and heart rate

Exercise data for the test group was acquired in-shoe, at the start and completion of a five-minute period of normal walking, following rest. The initial heart rate across the group was mean 64 BPM (range 58-70 BPM) rising to mean 79 BPM (range 66-84 BPM). Doppler spectra and corresponding blood flux values, for the two heart rates, were compared for each subject. Within the group, the maximum difference in the two flux values for an individual was 11% of full-scale. The experiment was repeated, with addition of an initial two minutes of normal walking, to allow the heart rate to stabilise at a relatively constant value throughout the measurement period. The variation in individual heart rates measured at the start of the third minute and on completion, fell to within five beats per minute and the maximum difference between the two flux values, to less than 3% of full-scale.

The results demonstrated that it is possible to establish stable measurement conditions for periods of five to ten minutes during walking for a non-diabetic test group. However, this is only correct for small variations in heart rate (<+/-10 BPM) and skin temperature (+/- 3^{o}C) over the test period. A further important advantage was the need for continuous monitoring of heart rate and skin temperature was replaced by quantification at the start and end of a test, only. This considerably simplified the acquisition system and measurement protocol.

Studies published in the literature have emphasised the significance of alcohol consumption, smoking and antihistamine on laser Doppler flux response (Li Kam Wa et al. 1990, Bircher et al. 1993). These factors were not considered in this study, however, subjects were requested to abstain from these and other stimulants, for a minimum of two hours prior, to participation.

6.2 Clinical evaluation of the plantar monitoring system

6.2.1 Study group

The main objective of clinical evaluation of the plantar monitoring system was to verify safe operation in vivo and to obtain in vivo data for analysis. Ethical approval was obtained from the Royal Bournemouth Hospital for a preliminary clinical evaluation of the system on diabetic subjects without previous plantar ulceration or prior foot trauma. A full longitudinal prospective study is needed to establish correlation between measured values and symptoms but this is beyond the scope of the present study. The hospital requested that the study group be restricted to a small group of ten patients, with follow up at 12 months. Furthermore, it was recommended that a diverse group be assessed to ensure reliable and safe operation across a range of neuropathic and vascular complications. One of the subjects was excluded at initial assessment due to an injured great toe proximal to the measurement site. The remaining subjects were all Caucasian males with a mean age of 61 years (range 53-72 years). All subjects had type II diabetes mellitus, minimum duration 12 months. These factors are important because subjects in this age range with type II diabetes mellitus have a high incidence of plantar ulceration (Williams 1994). Five nondiabetic Caucasian males, mean age 55 years (range 51-60 years), were used as a control group. The upper age limit was set to ensure a reasonable level of mobility for the dynamic test. All subjects were non-smokers and in otherwise good health, excepting the complications of the diabetic groups. The measurements were scheduled to avoid concurrent participation in pharmaceutical trials. All tests were carried out under controlled conditions at Bournemouth University and at the Diabetes and Endocrine Centre of the Royal Bournemouth Hospital. A summary of the composition of the study group is given in table 2.

Signals for subjects Control 1, Control 5 and BC exhibited drop out in some sections. This was traced to a particular sensor subsequently found to have an intermittent connection on the sensor PCB. Results for these subjects were excluded.

Subject	Age (years)	Diabetic type	Duration of diabetes (years)	Summary of existing complications
Control2	60	-	-	-
Control3	51	-	-	-
Control4	58	-	-	-
BP	53	II	2	Peripheral vascular disease, Aortic bifurcation graft (1996)
GL	54	II	4	Peripheral neuropathy
JCC	72	II	5	Peripheral neuropathy + Hypertension.
RC	57	II	2	Peripheral neuropathy
SF	59	II	15	Hypertension + Microalbuminuria
SS	72	II	1	Peripheral vascular disease + Hypertension

Table 2 General details of the study group.

6.2.2 Protocol for construction of measurement shoe

A manual inspection of the unclad right foot of each subject was performed to evaluate anatomical condition with emphasis on the plantar aspect of the first metatarsal head. Normal procedures were used to minimise cross infection. The height and weight of each subject was recorded and added to the patient record. A sheet of A3 matt paper was placed under the foot and an outline obtained, by drawing around the circumference of the foot with a marker pen. The pen was held vertical, such that the foot was contained within the outline, and the mark width was selected to be clearly visible to the seated subject. The foot was placed vertically onto a support stool and the first metatarsal head located manually, by palpation. The estimated centre of the bone was marked using a soluble marker pen. The heel was then placed to correspond with the outline and the foot carefully lowered, to transfer the centre mark to paper. This procedure was repeated three times to establish the accuracy of alignment, which was within 4mm across the whole group. Subjects JCC and RC had difficulty in aligning the foot with the outline, requiring assistance to guide the foot into position. As both subjects had peripheral sensory neuropathy this was attributed to an impaired tactile sensory or lower-leg muscular, function.

After foot size and location of the measurement site had been determined, the measurement shoe for each subject was constructed using the outline of the foot as a template. The centre position of the sensor was determined using the spatial average of the first metatarsal centre marks. The template was aligned with the orthopaedic insole such that a minimum clearance of 5mm was achieved between the sensor and outer edge of the insole. This was necessary to ensure that the sensor was adequately retained within the insole. The foot restraining straps were located immediately to the rear of the sensor location, on both sides of the insole. This provided optimum contact between the sensor and foot. A ring of double-sided adhesive tape was located on the sensor to provide adhesion to plantar skin.

Each measurement shoe was constructed to completion, except for bonding of the upper neoprene layer. Just prior to measurement, the sensor was located within the insole and the upper neoprene layer mounted using double sided adhesive tape. Tests were

performed using a set of three, final prototype sensors, in rotation. These devices were calibrated at five days prior to the first test date.

Subjects were given a prior verbal and written description of the test objectives and procedure, and formal consent was obtained. Most subjects expressed apprehension with regard to the laser, which was overcome by applying a standard laser pointer to their skin to demonstrate the technique painless.

6.2.3 Pre-test clinical assessment of study group

A qualified research nurse specialising in diabetes and familiar to the diabetic subjects assisted throughout the clinical evaluation. A comprehensive clinical evaluation of all subjects was performed within 14 days prior to the present study. Evaluation of peripheral sensory neuropathy was assessed subjectively using graded monofilaments and quantitatively using a vibration perception test (Biothesiometer). Tests were made at five sites on the foot with the biothesiometer threshold for neuropathy taken as 30V in accordance with previous studies (Cavanagh and Ulbrecht 1994). Two simple tests were used to detect autonomic neuropathy. The difference between maximum heart rate and minimum heart rate was counted for each of three ten second cycles with the subject inhaling deeply at a rate of six times per minute. The mean difference over the three cycles was calculated and a value of 15 used as the normal value. The second test measured blood pressure with the subject supine and then at one minute after standing. A drop of 10mmHg or less was considered normal and a drop of 30mmHg or more was considered indicative of autonomic neuropathy. The test was repeated three times and the mean recorded. Valsalva's manoeuvre was not used because of the possible risk to subjects with cardiovascular complications. Peripheral vascular disease was assessed by determination of the ankle:brachial index, with values at or above unity taken as normal. Urine testing of microalbumin was performed and an Albumin:Creatinine ratio (ACR) >2.5 considered an indication of microalbuminuria.

Data for glycosylated haemoglobin HBA1 was not available and blood glucose control was assessed from recent data on fructosamine levels. Concentrations higher then 360µmol/L indicated poor control. All of the subjects in the present study had good control achieved by diet.

None of the test subjects had a history or current evidence, of oedema in the right foot.

Full details regarding the pre-evaluation clinical assessment of these subjects is given in table 3.

Subject	Body Mass Index	Ankle: Brachial Index	Fructosamine concentration (μmol/L)	Albumin: Creatinine ratio	Vibration Perception (Volts)	Variation in heart rate (BPM)	Systolic pressure drop (mmHg)
Control2	18.7	>1.0	-	-	<30	14	8
Control3	21	>1.0	-	-	<30	22	3
Control4	19.3	>1.0	-	-	<30	17	7
BP	25.6	0.7	310	1.5	<30	24	17
GL	28.3	>1.0	280	1.2	46.1	8	31
JCC	27.7	0.9	310	0.8	38.7	5	38
RC	31.6	>1.0	260	1.9	41.2	3	34
SF	23	0.9	340	12.1	<30	16	6
SS	29.8	0.6	270	2.3	<30	28	21

Table 3 Clinical data for the study group assessed within 14 days prior to testing.

6.2.4 Measurement protocol

The testing procedure commenced with a rest period of ten minutes, after which plantar skin temperature, pulse and blood pressure were recorded. Blood oxygenation levels were assessed using a pulse oximeter (Nellcor model N100). The foot was then warmed in water at 30°C, for 3 minutes. During this period, the upper seal of the double-sided adhesive tape on the sensor was removed. The foot was dried and the heel located in the measurement shoe. The forefoot was lowered into position manually to ensure alignment of the first metatarsal head with the sensor. The foot restraining straps were adjusted to obtain a close and comfortable fit and a nominal signal level of two volts. The skin temperature of the foot was determined by inserting an electronic thermometer under the foot close to the first metatarsal head. The subjects heart rate was determined by counting the pulse manually at the wrist.

For static tests, the recorder and instrumentation were located on the floor close to the foot. For dynamic measurement the equipment was suspended from the left shoulder via a strap, the length of the sensor cable was adjusted, by coiling to suit each subject. The laser was activated and adjusted to an operating current of 50mA, corresponding to an optical power of 1mW at the skin. At rest and during recovery the subject was seated with the heel on the floor and the forefoot slightly elevated to prevent loading. For static loading the subject stood normally without support. Dynamic data was obtained during walking at normal speed. The following data was obtained: Three minutes at rest, two minutes static loading, two minutes recovery, one minute at rest, three minutes static loading, three minutes recovery, one minute at rest, four minutes static loading, four minutes recovery, five minutes walking. This protocol provided a means of determining if the blood flux response was proportional to the duration of loading. Between each loading cycle a further five minutes of recovery was allowed to ensure clearance of residual vasodilators and a return to rest level. Prior to dynamic measurement, a three-minute period of acclimatisation was used to stabilise the heart rate. Data was not acquired during these periods because of the limited capacity of the recording equipment.

During measurement, an indication of signal validity was available from the signal meter of the instrumentation recorder and audibly via headphones. It was not possible to

monitor the signals using an oscilloscope due to the requirement for electrical isolation of the subject, as stipulated by the Royal Bournemouth Hospital. After completion of the test sequence, the laser was switched off and the foot carefully removed from the shoe to avoid damage to the skin by the double-sided tape. It was noted that the sensor induced some weak marking of the skin at the location of the photodiodes and the foot was monitored visually until these marks disappeared. The longest period for post measurement recovery of skin was twelve minutes, (mean = 4 minutes, range 2-12minutes).

6.2.5 Processing and analysis of test data

Total test duration was limited by the capacity of the instrumentation battery, available disk space and the performance of the software. The test sequence typically generated 750 Megabytes of data and required four hours to download and process, per subject.

The laser Doppler algorithm was applied to extract the blood flux signal and a one Hertz averaging filter applied to the load signal. Additional signal processing was required, to remove noise, due to movement artefact and for extraction of event times. Some base line drift of both load and blood flux signals was observed, although this was less than 5% of the full-scale range, for both signals, across the study group.

It was noted that movement artefact could be observed directly from the load signal and was correlated with noise present in the blood flux signal. The amplitude of the movement artefact varied considerably from subject to subject. This was attributed to subject sway as part of the normal balance mechanism during standing. Consequently, load and blood flux signals were filtered using a first order, low pass Butterworth filter, with a cut-off of 5Hz, implemented in software.

Observation of the load signals from different subjects, indicated variation in the time at which loading and unloading occurred (within +/-10s), relative to the start of the static loading test, and in the duration of each load and recovery period. These variations occurred because of differences in subject response due to the method of manually specifying times of loading and unloading. Precise times of each event were obtained from the unfiltered load signal by applying a software comparator with an upper

threshold set at 75% and a lower threshold set at 25% of maximum load. These times were then used as indices to extract the blood flux signal corresponding to the unloaded recovery periods. This provided a method of identifying the regions of interest relative to loading and unloading events.

Mean resting blood flux values for each rest period were compared and found to differ by less than 10% for each subject for different loading times. This was considered to indicate that sufficient time had been allowed for a return to resting levels prior to each test. To simplify analysis the mean resting blood flux value for all tests was used to indicate the mean resting level.

Static data obtained for the study group was analysed and several important measurement limitations and signal characteristics were identified:

The restricted duration of the recovery period, for which data was obtained, was insufficient to show a return to resting levels. Other studies involving assessment of reactive hyperaemia have identified the rise time to the peak and the time to recover to 50% of the peak value, as the parameters of interest (Fagrell 1991). The results of the present study indicate a reduction close to 50% of the peak for most subjects, within the recorded portion of the recovery period.

6.2.6 Definition of biological zero

The general form of the recovery period of the blood flux signal following loading, is a rapid increase to a peak value, followed by a slow decay toward rest levels. This response is typical of a reactive hyperaemia following pressure-induced occlusion of the microcirculation (Fagrell 1991). Changes in optical intensity proportional to loading were noted. This was an important finding because the blood flux signal is directly proportional to optical intensity. This problem has been overcome in other studies by varying the laser output power to maintain constant intensity during loading (Sacks et al. 1988). However, in the current study these variations were observed to be subject specific. It could be argued therefore that varying the output intensity of the laser would invalidate the standard normalisation process, required for comparison between subjects, because of differences in pigmentation. To overcome this difficulty amplitude

scaling was done on a per sample basis rather than by mean intensity taken over a period equal to the update rate (Obied 1993). The approach used in the present study results in a consistent baseline and is considered a reliable representation of 'biological zero' because as previously estimated, the pressure on the skin is sufficient for capillary closure during full load. Therefore, comparisons in terms of amplitude of the blood flux signal were considered valid. This is important because it overcomes the difficulty associated with laser Doppler studies of tissue under load, which have been commented on by Sacks et al. (1988) and Kabagambe et al. (1994). For example Sacks et al. (1988) found that during expected zero flow conditions the instrument response was 30-40% above the instrument base line, and attributed this to random RBC movement within tissue. It is important to stress that the arguments given here in support of the instrument baseline being equal to 'biological zero' are based on estimates and manual observation that the pressure on the skin is sufficient to cause capillary closure. As there is no way of confirming the validity of these estimates, other forms of evaluation were also devised. The most obvious solution and one routinely used in general laser Doppler studies is to make comparisons based on changes in blood flux measured relative to the mean resting flux (Fagrell 1991).

6.2.7 Determination of minimum load period for a hyperaemic response

In the present study it was considered that the blood flux at peak hyperaemic response represents a well-defined physiological state - that of maximum flow. It could be argued that the impaired hyperaemic response that can occur with autonomic neuropathy would prevent identification of the peak in some subjects. However, an absent hyperaemic response is consistent with advanced autonomic dysfunction, which results in constant dilation of the affected vessels (Boulton 1994). Therefore, the maximum value of the blood flux could be considered similar to the hyperaemic peak for these cases. The results for the present study show a clearly discernible peaked response for all subjects. However, the duration of occlusion required to obtain a definite hyperaemic response under the foot was unknown. To estimate this value, a collateral study was performed on five healthy volunteers (mean age=32 years, range 25-60 years) using the plantar monitoring system. Static loading was applied for periods of 30 seconds to 300 seconds, in increments of 30 seconds, with a rest period of five minutes between each cycle. In all cases, the type of response obtained for load periods in excess of 90 seconds was a

rapid increase to a well-defined peak value. For load periods less than 90 seconds, the nature of the response was less well defined. For this reason, the minimum loading time used in the clinical evaluation was 120 seconds.

6.2.8 Physiological interpretation of the response

Following unloading, blood flux increased linearly from zero to maximum, at a rate that varied across the group. This type of response can be explained by considering the reperfusion of tissue following removal of load. During this period, the RBC concentration in the sample region must increase. This increase is intrinsically linked to RBC velocity and blood flow. It is therefore only possible for the blood flux to increase linearly if the RBC concentration is increasing linearly and the rate of blood flow is constant. It is suggested that the rate of increase of blood flux after unloading is proportional to mean blood flow into the tissue - a parameter of clinical interest.

Conversely, in the period following the hyperaemic peak, the sample volume has been re-perfused and the RBC concentration can be considered to have attained a relatively constant, nominal value. The character of the response during this period is, therefore, predominately determined by flow rate. Across the study group, this response was characterised by a consistent decay in blood flux for periods of between 40 and 100 seconds after the peak. Subsequent oscillations are observed in the response with considerable variation in amplitude and frequency between subjects. Although these oscillations are normal during a hyperaemic response (Fagrell 1991) it is unclear if they are important clinically. Therefore, analysis was restricted to the initial non-oscillatory period of the recovery. It is suggested that the response during this period is more likely to arise from the period of loading alone, whereas subsequently, local metabolic factors may become increasingly significant.

6.2.9 Problem of specifying blood flux measurement units

The remaining analysis problem relates to quantifying the results. As there is no 'gold standard' method of determining mean blood flow in a comparable sample of cutaneous tissue, in vivo calibration of a laser Doppler system is not generally feasible. One study (Simonen et al. 1997) has provided data on the normal variation in cutaneous RBC concentrations and RBC velocities, however this was based on a relatively small (n=28)

group of unmatched normal subjects. Changes in the rheology of blood in diabetes mellitus can occur which affect plasma viscosity (MacRury 1990) and nonenzymatic glycosylation can affect the deformability of the RBC membrane (Watala 1992). Either of these conditions could result in RBC velocities and concentrations outside the normal range for non-diabetics. It is therefore not valid in the present study to extract values for RBC velocity from the blood flux, without independent measurement of RBC concentration. Results are therefore expressed in terms of the standard laser Doppler parameter - blood flux, which has arbitrary units.

Figure 28 Indicates the parameters assessed in the static study. The rise time is defined as the time for the blood flux to reach maximum, relative to the time at which the load signal reaches zero. The recovery time is defined as the time for the blood flux to fall to 50% of the maximum value. The relative increase is defined as the percentage increase in blood flux from the mean resting level to the maximum value.

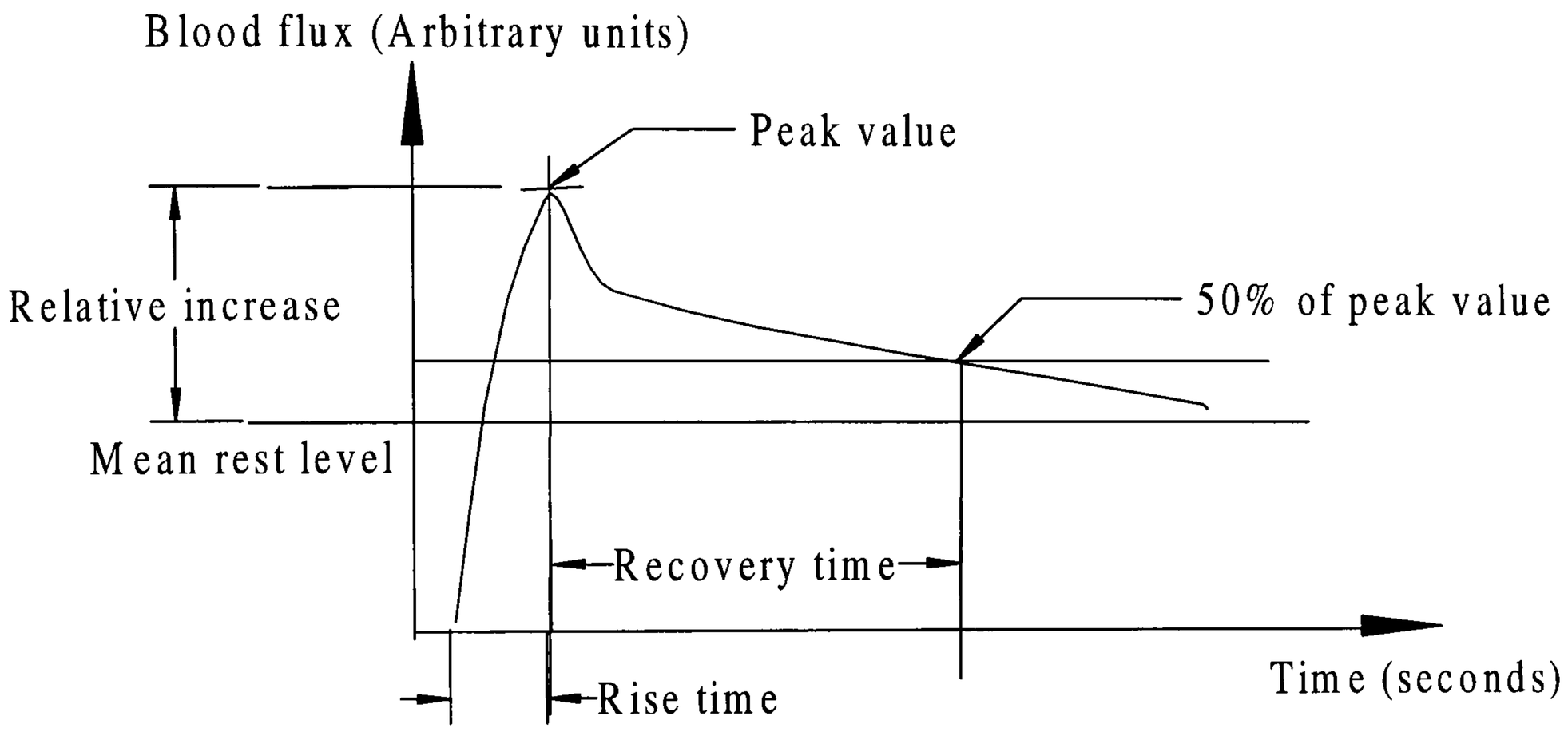

Figure 28 Method of characterisation for static tests results.

6.2.10 Results of static tests

The results for evaluation of the system during static loading are presented in this section. Table 4 (page 157) summarises general clinical data obtained at the time of testing. Changes in heart rate from rest to test conditions were low, indicating subjects were not stressed by testing. Blood pressures for some subjects were elevated consistent with existing hypertension noted in the hospital database. Values for oxygen saturation ($Sa0_2$) are above 95%, for all subjects, which suggests that RBC concentrations are normal and comparisons of blood flux are valid.

Table 5 (page 157) Summarises data regarding plantar skin temperature at the measurement site at rest, after pre-warming and on test completion. In all cases, the relative increase (Final temperature minus Pre-warm temperature) was sufficiently low to satisfy the measurement criteria for thermal stability (<+/-3°C).

Figures 29a-29c (page 158) show the blood flux response under the first metatarsal head for a non-diabetic control, diabetic neuropath and diabetic vascular subject for equal loading times of 120 seconds. The response for the control and neuropathic subjects show a hyperaemic response with a rapid rise to a well-defined peak followed by a gradual recovery. In contrast, the response for the vascular subject is a slower rise to a much broader peak. The control subject recovers to 50% of peak value within less than half of the recovery period, whereas the diabetic subjects have blood flux greater than 50% of peak at the end of the recovery period. Note that resting blood flux is substantially lower for the control subject than for the diabetic subjects.

Figure 30a,b (page 159) compares the response to different loading times for a control subject. Both graphs show a similar type of response.

Figures 31a-31c (page 160), compare the response to different loading times for a diabetic with neuropathic complications. All three graphs show similar features. The blood flux remains above the 50% peak value for all cases.

Figure 32a-32c (page 161) compares the response to different loading times for a diabetic with vascular complications. All three graphs show similar features. An

important observation for this subject is that the response in each case is substantially lower than the mean resting flux level.

Table 6 (page 162) summarises the results from the static loading study for all subjects.

Figure 33 (page 163) shows mean resting blood flux for all subjects. This data is included as it indicates increased resting flux in the diabetic foot in comparison to the normal foot, which is consistent with the findings of other studies (Flynn et al. 1988, Barnes et al. 1991, Shaw and Boulton 1997).

Figure 34 (page 163) shows the rise time to the peak of the response from the time at which the load falls to zero, for the various load times. The results suggest that the rise time is independent of load duration. The maximum difference in rise time is 3s in the control group and 9s in the neuropathic group. The rise time following loading for 180s, for subject BP was found to be due to a partial reloading of the foot during the recovery period. With this value excluded, the maximum difference in rise time is 14s in the vascular group.

The relative increase in blood flux from mean resting flux to the peak was assessed, figure 35 (page 163) compares the results for different loading times. Five subjects show a greater relative increase for the longer load time. Subject SS has a negative relative increase indicating that blood flux falls below mean resting levels following loading, a consistent finding for this subject.

6.2.11 Repeatability of static results

Measurement repeatability was assessed for one control and two diabetic subjects. Results are summarised in table 7 (page 164). The first two tests were made sequentially during which the subject continued to wear the measurement shoe. The third test was made on the following day with both the sensor and measurement shoe refitted. The same sensor was used for each subject in all tests. Differences in physiological factors including heart rate and plantar skin temperature were minimised as far as possible. These results suggest that repeatability is better than 10% for consecutive measurements without refit of the measurement shoe, increasing to 25%

after refit. The latter figure also includes the effects of physiological changes over the 24-hour period separating the non-consecutive tests. The control subjects exhibited repeatability of better than 5%. This difference in repeatability could relate to the impaired microcirculation in the diabetic subjects.

Figures 36 to 38 (page 165) show the variation in mean rest flow, rise time and relative increase from mean rest to peak, respectively, for different tests.

Subject	**Heart rate (Rest - BPM)**	**Heart rate (Test - BPM)**	**Blood pressure (mmHg)**	**SaO_2 (%)**
Control2	60	63	155/72	98
Control3	76	71	149/74	98
Control4	62	64	150/79	99
BP	68	70	152/77	97
GL	89	84	140/71	98
JCC	74	72	168/77	98
RC	82	81	159/81	97
SF	81	78	160/75	99
SS	58	65	180/86	96

Table 4 Clinical data obtained at time of testing.

Subject	**Rest** (°C)	**Pre-warm** (°C)	**Final** (°C)
Control2	27.8	29.1	28.4
Control3	27.6	28.8	28
Control4	28.6	29.7	30.3
BP	28.5	29.4	29.9
GL	30.8	30.4	30.5
JCC	29.4	30.2	29.8
RC	28.2	29.1	29.7
SF	27.6	29.1	30
SS	27.2	29.3	29.7

Table 5 Plantar skin temperatures measured under the metatarsal head.

(a)

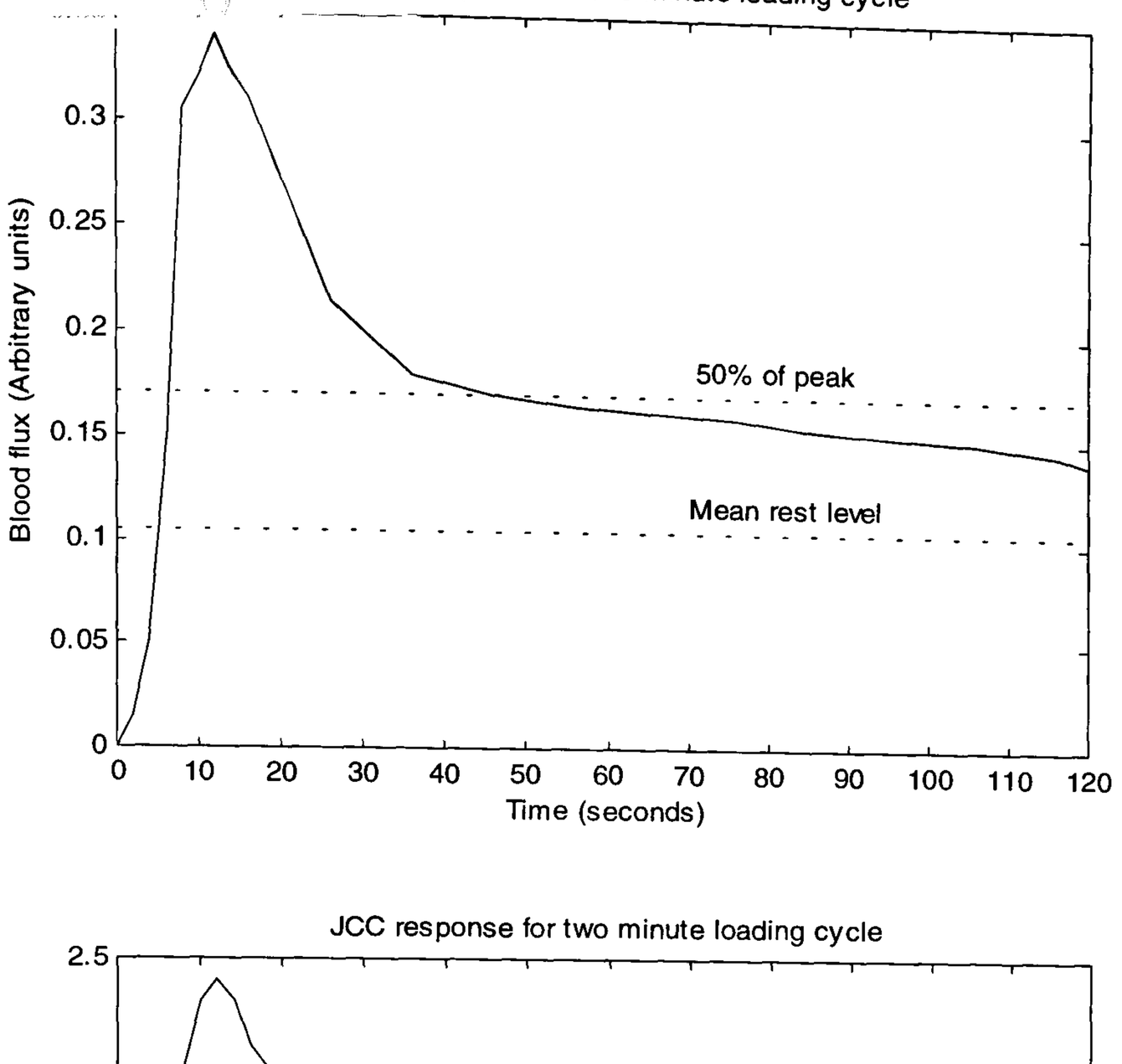

(b)

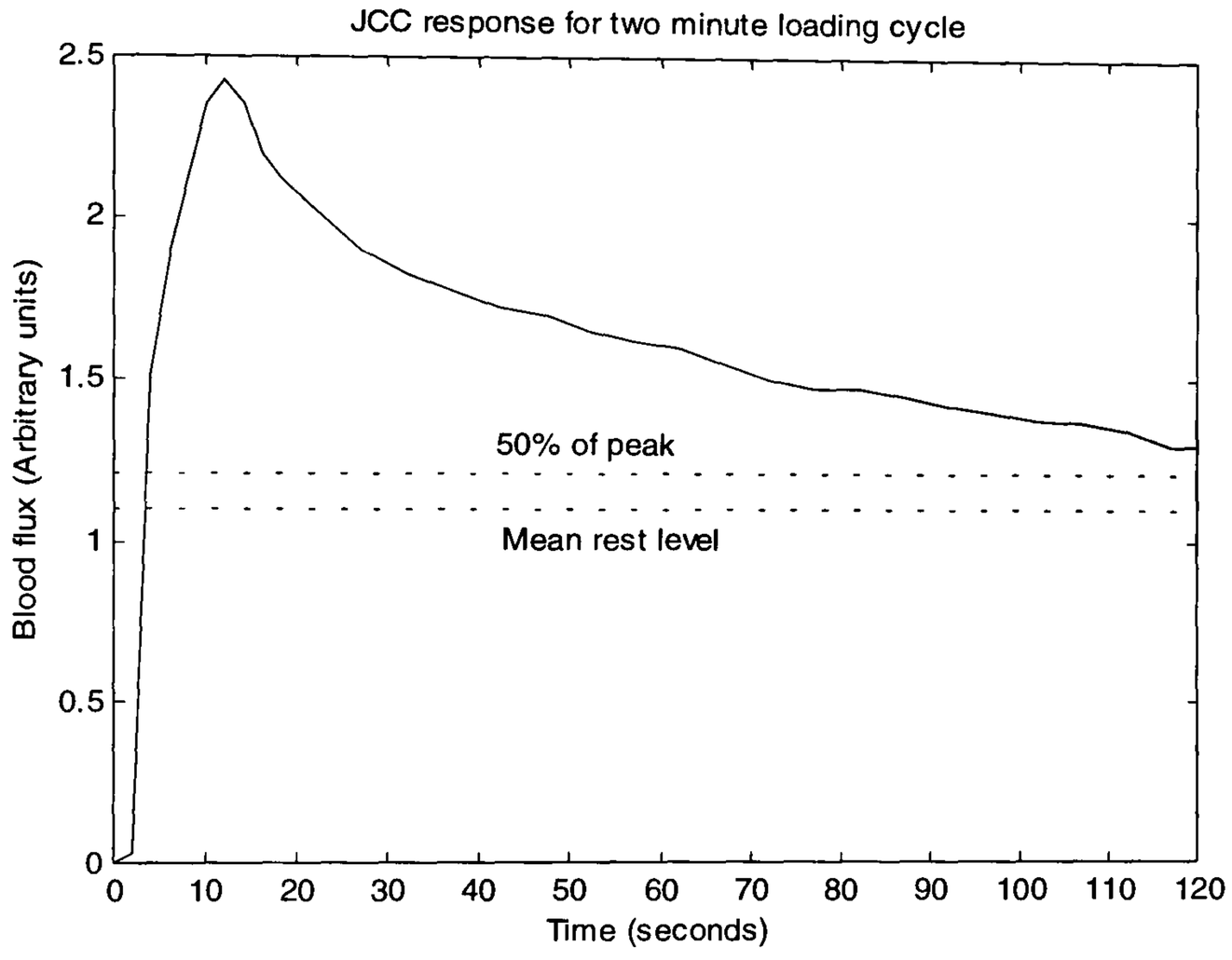

(c)

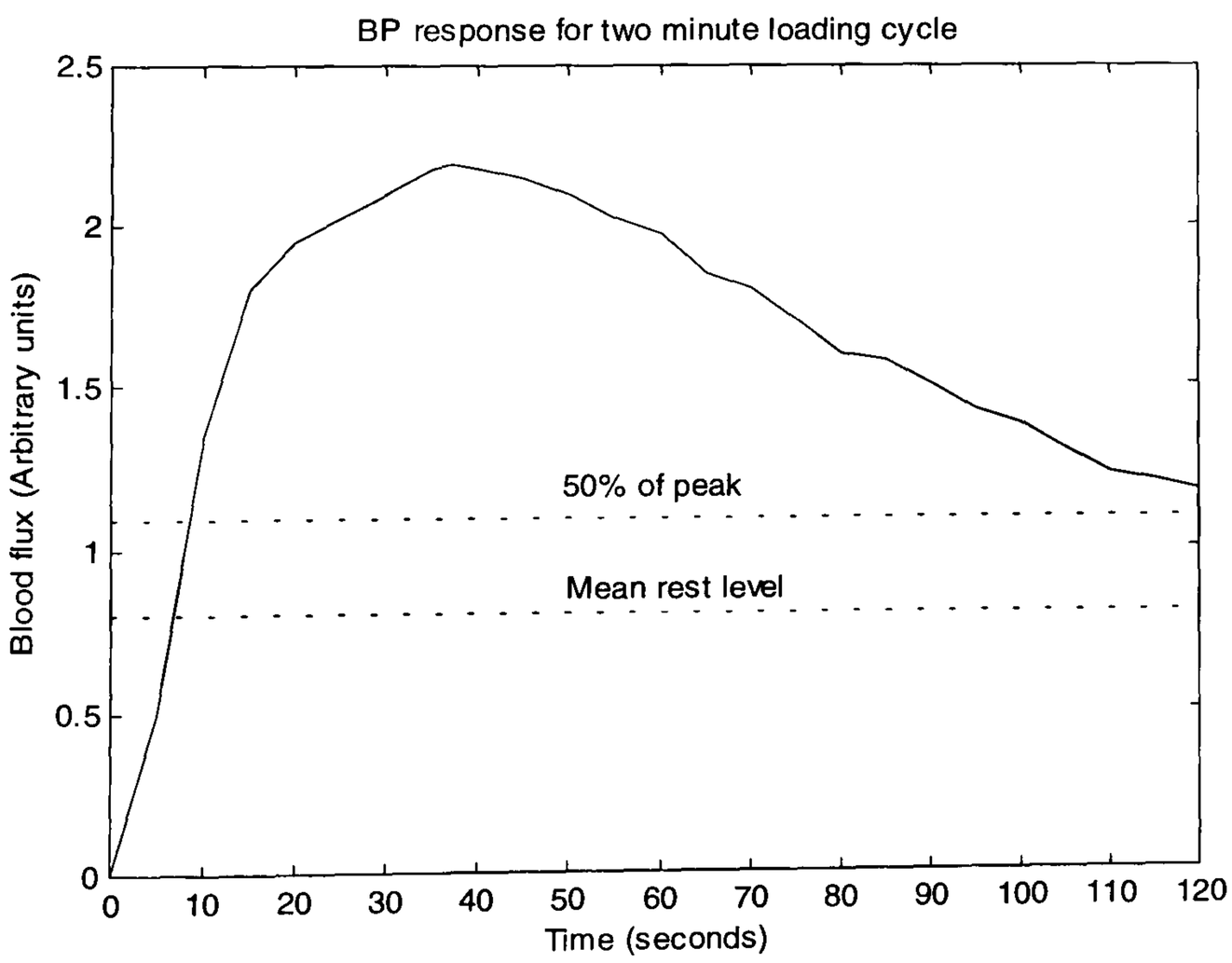

Figure 29(a-c) Hyperaemic response under first metatarsal head for **(a)** control, **(b)** diabetic with neuropathy, **(c)** diabetic with vascular complications.

(a)

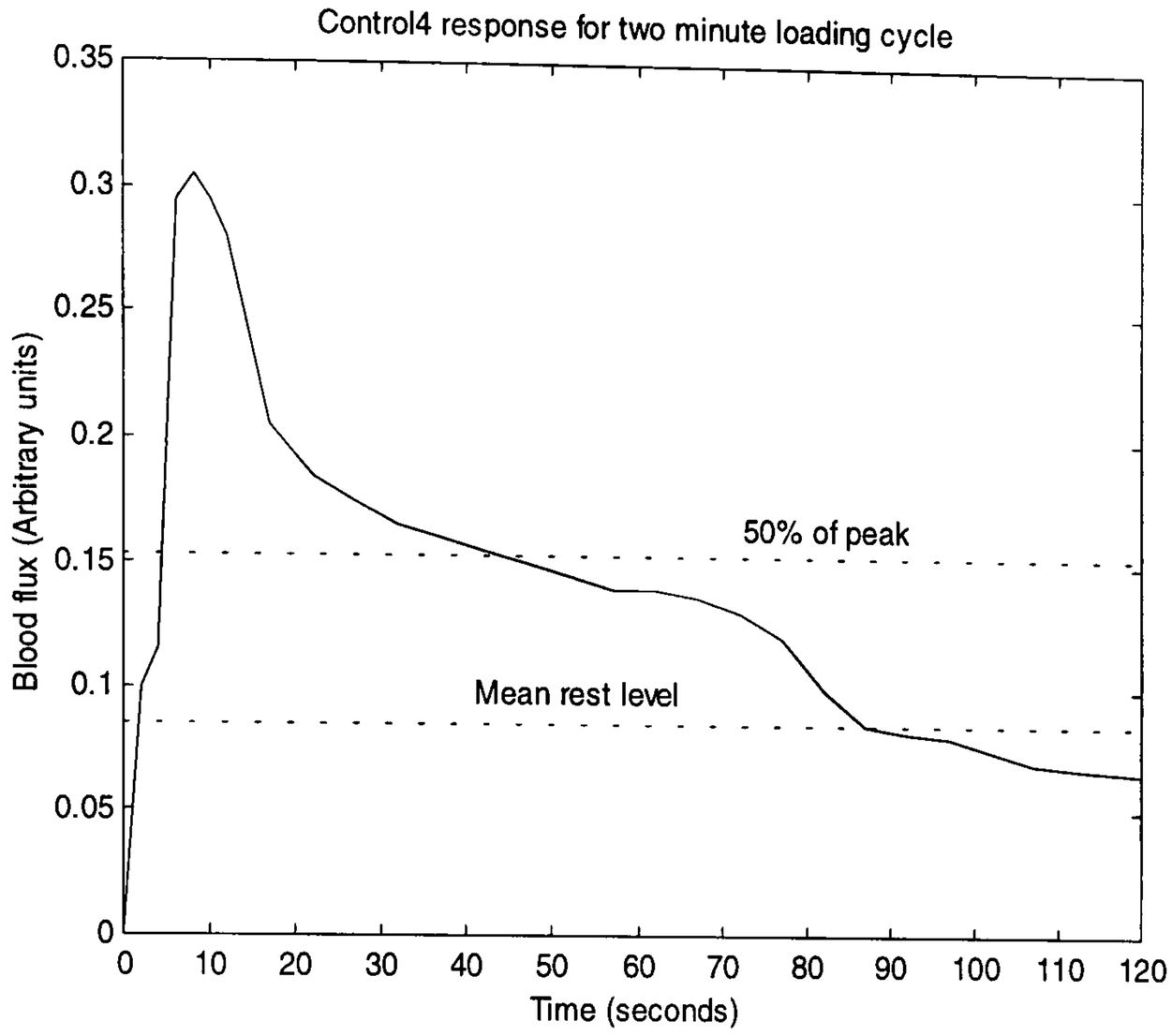

(b)

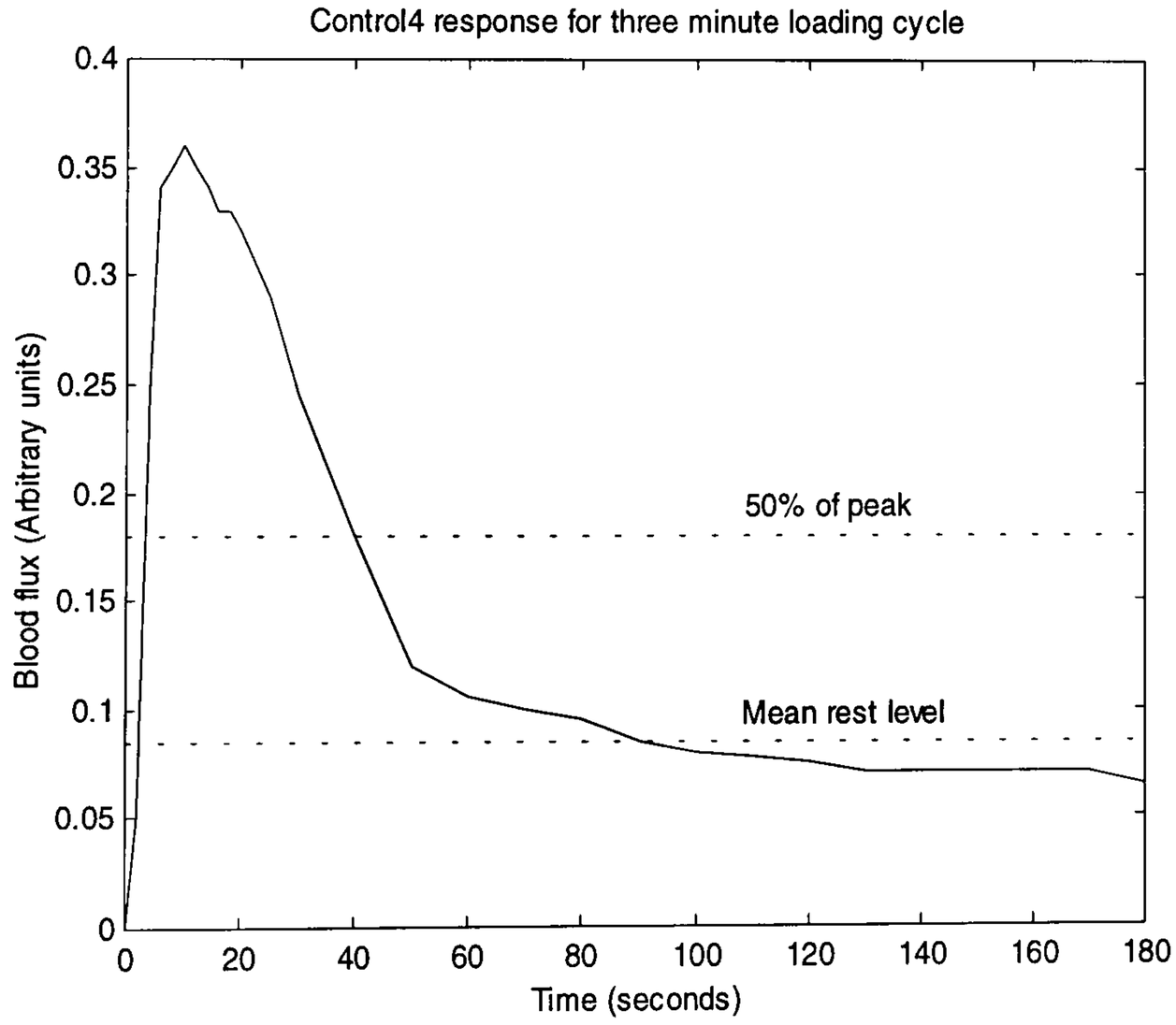

Figures 30(a,b) Hyperaemic responses under first metatarsal head for a control subject following removal of load after standing for **(a)** two and **(b)** three minutes, respectively. N.B. results of the four-minute loading were obtained under different experimental conditions and are excluded.

(a)

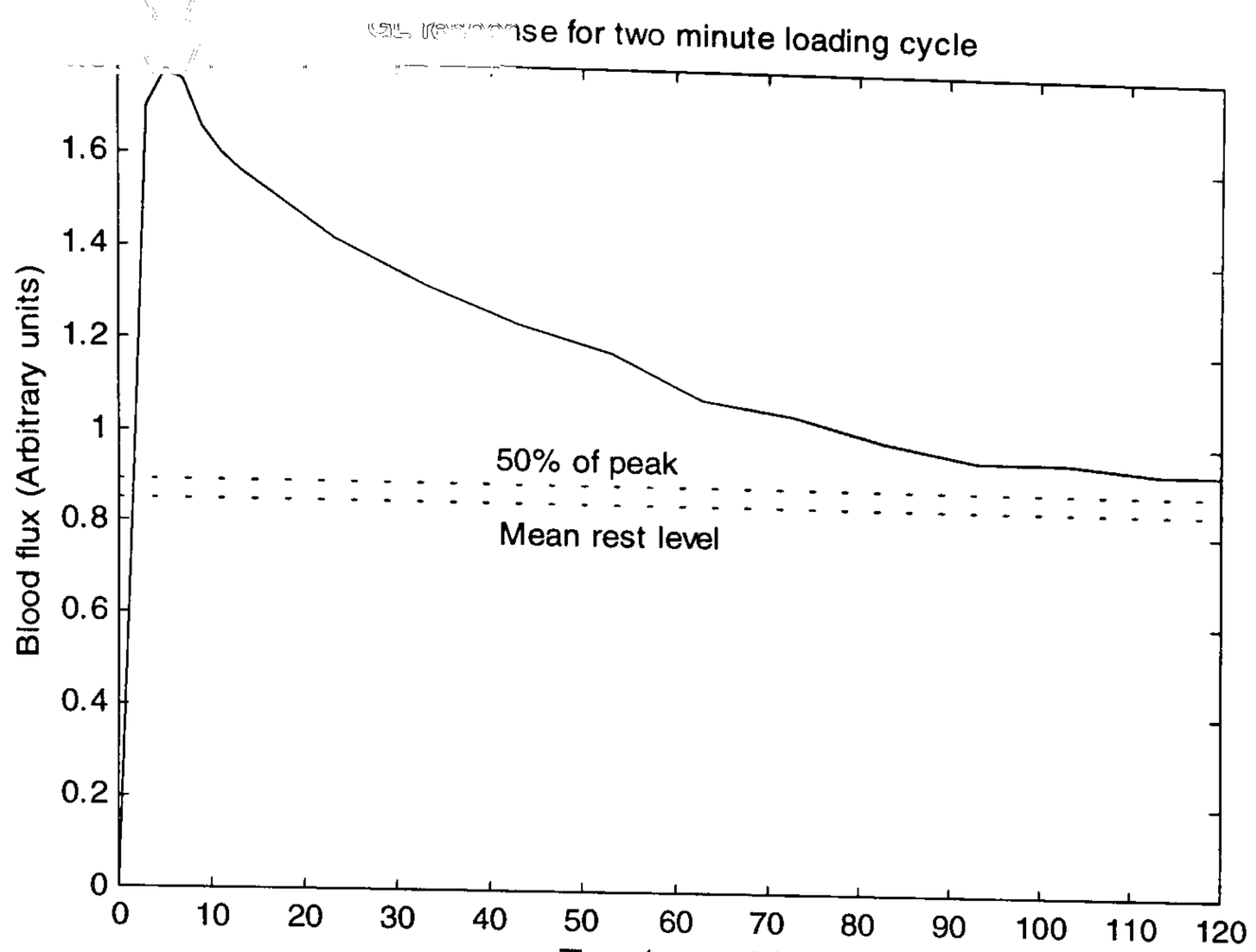

(b)

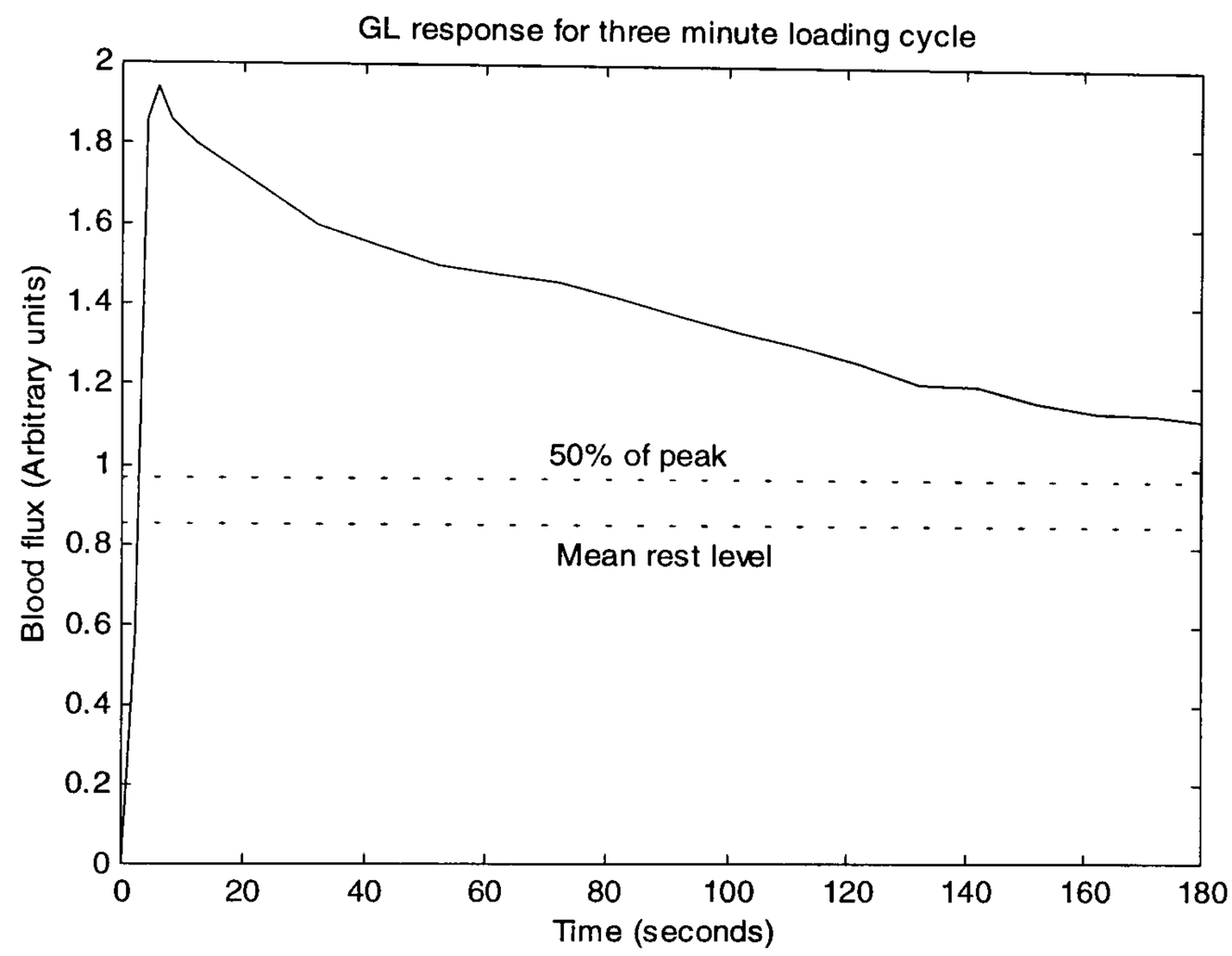

(c)

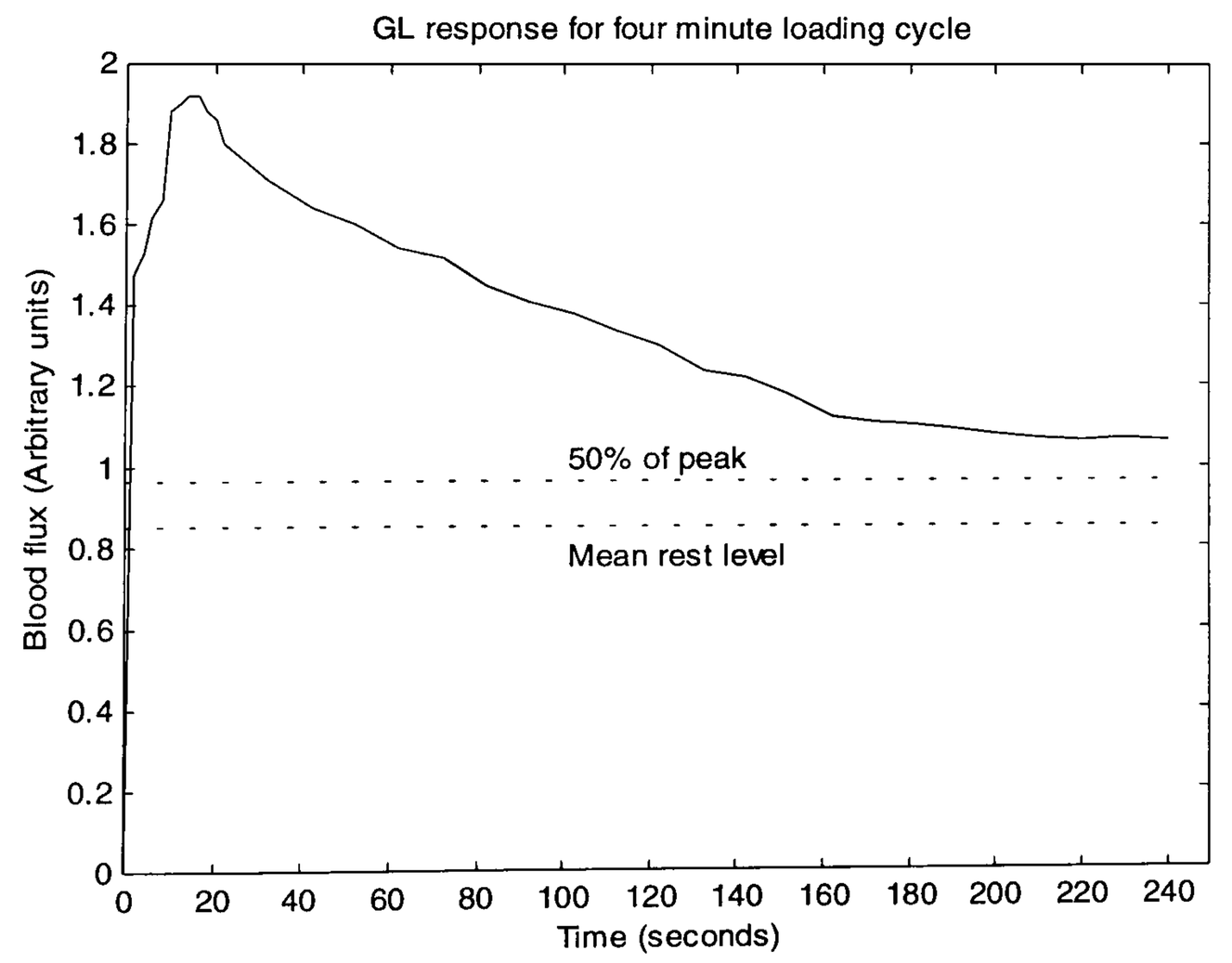

Figure 31(a-c) Hyperaemic responses under first metatarsal head for a diabetic subject with neuropathy, following removal of load after standing for (**a**) two, (**b**) three and (**c**) four minutes.

(a)

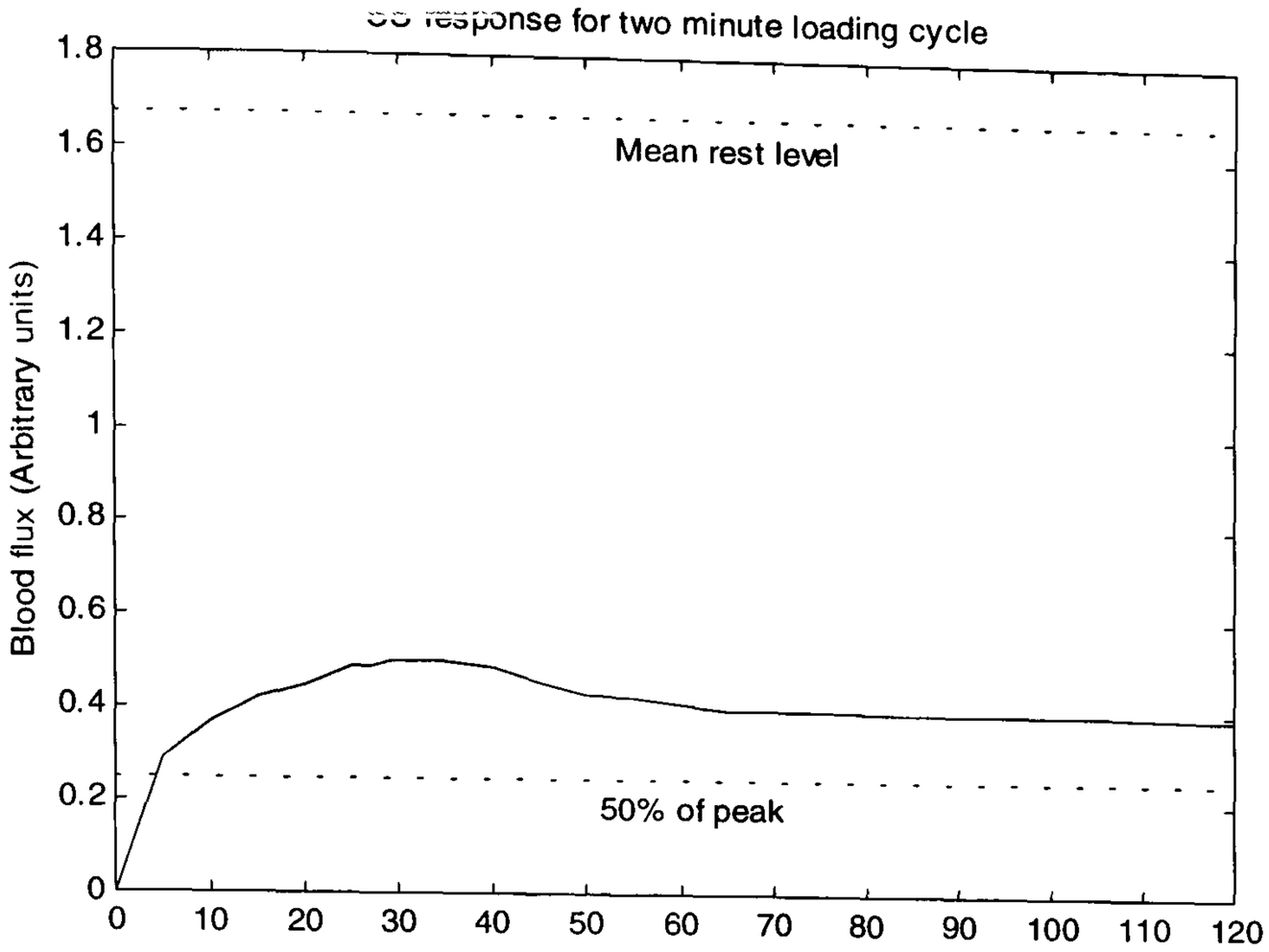

(b)

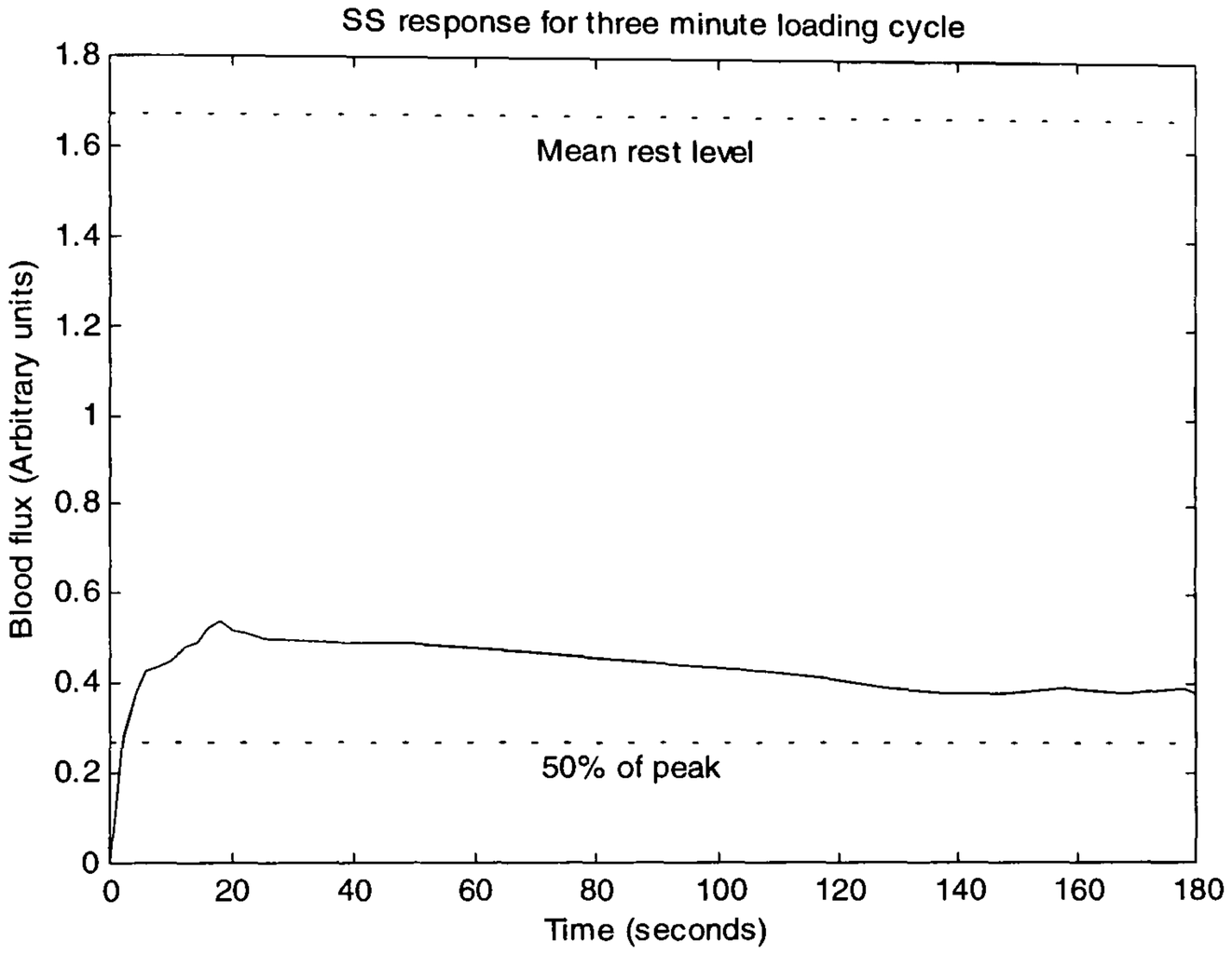

(c)

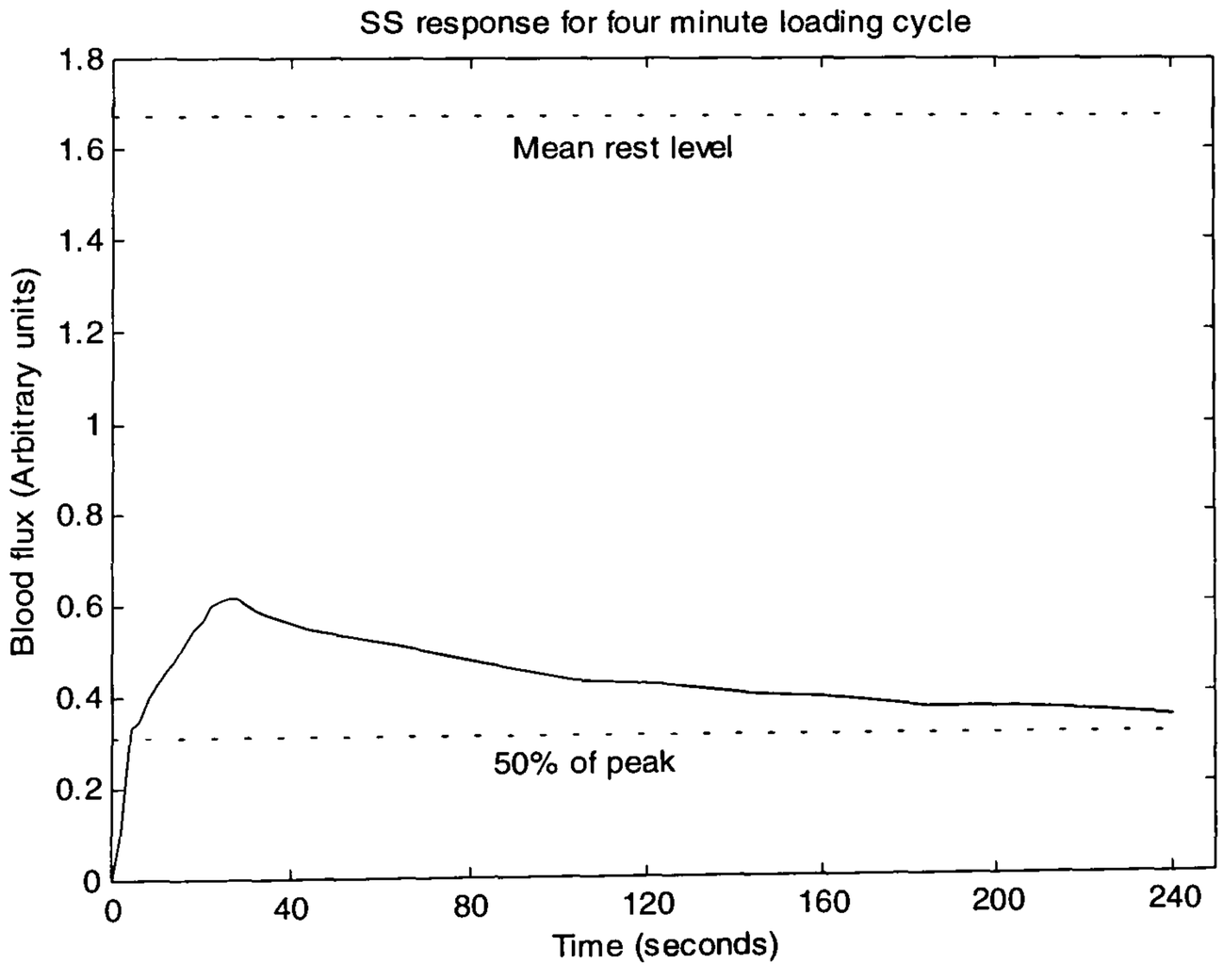

Figure 32(a-c) Hyperaemic responses under first metatarsal head for diabetic subject with vascular complications following removal of load after standing for (**a**) two, (**b**) three and (**c**) four minutes.

Subject	Mean rest Flux	Peak (Arbitrary units) Load time (seconds):			Rise time (seconds) Load time (seconds):			Recovery 50% peak (seconds) Load time (seconds):			% increase rest to peak Load time (seconds):		
		120	180	240	120	180	240	120	180	240	120	180	240
Control2	0.105	0.34	0.33	0	12	10	0	33	38	0	224	214	0
Control3	0.14	0.35	0.36	0	8	10	0	45	160	0	150	157	0
Control4	0.085	0.305	0.36	0	8	11	0	35	29	0	259	323	0
BP	0.8	2.19	1.88	0.54	37	119	28	>120	>180	>240	174	225	33
GL	0.85	1.78	1.94	1.92	5	6	14	>120	>180	>240	109	128	126
JCC	1.1	2.42	1.98	2.12	12	10	12	>120	>180	>240	120	80	93
RC	0.525	1.8	1.82	1.92	9	18	18	43	62	105	242	247	266
SF	0.75	1.34	0.82	1.38	50	68	48	>120	20	14	78	9	84
SS	1.675	0.5	0.54	0.62	32	18	26	>120	>180	>240	-70	-68	-63

N.B. Entries set to 0 for control subjects for load times of 240s indicate excluded results (Refer to text).

Table 6 Summary of results for static loading tests.

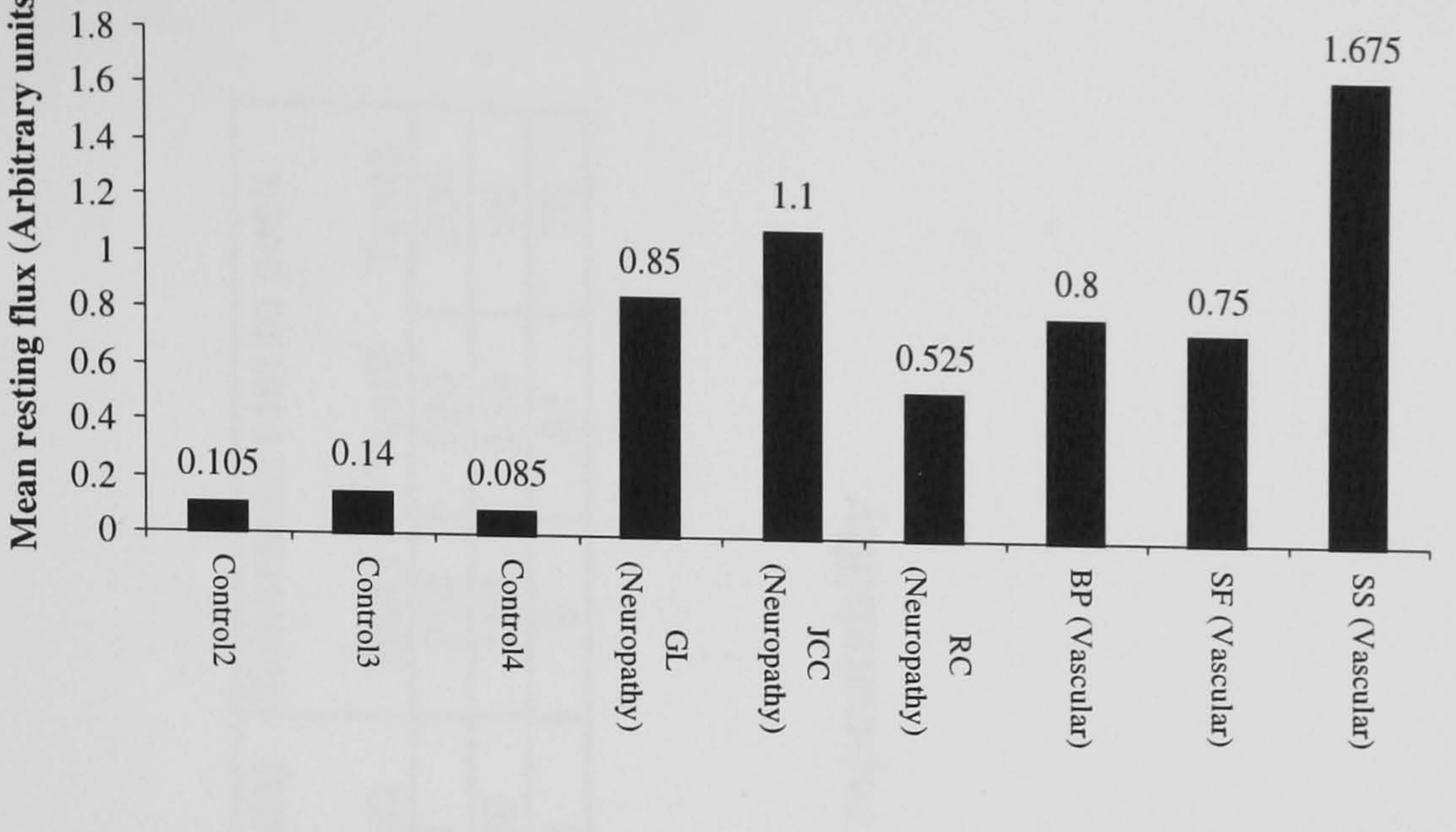

Figure 33 Mean resting flux measured under first metatarsal head for all subjects.

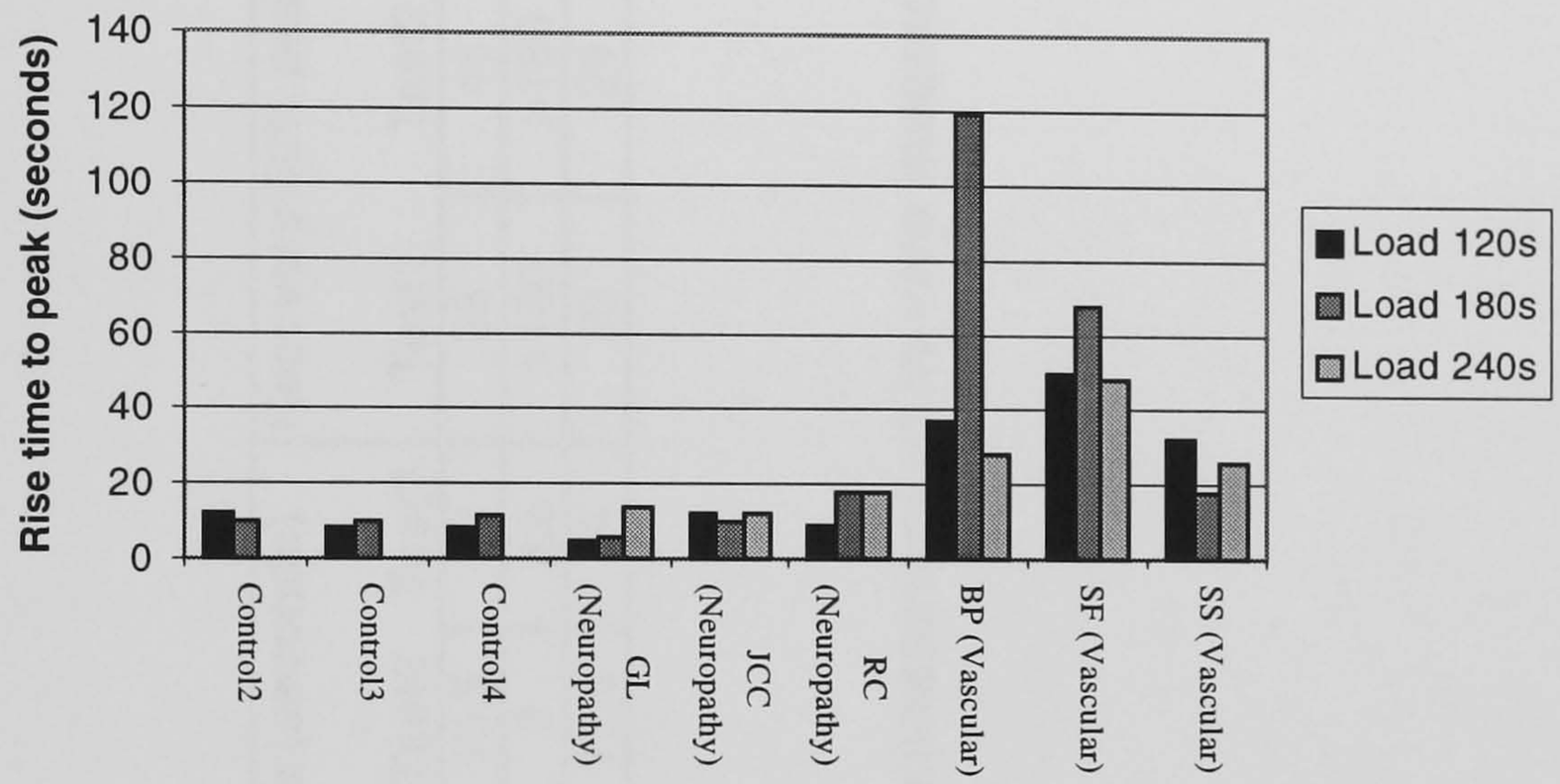

Figure 34 Comparison of rise time to peak of blood flux after unloading, for different loading times. (Value for BP for Load=180s is invalid due to movement artefact).

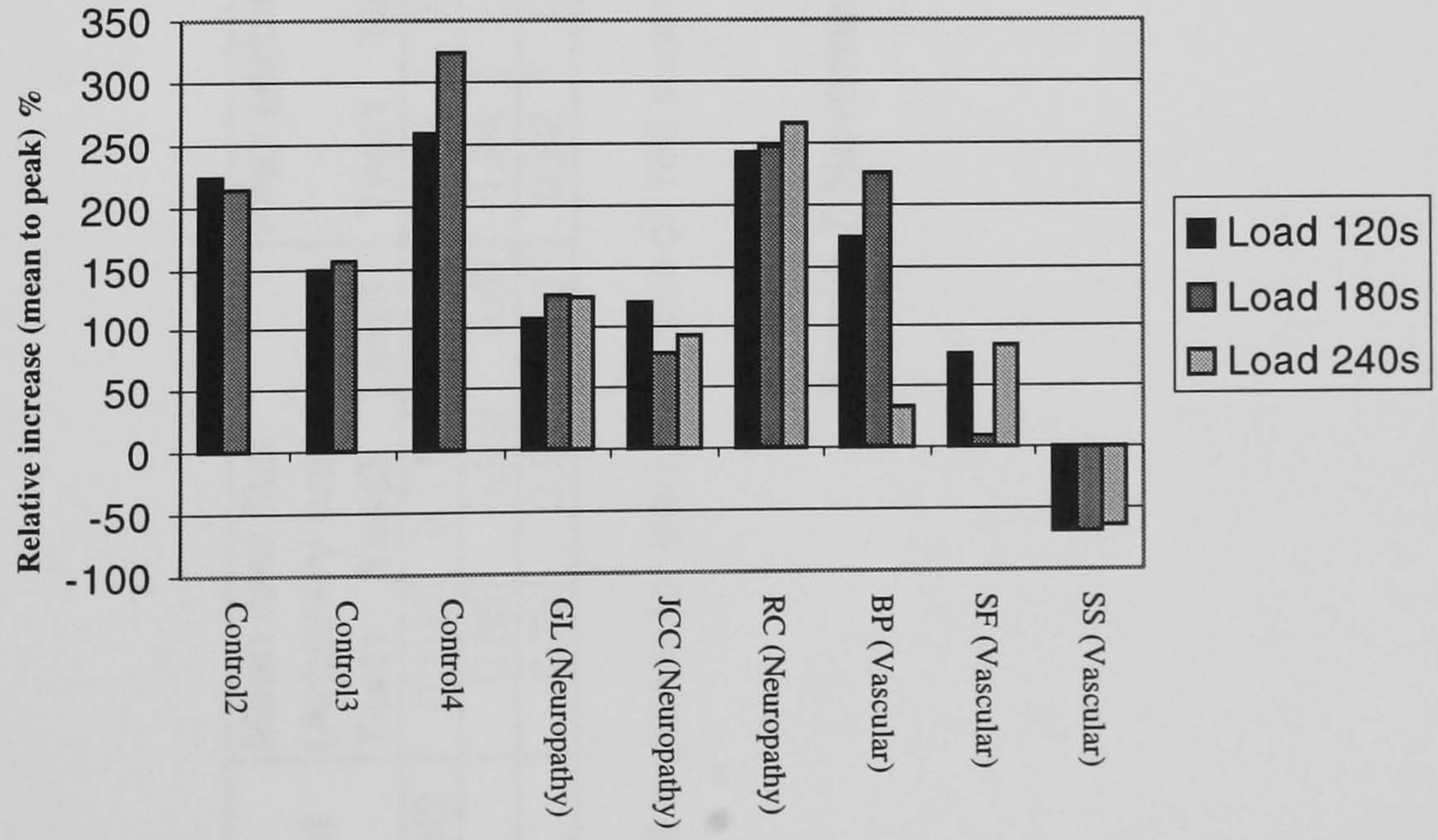

Figure 35 Comparison of relative increase from mean rest flux to peak flux for different loading times.

Subject	Mean rest flux (Arbitrary units)			Peak (Arbitrary units)			Rise time (seconds)			Recovery 50% peak (seconds)			% increase rest to peak		
	Test1	Test2	Test3	Test1	Test2	Test3	Test1	Test2	Test3	Test1	Test2	Test3	Test1	Test2	Test3
Control2	0.105	0.112	0.097	0.33	0.36	0.35	10	10.5	12	38	46	41	214	220	206
GL	0.85	0.93	0.67	1.94	2.04	1.31	6	8	8.5	>180	>180	>180	128	119	96
SF	0.75	0.69	0.81	0.82	1.25	1.43	68	72.3	54	20	29	38	9	81	76

N.B. All tests are for load durations of 180 seconds

Table 7 Summary of results for assessment of in-vivo measurement repeatability.

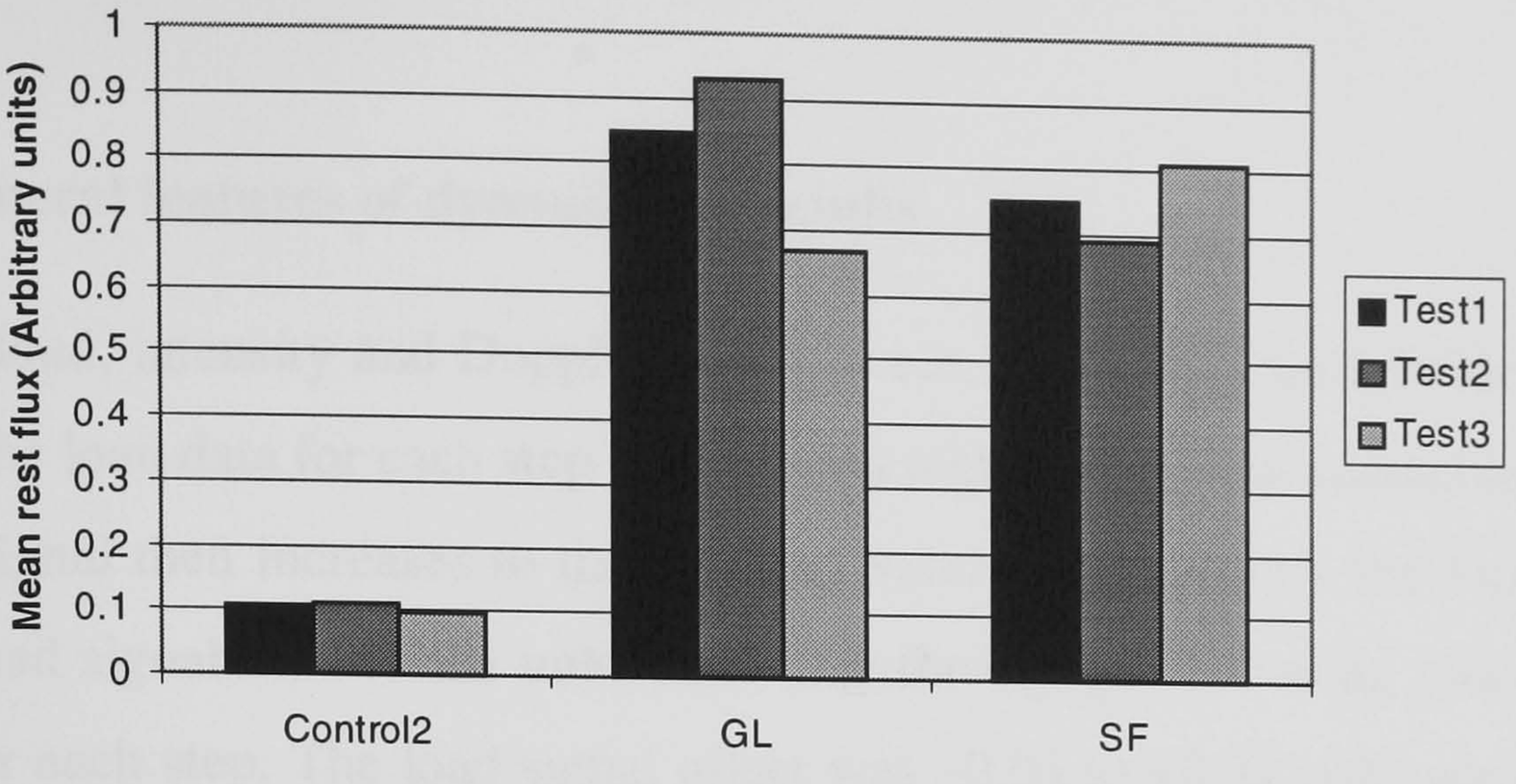

Figure 36 Mean resting blood flux for three subjects assessed for three separate loading tests. Note: test1 and test2 are sequential, test3 follows refitting of measurement shoe.

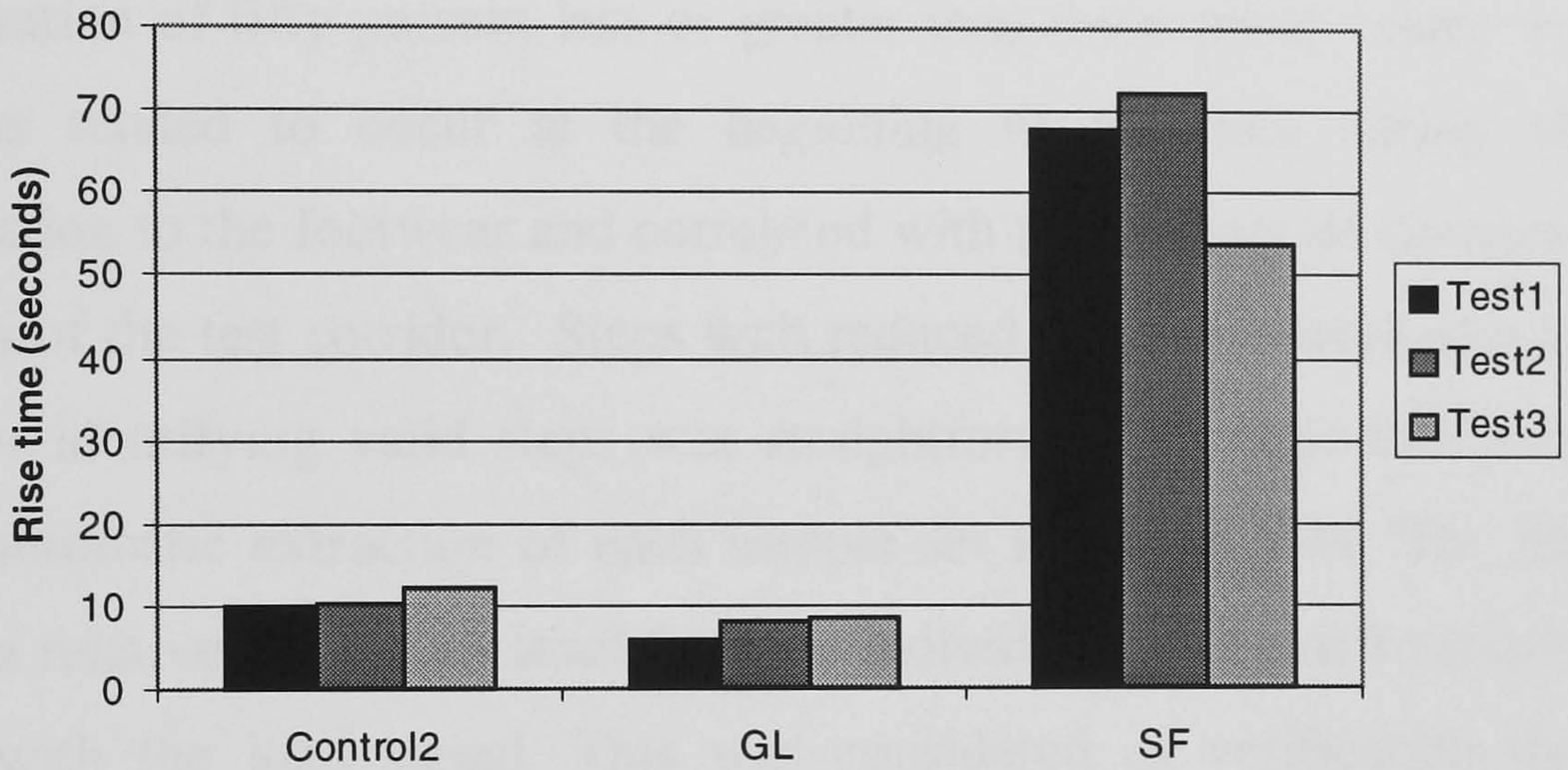

Figure 37 Rise time to peak of blood flux after unloading for three separate loading tests of 180s. Note: test1 and test2 are sequential, test3 follows refitting of measurement shoe.

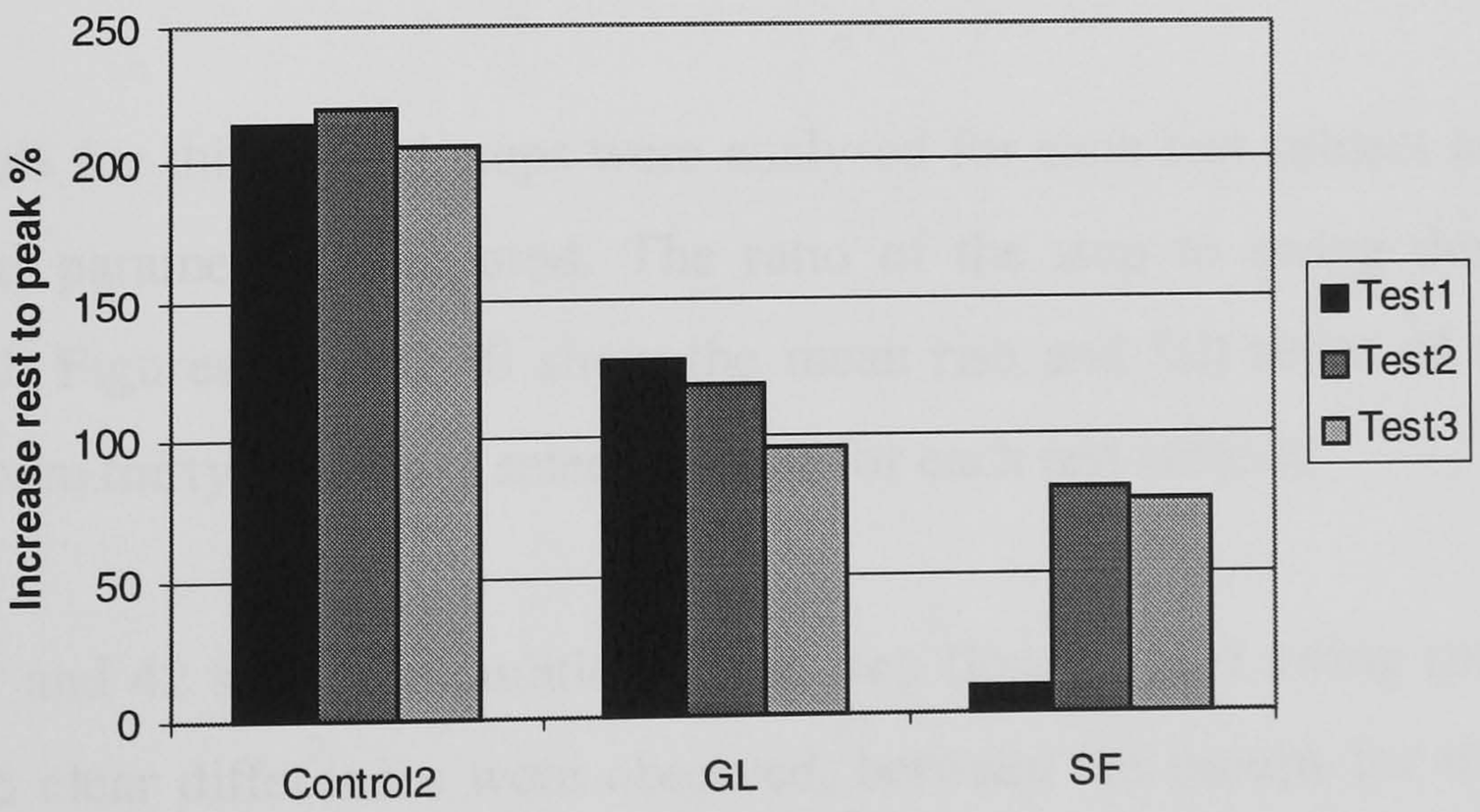

Figure 38 Relative increase in flux from rest to peak following unloading, for three separate loading tests each of 180s. Note: test1 and test2 are sequential, test3 follows refitting of measurement shoe.

6.2.12 General features of dynamic test results

Dynamic load, intensity and Doppler signals were, in general, well-defined continuous signals. The load data for each step commenced with the forefoot contacting the ground, the load signal then increases to the full load value. Subsequently the forefoot is lifted and the load signal falls to the unloaded value throughout the swing phase. This cycle repeats for each step. The load signal offset was –0.03 to +0.02 volts across the group, thus the load is effectively zero throughout the swing phase. The load data for each step was characterised in terms of, rise-time, step duration, fall-time, and swing duration. Mean values for the step and swing duration were used to establish normal values. Steps having duration of fifty percent less or greater than these mean values were excluded. Such steps tended to occur at the beginning of the data during the period of acclimatisation to the footwear and correlated with noted times of changes of direction, at the ends of the test corridor. Steps with reduced amplitude were also excluded. The process for identifying valid steps was straightforward to code into system software allowing automatic extraction of each sample set from test data. The intensity signal exhibited a relatively constant level for each individual, with small variations occurring in phase with the load signal. This was considered as verification that the sensor remained in contact with tissue during walking. On average, this signal was 10% larger during loading than the unloaded value. This is thought to occur as a result of reduced absorption by blood, with the fall in perfusion under load, so that tissue reflectance is increased.

Load signals for thirty valid steps were analysed for each test subject and mean values of the load parameters compared. The ratio of the step to swing duration was also determined. Figures 39 and 40 show the mean rise and fall times of the load signal, obtained from thirty randomly selected steps for each test subject.

Figures 41 and 42 show the duration of the step (loaded) and swing (unloaded) phases of gait. No clear differences were observed, between the groups for these parameters, for the example set or alternative sets of thirty steps. Histograms of duration of step and swing phases revealed that some subjects exhibited a normal distribution whereas others

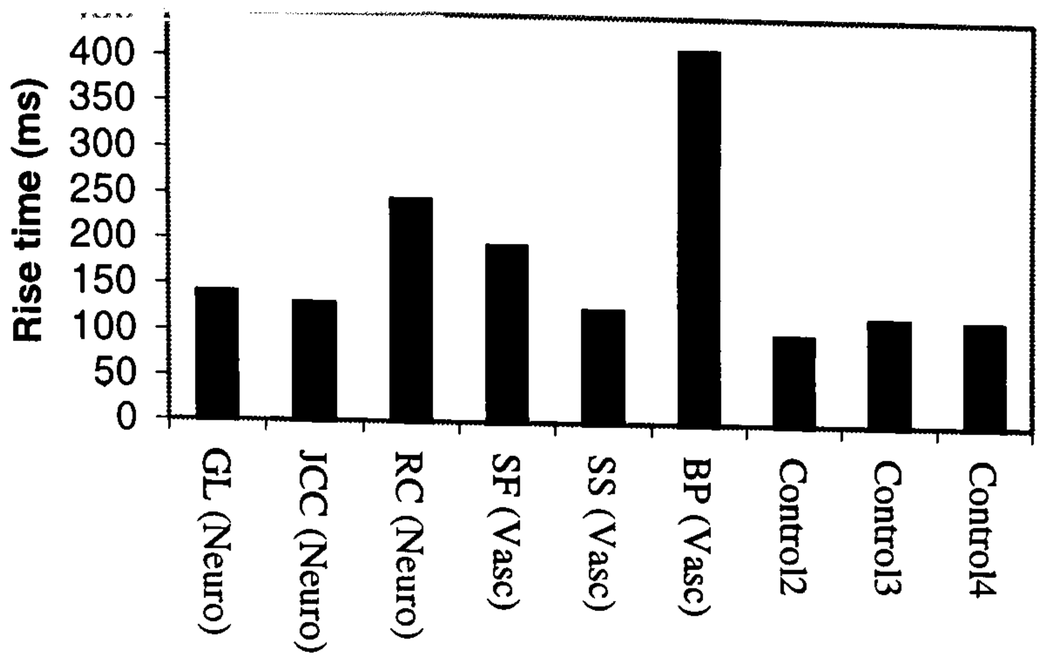

Figure 39 Rise times of dynamic load signal averaged over thirty steps.

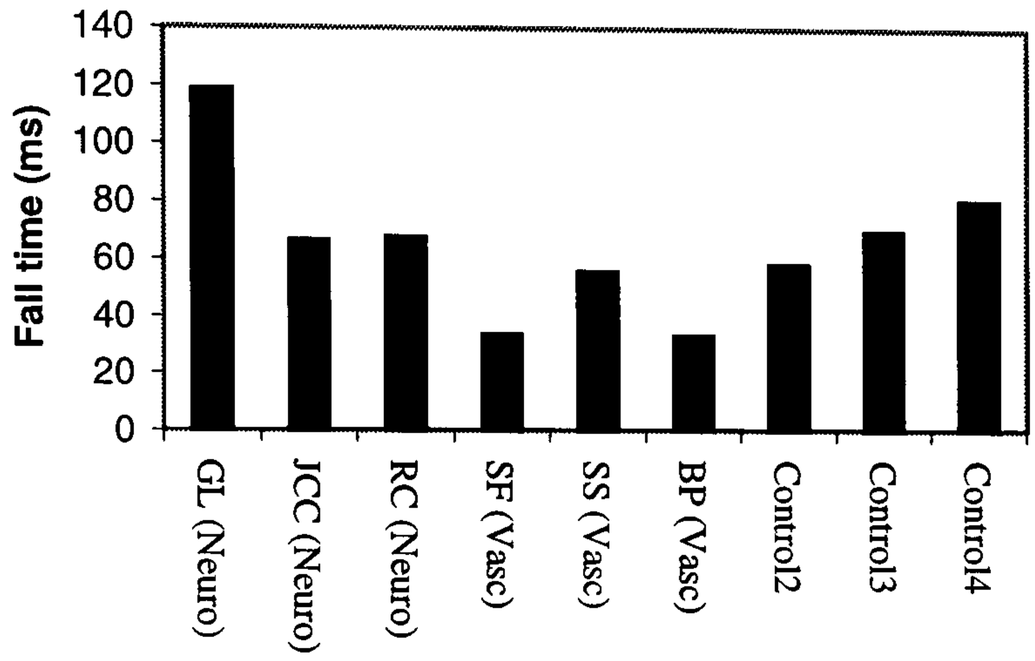

Figure 40 Fall times of dynamic load signal averaged of thirty steps.

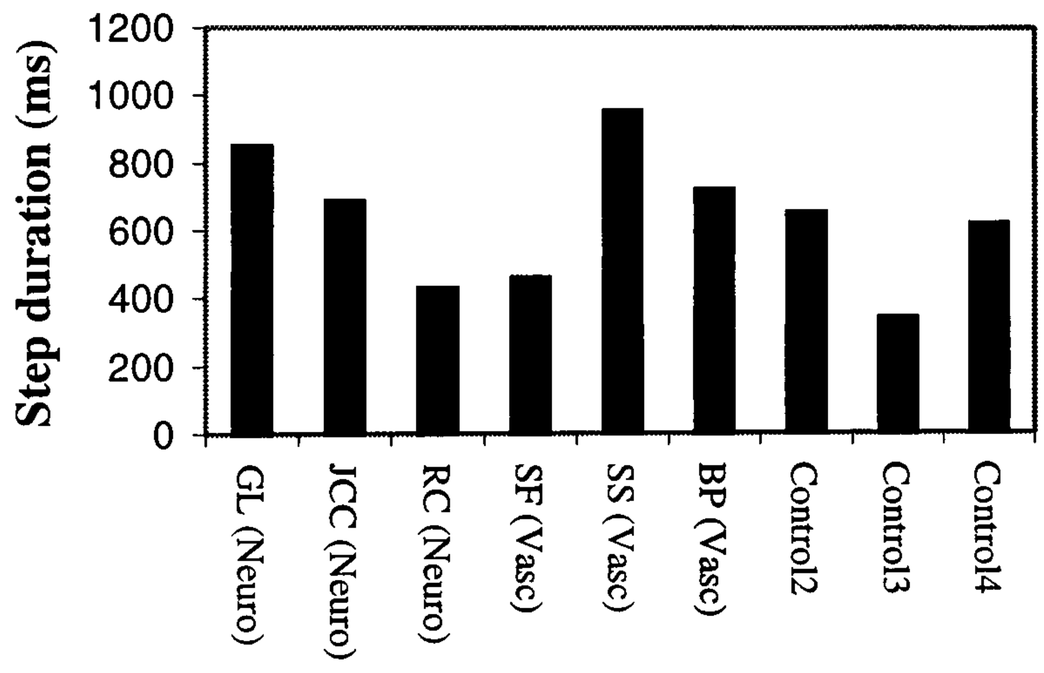

Figure 41 Duration of step (loaded) phase of gait averaged over thirty steps.

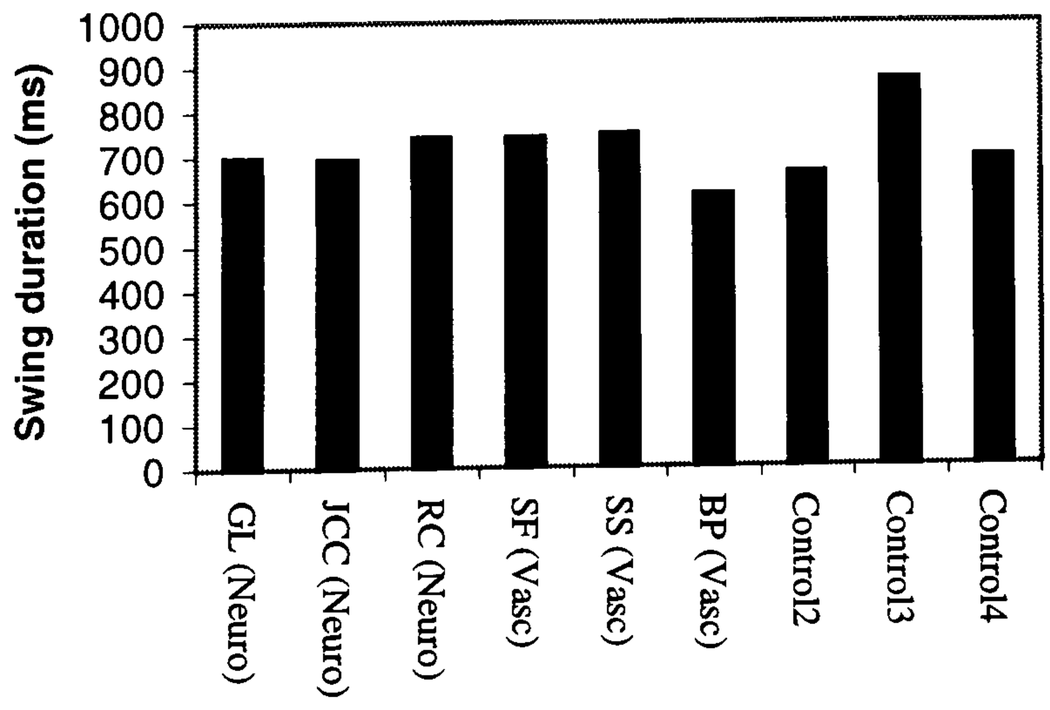

Figure 42 Duration of swing (unloaded) phase of gait averaged over thirty steps.

exhibit singled sided or uniform distributions. The form and range of the distribution was consistent throughout the test data for individuals. The results of this study allowed sets of data to be selected based on specified matching criteria. By restricting the size of the sample to ten steps, it was possible to obtain close matching of step parameters within each set.

6.2.13 Processing and interpretation of dynamic results

Doppler signals for each step within each sample were extracted and processed using the laser Doppler algorithm previously described. Figure 43 illustrates the Doppler signal during the swing phase of a step for a control subject; similar graphs were obtained for all subjects. The important characteristic of this data is the transient in the Doppler signal at the beginning and end of the swing phase. These transients are attributed to movement artefact caused by decompression of tissue and motion of the foot relative to the sensor.

Thus, there is a limited period within the swing phase, during which the Doppler signal is representative of blood flux. Furthermore, the duration of the transient following unloading was found to vary considerably (14ms to 76ms) from step to step and was independent of load parameters. These characteristics further complicated interpretation of blood flux. In the static case qualitative measurements of recovery times, were made relative to a well-defined biological reference – the peak hyperaemic response. For the dynamic data, the time at which the load fell to zero and the end of the Doppler-unloading transient were evaluated as suitable reference points. The Doppler flux at successive instants in time, relative to these points, were then compared for matched steps for each test subject. There was considerable variation (+/-40% of full scale) in the flux values, suggesting that the blood flux was independent of the loading parameters. However, blood flux was found to increase linearly within the swing phase before reaching a steady level. Furthermore, the flux value at the end of the Doppler-unloading transient was non-zero. By extrapolating the flux backward in time from this point, it was possible to predict that the blood flux starts to increase at a time within the transient period. Therefore, neither of the proposed event times were acceptable as reference points. The predicted time at which the blood flux signal began to increase was also

discarded as no valid physiological statement could be made regarding blood flux during the transient period.

Solution of the preceding problem required consideration of the rate of increase of the blood flux during the swing phase. A sample set of ten unmatched steps was obtained for each test subject. Blood flux values were calculated at successive 25ms intervals during the valid portion of the Doppler signal within the swing phase. This value was determined by the lower Doppler cut-off frequency. The mean value of the blood flux for each interval for the ten steps was established and plots produced of mean blood flux versus time. The linearly increasing portion of the blood flux was approximated by a best straight-line fit based on five data points. The number of data points is limited by the minimum period of flux increase of 125ms across the group. The slope of the linear fit was compared for different sample sets and was consistent to within 10% for each subject. Figure 44 is a comparison of these best straight-line fit approximations, to the mean increases in blood flux, calculated for the values obtained during the swing phase of ten random steps for each subject.

The variation in heart rate and plantar skin temperature for the dynamic tests were within the allowable range of +/-3^{o}C.

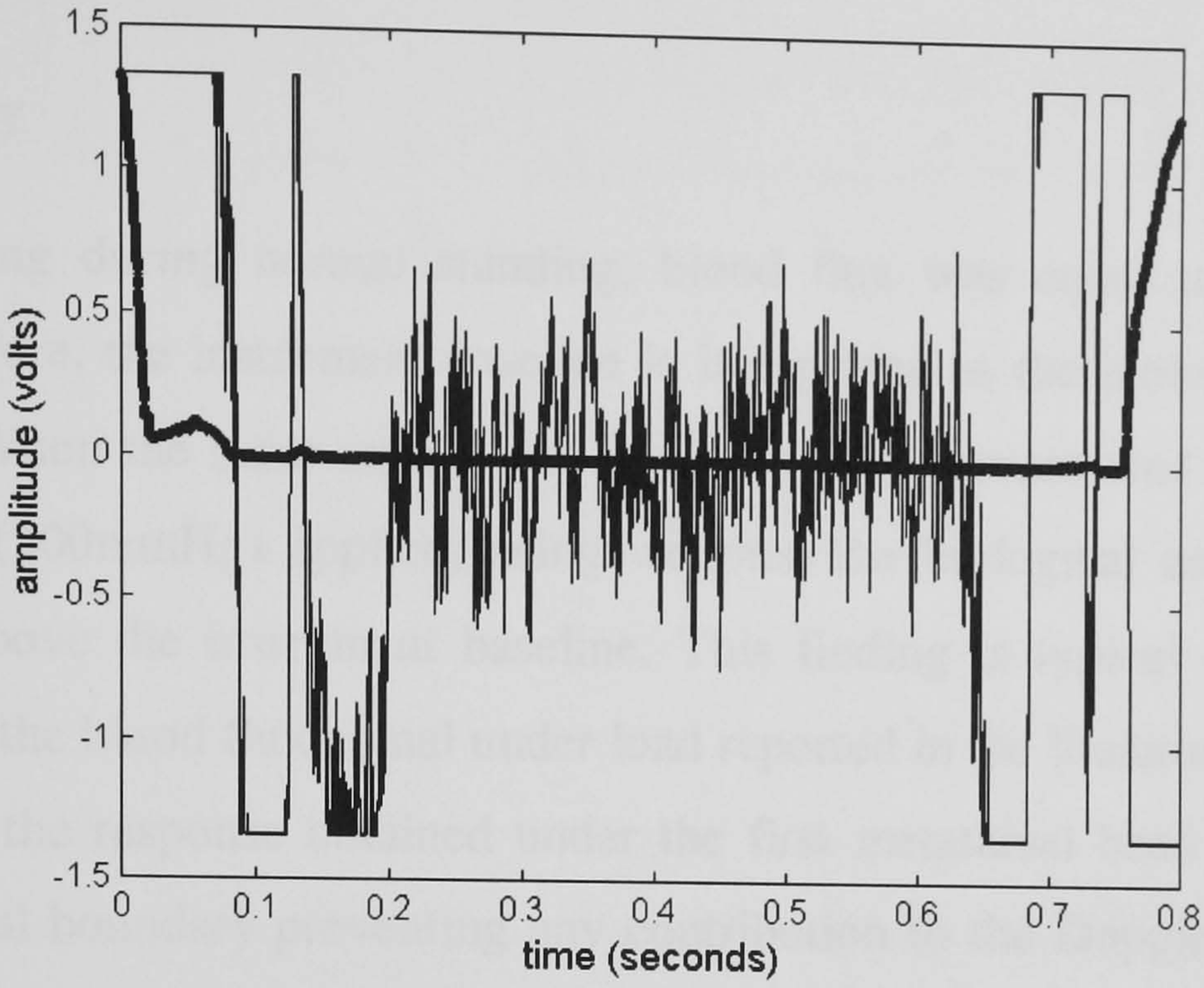

Figure 43 Doppler signal during the swing phase of one step, for a control subject. The bold line is the load signal. The Doppler signal is representative of blood flow for the period from 200-600 milliseconds.

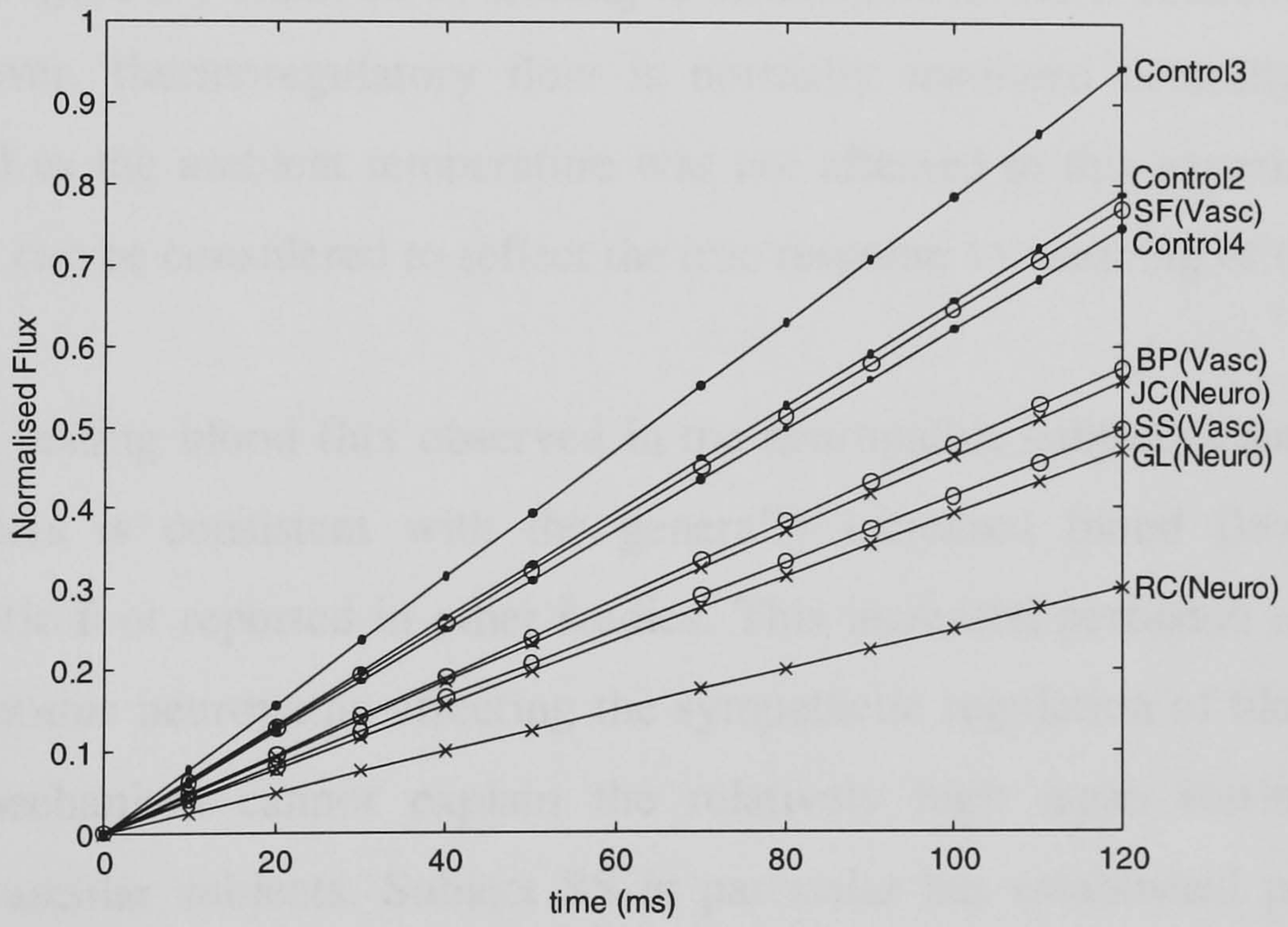

Figure 44 Plot of rates of increase of normalised blood flux (Flux / $Flux_{(max)}$) for the study group. Each line is a best straight-line fit to the mean rate obtained from ten randomly selected steps for each subject, at successive intervals of 25ms of the Doppler signal, within the swing phase. Control 1 is omitted due to sensor failure as discussed earlier in the text.

6.2.14 Summary

For static loading during normal standing, blood flux was equal to the instrument baseline. Therefore, the instrument baseline is interpreted as the biological zero in the present study. When the same sensor was applied to the forearm and a flow cessation load of 27kPa (200mmHg) applied, using weights, the biological zero level was on average 17% above the instrument baseline. This finding is typical of the results of other studies of the blood flux signal under load reported in the literature. The proposed explanation for the response obtained under the first metatarsal head is that the bone acts as an optical boundary preventing any contribution to the Doppler spectrum from deeper vessels.

Increasing skin temperature under the first metatarsal head by nearly 30°C, resulted in an increase in the area under the Doppler spectrum of approximately 50%. A much greater increase could be expected in response to this large temperature increase, due to additional thermoregulatory shunt flow, leading to an increase in RBC concentration in the tissue. However, thermoregulatory flow is normally mediated centrally by the hypothalamus and as the ambient temperature was not affected in this experiment the observed increase can be considered to reflect the true response to warming of the foot.

The greater mean resting blood flux observed in the neuropathic subjects compared to the control subjects is consistent with the generally increased blood flow in the neuropathic diabetic foot reported in other studies. This increased perfusion is usually attributed to autonomic neuropathy affecting the sympathetic regulation of blood flow. However, this mechanism cannot explain the relatively high mean resting levels observed in the vascular subjects. Subject SS in particular has established peripheral vascular disease. Inspection of the plantar skin of this subject revealed a mottled colouration suggesting an impaired distribution of blood. The mean rest value could then be explained by the sensor being located over a highly perfused region. However, this explanation cannot explain the relatively high resting blood flux in the vascular subjects BP and SS because plantar skin perfusion appeared normal in these subjects. The rise times for the neuropathic subjects (mean =18s, load=120s) were slower than those of the control subjects (mean=10s, load=120s). However the linear form of the

increase in blood flux for both cases suggests that reperfusion following unloading is relatively normal for the neuropathic group. In contrast, the times for the vascular subjects (mean=30s, load=120s) exhibit a different type of response, with an initially rapid increase to within 50-80% of the peak, followed by a much slower rate of increase to the peak response. As these subjects have no clinical evidence of neuropathy but clinical evidence of vascular disease, the physiological basis of this response is more likely to be related to the physics of the vascular system rather than to poor functional regulation. Further evidence of compromised blood flow for the vascular group is provided by the lower relative increase rest to peak of the response (mean=83%, load=120s) when compared to the controls (mean=211%, load=120s) and neuropaths (mean=134%, load=120s). Under these conditions of reduced flow in the vascular group, a relatively longer period would be required for clearance of vasodilators from the blood stream. This may explain why the recovery period is at least twice as long in the vascular group than for the controls. In contrast, the general features of the response for the neuropathic group suggest that the physical response of the vascular system following unloading is normal. However, the extended recovery period, which is at least three times greater than for the control group, suggests that autoregulation of blood flow is impaired consistent with the clinical evidence of autonomic neuropathy.

Assessment of repeatability indicates that the observed findings are consistent for closely matched measurement and physiological conditions. The variation in response is up to 30% for tests performed on separate days when the sensor is relocated. For sequential tests during which sensor position is maintained the variation in response falls to typically 10%, (excluding subject SF where a failure in reperfusion occurred between two sequential tests). This level of variation is consistent with the findings of other laser Doppler studies at other sites on the body.

Due to the short time scales involved in tissue reperfusion during the swing phase, the results of the dynamic study are considered to relate only to the vascular physics and not too functional regulation. It could therefore be expected, given the findings of the static study that the neuropathic subjects would exhibit a faster rate of reperfusion. However, the dynamic results indicate a mean reperfusion rate of 3.4 a.u/ms (Arbitrary units per millisecond) compared to 5.1 a.u/ms for the vascular group. For the vascular subjects the difference between the static and dynamic rates may be related to the

duration of loading with failure in reperfusion only becoming evident after a relatively long loading period i.e 120s. For the neuropathic subjects a possible explanation for the slow rates of reperfusion during walking is that the tissue remains partially perfused during the loading phase. Then the volume of blood re-entering the tissue during the swing phase would be comparatively low. A possible basis for this is the observation of over perfusion commonly observed in the neuropathic diabetic foot. The differences between the findings of the two studies also suggest that both static and dynamic data is required to fully assess the diabetic foot.

Given the current findings the plantar monitoring system appears to be capable of providing an indication of the status of the microcirculation under the first metatarsal head. Further clinical data is required to investigate the physiological basis for these findings and identify if the findings have clinical use in predicting the risk of ulceration.

Chapter 7 Conclusions

7.0 Introduction

A critical review of the development of the plantar monitoring system is presented in summary form. Results of the in vivo clinical evaluation of the system are discussed. Recommendations for further work are given. In the final section, the overall contribution of the work is considered.

7.1 Summary

The project is reconsidered in terms of the theoretical background and review of the literature made after the initial proposal. Justification is given for in-shoe measurement of blood flux by laser Doppler at the plantar surface of the diabetic foot during standing and walking. Such a study could not be performed using existing techniques and the requirement for a plantar monitoring system is identified. A critical review of the development of such a system is given in summary form.

7.1.1 Review of justification for the study

Previous studies have demonstrated changes in the blood supply to the foot of the diabetic at both macrovascular (Shaw and Boulton 1997) and microvascular levels (Japp and Tooke 1995). If the blood supply to the foot is reduced, by atherosclerosis, painful ischaemic ulcers can occur, which typically affect the dorsum of the foot and the toes. Ulceration is, however, considerably more prevalent in the neuropathic foot (Grunfeld 1992), occurring on the plantar surface at sites where tissue is subject to loading by bones such as the calcaneous and heads of the metatarsals (Lord 1986). In the ischaemic foot, the risk of ulceration can be estimated by assessing blood flow at the ankle by Doppler ultrasound and blood flux at the great toe by laser Doppler (Stevens et al. 1993). When these techniques are applied to the neuropathic foot, a normal or elevated blood flow is frequently observed suggesting that the vascular supply is adequate, both to and within the foot. Therefore, in the neuropathic foot, risk of ulceration is routinely assessed, by measurement of plantar pressure and determination of the extent of sensory neuropathy. However, the usefulness of the results obtained is limited by a lack of consensus on the levels of pressure/duration that cause ulceration

(Cavanagh and Ulbrecht 1994). Furthermore, the mechanisms that lead to tissue damage and initiate ulceration cannot be established using these techniques. An impaired nutritional supply to tissue is usually proposed as the underlying cause of neuropathic ulceration. This stems from observed similarities with the formation of pressures sores (decubitus ulcers) which often occur in otherwise healthy tissue if the product of the magnitude and duration of applied pressure exceeds a certain level. Damage to tissue can normally be avoided if pressure is removed within a reasonable time. Following unloading, a period of increased blood flow, reactive hyperaemia compensates for the nutritional deficit. This mechanism has been previously demonstrated to be impaired in the neuropathic diabetic foot (Rayman et al. 1986b). However, there is no conclusive evidence of increased loading times under the neuropathic foot. The basis for the depletion in the nutritional supply could therefore be considered to arise from increased plantar pressure together with impaired vascular regulation due to autonomic neuropathy, preventing a compensatory increase in blood flow to the region. Previous studies have demonstrated increased plantar pressure (Lord 1986), and impaired regulation of perfusion has been demonstrated on the dorsum and at the great toe (Stevens et al. 1993) of the neuropathic diabetic foot. This evidence cannot be considered sufficient to validate the preceding hypothesis because plantar ulceration in the neuropathic diabetic foot is normally a singular, localised event, classically presenting under the metatarsal head (Edmonds and Foster 1994). One previous study has simultaneously attempted to assess both pressure and perfusion on the plantar surface (Castronouvo 1987). However for reasons previously discussed, the methods used were, in the opinion of the present author, inappropriate. In particular the blood supply at the surface of the foot appeared to be altered by application of a pressure cuff around the foot, when this procedure was replicated. Furthermore, previous studies have only assessed blood flow for the unclad foot during static conditions. Clinical evidence suggests that ulceration is linked to dynamic loading of the foot (Cavanagh and Ulbrecht 1994). It can therefore be argued that such a study should obtain results during normal walking, with the foot in-shoe.

7.1.2 Re-evaluation of objectives

The preceding discussion provides justification for the focus of the present study on assessing the effect of pressure on plantar cutaneous blood flow, at a prevalent site of ulceration in the neuropathic diabetic foot. The original objective was to perform a clinical trial to satisfy this requirement. Initially this appeared to be a straightforward clinical measurement problem. The laser Doppler technique was identified as most appropriate for this application because of the fast response time, the small size and flexible geometry of the probe head and ability to obtain data continuously and non-invasively. The technique has also been used successfully, in other studies of cutaneous blood flow in diabetes mellitus (Chittenden and Shami 1993). However, commercial laser Doppler systems were found to be unsuitable, because the use of fibre optic connections to the probe head resulted in the Doppler signal being swamped by movement artefact noise. In the present study, it has been confirmed that this problem cannot be resolved by mechanical restriction of the optical fibres or by signal processing.

Consequently, the objective of the project became the development of a system capable of assessing plantar blood flow, in-shoe during normal walking.

7.1.3 System development

The problem of movement artefact noise was substantially reduced by eliminating optical fibre connections to the laser Doppler probe head. This required that the laser diode and photodetectors were situated at the measurement site. Furthermore, without amplification at the measurement site, an acceptable signal to noise ratio could not be achieved. With these constraints, the construction of an integrated probe containing these components and sufficiently small to fit into normal footwear proved difficult to realise. To solve this problem a measurement shoe was developed that because of variation in the size of the foot and location of the metatarsal head, had to be custom made for each test subject. This solution was acceptable for the small clinical study used to verify operation of the probe and to obtain initial results. However, for a large clinical trial the time required to construct the measurement shoes would be prohibitive.

Development of the laser Doppler probe required solving of a number of problems. An adequate signal to noise ratio (SNR) could not be achieved using the smallest available photodiodes because the optical output power of the laser diode had to be limited to 1mW for safety. To operate at this power level, photodiodes with a large photosensitive area were necessary. The SNR was further improved by using a low noise, laser diode with a single longitudinal output and by implementing automatic power control in the laser diode power supply. Low noise amplifiers were also used in the Doppler signal path. Electrical interference coupled through the subject was avoided by making the plantar contact face a conductive path to the instrumentation ground. These techniques only gave an acceptable signal to noise ratio provided the probe was maintained at a constant temperature. It was not feasible to regulate the probe temperature using a Peltier heat pump and measurements were made on pre-warmed feet that were insulated within the measurement shoe. This required lining the plantar surface of the measurement shoe with neoprene rubber. The temperature to which the foot is pre-warmed is determined by physiological considerations. It is, therefore, essential that the operating wavelength of the laser diode is stable at the selected measurement temperature.

To allow the foot normal flexion during walking the maximum plantar dimension of the probe was determined as 30mm. It was demonstrated that this value also provides adequate support for the first metatarsal head during walking. This was important to avoid abnormal loading and to prevent shear between the edge of the probe and the skin. By locating the probe in a compressible insole, normal loading was maintained throughout the gait cycle. Plastazote foam was the most suitable material for construction of the insole, however this material was observed to reduce in thickness after use. This resulted in short term marking of the skin of some test subjects. The use of properly tensioned straps together with adhesive tape was essential to maintain the probe in contact with plantar tissue and to minimise lateral movement between tissue and probe.

7.1.4 Limitations of system hardware

The preceding techniques allowed a Doppler signal to be obtained from the plantar surface of the foot, during walking. However, the Doppler signal was subject to spurious noise, which could not be eliminated by signal processing remote from the sensor. For this reason, the instrumentation within the probe was further modified to include a differential amplification scheme. This resulted in a reliable Doppler signal of sufficient amplitude to allow coupling directly from the probe to an instrumentation recorder worn by the subject at waist level. Use of a multi-channel, high capacity, instrumentation recorder was necessary to record the Doppler, optical intensity and load signals. Recording of the raw Doppler signal allowed different laser Doppler signal processing algorithms to be evaluated, off-line. However, the approach had several disadvantages compared to a real-time processor: The test subject was required to carry a bulky instrumentation recorder; the signal could not be effectively monitored during the measurement period; several hours were required to download and process the data for each test subject.

7.1.5 Limitations of the software system and signal processing

To obtain an acceptable level of performance system software was developed as a set of modules, each optimised for a given task by using an optimising compiler and low-level programming. Using these techniques total processing time for the data for each subject was reduced to two hours. During the downloading phase, data from the instrumentation recorder is obtained in real-time and stored to hard disk. The implementation of this routine is critical to avoid data loss because of the asynchronous nature of the transfer. Downloaded data was inspected, for the entire test period, to ensure integrity of the signals and to identify any anomalies. In the majority of cases, the characteristics of the signals were consistent throughout the test period. The signal-processing phase involves the application of a standard laser Doppler, processing algorithm, to extract the blood flux signal from the raw data. The signal to noise ratio of the system can be improved at this stage by averaging several sets of Doppler data, however the update rate of the blood flux signal is then reduced. In the present study, an update rate of one second was acceptable for static measurements and an update rate of once per hundred milliseconds, for dynamic measurements. The final stage of the signal

processing is normalisation by the optical intensity signal. The intensity signal obtained from static and dynamic studies varied with loading and required normalised values to be calculated on a sample by sample basis. This considerably increases the total time required for processing of dynamic data.

7.1.6 Limitations of calibration and measurement

The signal-processing algorithm used in this system was selected to simplify calibration by allowing comparison with published data. This approach was necessary because of the lack of a standard calibration technique for laser Doppler and the difficulties associated with performing an empirical study. The algorithm is only linear over a limited range of red blood cell concentrations, which limits application to assessment of the microvasculature. An important limitation of the present study is that the red blood cell concentration is not determined independently at the measurement site. This gives rise to a potential error because the expectation of normal red blood cell concentrations may be invalidated by changes in the haematocrit that can occur with diabetes mellitus (Bell 1994). In other systems, the operating range has been extended by use of empirically derived algorithms or by techniques to linearise the response. This requires calibration phantoms that are generally poor models of the microcirculation and the methods used to calibrate the present system are only sufficient to verify the linearity of the system. It must be stressed, however, that the original derivation of the algorithm used in this system includes a dependency on the non-spherical geometry of the red blood cell. The use of scattering particles with different geometries can increase the probability of multiple scattering, resulting in an overestimate of blood flow.

7.1.7 Operational measurement limitations

Refinement of the sensor resulted in individual measurement repeatability with a worst case drift 5% of full scale over a period of six months. However, the sensor to sensor measurement repeatability is relatively poor at 11% of full scale, across five devices. This value could be substantially improved by adding extra instrumentation, within the probe to allow the gain to be adjusted to compensate for differences in optical sensitivity. This was not possible in the present design due to the lack of space imposed by the upper limit on the probe size. Sensitivity to changes in flow rate and

concentration has been assessed over a limited range. For normal physiological monitoring, the response is adequate, however the response to small changes in either parameter was poor. This was not a problem in the present study because large variations in blood flux are associated with the hyperaemic response and during dynamic loading of tissue. A more important parameter under these conditions is the sensor bandwidth, which was shown to extend to 25kHz. This value imposes a limit on the maximum particle velocity that can be resolved by the system. This is important because the maximum particle velocity occurring during reactive hyperaemia, was demonstrated as being proportional to the duration of loading, for periods up to ten minutes. Consequently, it became necessary to limit the maximum duration for static loading to five minutes, to ensure the sensor remained within the linear operating region. The variation in sensor response with operating temperature was compensated for by introducing correction factors into the processing algorithm. Skin temperatures were determined manually at the beginning and end of each test and the mean value used to determine the compensation factor. The validity of this approach is questionable because changes in temperature during a test are not taken into consideration.

The response of the system was demonstrated to be consistent with expected physiological behaviour during increases in skin temperature and loading of tissue. It was shown that a period of two minutes of normal walking is required to eliminate the affects of variations in heart rate on flux response. Characterisation confirmed that reliable assessment of blood flux from the plantar surface of the foot could be obtained under controlled conditions.

7.2 Discussion

7.2.1 Measurement validation – types of vessel sampled

It is important to stress that the small size of the study group prevents any general conclusions being made with regard to these results.

The focus of the clinical evaluation of the system was assessment of blood flux in the superficial capillaries of plantar skin. This is justified by the high incidence (around 80%) of ulcers originating within the upper dermis (Grunfeld 1992). The affect of vertical loading was considered, as this is a higher impact on superficial blood flow than shear, which tends to affect flow deeper in the dermis (Tsay 1991).

This study has assessed total blood flux in plantar cutaneous tissue, which comprises thermoregulatory blood flow through arteriovenous anastomoses and nutritional blood flow through superficial capillaries. It is the flow in the nutritional capillaries, which is of clinical interest because thermoregulatory vessels are not active in tissue nutrition. However, nutritional capillaries only account for about 15% of total blood flux (Fagrell 1991). As it is not possible to separate information on blood flow for each type of vessel from the Doppler signal (Chittenden and Shami 1993), the blood flux is dominated by the contribution from thermoregulatory vessels. In the present study, thermoregulatory blood flow has been controlled by maintaining the sampled tissue in a temperature range that minimises thermoregulatory flow for normal nutritional flow levels (Stevens et al. 1993, Netten et al. 1996). Under these conditions, it is proposed that changes in blood flux reflect changes in nutritional flow. An important limitation of this approach is that thermoregulatory flow is predominantly controlled centrally by the hypothalamus. Changes in ambient and core temperature could affect thermoregulatory flow independent of constant local temperature. For this reason, measurements were made at closely matched ambient and skin temperatures for each subject and over relatively short time scales. There remains, however, some doubt that the changes in blood flux observed are due solely to nutritional flow. The importance of this uncertainty on interpreting the results of the present study depends on the extent to which both types of vessel are affected by neuropathy and/or microvascular disease, in the diabetic foot. If both types of vessel are equally affected, changes in blood flux are representative of general functional and/or physical changes in the vessels of the sample

tissue. This would, however be contrary to the 'capillary steal' hypothesis in which sympathetic denervation affects only the thermoregulatory vessels. Conversely, a study by Netten et al. (1996) found that nutritional blood flow under the nail fold of the great toe, which is absent of arteriovenous anastomoses, was increased in diabetic feet. In the same subjects blood flow in the skin under the great toe, which is rich in arteriovenous anastomoses was also increased. This together with the increasing consensus in favour of the haemodynamic hypothesis (Japp and Tooke 1995) suggests that measurement of changes in total blood flow do reflect general impairment of the microvasculature in the diabetic foot.

7.2.2 Measurement validation – types of response

It is important to state that changes in blood flow assessed by laser Doppler can only be properly compared if detailed knowledge of capillary density and red blood cell concentration in the sample volume is available. As this information is normally unavailable, comparison must be made based on responses to events that induce local changes in cutaneous blood flow, for example by thermal injury (Rayman et al. 1986b). Although this type of approach is useful in demonstrating an impaired response, it does not represent the typical environment of the diabetic foot. For example, in plantar assessment the subject is normally supine, which due to postural vasoconstriction affects blood flow in the foot (Khodabandehlou et al. 1997). Furthermore, the normal extrinsic stimulus for changes in plantar blood flow is from partial or full occlusion due to variations in plantar skin pressure. Consequently, changes in blood flow due to skin pressure have both a physical and a physiological basis. The physical basis arises from the movement of blood out of a loaded region of tissue and the return of blood when the load is removed; this is a short-term transient response. The physiological basis arises from the hyperaemic response that compensates for the nutritional deficit that occurs during loading, and requires a longer period of reduced blood flow. It is suggested that the transient response is likely to be determined primarily by the properties of the sample tissue and vessels, whereas the hyperaemic response reflects the adequacy of the regulation of blood flow. If correct, this could allow vascular and neuropathic complications to be separately assessed at the same site. The current study has demonstrated that sufficiently stable conditions can be achieved to allow both the transient and hyperaemic responses to be assessed in vivo.

7.2.3 Other physiological measurement limitations

Despite these justifications for the general validity of the study, several other factors require comment. The in vivo tests to establish the effect of physiological factors such as load, skin temperature and heart rate were performed on a younger age group and the findings may not apply to the study group. In particular the mechanical properties of skin are known to alter with age. The study group itself although diverse, was not a random sample of diabetic subjects. Although this was partly by design, further bias was imposed by recruitment of the subjects, from a study of dietary control. Therefore, unlike the wider diabetic population, none of the test subjects used metabolic control or vasodilators. The marking of the skin is of some concern, but seemingly unavoidable because the sensor must remain in contact with the skin to reduce movement artefact. No adverse affects have been reported by the hospital in the intervening eight months since the study was performed.

7.2.4 In vivo static results

It is important to stress that the small size of the test group and the nature of the study prevented application of statistical inference methods and therefore no clinical significance can be attributed to the results presented in chapter six and discussed in this section. However, some general comments can be made regarding the results. For all subjects the form of the response was similar for different loading times. Similar responses were obtained for all subjects in the control group and similar responses were obtained for all subjects in the neuropathic group. The responses of subjects in the vascular group were more variable. There are clear differences between the responses obtained from each group. The control subjects exhibit a rapid rise to a peak followed by a fast recovery to 50% of peak within 30-50seconds. The neuropathic subjects exhibit a fast rise to peak followed by a slower recovery rate than the controls. The vascular subjects exhibit a much slower rise, to a broad maximum followed by a slow recovery. In most cases, the time to recover to 50% of the peak increases for longer loading times. This is consistent with the requirement to maintain a higher flow rate, for longer, to compensate for the greater nutritional deficit (Fagrell 1991). These results provide preliminary evidence to suggest that the system can demonstrate differences in blood flux responses between non-diabetic subjects, diabetic subjects with neuropathy and diabetic subjects with vascular complications.

The values for mean resting blood flux are substantially higher in the diabetic subjects than the controls. This is consistent with microvascular over-perfusion observed in the diabetic foot at rest (Japp and Tooke 1995). It is interesting to note that despite clinical evidence of an ischaemic foot, vascular subject SS has a high rest flux.

The rise times for the control and neuropathic subjects are all less than 20 seconds, whereas the minimum rise time for the vascular group is 18 seconds and is typically in the range of 20s to 60s. These values are broadly comparable to values stated by Fagrell (1991) for rise times measured at the ankle of greater than thirty seconds for subjects with macrovascular disease and less than thirty seconds for controls. In the present study, rise times for the vascular subjects do not appear to correlate with the extent of vascular impairment. Subject SS for example shows fast rise times despite having the lowest ankle:brachial index (0.6). It is possible that this is due to the difficulty of determining valid ankle pressures in some diabetic subjects due to calcification of lower limb arteries which can prevent closure at normal pressures (Sandeman and Shearman 1999).

The relative increase in blood flux from mean rest to peak is reasonably consistent for the control and neuropathic groups. The low relative increase for neuropaths GL and JCC, compared to the control group, is consistent with the impaired hyperaemic response previously observed in the neuropathic foot (Rayman et al. 1986). Conversely, neuropath RC has a similar relative increase to the control group despite clinical evidence of autonomic neuropathy. The relative increases in the vascular group differ considerably. Vascular subject SS has a consistent response below the mean resting level. As the mean resting level for all tests for this subject was relatively constant it is suggested that the response represents a failed re-perfusion that eventually recovers to normal rest levels.

Repeatability of the static loading results is good, however these results are for a small number of subjects under well matched conditions. The values obtained for the same fitting are generally closer than after refitting of sensor and shoe, which suggests that repeatability is affected by this procedure.

7.2.5 In vivo dynamic results

The results of the dynamic assessment of the study group are based on the rate of flux increase (re-perfusion) during the unloaded swing phase of gait. To allow comparison, flux values, normalised by the maximum flux during the swing phase, are expressed as arbitrary units per millisecond (a.u)/ms. The control group demonstrated the fastest rates of increase (range 6.1 a.u/ms to 7.9 a.u/ms), the vascular group has intermediate rates (range 4 a.u/ms to 6.2 a.u/ms) and the neuropathic group the slowest rate of increase (range 2.3 a.u/ms to 4.5 a.u/ms). Some overlap occurs between the groups. A possible explanation for these differences is that the properties of plantar tissue are changed in the diabetic foot so that decompression of tissue after unloading is slower leading to a consequent reduction in the rate of re-perfusion. This idea is supported by existing evidence of changes in the mechanical properties of skin in the diabetic foot (Brash et al. 1999). To test this idea, the duration of the Doppler-unloading transient, which is considered proportional to the rate of de-compression of the tissue, was measured over thirty steps for each subject. Mean values were calculated, giving a range of 130ms to 240ms across the group. The range for the control group was 140ms to 235ms, for the neuropathic group 130ms to 180ms and for the vascular group 160ms to 240ms. Thus, the decompression rate of plantar tissue, quantified by measuring the unloading transient, does not indicate clear differences between the groups. Additional work is required to investigate these findings further.

7.3 Recommendations for further work

Application of the plantar monitoring system for a full clinical trial requires further integration of the sensor to allow location within normal footwear. This could be achieved by locating the sensor within the type of insole that can be inserted in-shoe. These typically have a depth of 3mm are widely available and low cost. To implement the sensor within this depth, surface mount components would be required. All of the components of the present sensor are available in this technology. Encapsulation within a rigid or semi-flexible compound would be required to prevent ingress of moisture and protect the skin. To eliminate the requirement of pre-warming of the foot, a continuous temperature sensor would need to be incorporated. However, the problem of maintaining a consistent operating temperature to stabilise operating wavelength

remains. Improved matching of the transimpedance stages is necessary to overcome the variations in device to device response that arise from small differences in photodiode sensitivity and the coherence parameter β.

The ability to independently determine red blood cell concentration at the measurement site would allow blood flow to be separated from the blood flux value. This would normally require some form of optical spectroscopy across several wavelengths and would not be easy to integrate within a small probe. A method of selective sampling of nutritional capillary flow is desirable. This cannot simply be achieved using a lower wavelength laser because at wavelengths below 600nm absorption by chromophores increases significantly.

The present study has been limited to assessment of plantar blood flow under the first metatarsal head and the size of the sensor housing is specific to this measurement site. Furthermore, the reliable biological zero is thought to result from compression of the sample tissue volume, between the metatarsal bone and the external load. The same argument can be applied to other bony prominences such as under the calcaneous, another prevalent site of neuropathic ulceration. However, for general studies, the contribution from deeper vessels during loading of the skin is likely to invalidate the biological zero signal and requires further consideration.

A telemetry system is proposed to eliminate the need for the subject to carry an instrumentation recorder. This is complicated by the need to encode Doppler, load and optical intensity signals on the transmission channel. The bandwidth of the signals would require a large transmission and storage overhead. This problem could be solved by performing real-time processing of the data before transmission, using an integrated processing for example a Digital Signal Processor such as the TMS320 series (Texas Instruments). It is likely that the processing and telemetry system would need to be situated external to the shoe, possibly mounted on the heel. A telemetry system would provide a real-time indication of blood flow and reduce the time currently required to download and process the data.

It is recommended that the Force Sensing Resistor is retained and instrumentation included to linearise the response, so that blood flow can be reliably assessed across a range of static loads.

To further improve the signal to noise ratio of the Doppler signal a low-noise constant current controller could be developed to replace the present automatic power control approach. However, this would increase the cost and complexity of the controller.

The present study has not included diabetic subjects without complications, this group needs to be represented in a full clinical study.

7.4 Contribution

A laser Doppler system has been developed which has been shown through standard in vitro, calibration techniques to have a level of performance comparable to commercial systems. The system extends application of the technique to assessment of blood flux in-shoe during standing and walking. Despite the constraints imposed by movement artefact, results have been obtained for the unloaded swing phase of gait. Clinical evaluation has demonstrated that the system can be applied safely to assessment of the asymptomatic diabetic foot. Initial results for a small study group indicate differences in the hyperaemic response, following a period of static loading, and in rates of tissue re-perfusion during walking, between control, neuropathic and vascular subjects.

Appendices.

Appendix A. The St Vincent Declaration.

Appendix B. Details of system software.

Appendix C. Technical drawings for second prototype.

Appendix D. Artwork for final prototype.

Appendix E. Supporting publications.

Appendix F. Noise figures for evaluated laser diodes.

Appendix A

The St Vincent Declaration

Appendix to The Government St Vincent Response Declaration

To promote:

- detection and control of diabetes and its complications
- awareness among public, patients and health care professionals of present opportunities and future potential for prevention of diabetic complications
- specialised paediatric care for children with diabetes
- reinforcement of existing centres of excellence for diabetes care, education and research and creation of new ones
- independence, equity and self-sufficiency for all people with diabetes
- fullest possible integration of the diabetic citizen into society
- prevention of severe diabetic complications by ensuring better use of measures currently known to be effective, thereby:
  - reducing new blindness due to diabetes by one third or more
  - reducing number of people entering end stage diabetic renal failure by at least one third
  - reducing by one half the rate of limb amputations for diabetic gangrene
  - cutting morbidity and mortality from coronary heart disease in the diabetic by vigorous programmes of risk factor reduction
  - achieving pregnancy outcome in the diabetic woman that approximates that of the non-diabetic woman

- establishment of modern information technology systems to monitor the quality of the health care provided for diabetes and the validity of laboratory and technical procedures used in diagnosis and self-management

- collaboration in diabetes research and development in Europe and internationally, through appropriate agencies and in partnership with national diabetes patient organisations

Appendix B

Labview 'G-code' for laser Doppler flux extraction algorithm.

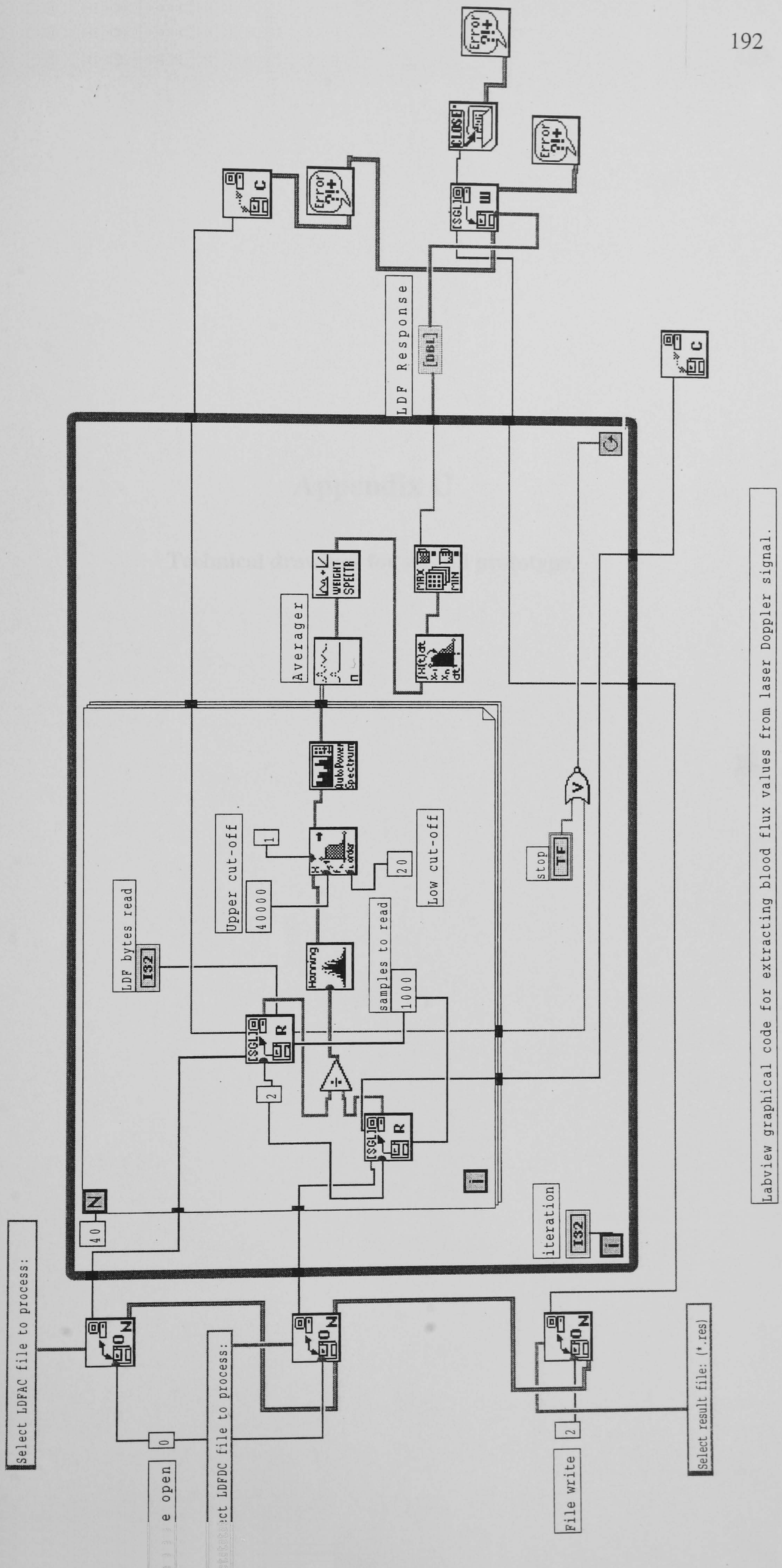
Error
CLOSE
[SGL]
C
LDF Response
[DBL]
MAX
MIN
Averager
WEIGHT SPEITR
Auto Power Spectrum
Hanning
Upper cut-off
40000
1
Low cut-off
20
samples to read
1000
LDF bytes read
I32
[SGL] R
2
40
N
stop
TF
iteration
i
0
File write
Select LDFAC file to process:
Select LDFDC file to process:
Select result file: (*.res)
Labview graphical code for extracting blood flux values from laser Doppler signal.

Appendix C

Technical drawings for second prototype.

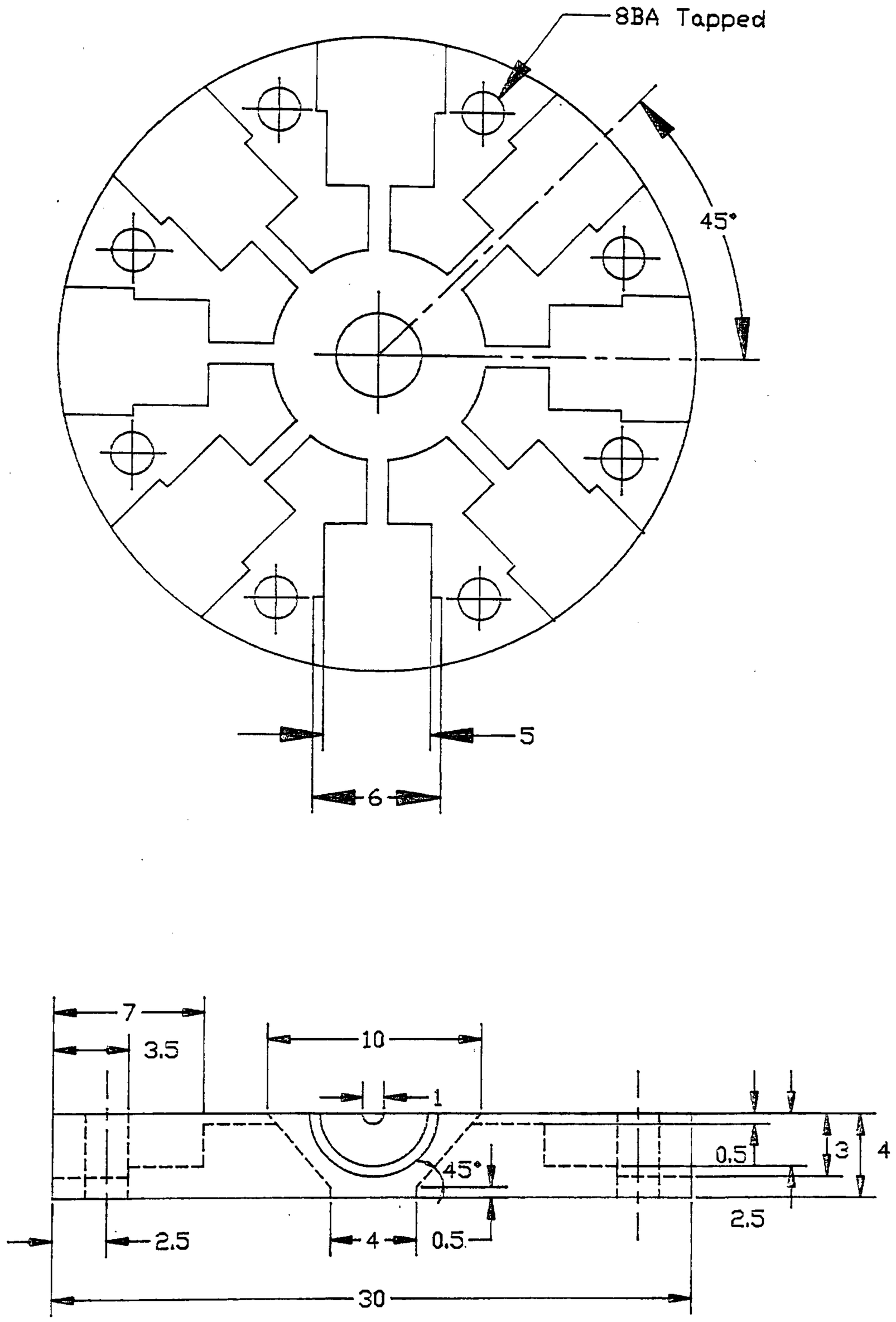

LDF Probe 2 LOWER HALF		
Jon Cobb DEC EXT 5107		
4mm = 1mm	DWG01V1	11 AUG 97

Notes: FAO: Brian Wright - TBlock.
Tony Brooker - Riverway.
Material: Cast Acrylic.

Approval:

1 of 4

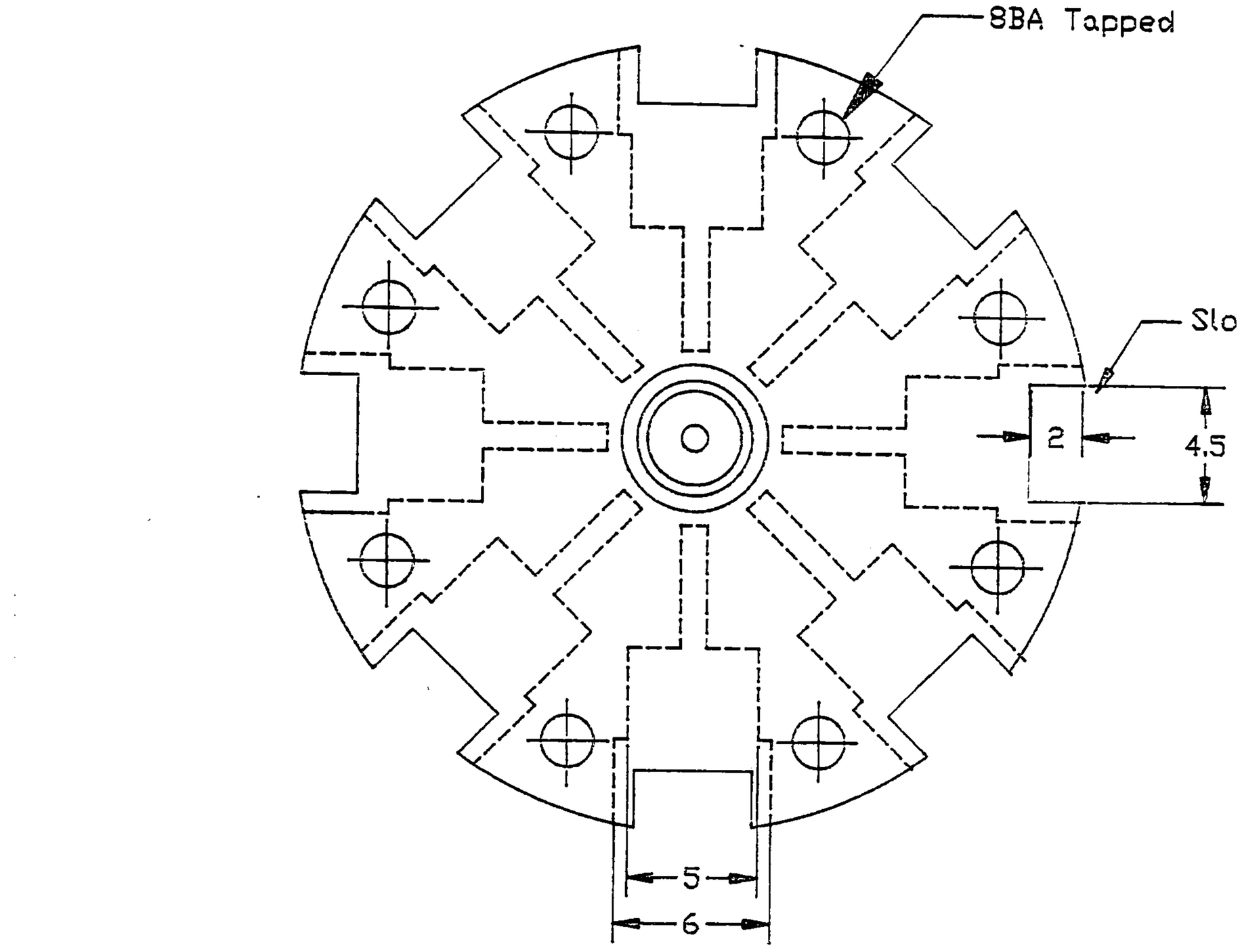

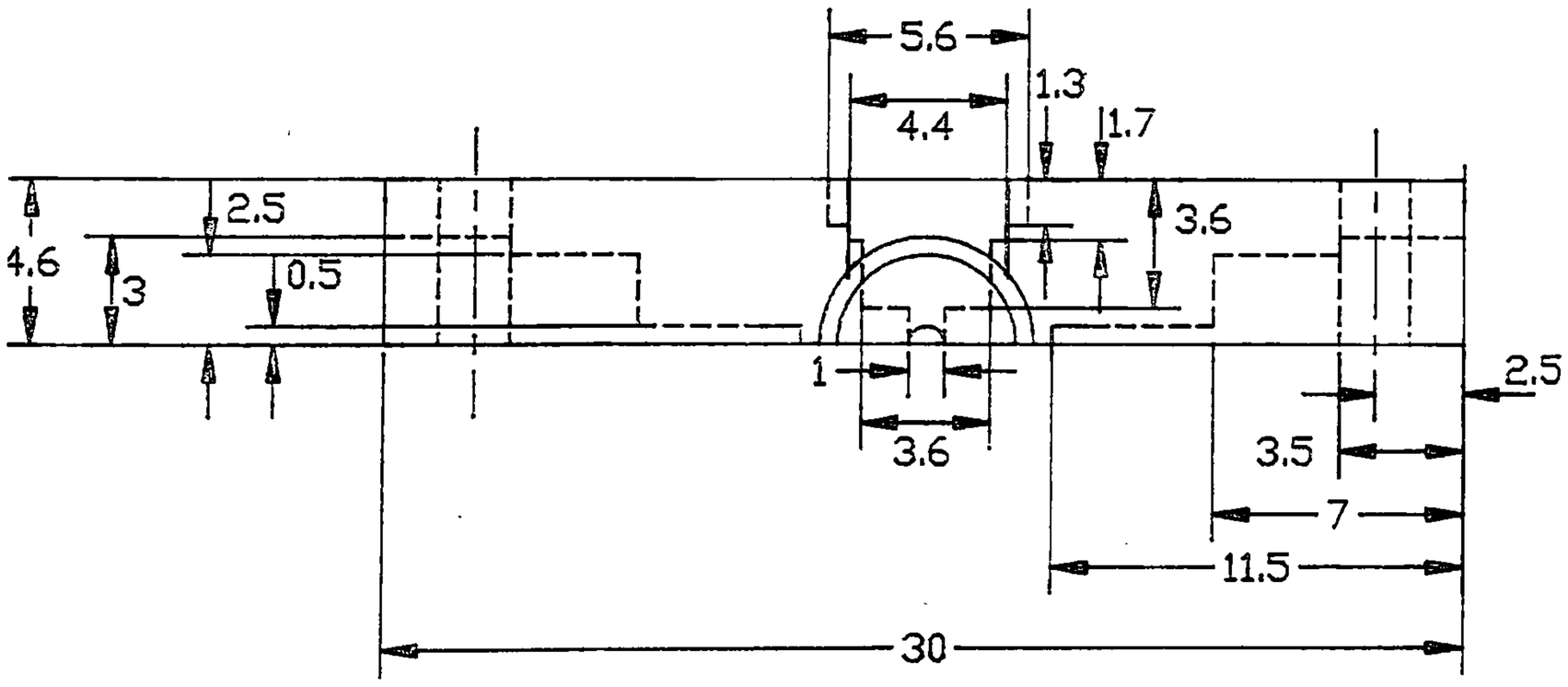

LDF Probe 2 UPPER HALF		
Jon Cobb DEC EXT 5107		
4mm = 1mm	DWG02V1	11 AUG 97

Notes: FAO: Brian Wright TBlock.
Tony Brooker - Riverway.
Material: Cast Acrylic.

Approval:

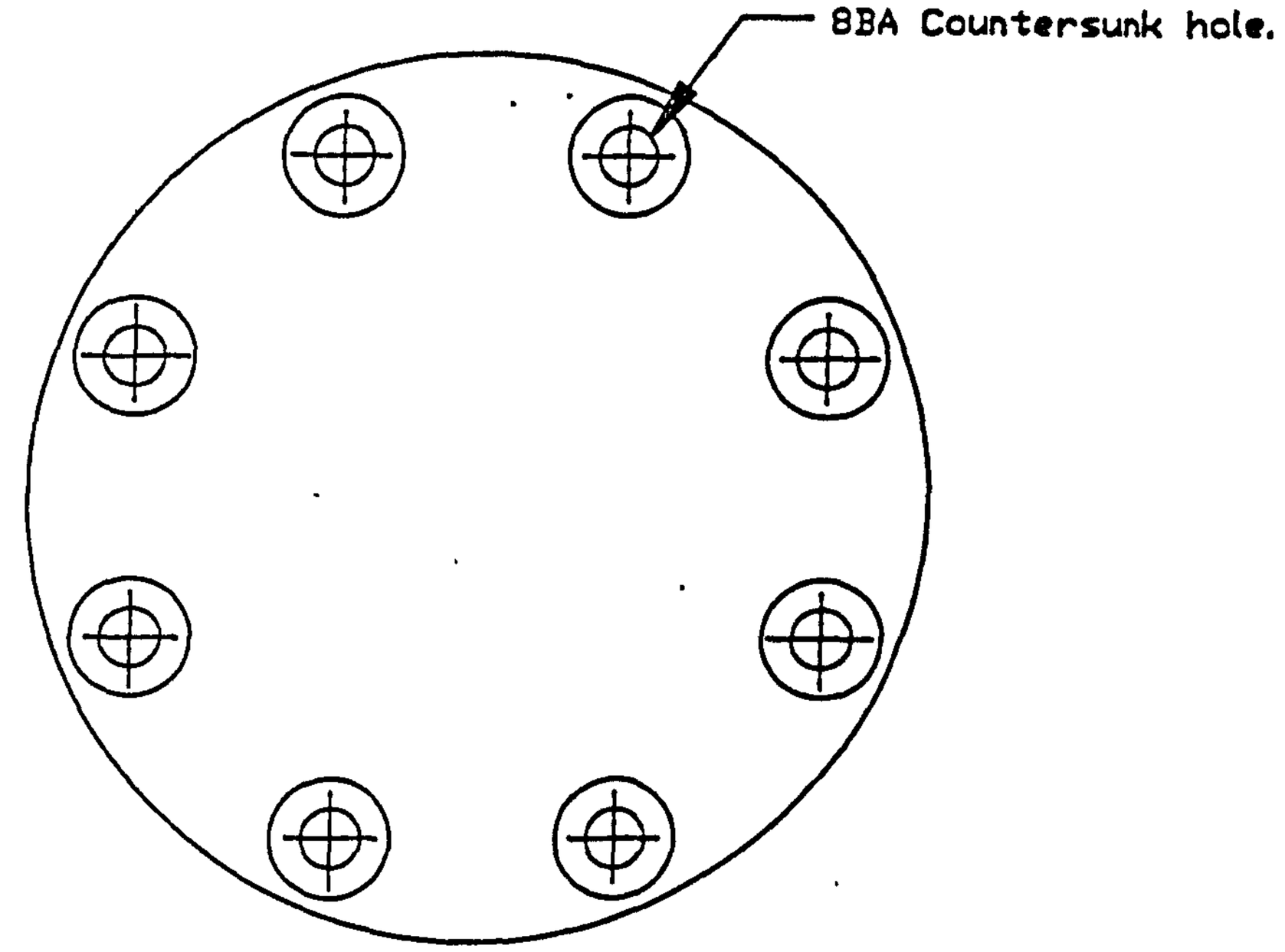

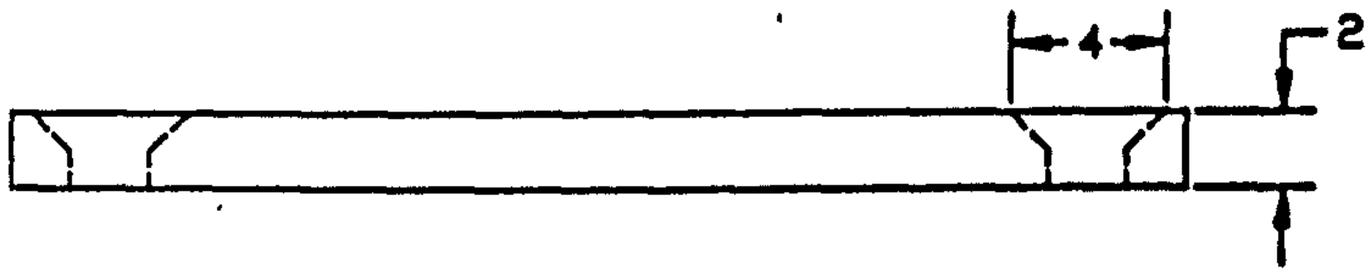

LDF Probe Top Cap.		
Jon Cobb DEC EXT 5107		
4mm = 1mm	DGW03V1	11 AUG 97

Notes: FAO: Brian Wright - TBlock.
Tony Brooker - Riverway.

Material: Cast Acrylic.

Approval:

3 of 4

All drawings viewed from top.

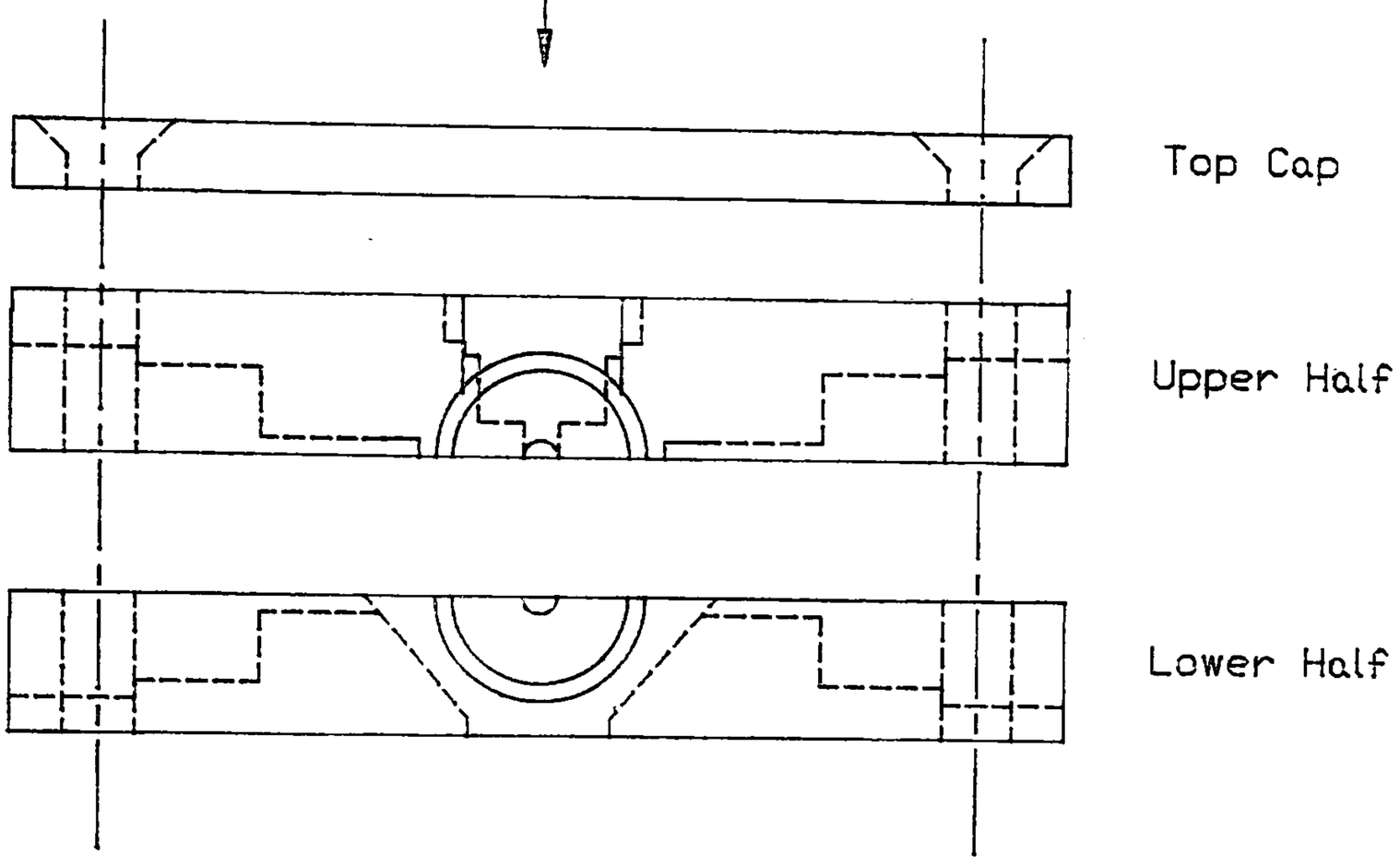

LDF Probe - ASSEMBLY & DRAWING KEY		
Jon Cobb DEC EXT 5107		
4mm = 1mm	DWG04V1	11 AUG 97

Notes: FAO: Brian Wright TBlock.
Tony Brooker - Riverway.
Material Cast Acrylic.

Approval:

4 of 4

Appendix D

Artwork for final prototype.

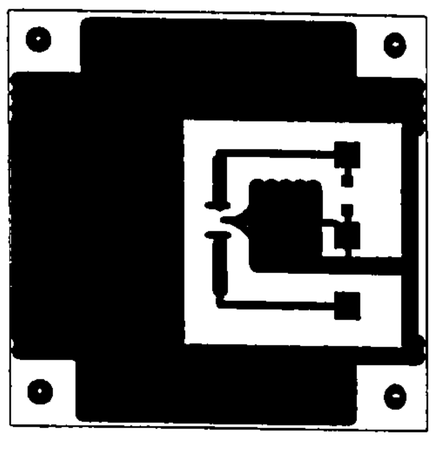

Laser board ground side.

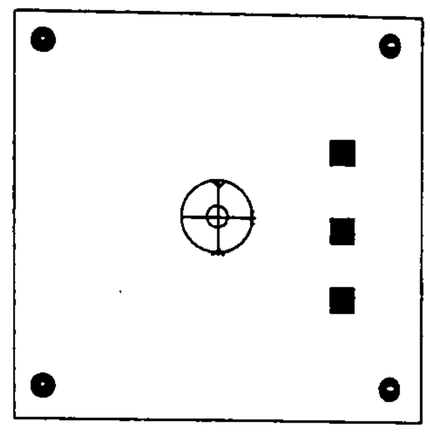

Laser board plantar side.

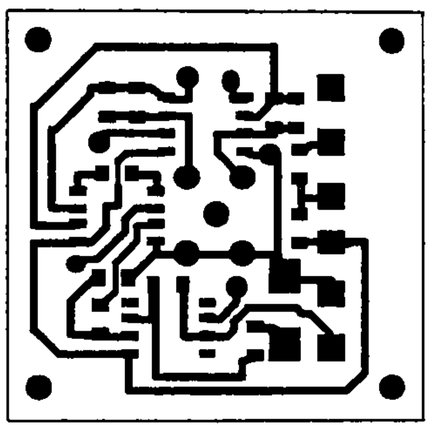

Instrumentation board ground side.

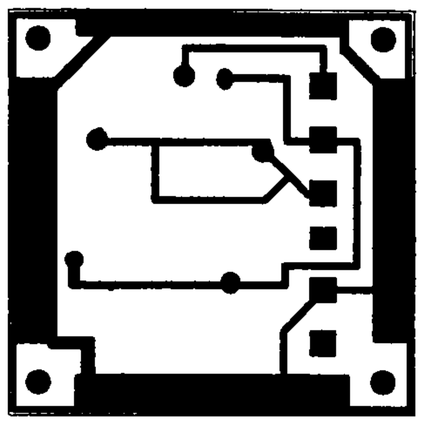

Instrumentation board plantar side

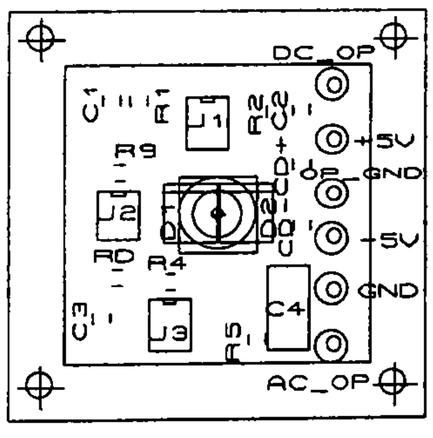

Instrumentation component ID

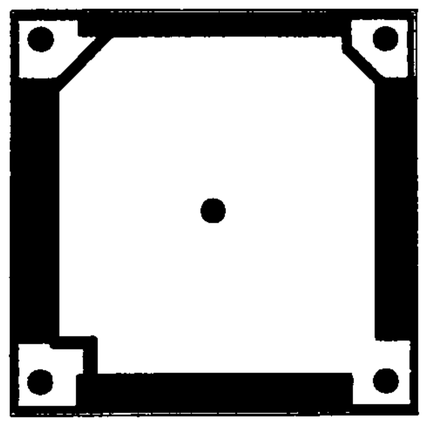

Plantar board ground side.
(Plantar side continuous copper)

PCB artwork scale 1:1 for final prototype sensor.

Appendix E

Supporting publications.

Review

Transducers for foot pressure measurement: survey of recent developments

J. Cobb **D. J. Claremont**

Department of Applied Computing and Electronics, Bournemouth University, Fern Barrow, Poole, Dorset BH12 5BB, UK

Abstract—*Recent advances in the development of transducers for the measurement of vertical and shear forces acting on the plantar surface of the foot are reviewed. Barefoot and in-shoe discrete and matrix transducers are reviewed in terms of structure, operation, performance and limitations. Examples of capacitive, piezoelectric, optical, conductive and resistive types of transducer are presented. Where available, the current clinical status is specified.*

Keywords—*Foot pressure measurement, Force, In-shoe measurement, Pressure transducers*

Med. & Biol. Eng. & Comput., 1995, **33**, 525–532

1 Introduction

THE AIM of this review is to summarise the performance of recent barefoot and in-shoe plantar pressure transducers to enable medical physicists, biomedical engineers and researchers to assess the suitability of devices and techniques for their particular applications. Previous reviews (LORD, 1981; ALEXANDER *et al.*, 1990; CAVANAGH *et al.*, 1992) have described the technology, operation and clinical applications of plantar pressure transducers without quantifying performance in detail. An excellent review of clinical findings can be found in Lord and Reynold's work (LORD and REYNOLDS, 1986).

Knowledge of the forces acting under the foot is important in the assessment of various foot pathologies (LORD and REYNOLDS, 1986). In diabetic neuropathy, measurement of plantar forces has indicated a relationship between excessive localised pressure and ulceration of the foot (CAVANAGH *et al.*, 1985). These abnormally high pressures occur as a result of a failure to achieve optimum load distribution, a consequence of the reduced sensitivity of the foot. The information obtained from these measurements can allow preventative measures to be undertaken to reduce the risk of further complication.

Other clinical applications where knowledge of plantar forces is of use include monitoring the affect of degenerative diseases on the foot such as leprosy (PATIL and SRINATH, 1990); analysis of changes in gait due to injury or deformity, for example, spina bifida (BETTS *et al.*, 1980b); and post-operative assessment following corrective surgery for conditions such as hallux rigidus (BETTS *et al.*, 1980b).

2 Methods of measuring vertical forces under the foot

2.1 *Barefoot load distribution measurement*

Static and dynamic studies of plantar forces can be achieved efficiently, using force and load distribution measurement platforms. Force platforms have been developed to a high level of performance. For example, the Kistler force plate* provides independent measurement of total vertical and shear forces with an accuracy of greater than 1 %, nonlinearity and hystersis of <1 % and sensitivity to 0·05 Pa, over full-scale ranges of typically 200 kPa for vertical forces and +/−50 kPa for shear forces. The system is primarily used for gait analysis and is not capable of measuring plantar load distribution. However, the high specification, good repeatability and long-term stability have resulted in the use of the Kistler force plate as the 'Gold standard' against which other systems are evaluated.

Since the early 1980s, several improved methods of measuring plantar load distribution under the barefoot have been developed. The commercially available Musgrave Footprint system† uses force-sensing resistors, comprising two polymer sheets, one with deposited pectinate electrodes and the other coated with the semiconducting material (molybdenum disulphide). Contact area between the electrodes and the semiconducting material increases with applied force, resulting in a large change in resistance. The devices are between 0.25 and 0.7 mm thick. The characteristic is logarithmic, with precise response dependent on substrate type, conductor geometry and the semiconducting material used. The structure of a basic force sensing resistor is depicted in Fig. 1.

Correspondence should be addressed to Dr. D. Claremont.

First received 20 December 1993 and in final form 9 December 1994

© IFMBE: 1995

* Kistler Instruments Ltd., Whiteoaks, The Grove, Hartley Wintney, Hants, UK

† Musgrave Footprint, Preston Communications Ltd., Llangollen, Clwyd, UK

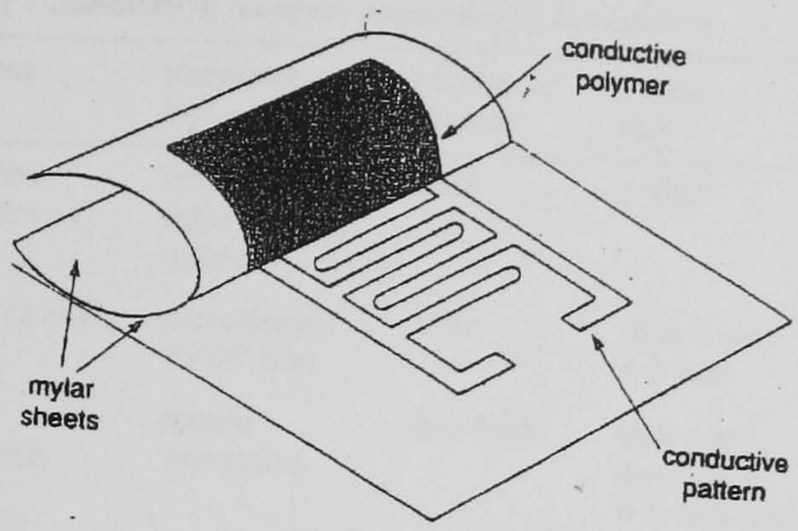

Fig. 1 *Structure of force-sensing resistor (characterised by MAALEJ et al., 1988): reproduced with kind permission of the IEEE, © 1988 IEEE, Proc. IEEE Engineering in Medicine & Biology Society 10th Ann. Int. Conf.*

The Musgrave system incorporates a matrix of 2048 Interlink§ 3 × 3 mm force-sensing resistors, with a measurement range of 0–4 MPa per sensor. The devices can be used within the range of 11 kPa to 110 kPa, giving a typical variation in resistance from 1 MΩ to 2 kΩ. Above 110 kPa, a sensor's response to a given load can vary by +/−2% per loading cycle. Above 1 MPa, the response of different sensors to the same load can vary by +/−15%. The temperature coefficient is load-dependent, typically around 0·1% per Kg $°C^{-1}$. A possible clinical limitation is the reduction in sensitivity with increasing load.

Several clinical studies have been undertaken using this system, Bennet and Duplock undertook clinical trials on 86 asymptomatic subjects and obtained results comparable with other methods (BENNET and DUPLOCK, 1993). Roggero *et al.* investigated the effectiveness of reconstructive surgery resulting from a wide range of foot pathologies (ROGGERO *et al.*, 1993). In all studies, a period of accustomisation was normally required.

In some clinical applications, such as the early detection of ulceration, high-resolution imaging of plantar load distribution is desirable to pinpoint sites of excessive pressure (LORD and REYNOLDS, 1986). Optical techniques have provided the highest levels of resolution for barefoot measurement. In the pedobarograph (BETTS *et al.*, 1980a, b; FRANKS *et al.*, 1983), the upper surface of a glass plate is covered with a thin opaque material, typically a plastic sheet. Under load, variations in the level of contact at the glass/plastic interface result in a change in the refractive index and attenuation of light propagating in the glass plate. When viewed from below, areas of contact are seen as low-intensity regions. The structure of the pedobarograph and the behaviour at the plastic/glass interface are depicted in Fig. 2.

With careful selection of the transducer sheet material, it is possible to obtain an almost linear relationship between applied pressure and light intensity. Criteria for the selection of the transducer material are described by Franks and Betts, who identify several problems occurring across a range of materials: nonlinearity; adhesion to the glass plate; saturation within the range of interest; material deformation and wear; poor dynamic response time; image intensity and uniformity dependent on surface granularity (FRANKS and BETTS, 1988). The dependence of sensitivity on temperature is particularly significant, varying by 10–15% over the range 20–30°C. The importance

§ Cryodom Europe, Coulsdon, Surrey, UK

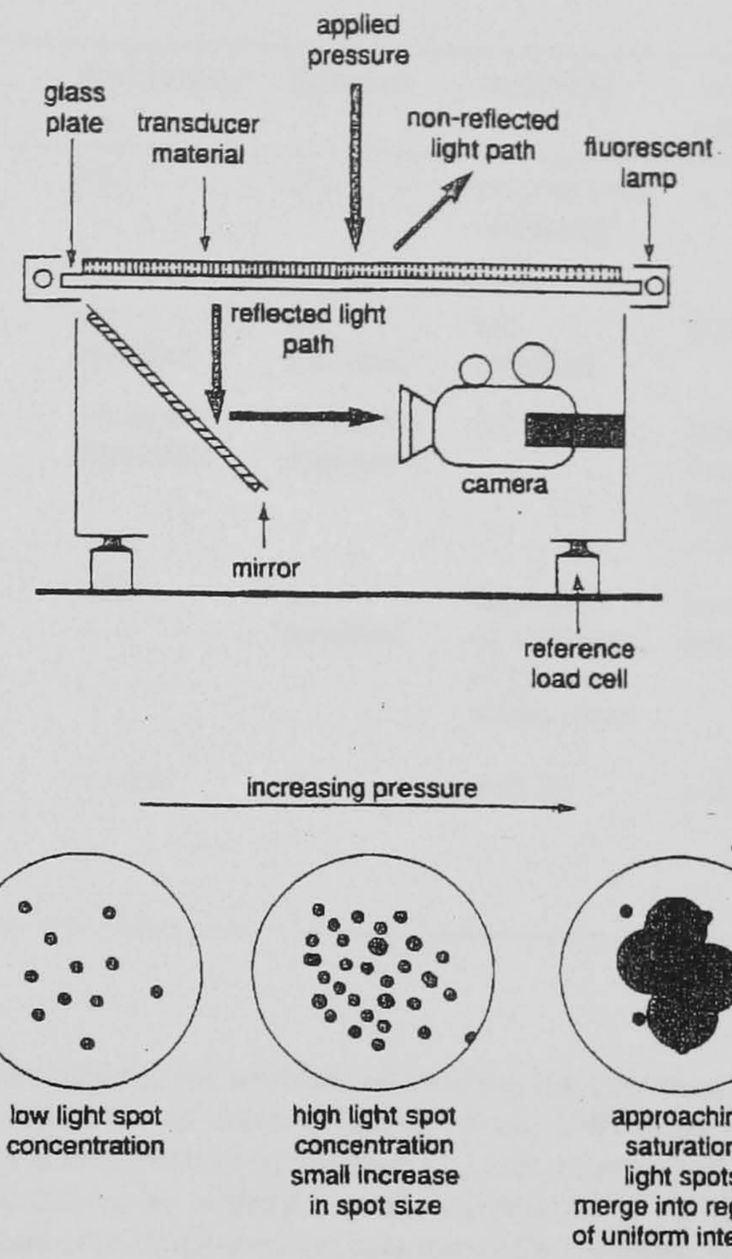

Fig. 2 *Elements of pedobarograph transducer system and behaviour at plastic/glass interface*

of load-dependent variations in light intensity in the waveguide has not been quantified.

Several clinical studies have been undertaken using the pedobarograph. Betts *et al.* investigated load distribution for two subjects with foot deformity resulting from spina bifida, and they undertook a post-operative assessment of four subjects with hallux rigidus (BETTS *et al.*, 1980b). Minns used the pedobarograph for static measurement in an evaluation of direct printing methods and noted that a stabilisation period of 30 s was required before obtaining an image, due to creep of the transducer material (MINNS, 1982). Image-processing techniques to overcome the low-intensity, low-contrast image obtained from the pedobarograph have been developed by Patil (PATIL, 1990). Pedobarograph images from 92 normal subjects have been analysed and objectively compared by Facey (FACEY, 1993).

The pedobarograph is now routinely used by Orthopaedic departments in Sheffield*.

A high-resolution imaging technique has been developed by Rhodes *et al.* using a 500 × 380 × 2·4 mm photoelastic sheet (polyurethane) and a polariser, bonded to a walkway constructed from 19 mm thick transparent acrylic (RHODES *et al.*, 1988). A thin sheet of silver-sprayed polycarbonate above the photoelastic sheet acts as a reflector. The load is transmitted to the photoelastic sheet through a 3 mm pitch corrugated plastic indenter to provide a maximum difference in the two orthogonal directions of strain to which the photoelastic effect is proportional. With increasing load, the light transmitted through the photoelastic sheet is rotated about the axis of propagation and can pass through the polariser to form a

* Personal communication: Dr R. P. Betts

Table 1 Summary of barefoot measurement transducers

reference	transducer type	number of sensors	sensor size	full- scale range/sensor	nonlinearity	hysterisis	sensitivity	frequency response
Musgrave Footprint	Interlink force-sensing resistor	2048	3 mm^2	0–4 MPa	7%	2%	reduces with increasing load	> 50 Hz
ASSENTE *et al.*, 1985	piezoelectric PVDF film	1024	10 × 7 mm × 3 mm	not specified	not specified	not specified	not specified	0·1–100 Hz
Pedo-barograph	optical waveguide	full-field	each pixel mapped to 2–3 mm area	>100 kPa per mm^2	material-dependent	material-dependent	2·5 kPa	material-dependent typically <20 Hz
RHODES, 1988	optical photoelastic	full-field	each pixel mapped to 3 mm area	not specified	<3%	not specified	dependent on thickness of photo-elastic sheet	not specified
Kistler platform (type 9284)	piezoelectric total vertical and shear forces	4 load cells/ 3 quartz rings per cell	force plate area = 500 mm^2	vertical 200 kPa shear +/−50 kPa	+/−1%	1%	0·05 Pa	>100 Hz

parallel line image of the indenter, with point intensity proportional to applied force. The image is captured by a camera adjacent to the walkway, with each pixel representing a physical area of 0·96 × 0·79 mm. To filter out surface irregularities and simplify interpretation, pixels are assigned the average intensity value within each 3 mm^2 area.

Calibration typically indicated nonlinearity errors of <3 %. Sensitivity is controlled by the thickness and hardness of the photoelastic sheet. The significance of spatial and temporal distortion (LORD, 1981) introduced by the polycarbonate reflector is not considered. With further evaluation, this technique may provide comparable performance to the pedobarograph with several advantages, particularly temperature-independent response.

Transducers employing piezoelectric materials are not well suited to static measurements due to the charge leakage arising from the non-ideal characteristics of charge amplifiers. The unacceptably high time constant required for accurate static measurements imposes a typical low-frequency limit of around 0.1 Hz on systems using piezoelectric materials (Kynar Technical Manual, 1987).

Assente *et al.* constructed a 580 × 380 mm platform using poled 40 μm piezoelectric PVDF (polyvinylidene fluoride) film, bonded to a double-sided printed circuit board containing 7 × 10 mm rectangular copper pads (ASSENTE *et al.*, 1985). Each of the 1024 pads is capacitively coupled to the piezoelectric film and connected to the instrumentation on the reverse side of the board via through hole plating. The upper side of the film is pre-plated with aluminium to provide a common ground reference. Charge amplifiers sample the output from each transducer at a rate of 100 Hz. Details of the transducer performance are not presented.

A summary of barefoot pressure transducer characteristics is given in Table 1.

2.2 *Discrete sensors for in-shoe pressure measurement*

Two significant disadvantages of barefoot measurement systems are the inability to assess behaviour at the foot-shoe interface (CAVANAGH *et al.*, 1992) and the difficulty of synchronising measurement to specific phases of the gait cycle (HENNIG *et al.*, 1994). In-shoe discrete transducers for measurement at selected plantar sites overcome these problems, while introducing the problem of locating the transducers at the appropriate sites of interest (LORD *et al.*, 1992). An accurate and repeatable method of aligning discrete sensors has recently been described by Akhlaghi *et al.* (AKHLAGHI *et al.*, 1994).

Kothari *et al.* evaluated the commercially available Orthoflex Hercules capacitive pressure transducer to measure pressure at seven locations under the foot (KOTHARI *et al.*, 1988). The transducer structure comprises five corrugated metal electrodes in parallel, separated by mica. The structure is formed as a thin cylinder, with a depth of 2·44 mm and a diameter of 18 mm.

Compression of the structure results in a change in capacitance from 230pF to 460pF over the full load range of 0–1·3 MPa. Maximum nonlinearity of 11 % and hysterisis of 10 % are stated for the range 0–700 kPa. Sensitivity varies over sensor area, reducing nonlinearly from a value of +/−5 kPa at the centre to +/−30 kPa at the periphery. The accuracy of the output is therefore dependent on load distribution. The transducer bandwidth is 12 Hz, limiting measurement to slow walking speeds. Kothari *et al.* intend to use these transducers in an 'electrotactile' feedback system to restore sensation to subjects with diabetic neuropathy.

Gross and Bunch constructed discrete piezoelectric ceramic (lead-zirconate-titanate) transducers, of dimensions 4·83 mm^2 ×1·3 mm, sealed in a polyurethane casing to provide protection from moisture, uniform load distribution and minimal sensitivity to lateral strain (GROSS and BUNCH, 1988). Maximum nonlinearity of 3·4 % and maximum hysterisis of 5·8 % are stated. Transducer-to-transducer sensitivity can vary by 20 % due to the difficulty of connection at the ceramic surface, requiring individual calibration of each transducer.

A clinical evaluation of transducer performance was undertaken on an unspecified number of asymptomatic subjects. For day-to-day tests, the combined error due to subject variation, transducer displacement and random factors, averaged over eight transducers, was 9·9 %. For single-day tests where transducers did not require relocation, the combined error was reduced to 3·1 %. Maximum errors were found to occur under the medial-midfoot and hallux due to the difficulty in attachment at these sites.

Discrete in-shoe transducers can introduce errors by causing the load to become concentrated at the measurement site, leading to high readings or saturation (NEVILL, 1991). The

situation can be improved by reducing transducer thickness, ideally below 0·5 mm (FERGUSON-PELL, 1980). However, the mechanical properties of the transducer, the use of an insole and the insole of the shoe can also significantly affect the load distribution.

The Electrodynagram system† provides seven discrete sensors with a thickness of only 0·3 mm. These sensors are suitable for both in-shoe and barefoot measurement. Each sensor is an integrated circuit containing a resistive bridge (NEW SCIENTIST, 1985) with temperature compensation. The measurement range is 0–1·5 MPa with sensitivity of +/−30 kPa. The sensors exhibit nonlinearity of 5–10 %, a high hysterisis error of 15–20 % and drift of 8 % after 1 min. Readings are stored in a waist-mounted instrumentation unit with the ability to sample at up to 200 Hz per sensor.

This system has been used in assessing variations in load distribution as a result of limb length discrepancy (D'AMICO *et al.*, 1985), diabetic foot ulceration (SMITH *et al.*, 1989) and assessment of the affect of varying shoe heel height on foot function (GASTWIRTH *et al.*, 1991).

Nevill *et al.* developed piezoelectric transducers using P(VdF-TrFE) copolymer film (NEVILL *et al.*, 1991). Discrete 10 × 10 × 2·8 mm transducers were cut from a laminate formed by bonding 500 μm non-electroded copolymer film between an upper brass sheet and a lower double-sided copper-clad board. The laminate provided sufficient stiffness to prevent significant errors caused by lateral stretching and bending of the film.

Transducers were located in recesses cut into a 3 mm thick rubberised cork insole at eight sites. An instrumentation unit containing eight charge amplifiers is strapped to each ankle. A further waist-mounted unit provides power to the two ankle units and an interface to the host computer.

The unit was calibrated by applying weights up to 10 kg through a loading piston. To simulate bending stresses, different types of test head were employed. Over the measurement range of 0–1 MPa, the transducers are linear to within 1·5 % and have a hysterisis error < 1·5 %. Sensitivity is +/−1 kPa within the calibration range. Errors due to lateral or transverse bending of the transducers resulted in a worst case reduction in sensitivity of 3 %. The frequency response extends from 0·008 Hz to 250 Hz.

The upper brass plate was found to reduce pyroelectric charge generation by conducting heat away from the film. Temperature compensation is applied to the data to account for differences between the calibration and measurement temperatures. The transducers require periodic re-laquering to reduce charge leakage arising from in-shoe humidity.

Clinical trials were undertaken with 41 normal subjects to assess pressure distribution and with seven asymptomatic subjects to assess hindfoot pain, knee failure and the effectiveness of pressure relief insoles. Transducers were sited under the heel, lateral arch, metatarsal heads and hallux. The results were comparable to those obtained for the same subjects using a dynamic pedobarograph (BETTS *et al.*, 1991). Variations in peak pressures occurring within single and between repeated tests required an average of ten footsteps per test to achieve an acceptable measurement repeatability. The significance of these variations have been assessed by Akhlaghi *et al.* (AKHLAGHI *et al.*, 1994). Measurement repeatability averaged across transducers was within 16 %. Reliability was excellent, with no transducer failure and a single connection failure in 10 000 footsteps. Clinical application maybe restricted by the need to make the insoles for each individual subject, which is both time-consuming and requires experience to mount the transducers.

The Gaitscan system arising from this work is currently in use as a clinical and research tool at Dundee Royal Infirmary and the Department of Podiatry, Leaf Hospital, Eastbourne (personal communication: Dr M. G. Pepper).

A discrete in-shoe electro-optical force transducer has been described by Maalej *et al.*, which employs an asymmetric U-shaped steel spring, mounted in an extra depth shoe (MAALEJ *et al.*, 1988). The spring has a lower beam length of 4 mm, upper beam length of 3·5 mm and radius of curvature of 1·5 mm. The upper beam has a curved end, which under load, acts to occlude transmission of light between an LED and photodetector mounted on the lower beam. The transducer is encapsulated in silicone rubber to provide even loading and protect against ingress of moisture and dirt. The load range is 0–1·6 MPa, giving a maximum deflection of 0·11 mm; good sensitivity is reported. Figures for nonlinearity of +/−2·5 % and hysteresis of 1·5 % are stated.

The use of this transducer in a clinical environment is limited by the need to use specialised footwear and the difficulty of aligning the sensors. Care is also required to exclude any external light. The silicone rubber used was found to break-down at around 1000 loading cycles, and a stronger elastomer is required. By employing fibre optics, Maalej *et al.* claim that a large increase in spatial resolution is possible.

A summary of discrete plantar pressure transducer characteristics is given in Table 2.

2.3 *Matrix insoles for in-shoe measurement*

Several of the problems associated with the use of discrete transducers can be overcome by incorporating transducers in an insole; for example, the affect on gait is minimised and lateral displacement from the measurement location is reduced (NEVILL, 1991). This 'matrix insole' approach has resulted in several commercial developments. However, there are several difficulties: repeatability between elements within an insole and between insoles; the problem of crosstalk between elements; errors due to bending forces; and the difficulty of calibration.

Nicol and Hennig developed a barefoot measurement mat using a flexible, capacitive sensor matrix; an improved version is employed in the Emed Pedar§ system.

This system provides 99 sensors on a 2 mm thick insole, with individual sensors occupying an area of 17 mm^2. Sensor measurement range is 30 kPa–0·6 MPa with sensitivity of 1 kPa varying by +/−5 % over the temperature range 10–40°C. Significant improvements in performance over other types of capacitive transducers are the low hysterisis of <3 %, frequency response to 50 Hz and good day-to-day repeatability. Mechanical decoupling of the sensing elements allows performance to be maintained when bending forces are applied. The instrumentation is located in a portable waist-mounted unit.

Using this technology, Hennig *et al.* compared the barefoot pressure distributions of 125 children and 111 adults with no history or indication of pathology, and obtained comparable results with other methods, despite some difficulty in targeting the sensor area (HENNIG *et al.*, 1994).

Hennig *et al.* also constructed an insole containing an array of 499 piezoelectric ceramic (lead-zirconate-titanate) transducers, 4·7 mm^2 × 1·2 mm, embedded in silicone rubber (HENNIG *et al.*, 1982). Over the measurement range of 0–1·5 MPa, sensitivity is 0·5 kPa varying by 1·5 % over 10–40°C. Excellent figures for nonlinearity of +/−2 % and

† Langer Biomechanics Group Ltd., The Green, Cheadle, Stoke-on-Trent, UK

§ Novel Gmbh, 80802 München, Germany

Table 2 Summary of discrete foot pressure transducers

reference	transducer type	number of sensors used	sensor size	full-scale range/ sensor	non-linearity	hysterisis	sensitivity	frequency response
KOTHARI *et al.*, 1988	capacitive	7	18 mm diameter × 2·4 mm	0–1.3 MPa	11%	10%	±5 kPa	12 Hz
GROSS and BUNCH, 1988	piezoelectric ceramic	8	483 mm^2 × 1·3 mm	2 MPa	3·4%	5·8%	not specified	>50 Hz
Electrodynogram (Langer)	polysilicon resistive bridge	7	10 mm^2 × 0·3 mm	0–1·5 MPa	5–10%	15–20%	±30 kPa	200 Hz
MAALEJ *et al.*, 1988	optical LED & photodiode	4	5 × 6 × 3 mm	0–1·6 MPa	±2·5%	1·5%	very high	>20 Hz
NEVILL, 1991	piezoelectric PVDF film	8	10 × 10× 2·8 mm	0–1 MPa	1·5%	< 1·5%	1 kPa	0.008–250 Hz
LORD *et al.*, 1992	magneto-resistor (shear transducer)	6	16 mm diameter × 4 mm	0–250 kPa over area 200 mm^2	not specified	not specified	high	500 Hz, 70 Hz used in practice

hysterisis of 1 % were achieved. The variation in the sensitivity of the sensors within the matrix, resulting from material and fabrication tolerances, was sufficient to require individual calibration of each sensor. Several sources of error were identified: pyroelectric charge generation, susceptibility to electrical interference and sensitivity to lateral strain.

A charge amplifier converts the output from each transducer to a proportional output voltage at a sampling rate of up to 200 Hz. The sensor was used to monitor one asymptomatic subject; no significant problems were reported.

Transducer arrays employing piezoelectric ceramic materials can be difficult to construct and can be subject to rapid mechanical fatigue; both problems may be reduced by using piezoelectric polymer film (NEVILL, 1991).

Pedotti *et al.* produced an insole from a film of the piezoelectric polymer, polyvinylidene fluoride (PVDF) (PEDOTTI *et al.*, 1984). Circular aluminium discs of 6 mm diameter were deposited onto the film to form transducer electrodes at 16 sites. Aluminium tracks transfer the output signal from each transducer to the periphery of the insole for connection to remote instrumentation. A 20 μm unpoled PVDF film was silver sprayed and bonded to the film to provide shielding from electrical interference.

The transducer is linear to within +/−0·2 % over the full load range of 0–4 MPa. Repeatability of response between the 16 transducers on the insole is within +/−3 %. Sources of error were identified as additional charge generation due to lateral stretching, pyroelectric charge generation arising from compressional heating of the polymer and from frictional heating during gait.

A clinical evaluation was undertaken with a single symptom-free subject; no problems were reported. Pedotti *et al.* claim excellent repeatability between tests. This technique is not appropriate for routine clinical use because of the need to make the insoles for each individual subject.

Several examples of transducer arrays based on conductive and resistive technologies have been developed during the last five years. Peruchon *et al.* fabricated an insole to measure the variation in conductance of a conductive polymer under load (PERUCHON *et al.*, 1989). A cross-sectional diagram of the transducer is shown in Fig. 3.

Electrodes are etched on a copper-plated flexible, printed circuit substrate (polyimide) to form an array of 127 elements with centre-to-centre spacing of 1 cm. Conductive tracks from each transducer converge at the periphery of the insole for connection to a waist-mounted instrumentation unit. The insole is 2·5 mm thick.

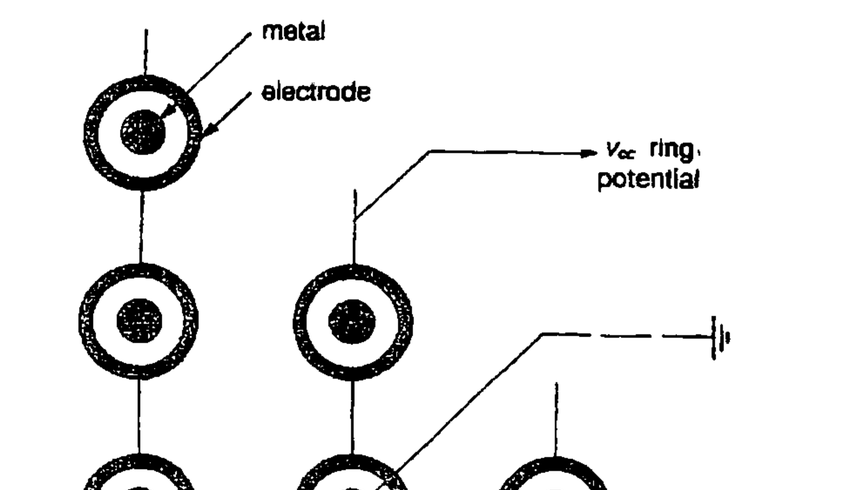

Fig. 3 *Cross-sectional diagram of multiple sensor insole (developed by PERUCHON et al., 1989)*

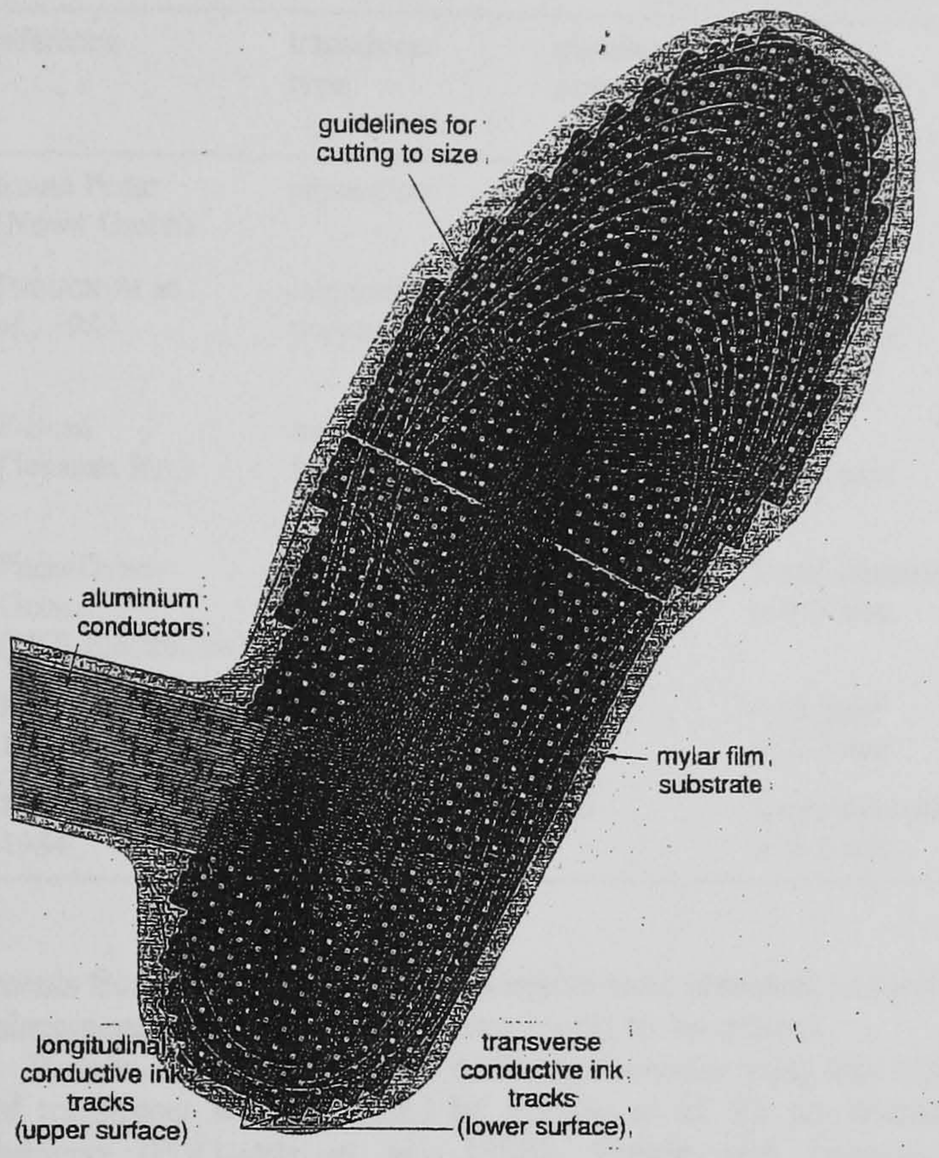

Fig. 4 *Tekscan F-scan insole; each resistive ink sensing element is formed between overlapping transverse and longitudinal conductors*

Each transducer element consists of a circular ground electrode and a concentric, isolated, outer reference electrode. Current flow between electrodes increases with compression of the polymer.

The calibrated measurement range is 0–300 kPa; from 0 to 225 kPa material compression is 15%, nonlinearity 16% and hysterisis 12%. For material compression in the range 15–25%, nonlinearity increases to 26%, requiring a look-up table to provide compensation. The resultant sensitivity is +/−20 kPa. Transducer bandwidth extends to 100 Hz. Response is temperature-independent in the range 15–35°C.

Sealing the conductive polymer in a polyurethane film increases its operational lifetime by reducing abrasion of the copper tracks. Compensation is required to reduce errors due to charge leakage between different elements. The limited range of conductive polymers is a problem; response times are typically low.

Clinical trials were undertaken on ten asymptomatic subjects; poor reliability was found to be a significant problem.

The F-Scan system* uses conductive and resistive inks on a flexible mylar substrate to form a matrix of 960 sensors on a disposable, 0·1 mm thick, insole (SENSORS, 1991). Each 5 mm^2 sensing element is formed by depositing a layer of resistive ink between two orthogonal conductors. Aluminium tracks deposited on the external surfaces provide connection to a small instrumentation unit worn on the ankle. These tracks are routed along the longitudinal centre line, allowing the insoles to be cut to size. A photograph of the insole is given in Fig. 4.

The matrix is scanned at 165 Hz per sensor with a resolution of 8 bits, yielding a sensitivity of +/−4 kPa. Data are transmitted over a lightweight cable to a host computer.

Details of the performance of the device are not given in the Tekscan literature. An evaluation of these insoles (ROSE *et al.*, 1992) indicated closely reproducible static and dynamic measurements for normal test subjects under certain conditions. However, calibration between sensors was found to be poor and the sensors showed significant wear with use. The thermal coefficient of the resistive ink may also be significant.

Clinical studies of one subject with a plantar callus below the second metatarsal head and a second subject with submetatarsaglia pain have been reported by Young (YOUNG, 1993).

The recently developed Podo-Dyno-Gram system† uses a matrix of 64 circular Interlink force-sensing resistors deposited onto a mylar film to form an insole. The measurement range is 0–0·8 MPa with a sensitivity of +/−20 kPa. Nonlinearity is less than 10%.

A summary of matrix insole characteristics is given in Table 3.

3 Methods of measuring shear forces under the foot

To investigate the possible effect of shear forces on various foot pathologies, a discrete shear transducer was developed by Tappin and Pollard (TAPPIN and POLLARD, 1980). The same principle is used in the transducer designed by Lord *et al.* (LORD *et al.*, 1992), illustrated in Fig. 5.

Movement of the permanent magnet relative to the magneto-resistive element results in a change in resistance proportional to applied force. The elasticity of the silicone rubber bonding the two halves of the transducer provides a restoring force to return the magnet to its equilibrium position. The maximal excursion of 0·6 mm corresponds to a shear stress of 250 kPa. By aligning the locking groove in either a longitudinal or transverse direction, relative to the foot, the related shear component can be measured. A bridge circuit provides a temperature-compensated output voltage. The frequency response extends to 500 Hz. In clinical tests, a high-frequency cut-off of 70 Hz was found to be acceptable. Shear measure-

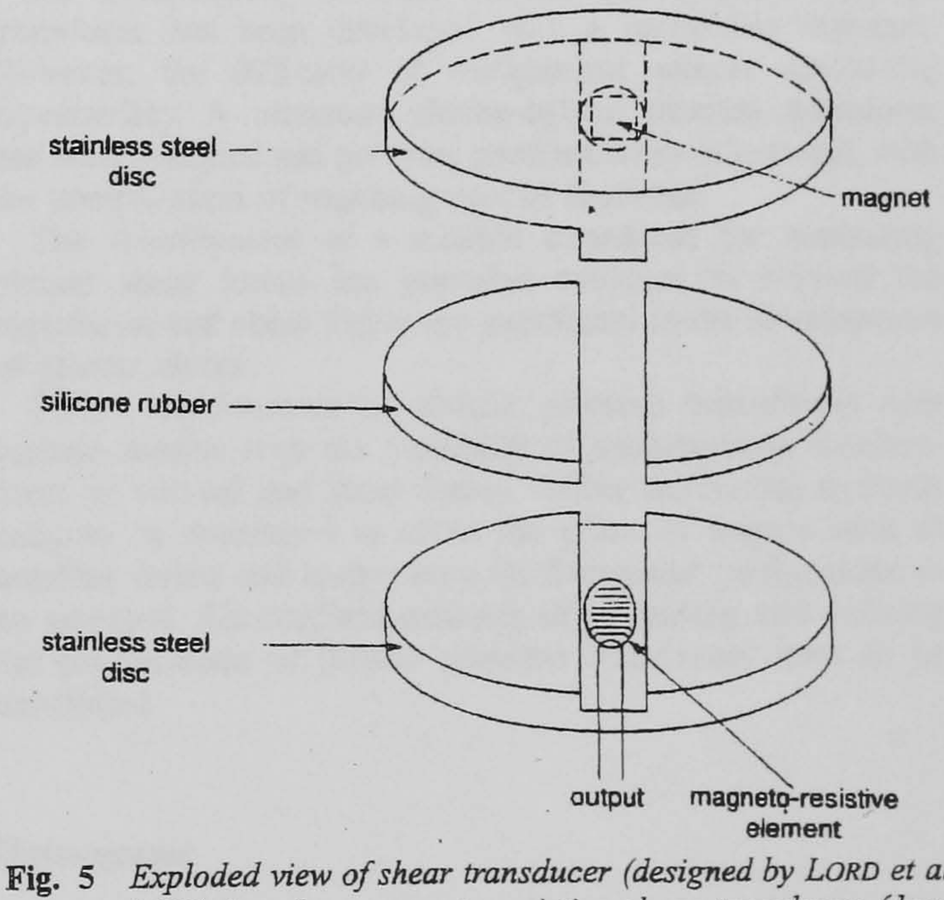

Fig. 5 *Exploded view of shear transducer (designed by LORD et al., 1992) based on magneto-resistive shear transducer (developed by TAPPIN, 1980)*

* Tekscan Inc., 307 West First Street, South Boston, Massachusetts, USA

† PKS Electronics, Belgium

Table 3 Summary of transducer matrix insoles for foot pressure measurement

reference	transducer type	number of sensors/ insole	sensor size	full-scale range/ sensor	nonlinearity	hysterisis	sensitivity	frequency response
Emed Pedar (Novel Gmbh)	capacitive	99	17 mm^2	30 kPa–0·6 MPa	not stated	<3%	1 kPa	50 Hz
PERUCHON *et al.*, 1989	conductive polymer	127	10 mm diameter × 2·5 mm	0–300 kPa	16% @ 75% full-scale	12% @ 75% full-scale	±20 kPa	100 Hz
F-Scan (Tekscan Inc.)	resistive ink	960	5 mm^2 × 0·1 mm	0–1 MPa	not specified	not specified	±4 kPa	165 Hz/ sensor sample rate
Podo-Dyno-Gram. (PKS Electronics)	piezo-electrical force sensing resistor	64	5 mm diameter × 0·7 mm	0–300 kPa	<10%	not available	±20 kPa	150 Hz
HENNIG *et al.*, 1982	piezoelectric ceramic	499	4·78 mm^2 × 1·2 mm	>1500 kPa	2%	1%	0·5 kPa	>50 Hz
PEDOTTI *et al.*, 1984	piezoelectric PVDF film	16	6 mm diameter < 0·1 mm	0–4 MPa	0·2%	not specified	not specified	>50 Hz

ments from four asymptomatic subjects were obtained; accurate placement of the transducers was found to be critical.

Results of clinical tests for differing footwear using this type of transducer were reported by Pollard *et al.* for ten normal subjects (POLLARD *et al.*, 1983). Tappin and Robertson undertook barefoot measurements on a group of 20 normal subjects and in-shoe measurement for a variety of footwear on ten normal subjects (TAPPIN and ROBERTSON, 1991). Their results indicated that the magnitude of the vertical forces required to occlude blood flow can be reduced by up to 50% when sufficient shear force is simultaneously present.

Further developments of this type of shear transducer are curently under investigation (LAING *et al.*, 1992), including possible improvements to instrumentation§. Modification to allow simultaneous measurement of vertical and shear forces has been made by Williams *et al.* in order to investigate stresses at the prosthetic interface of lower limb amputees (WILLIAMS *et al.*, 1992). A shear transducer using copolymer piezoelectric film has been reported and is currently being clinically evaluated (AKHLAGHI and PEPPER, 1993).

4 Conclusions

In assessing and presenting results from clinical studies involving measurement of plantar pressure, it is important to identify and quantify the limitations of the devices used to allow an objective comparison to be made with the findings from other studies. This review has detailed the performance of several plantar pressure transducers designed during the last 15 years. The most significant developments are summarised below.

The Musgrave Footprint provides high-resolution imaging and is well suited for inclusion in a walkway. There are some inherent problems with the force-sensing resistors employed, in particular poor measurement repeatability and nonlinear sensitivity. The Dynamic Pedobarograph provides very high resolution images; sources of error include significant temperature dependence and creep of the transducer material.

The Electrodynagram system provides reasonable performance and uses very thin transducers; there are some problems with drift and hysterisis.

The Emed-Pedar insoles use specially developed capacitive elements, yielding improved performance compared to previous capacitive transducers. The Tekscan insoles allow high-resolution imaging using a very thin low-cost insole which can be scaled in size; there are possible problems with repeatability.

The majority of these commercial devices have been evaluated in clinical studies with comparable results between systems. Most have wide clinical applicability. There have been several non-commercial transducer developments.

In the Gaitscan system, the use of discrete piezoelectric film transducers in an insole provides good performance and reliability. However, the need to fabricate the insole for each individual subject may limit the extent of its clinical applications. This system is being evaluated clinically and may soon be a commercial option.

A photoelastic sheet has been used in a walkway, providing high resolution at low cost and possible advantages over the pedobarograph.

An exceptionally accurate discrete piezoelectric ceramic transducer has been developed with a repeatable response. However, the difficulty of realignment affects day-to-day repeatability. A miniature electro-optical discrete transducer has been designed and provides good accuracy at low cost, with the complication of requiring special footwear.

The development of a reliable transducer for measuring plantar shear forces has provided evidence to support the hypothesis that shear forces are significant in the development of plantar ulcers.

Future development of plantar pressure transducers may include insoles with the capability of simultaneous measurement of vertical and shear forces. Better calibration methods need to be developed to allow the effect of factors such as bending forces and temperature on transducer performance to be assessed. Standardised methods of evaluating and defining the performance of plantar pressure transducers need to be developed.

§ Personal communication: Dr M. Lord

References

AKHLAGHI, F., PEPPER, M., *et al.* (1993): Assessment of in-shoe foot pressure patterns over multiple footsteps. *Proc. IPSM/HPA 49th Ann. Conf.*, Lincoln, UK, p. 68

AKHLAGHI, F., DAW, J., *et al.* (1994): In-shoe step-to-step pressure variations. *Foot*, 4, pp. 62–68

ALEXANDER, I. J., CHAO, E. Y., *et al.* (1990): 'The assessment of dynamic foot-to-ground contact forces and plantar pressure distribution: a review of the evolution of current techniques and clinical applications'. *Foot Ankle*, **11**, pp. 152–167

ASSENTE, R., FERRIGNO, G., *et al.* (1985): 'Distributed multiplexing architecture for PVDF multitransducer platform scanning: a theoretical and practical approach'. *Proc. 5th Symp. Electrets, Heidelberg, Germany*, pp. 795–800

BENNET, J. P. and DUPLOCK, L. R. (1993): 'Pressure distribution beneath the human foot'. *J. Am. Podiatric Med. Assoc.*, **83**, (12), pp. 674–678

BETTS, R. P., DUCKWORTH, T., *et al.* (1980a): 'Critical light reflection at a plastic/glass interface and its application to foot pressure measurements'. *J. Med. Eng. Technol.*, **4**, (3), pp. 136–142

BETTS, R. P., FRANKS, C. I., *et al.* (1980b): 'Static and dynamic foot-pressure measurements in clinical orthopaedics'. *Med. Biol. Eng. Comput.*, **18**, (5), pp. 674–684

BETTS, R. P., FRANKS, C. I. and DUCKWORTH, T. (1991): 'Foot pressure studies: normal and pathological gait analysis'. In *Disorders of the foot*. JAHSS, M. H. (Ed.). (W. B. Saunders, Philadelphia, Pennsylvania), Vol. 1, Chap. 18, pp. 484–519

CAVANAGH, P. R., HENNIG, E. M., *et al.* (1985). In: *'Biomedical measurement in orthopaedic practice'*. WHITTLE, M. (Ed.). (Oxford Science Publications), pp. 159–165

CAVANAGH, P. R., HEWITT, Jr, J. E., *et al.* (1992): 'In-shoe plantar pressure measurement: a review'. *Foot*, **2**, pp. 185–194

D'AMICO, J. C., DINOWITZ, H. D., *et al.* (1985): 'Limb length discrepancy—an electrodynographic analysis'. *J. Am. Podiatric Med. Assoc.*, **75**, pp. 639–643

FACEY, O. E., HANNAH, I. D., *et al.* (1993): 'Analysis of the reproducibility and individuality of dynamic pedobarograph images'. *J. Med. Eng. Technol.*, **17**, (1), pp. 9–15

FERGUSON-PELL, M. W. (1980): 'Design criteria for the measurement of pressure at body/support interfaces'. *Eng. Med.*, **9**, (4), pp. 209–213

FRANKS, C. I., BETTS, R. P., *et al.* (1983): 'Microprocessor-based image processing system for dynamic foot pressure studies'. *Med. Biol. Eng. Comput.*, **21**, (5), pp. 566–572

FRANKS, C. I. and BETTS, R. P. (1988): 'Selection of transducer material for use with 'Optical' foot pressure systems'. *J. Biomed. Eng.*, **10**, (4), pp. 365–367

GASTWIRTH, B. W., O'BRIEN, T. D., *et al.* (1991): 'An electrodynagraphic study of foot function in shoes of varying heel heights'. *J. Am. Podiatric Med. Assoc.*, **81**, pp. 463–472

GROSS, T. S. and BUNCH, R. P. (1988): 'Measurement of discrete vertical in-shoe stress with piezoelectric transducers'. *J. Biomed. Eng.*, **10**, (3), pp. 261–265

HENNIG, E. M., CAVANAGH, P. R., *et al.* (1982): 'A piezoelectric method of measuring the vertical contact stress beneath the human foot'. *J. Biomed. Eng.*, **4**, (3), pp. 213–222

HENNIG, E. M., STAATS, A., *et al.* (1994): 'Plantar pressure distribution patterns of young school children in comparison to adults'. *Foot Ankle*, **15**, (1), pp. 35–40

KOTHARI, M., WEBSTER, J. G., *et al.* (1988): 'Capacitive sensors for measuring the pressure between the foot and shoe'. *IEEE Eng. Med. Biol.*, **2**, pp. 805–806

KYNAR TECHNICAL MANUAL (1987): Pennwalt Corporation, P. O. Box 799, Valley Forge, Philadelphia, USA

LAING, P., *et al.* (1992): 'The development of the low profile Liverpool shear transducer'. *Clin. Phys. Physiol. Meas.*, **13**, (2), pp. 115–124

LORD, M. (1981): 'Foot pressure measurement: a review of methodology'. *J. Biomed. Eng.*, **3**, pp. 91–99

LORD, M. and REYNOLDS, D. P. (1986): 'Foot pressure measurement: a review of clinical findings'. *J. Biomed. Eng.*, **8**, pp. 283–294

LORD, M., HOSEIN, R., *et al.* (1992): 'Method for in-shoe shear stress measurement'. *J. Biomed. Eng.*, **14**, (5), pp. 181–186

MAALEJ, N. and WEBSTER, J. G. (1988): 'A miniature electroptical force transducer'. *IEEE Trans.*, **BME-35**, pp. 93–99

MINNS, R. J. (1982): 'Two simple plantar pressure recording devices in clinical use: evaluation using a pedobarograph'. *J. Eng. Med.*, **11**, (3), pp. 117–120

NEVILL, A. J. (1991): 'A foot pressure measurement system utilising PVDF and copolymer piezoelectric transducers'. *PhD Thesis*. University of Kent at Canterbury, UK

NEVILL, A. J., PEPPER, M. G. and WHITING, M. (1995): 'In-shoe foot pressure measurement system utilising piezoelectric transducers'. *Med. Biol. Eng. Comput.*, **33**, (1), pp. 76–81

NEW SCIENTIST (1985): 'Measuring the weight on your feet'. *New Scientist*, 13 June, p. 24

NICOL, K. and HENNIG, E. M. (1978): 'Measurement of pressure distribution by means of a flexible, large surface mat'. In *Biomechanics VI-A*. (University Park Press, Baltimore, USA), pp. 374–380

PATIL, K. M. and SRINATH, M. S. (1990): 'New image-processing system for analysis, display and measurement of static and dynamic foot pressures'. *Med. Biol. Eng. Comput.*, **28**, (5), pp. 416–422

PEDOTTI, A., ASSENTE, R., *et al.* (1984): 'Multisensor piezoelectric polymer insole for pedobarography'. *Ferroelectrics*, **60**, (1–4), pp. 163–174

PERUCHON, E., JULLIAN, J. M., *et al.* (1989): 'Wearable unrestraining footprint analysis system. Applications to human gait study'. *Med. Biol. Eng. Comput.*, **27**, (6), pp. 557– 565

POLLARD, J. P., LE QUESNE, L. P., *et al.* (1983): 'Forces under the foot'. *J. Biomed. Eng.*, **5**, pp. 37–40

RHODES, A., SHERK, H., *et al.* (1988): 'High resolution analysis of ground foot reaction forces'. *Foot Ankle*, **9**, pp. 135–138

ROGGERO, P., BLANC, Y., *et al.* (1993): 'Foot reconstruction in weight bearing area: long term results and gait analysis'. *Eur. J. Plastic Surg.*, **16**, pp. 186–192

ROSE, N. E., FEIWELL, L. A., *et al.* (1992): 'A method for measuring foot pressures using a high resolution, computerised insole sensor: the effect of heel wedges on plantar pressure distribution and center of force'. *Foot Ankle*, **13**, pp. 263–170

SENSORS (1991): 'A pressure mapping system for gait analysis'. *Sensors*, pp. 21–23

SMITH, L., PLEHWE, W., *et al.* (1989): 'Foot bearing pressure in patients with unilateral diabetic foot ulcers'. *Diabetic Med.*, **6**, pp. 573–575

TAPPIN, J. W. and POLLARD, J. P. (1980): 'Method of measuring shearing forces on the sole of the foot'. *Clin. Phys. Physiol. Meas.*, **1**, pp. 83–85

TAPPIN, J. W. and ROBERTSON, K. P. (1991): 'Study of relative timing of shear forces on the sole of the forefoot during walking'. *J. Biomed. Eng.*, **13**, pp. 39–42

WILLIAMS, R. B., PORTER, D., *et al.* (1992): 'Triaxial force transducer for investigating stresses at the stump/socket interface'. *Med. Biol. Eng. Comput.*, **30**, pp. 89– 96

YOUNG, R. C. (1993): 'The F-scan system of foot pressure analysis'. *Clinics Podiatric Med. Surg.*, **10**, (3), pp. 455–461

Authors' biographies

John Cobb was born in Poole, UK, in 1966. He received his HND in Electronic Engineering from Bournemouth University in 1990 and his MSc in Microelectronic Systems Design from the University of Southampton in 1991. He is currently undertaking research and development in the field of Medical Instrumentation and Computing at the Department of Applied Computing and Electronics, Bournemouth University. He is studying for his PhD at Bournemouth University on the development of new biomedical force sensors.

Denzil Claremont obtained his honours degree in Physiology from the University of London in 1975 and his MSc in Bioengineering from Strathclyde University in 1976. In 1981 he was awarded his D Phil from Sussex University for work performed at the Brompton Hospital on the pathophysiology of cardiopulmonary bypass. He then worked for nine years on the development of *in vivo* glucose sensors at Guy's Hospital Medical School, London. Currently, he is a Principal lecturer in the Department of Applied Computing and Electronics at Bournemouth University and an Honorary Consultant Clinical Scientist at Poole Hospital. His research interests are metabolic monitoring and in the application of engineering in the management of patients with diabetes mellitus.

2nd Meeting on Measurements in Wound Healing

University of Southampton
Southampton, England

24 - 25 March 1997

FINAL PROGRAMME

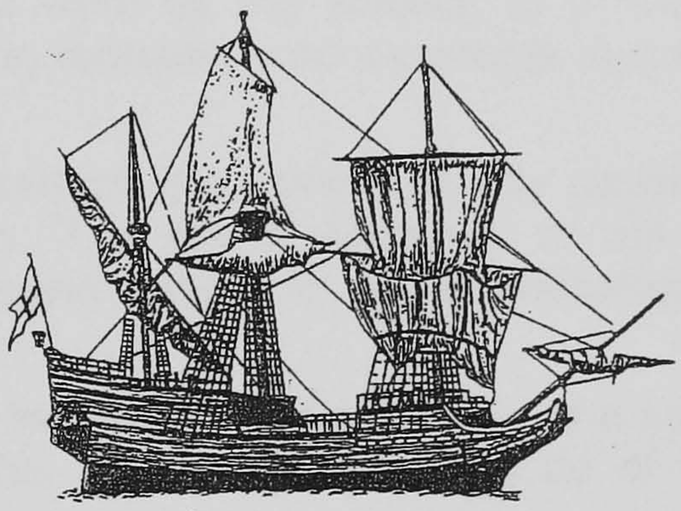

Organised by the Vascular Research Group of Southampton University Hospitals NHS Trust with Co-sponsorship by ETRS

★★★ **Continuing Educational credits are offered with this meeting (up to a maximum of 11 credits)** ★★★

A SENSOR FOR PLANTAR BLOOD FLOW AND PRESSURE MEASUREMENT

J E Cobb, D J Claremont
Department of Electronics, Bournemouth University, Fern Barrow, Poole, Dorset

---

A prototype instrument is described for the simultaneous noninvasive evaluation of microvascular blood flow and plantar pressure. A miniature laser diode and surface mount photodiode are integrated in the sensor together with instrumentation. A Force Sensing Resistor (FSR) bonded to the probe measures applied load. The probe temperature is measured using a small thermocouple to provide compensation for the FSR.

The system is calibrated using a low friction syringe, driven by different weights to control the weight of flow of the scattering media, a linear response was obtained over the range of interest from 20KHz to 12KHz.

The laser Doppler, pressure and temperature signals from the sensor are connected to an external instrumentation unit worn by the subject, to provide further amplification and filtering prior to the data being recorded onto a portable digital audio recorder attached to the subject.

The recorded data is analysed off line using specially developed software implemented using the Labview program. The power spectrum of the photocurrent is coherently averaged and signal processing applied to allow evaluation of different laser Doppler algorithms.

The probe is designed to be incorporated into the sole of a surgical shoe, sited under one of the metatarsal heads. This type of sensor could be of use in the study of plantar ulceration in diabetic patients.

IPEM Meetings

FINAL PROGRAMME

Annual Scientific Conference & Business Meeting of the IPEM South Western Group

Postgraduate Centre, Poole Hospital

7-8 May 1999

(Organised by the IPEM South Western Group)

★★★ **3 CPD credits applicable** ★★★

The Institute of Physics and Engineering in Medicine
Fairmount House, 230 Tadcaster Road
York YO24 1ES
Tel: 01904 610821 Fax: 01904 612279 Email: meetings@ipem.org.uk

Registered in England and Wales (no. 3080322) **Registered Charity (No. 1047999)**

PRELIMINARY EVALUATION OF A SENSOR FOR PLANTAR BLOOD FLOW AND PRESSURE MEASUREMENT.

J E Cobb & D J Claremont, Dept of Electronics, Bournemouth University, Fern Barrow, Poole.

To gain further insight into the pathopsychology of diabetic plantar ulceration, a monitoring system has been developed. A sensor of diameter 30mm is embedded in a measurement shoe sited under the first metatarsal head. An indication of blood flow is obtained using laser Doppler flowmetry and load data is obtained using a force sensing resistor. We conducted a pilot study of the system in a group of five non-diabetic subjects.

The test group had no history of foot problems or vascular disorders and were all non-smokers. The group had a mean age of 28.2 years +/- 5 years. The location of the sensor was identified by palpatation, marked and transferred to a template for construction of the measurement shoe. The location of the alignment mark was repeatable to within +/- 3mm. To ensure changes in blood flow were independent of variation in skin temperature, the foot was warmed to 30 deg C. A static test consisted of a sequence of blood flow obtained from the unloaded foot, two minutes under standing load and a further three minutes from the unloaded foot. The mean time for the blood flow to fall from rest to cessation level was 18.2 seconds (range 16-19.6 secs). Following removal of load a hyperaemic type response was noted. The mean duration for the blood flow to rise from cessation to the peak of the response was 12.4 seconds (range 11.6-13.85 secs). The mean duration from the peak of the hyperaemic response for a return to resting levels was 64.1 secs (range 59.7-80.0 secs). The measured response times were found to be inversely proportional to the mean heart rate during the test.

A dynamic test consisted of a continuation period of five minutes of dynamic gait. The mean blood flow, during the swing phase of the gait was determined. The standard deviation for each individual was <0.2 over thirty steps. Across the group the calculated normalised blood flow value ranged from 0.705-0.840. The variation within the values for four sets of 30 steps obtained from a single five minutes measurement period was <10%.

Appendix F

Noise figures for evaluated laser diodes.

Device	Manufacturer	Measured noise figure	Action
HL7806G	Hitachi	-56dB	Excluded
HL7836G	Hitachi	-62dB	Retained
LTO22MS	Sharp	-65dB	Retained
LTO23MS	Sharp	-60dB	Excluded
ML40123N	Mitsubishi Electric	-75dB	Retained
RLD78MC	ROHM	-45dB	Excluded
RLD78NP10	ROHM	-40dB	Excluded
SLD231VC	Sony	-55dB	Excluded
SLD1121VS	Sony	-47dB	Excluded

NB This tables gives noise figures for the for the evaluated laser diodes, refer to the discussion on page 76.

Glossary

Antialiasing filter	Input filter restricting signal bandwidth to satisfy Nyquist criteria.
Arteriovenous anastomoses	The vessels of the skin supporting thermoregulation also referred to as AV shunts.
Automatic power control	Regulation of optical output from laser diode by feedback
Avascular	Without blood, for example the epidermis.
Backscattered	Light reflected outward from tissue to the skin surface.
Biomechanical	Physical stresses acting on tissue.
Blood flux	Product of mean red blood cell velocity and concentration.
Coherence	Measure of temporal and spatial correlation of optical waves.
Cutaneous	Of the skin.
Erythrocyte	The red blood cell.
Force sensing resistor	A thin film resistance device for measuring load.
Haemodynamic	Relating to physical characteristics of blood flow.
Heparinised	Addition of anticoagulant to blood.
Heterodyne	Difference frequency when two different frequencies are summed
Hysterisis	Difference in dependent response at same values, for increasing and decreasing values of the independent variable.
Ischaemic	Inadequacy of blood supply.
Laser Doppler flowmetry	Method of assessing skin blood flow.
Linearity	A measure of the difference between the actual response and the ideal linear response.
Microspheres	Microscopic beads used to simulate red blood cells in-vitro.
Microvasculature	The small vessels supporting blood flow in the skin.
Microangiopathy	Thickening of capillary membrane in disease.

Neuropathy	Disease of peripheral nerves especially in diabetes mellitus.
Non-enzymatic glycosylation	Abnormal molecular linking with glucose in diabetes mellitus.
Peltier device	Method of cooling by electrical current.
Plastazote foam	High density foam used in orthopaedic applications.
Haemorheology	Study of blood flow in relation to constituents of blood.
Heterodyne	Production of audio frequency by combining higher frequencies.
Heterogeneous	Diversification of structure / composition.
Swing phase	Period of the gait cycle when the foot is not in ground contact.
Thermoregulatory	Control of body core temperature by varying skin blood flow.
Type I	Insulin dependent diabetes mellitus.
Type II	Non-insulin dependent diabetes mellitus.
Vasomotion	Changes in blood vessel contraction and dilation.

List of References

Akhlaghi, F. and Pepper, M.G. 1996. In-shoe biaxial shear force measurement: the Kent shear system. Medical and biological engineering and computing. 34, 315-317.

Alexander, I.J., Chao, E.Y. and Johnson, K.A. 1990. The assessment of dynamic foot-to-ground contact forces and plantar pressure distribution: a review of the evolution of current techniques and clinical applications. Foot and Ankle. 11, 152-167.

Analog devices. 1994. Design reference manual, amplifiers. Norwood, Massachusets. Analog devices.

Anderson, R.R. and Parrish, J.A. 1981. The optics of human skin.
Journal of investigative dermatology. 77(1), 13-19.

Apelqvist, J., Larsson, J. and Agardh, C.D. 1993. Long term prognosis for diabetic patients with foot ulcers. Journal of internal medicine. 233(6), 485-491.

Bader, D.L. 1990. Effects of compressive loading regimens on tissue viability. In: Bader, D.L. (editor), Pressure sores clinical practice and scientific approach. London, The Macmillan Press Ltd. 191-201.

Barnes, M.D., Peppiatt, T.N. and Mani, R. 1991. Glimpses into measurements of the mircocirculation in the skin. Journal of biomedical engineering. 13, 185-188.

Barnett, N.J., Dougherty, G. and Pettinger, S.J. 1990. Comparative study of two laser Doppler blood flowmeters. Journal of medical engineering and technology. 14(6), 243-249.

Barton, A. and Barton, M. 1981. The management and prevention of pressure sores. London, Faber and Faber.

Basel, T. 1990. Behaviour to prevent pressure sores. In: Bader, D.L. (editor), Pressure sores clinical practice and scientific approach. London, The Macmillan Press Ltd. 50-55.

Bell, P. 1994. Vascular disease: aetiology and presentation. In: Boulton, A.J.M, Connor, H. and Cavanagh, P.R. (editors), The foot in diabetes (second edition). Chichester, Wiley. 121-135.

Bertone, N. and Webb, P. 1998. Noise and stability in pin detectors. EG&G optoelectronics journal. 3, 27.

Bircher, A., De Boer, E.M., Agner, T., Wahlberg, J.E. and Jorgen, S. 1993. Guidelines for measurement of cutaneous blood flow by laser Doppler flowmetry. Contact dermatitis. 28, 1-8.

Boggett, D., Obied, A., Blond, J. and Rolfe, P. 1986. Calibration of a laser Doppler skin blood flow meter using a simple fluid model and digital signal processing. In: Copeland, K. (editor), Electronics in medicine and biology - selected papers. London, IERE. 241-247.

Bonner, R. and Nossal, R. 1981. Model for laser Doppler measurements of blood flow in tissue. Applied optics. 20(12), 2097-2107.

Bonner, R.F. and Nossal, R. 1990. Principles of laser-Doppler flowmetry. In: Shepherd, A.P. and Oberg, P.A. (editors), Laser-Doppler blood flowmetry. Massachusetts, Kluwer Academic Publishers. 17-31.

Borgos, J.A. 1990. TSI 'S LDV Blood flowmeter. In: Shepherd, A.P. and Oberg, P.A. (editors), Laser Doppler blood flowmetry. Massachusetts, Kluwer Academic Publishers, 73-82.

Boulton, A.J.M., Hardisty, C.A., Betts, R.P., Franks, C.I., Worth, R.C., Ward, J.D. and Duckworth, T. 1983. Dynamic foot pressure and other studies as diagnostic and management aids in diabetic neuropathy. Diabetes care. 6(1), 26-33.

Boulton, A.J.M. 1994. The pathway to ulceration: aetiopathogenesis. In: Boulton, A.J.M., Connor, H. and Cavanagh, P.R. (editors), The foot in diabetes. (Second edition). Chichester, Wiley. 37-48.

Brand, P.W. 1990. The diabetic foot. In: Rifkin, H. and Ponte, D. (editors), Ellenberg and Rifkin's diabetes mellitus: Theory and practice. (Fourth edition). New York, Elsevier. 829-849.

Brash, P.D., Foster, J., Vennert, W., Anthony, P. and Tooke, J.E. 1999. Magnetic resonance imaging techniques demonstrate soft tissue damage in the diabetic foot. Diabetic medicine. 16(1), 55-61.

Brownlee, M., Vlassara, H. and Cerami, A. 1984. Nonenzymatic glycosylation and the pathogenesis of diabetic complications. Annals of internal medicine. 101, 527-537.

Brownlee, M., Cerami, A., Vlassara, H., Flier, J.S. and Kahn, C.R. 1988. Advanced glycosylation end products in tissue and the biochemical basis of diabetic complications. New England journal of medicine. 318, 1315-1321.

Cai, H., Pettersson, H., Rohman, H., Larsson, S.E. and Oberg, P.A. 1996. A new single-fibre laser Doppler flowmeter based on digital signal processing. Medical engineering and physics. 18, 523-528.

Campbell, W. and Lebovitz, H. 1996. Diabetes Mellitus - Fast facts. Oxford, Health Press.

Castronuovo, J.J., Pabst, T.S., Flanigan, D.P. and Foster, L.G. 1987. Non-invasive determination of skin perfusion pressure using a Laser Doppler. Journal of cardiovascular surgery. 28, 253-257.

Cavanagh, P.R., Sims, D.S. and Sanders, L.J. 1991. Body mass is a poor predictor of peak plantar pressure in diabetic men. Diabetes care. 14(8), 750-755.

Cavanagh, P.R. and Ulbrecht, M.D. 1992. Biomechanics of the foot in diabetes mellitus. In: Levin, M.E., O'Neal,W. and Bowker, J.H. (editors), The diabetic foot (Fifth edition). St Louis, Mosby. 199-232.

Cavanagh, P.R., Hewitt, F.G. and Perry, J.E. 1992. In-shoe plantar pressure measurement: a review. The foot. 2, 185-194.

Cavanagh, P.R. and Ulbrecht, J.S. 1994. Biomechanical aspects of foot problems in diabetes. In: Boulton, A.J.M., Connor, H. and Cavanagh, P.R. (editors), The foot in diabetes. (Second edition). Chichester, Wiley. 25-35.

Cavanagh, P.R., Ulbrecht, J.S. and Caputo, G.M. 1996. Biomechanical aspects of diabetic foot disease: Aetiology, treatment and prevention. Diabetic medicine. 13(S1), S17-S22.

Challoner, A.V.J. 1975. Accurate measurement of skin blood flow by a thermal conductance method. Medical and biological engineering. 3, 197-201.

Challoner, A.V.J. 1979. Photoelectric plethysmography for estimating cutaneous blood flow. In: Rolfe, P. (editor) Non-invasive physiological measurement. London. Academic press. 125-151.

Cheong, W., Prahl, S.A. and Welch A.J. 1990. A review of the optical properties of biological tissues. IEEE Journal of quantum electronics. 26(12), 2166-2185.

Chien, S. and Usami, S. 1967. Blood viscosity: influence of erythrocyte deformation. Science. 157, 827.

Chittenden, S.J. and Shami, S.K. 1991. Microangiopathy in diabetes mellitus: 1. causes, prevention and treatment. Diabetes research. 17, 105-114.

Chittenden, S.J. and Shami, S.K. 1993. Microvascular investigations in diabetes mellitus. Postgraduate medical journal. 69, 419-428.

Cobb, J.E. and Claremont, D.J. 1995. Transducers for foot pressure measurement: survey of recent developments. Medical & biological engineering and computing. 33, 525-532.

Connor, H. 1994. Prevention of diabetic foot problems: Idenitification and the team approach. In: Boulton, A.J.M., Connor, H. and Cavanagh, P.R. (editors), The foot in diabetes (Second edition). Chichester, Wiley. 57-68.

Cook, T.A., Rahim, N., Simpson, H.C.R. and Galland, R.B. 1996. Magnetic resonance imaging in the management of diabetic foot infection. British journal of surgery. 83(2), 245-248.

Corbett, J.A. and McDaniel, M.L. 1995. Intraislet release of interleukin-1 inhibits beta-cell function by inducing beta-cell expression of inducible nitric-oxide synthase. Journal of experimental medicine. 181(2), 559-568.

Daly, C.H., Chimoskey, J.E., Holloway, G.A. and Kennedy, D. 1976. The effect of pressure loading on the blood flow rate in human skin. In: Kenedi, R.M. and Cowden, J.M. (editors), Bedsore biomechanics. London, Macmillan. 69-77.

Daniel, R.K., Priest, D.L. and Wheatley, D.C. 1981. Etiologic factors in pressure sores: an experimental model. Arch. Phys. Med. Rehabil. 62(10), 492-498.

De Mul, F.F.M., Van Spijker, D., Van der Plas, J., Aarnoudse, J.G. and Smits, T.M. 1984. Mini laser-Doppler (blood) flow monitor with diode laser source and detection integrated in the probe. Applied optics. 23(17), 2970-2973.

Delbridge, L. and Ctercteko, G. 1985. The etiology of diabetic neuropathic ulceration of the foot. British journal of surgery. 72, 1-6.

Delbridge, L., Ellis, C.S., Robertson, K. and Lequesne, L.P. 1985. Nonenzymatic glycosylation of keratin from the strateum corneum of the diabetic foot. British journal of dermatology. 112, 547-554.

Drain, L.E. 1980. The laser Doppler technique. Chichester, John Wiley and Sons.

Dryden, C.M., Gray, W.M., Asbury, A.J. 1992. Oxford Optronix MPM 3S: a clinical assessment of a microvascular perfusion monitor.
Journal of medical engineering and technology. 16(4), 159-162.

Duck, F.A. 1990. Physical properties of tissue. London, Academic press limited.

Dyet, J.F. 1994. The role of radiology in the assessment and treatment of the diabetic foot. In: Boulton, A.J.M., Connor, H. and Cavanagh, P.R. (editors), The foot in diabetes. (Second edition). Chichester, Wiley. 137-164.

Edelman, D., Hough, D.M., Glazebrook, K.N. and Oddone E.Z. 1997. Prognostic value of the clinical examination of the diabetic foot ulcer.
Journal of general internal medicine. 12(9), 537-543.

Edmonds, M.E. and Foster, A.V.M. 1994. Classification and management of neuropathic and neuroischaemic ulcers. In: Boulton, A.J.M., Connor, H. and Cavanagh, P.R. (editors), The foot in diabetes. (Second edition). Chichester, Wiley. 109-120.

EG & G Optoelectronics. 1998. Silicon photodiode – application notes.
Montreal, EG & G Optoelectronics.

Elkeles, R.S. and Wolfe, J.H.N. 1991. The diabetic foot. British medical journal.
303, 1053-1055.

Elkhawand, C., Jamart, J., Donckier, J., Chatelain, B., Lavenne, E., Moriau, M. and Buysschaert, M. 1993. Hemostasis variables in type-1 diabetic-patients without demonstrable vascular complications. Diabetes Care. 16, 1137-1145.

Ellenberg, M. 1990. Diabetic neuropathy. In: Rifkin, H. and Ponte, D. (editors), Ellenberg and Rifkin's diabetes mellitus: Theory and practice. (Fourth edition).
New York, Elsevier. 777-799.

Evans, D.H., McDicken, W.N., Skidmore, R. and Woodcock, J.P. 1989. Doppler ultrasound – Physics, instrumentation, and clinical applications. Chichester, Jon Wiley and Sons Ltd.

Faglia, E., Favales, F., Quarantiello, A., Calia, P., Brambilla, G., Rampoldi, A. and Morabito, A. 1996. Feasibility and effectiveness of peripheral percutaneous transluminal ballon angioplasty in diabetic subjects with foot ulcers. Diabetes care. 19(11), 1261-1264.

Fagrell, B., Fronek, A. and Intaglietta, M.A. 1977. Microscope television system for studying flow velocity in human skin capillaries. American journal of physiology. 233, H318-H321.

Fagrell, B. 1991. Peripheral vascular diseases. In: Shepherd, A.P. and Oberg, P.A. (editors), Laser-Doppler blood flowmetry. Massachusetts, Kluwer Academic Publishers. 201-213.

Ferguson-Pell, M.W. 1980. Design criteria for the measurement of pressure at body/support interfaces. Engineering in medicine. 9(4), 209-213.

Flynn, M.D., Edmonds, M.E., Tooke, J.E. and Watkins, P.J. 1988. Direct measurement of capillary blood flow in the diabetic neuropathic foot. Diabetologia. 31: 652-656.

Flynn, M.D. and Tooke, J.E. 1995. Diabetic neuropathy and the microcirculation. Diabetic Medicine. 12: 298-301.

Fraden, J. 1996. Handbook of modern sensors, physics design and applications. Berlin, Springer-Verlag.

Francis, J.R.D. 1976. Fluid mechanics for engineering students. (Fourth edition). London, Edward Arnold publishers Ltd.

Fronek, A. 1989. Noninvasive diagnostics in vascular disease.
Philadelphia, McGraw Hill.

Giansanti, R., Rabini, R.A., Boemi, M. and Fumelli, P. 1996. Blood rheology changes and disturbances in mircocirculation. Clinical rheology. 16(4), 543-548.

Goodman, S.R. and Shiffer, K. 1983. The spectrin membrane skeleton of normal and abnormal human erythrocytes: a review. American journal of physiology. 244, C121-C141.

Green, J.F. 1987. Fundamental cardiovascular and pulmonary physiology. (Second edition). Philadelphia, Lea and Febiger.

Grunfeld, C. 1992. Diabetic foot ulcers: Etiology, treatment, and prevention. Advances in internal medicine. 37:103-132.

Gush, R.J. and King, T.A. 1987. Investigation and improved performance of optical fibre probes in laser Doppler blood flow measurement. Medical and biological engineering and computing. 25, 391-396.

Gush, R. and King, T. 1991. Discrimination of capillary and arterio-venular blood flow in skin by laser Doppler flowmetry. Medical and biological engineering and computing. 29, 387-392.

Guyton, A.C. 1992. Human physiology and mechanisms of disease. (Fifth edition). Philadelphia, W.B.Saunders Company.

Hill, R. 1987. Diabetes health care: a guide to the provision of health care services. London, Chapman and Hall. 177-190.

Hilsted, J. and Christensen, N.J. 1992. Dual effect of insulin on plasma-volume and transcapillary albumin transport. Diabetologia. 35, 99-103.

Holloway, G.A. and Watkins, D.W. 1977. Laser Doppler measurement of cutaneous blood flow. Journal of investigative dermatology. 69, 306-309.

Horowitz, P. and Hill, W. 1984. The art of electronics. Cambridge, Cambridge University Press.

Huether, S.E. 1998. Structure, function and disorders of the integument. In: McCance, K.L. and Huther, S.E. (editors), Pathophysiology the biological basis for disease in adults and children. (Third edition). Mosby-Year Book Inc. 1594-1654.

International Diabetes Federation. 1998. Diabetes Health Economics: Facts, Figures and Forecasts. Brussels, International Diabetes Federation.

Jaap, A.J., Shore, A.C., Gartside, I.B., Gamble, J. and Tooke, J.E. 1993. Increased microvascular fluid permeability in young type 1 (insulin-dependent) diabetic patients. Diabetologia. 36, 648-652.

Jaap, A.J. and Tooke, J.E. 1994. Is microvascular disease important in the diabetic foot? In: Boulton, A.J.M., Connor, H. and Cavanagh, P.R. (editors), The foot in diabetes. (Second edition). Chichester, Wiley. 49-56.

Jaap, A.J. and Tooke, J.E. (1995). Pathophysiology of mircovascular disease in non-insulin-dependent diabetes. Clinical science. 89, 3-12.

Jakobsson, A. and Nilsson, G.E. 1993. Prediction of sampling depth and photon pathlength in laser Doppler flowmetry. Medical and biological engineering and computing. 31, 301-307.

Jeffcoate, W.J. and Finch, R.G. 1994. The use of antibiotics in lesions of the diabetic foot: A British perspective. In: Boulton, A.J.M., Connor, H. and Cavanagh, P.R. (editors), The foot in diabetes. (Second edition). Chichester, Wiley. 211-217.

Johnson, J.M. 1990. The cutaneous circulation. In: Shepherd, A.P. and Oberg, P.A. (editors), Laser Doppler blood flowmetry. Massachusetts, Kluwer Academic Publishers, 121-140.

Jung, W.G. 1989. IC Opamp-cookbook. (Third edition). Indianapolis, Sams & Co.

Kabagambe, M.K., Swain, I. and Shakespeare, P. 1994. An investigation of the effects of local pressure on the microcirculation of the skin (reactive hyperaemia) in spinal cord injured patients. Journal of tissue viability. 4(4), 110-123.

Kelleher, D. 1988. Diabetes. London, Routledge.

Kenedi, R.M. 1980. Human body biomechanics. In: Kenedi, R.M. (editor), A textbook of biomedical engineering. Glasgow, Blackie and Son Limited. 1-76.

Khodabandehlou, T., Zhao, H., Vimeux, M. and Le Devehat, C. 1997. The autoregulation of the skin mircocirculation in healthy subjects and diabetic patients with and without vascular complications. Clinical haemorheology and microcirculation. 17, 357-362.

Knowles, E.A. and Boulton, A.J.M. 1996. Do people with diabetes wear their prescribed footwear? Diabetic medicine. 13(12), 1064-1068.

Kothari, M., Webster, J.G., Tompkins, W.J., Wertsch, J.J., and Bach-y-Rita, P. Capacitive sensors for measuring the pressure between the foot and shoe. IEEE engineering in medicine and biology 10th annual conference. 1988. 2, 805-806.

Laing, P., Deogan, H., Cogley, D., Crerand, S., Hammond, P. and Klenerman, L. 1992. The development of the low profile Liverpool shear transducer. Clinical physiology and physiological measurement. 13(2), 115-124.

Lavery, L.A., Armstrong, D.G., Vela, S.A., Quebedeaux, T.G. and Fleischli, J.G. 1998. Pratical criteria for screening at high risk for diabetic foot ulceration. Archives of internal medicine. 158(2), 157-162.

Leslie, P., Jung, R.T., Isles, T.E., Baty, J., Newton, R.W. and Illingworth, P. 1986. Effect of optimal glycaemic control with continuous subcutaneous insulin infusion on energy expenditure in type 1 diabetes mellitus. British medical journal. 293, 1121-1126.

Levin, M.E. and O'Neal, L. 1988. Peripheral vascular disease. In: Levin, M.E., O'Neal, L.W. and Bowker, J.H. The diabetic foot. (Fourth edition). Missouri, The C.V. Mosby Company. 803-827.

Levin, M.E., 1988. The diabetic foot: Pathophysiology, evaluation and treatment. In: Levin, M.E., O'Neal, L.W. and Bowker, J.H. The diabetic foot. (Fourth edition). Missouri, The C.V. Mosby Company. 1-49.

Li Kam Wa, T.C., Almond, N.E., Cooke, E.D. and Turner, P. 1990. Skin blood flow changes following intradermal bradykinin injections measured by laser Doppler flowmetry: comparison with weal and flare. Journal of medical engineering and technology. 14(5), 190-193.

Libbrecht, K.G. and Hall, J.L. 1993. A low noise high-speed diode laser current controller. Reviews of scientific instrumentation. 64(8), 2133-2135.

Liebert, A., Leahy, M. and Maniewski, R. 1998. Multichannel laser-Doppler probe for blood perfusion measurements with depth discrimination. Medical and biological engineering and computing. 36, 740-747.

Lindberg, L.G., Tamura, T. and Oberg, P.A. 1991. Photoplethysmography – Part 1 Comparison with laser Doppler flowmetry. Medical and biological engineering and computing. 29, 40-47.

Little, R.C. and Little, W.C. 1989. Physiology of the heart and circulation, (Fourth edition). Chicago, Medical Publishers Incorporated.

Lord, M. 1981. Foot pressure measurement: a review of methodology. Journal of biomedical engineering. 3, 91-99.

Lord, M., Reynolds, D.P. and Hughes, J.R. 1986. Foot pressure measurement: a review of clinical findings. Journal of biomedical engineering. 8, 283-294.

Lord, M., Hosein, R. and Williams, R.B. 1992. Method for in-shoe shear stress measurement. Journal of biomedical engineering. 14, 181-186.

Maalej, N., Webster, J.G., Tompkins, W.J. and Wertsch, J.J. 1989. A conductive polymer pressure sensor array. In: Eleventh annual international conference in: Engineering in medicine and biology society. Washington, IEEE.1116-1117.

MacRury, S.M. and Lowe, G.D.O. 1990. Blood rheology in diabetes mellitus. Diabetic medicine. 8, 285,291.

Manduteanu, I., Calb, M., Lupu, C., Simionescu, N. and Simionescu, M. 1992. Increased adhesion of human diabetic platelets to cultured valvular endothelial cells. Journal of submicroscopic cytology and pathology. 24, 539-547.

Mani, R. and White, J.E. 1988. The use of surface sensors to study venous ulcers. Bioeng skin. 4, 229-242.

Mani, R., Ross, J.N. and Keefe, M. 1995. Measurements of limb oedema in chronic venous disease: a review. Skin research and technology. 1, 51-54.

Mani, R. 1999. Science of measurements in wound healing. Wound repair and regeneration. 7(5), 330-334.

Marchesi, V.T. 1983. The red cell membrane skeleton: recent progress.
Blood. 61, 1-11.

Marion, J.B. and Hornyak, W.F. 1985. General physics with bioscience essays. (Second edition). Chichester. Wiley.

Marova, I., Zahejsky, J. and Sehnalova, H. 1995. Nonenzymatic glycation of epidermal protiens of the stratum-corneum in diabetic patients. Acta diabetologica. 32(1), 38-43.

Matcher, S.J. and Copper, C.E. 1994. Absolute quantification of deoxyhaemoglobin concentration in tissue near infrared spectroscopy. Physical, medical and biological. 39, 1295-1312.

McCabe, C.J., Stevenson, R.C. and Dolan, A.M. 1998. Evaluation of a diabetic foot screening and protection programme. Diabetic medicine. 15(1): 80-84.

McInnes, A.D. 1994. The role of the chiropodist. In: Boulton, A.J.M., Connor, H. and Cavanagh, P.R. (editors), The foot in diabetes. (Second edition). Chichester, Wiley. 77-92.

McKeown, K.C. 1994. The history of the diabetic foot. In: Boulton, A.J.M., Connor, H. and Cavanagh, P.R. (editors), The foot in diabetes. (Second edition). Chichester, Wiley. 5-14.

Michel, C.C. and Gillott, H. 1990. Microvascular mechanisms in stasis and ischaemia. In: Bader, D.L. (editor), Pressure sores clinical practice and scientific approach. London, Macmillan Press Ltd. 153-163.

Mito, K. 1992. Characteristics of laser Doppler flowmeters with differing optical arrangements. Journal of medical engineering and technology. 16(6), 236-242.

Morris, A.S. 1993. Principles of measurement and instrumentation. Hemel Hempsted, Prentice Hall.

Mueller, M.J. 1997. Therapeutic footwear helps protect the diabetic foot. Journal of the american podiatric medical association. 87(8), 360-364.

Muller, R. 1981. Haemorheology and peripheral vascular diseases: a new therapeutic approach. Journal of medicine. 12, 209-235.

Murray, H.J., Young, M.J. and Boulton, A.J.M. 1996. The association between callus formation, high pressures and neuropathy in diabetic foot ulceration. Diabetic medicine. 13(11), 979-982.

Netten, P.M., Wollersheim, H., Thien, T. and Lutterman, J.A. 1996. Skin microcirculation of the foot in diabetic neuropathy. Clinical science. 91, 559-565.

Nevill, A.J. 1991. A foot pressure measurement system utilising PVDF and copolymer piezoelectric transducers. PhD Thesis. University of Kent at Canterbury, UK.

Nevill, A.J., Pepper, M.G. and Whiting, M. 1995. In-Shoe foot pressure measurement system utilising piezoelectric film transducers. Medical and biological engineering and computing. 33, 76-81.

Newson, T.P., Obied, A., Wolton, R.S., Boggett, D. and Rolfe, R. 1986. Laser Doppler velocimetry: the problem of fibre movement artefact. Journal of biomedical engineering. 9, 169-172.

Nikkels-Tassoudji, N., Henry, F., Letawe, C., Pierard-Franchimont, C., Lefebvre, P., and Pierard, G.E. 1996. Mechanical properties of the diabetic waxy skin. Dermatology. 192(1), 19-22.

Nilsson, G.E. and Tenland, T. 1980. A new instrument for continuous measurement of tissue blood flow by light beating spectroscopy.
IEEE Transactions on biomedical engineering. 27(1), 12-19.

Nilsson, G.E., Tenland, T. and Oberg P. 1980. Evaluation of a laser Doppler flowmeter for measurement of tissue blood flow.
IEEE Transactions on biomedical engineering. 27(10), 597-604.

Nilsson, G.E. 1984. Signal processor for laser Doppler tissue flowmeters. Medical and biological engineering and computing. 22, 343-348.

Nilsson, G.E. 1990. Perimed's LDV flowmeter. In: Shepherd, A.P. and Oberg, P.A. (editors), Laser Doppler blood flowmetry. Massachusetts, Kluwer Academic Publishers, 57-72

Norton, D., McLaren, R. and Exton-Smith, A.N. 1975. An investigation of geriatric nursing problems in hospital. Edinburgh, Churchill-Livingstone.

O'Flynn, M. 1982. Probabilities, random variables, and random processes. New York, Harper and Row.

Obeid, A.N., Boggett, D.M., Barnett, N.J., Dougherty, G. and Rolfe, P. 1988. Depth discrimination in laser Doppler skin blood flow measurement using different lasers. Medical and biological engineering and computing. 26, 415-419.

Obied, A.N. 1989. The measurement of blood flow in the microcirculation using laser Doppler flowmetry. PhD. Thesis. Oxford Polytechnic.

Obied, A.N., Barnett, N.J., Dougherty, G. and Ward, G. 1990. A critical review of laser Doppler flowmetry. Journal of medical engineering and technology. 14(5), 178-181.

Obied, A.N. 1993. In vitro comparison of different signal processing algorithms used in laser Doppler flowmetry. Medical and biological engineering and computing. 31, 43-52.

Oberg, P.A., 1990. Innovations and precautions. In: Shepherd, A.P. and Oberg, P.A. (editors), Laser Doppler blood flowmetry. Massachusetts, Kluwer Academic Publishers, 93-109.

Palastanga, N., Field, D. and Soames, R.1994. Anatomy and Human Movement. (Second edition). Oxford, Butterwoth Heinemann.

Patton, J.T. 1991. Imaging of bone and joint infections. Current opinion in radiology. 3(5), 713-718.

Pfeffer, J. 1991. The cause of pressure sores. In: Webster, J.G. (editor), Prevention of pressure sores – Engineering and clinical aspects. Bristol, Adam Hilger. 1-18.

Pham, H.T., Economides, P.A. and Veves, A. 1998. The role of endothelial function on the foot- microcirculation and wound healing in patients with diabetes. Clinical podiatric medical surgery. 15(1), 85-93.

Phillips, J. 1997. Pressure sores. London, Churchill Livingstone.

Rayman, G., Hassan, A. and Tooke, J.E. 1986(a). Blood flow in the skin of the foot related to posture in diabetes mellitus. British medical journal. 292, 87-90.

Rayman, G., Williams, S.A., Spencer, P.D., Smaje, L.H., Wise, P.H. and Tooke, J.E. 1986(b). Impaired microvascular hyperaemic response to minor skin trauma in type I diabetes. British medical journal. 292, 1295-1298.

Rayman, G., Williams, S.A., Gamble, J. and Tooke, J.E. 1994. A study of factors governing fluid filtration in the diabetic foot. European journal of clinical investigation. 24(12), 830-836.

Rayman, G., Malik, R.A., Sharma, A.K. and Day, J.L. 1995. Microvascular response to tissue-injury and capillary ultrastructure in the foot skin of type-1 diabetic patients. Clinical science. 89(5), 467-474.

Reddy, N.P. 1990. Effects of mechanical stresses on lymph and interstitial fluid flows. In: Bader, D.L. (editor), Pressure sores clinical practice and scientific approach. Macmillan Press. 1990. 2-20.

Robertson, J., Swain, I. and Gaywood, I. 1990. The importance of pressure sores in total health care. In: Bader, D.L. (editor), Pressure sores - clinical practice and scientific approach. London, Macmillan Press. 3-12.

Romanelli, M. and Falanga, V. 1999. Measurement of transcutaneous oxygen tension in chronic wounds. In: Mani, R., Falanga, V., Shearman, C.P., Sandeman, D. (editors), Chronic wound healing – clinical measurement and basic science. London, W.B. Saunders company Ltd. 68-80.

Ryan, T.J. 1985. Dermal vasculature. In: Skerrow, D. and Skerrow, C.J. (editors), Methods in skin research. London, Wiley. 527-558.

Ryan, T.J. 1990. Cellular responses to tissue distortion. In: Bader, D.L. (editor), Pressure sores - clinical practice and scientific approach. London, Macmillan Press. 141-152.

Sacks, A.H., Ksander, G. and O'Neill, H. (1988). Difficulties in laser Doppler measurement of skin blood flow under applied external pressure. Journal of rehabilitation research and development. 25(3), 19-24.

Sage, R.A. 1987. Diabetic ulcers: evaluation and management. Clin Podiatr Med Surg. 4(2), 383-93.

Sandeman, D. and Shearman, C.P. 1999. Clinical aspects of lower limb ulceration. In: Mani, R., Falanga, V., Shearman, C.P., Sandeman, D. (editors), Chronic wound healing – clinical measurement and basic science. London, W.B. Saunders company Ltd. 4-25.

Sargent,W.Q. 1988. Haemorheology. In: Levin, M.E., O'Neal, L.W. and Bowker, J.H. (editors), The diabetic foot. Missouri, CV Mosby Company. 71-75.

Sarrafian, S.K. 1993. Anatomy of the Foot and Ankle: Descriptive, Topographic, Functional. (Second edition). Philadelphia, J.B.Lippincott Company.

Scales, J.T. 1990. Pathogenesis of pressure sores. In: Bader, D.L. (editor), Pressure sores clinical practice and scientific approach. London, The Macmillan Press Ltd. 15-26.

Schaff, P.S. and Cavanagh, P.R 1990. Shoes for the insensitive foot – the effect of a rocker bottom shoe modification on plantar pressure distribution. Foot & Ankle. 11(3), 129-140.

Schmidt, R.F. and Thews, G. 1987. Human physiology. (Second edition). New York, Springer-verlag.

Schmitt, J.M., Meindl, J.D. and Mihm, F.G. 1986. An intergrated circuit-based optical sensor for in-vivo measurement of blood oxygenation. IEEE Transactions on biomedical engineering. BME-33(2), 98-107.

Scott, E.M. 1986. Cardiovascular physiology – An integrative approach. Manchester, Manchester university Press.

Sharp. 1997. Laser diode user's manual. Oxford, Sharp laboratories of Europe.

Shaw, J.E. and Boulton, A.J.M. 1997. The pathogenesis of diabetic foot problems an overview. Diabetes. 46(2), S58-S61.

Shohet, S.B. and Lux, S.E. 1984. The erythrocyte membrane skeleton pathophysiology. Hospital practice. 19, 89.

Simonen, P., O'Brien, M., Hamilton, C., Ashcroft, J. and Denham, J. 1997. Normal variation in cutaneous blood content and red blood cell velocity in humans. Physiological measurement. 18, 155-170.

Simpson, A., Bowers, K. and Weir-Hughes, D. 1996. Pressure sore prevention. London, Whurr publishers Ltd.

Sinagra, D., Greco, D., Scarpitta, A.M. and Brigandi, M. 1997. Feedback inhibition of insulin secretion in obese female subjects with different insulin-resistant states. Diabetes nutrition and metabolism. 10(4), 185-188.

Slaaf, D., Tangelder, G.J. and Reneman, R. 1993. Physics of the microcirculation. In: Strackee, J. and Westerhof, N. (editors), The physics of heart and circulation. Bristol, IOP Publishing Ltd.

Steed, D.L, Donohoe, D., Webster, M.W., Lindsley, L., Ricotta, J.J, Luterman, A., Brown, S., Comeerota, A.J., Walsh, D.B., Bergamini, T.M., Baker, W.H., Boltax, R.S., Schwarcz, T.H., Donohoe and D.J., Fleishman, A. 1996. Effect of extensive debridement and treatment on the healing of diabetic foot ulcers. Journal of the American college of surgeons. 183(1), 61-64.

Stern, M.D. 1975. In vivo evaluation of microcirculation by coherent light scattering. Nature. 254, 56-58.

Stess, R.M, Jensen, S.R. and Mirmiran, R. 1997. The role of dynamic plantar pressures in diabetic foot ulcers. Diabetes care. 20(5), 855-858.

Stevens, M.J., Goss, D.E., Foster, A.V.M, Pitei, D., Edmonds, M.E., Watkins, P.J. 1993. Abnormal digital pressure measurements in diabetic neuropathic foot ulceration. Diabetic medicine. 10, 909-915.

Stonebridge, P.A. and Murie, J.A. 1993. Infrainguinal revascularization in the diabetic patient. British journal of surgery. 80(10), 1237-1241.

Strackee, J. and Westerhof, N. 1993. The physics of heart and circulation. London, IOP publishing.

Sykes, M.K., Vickers, M.D. and Hull, C.J. 1981. Principles of clinical measurement. Oxford, Blackwell Scientific Publications.

Tagare, P. 1993. Signal averaging. In: Tompkins, W.J. (editor), Biomedical digital signal processing. New Jersey, Prentice Hall. 184-192.

Tooke, J.E. and Brash, P.D. 1996. Microvascular aspects of diabetic foot disease. Diabetic medicine. 13(S1), S26-S29.

Tsay, D. 1991. Pressure distribution in tissue. In: Webster, J.G. (editor), Prevention of pressure sores - engineering and clinical aspects. Bristol, Adam Hilger. 19-33.

Uccioli, L., Mancini, L., Giordano, A., Solini, A., Magnani, P., Manto, A., Cotroneo, P., Greco, A.V. and Ghirlanda, G. 1992. Lower limb arteriovenous shunts, autonomic neuropathy and the diabetic foot. Diabetes research and clinical practice. 16(2), 123-130.

Ulbrecht, J.S., Norkitis, A. and Cavanagh, P.R. 1988. Plantar pressure and plantar ulceration in the neuropathic diabetic foot. In: Levin, M.E., O'Neal, L.W., Bowker, J.H., (editors), The diabetic foot. (Fourth edition). Missouri, C.V. Mosby Company. 29-45.

Van De Graff, K.M. and Fox, S.I. 1992. Concepts of human anatomy and physiology. (Third edition). Urbana, Wm. C. Brown Publishers.

Van der Zee P. 1993. Measurement and modelling of the optical properties of biological tissues in the near infrared. PhD Thesis. University of London.

Vermillon, B.D. 1986. Clinical effects of diabetes mellitus on the arterial system. Bruit. 10: 187.

Veves, A., Murray, H.J., Young, M.J. and Boulton, A.J.M. 1992. The risk of foot ulceration in diabetic patients with high foot pressure: a prospective study. Diabetologia. 35, 660-663.

Vigilance, J.E., Reid, H.L., Richards-George, P. and Mills, J. 1997. Impaired vasodilatory reserve in diabetics with and without neuropathy. Medical science research. 25, 561-564.

Watala, C. 1992. Hyperglycemia alters the physiochemical properties of proteins in erthrocyte-membranes of diabetic patients. International journal of biochemistry. 24(11), 1755-1761.

Watkins, P.J. and Edmonds, M.E. 1983. Sympathetic nerve failure in diabetes. Diabetologia. 25, 73-77.

Weidner, R.T. and Sells, R.L. 1980. Elementary modern physics. (Third edition). New York, Allyn and Bacon, Inc.

Weinstien, D., Wang, A., Chambers, R., Stewart, C.A. and Motz H.A. 1993. Evaluation of magnetic-resonance-imaging in the diagnosis of osteomyelitis in diabetic foot infections. Foot & Ankle. 14(1), 18-22.

Whittle, M. 1991. Gait analysis – An introduction. Oxford, Butterworth-Heinemann Ltd.

World Health Organisation. 1990. Diabetes care and research in Europe – The St Vincent declaration. London, HMSO.

Williams, D.R.R. 1994. The size of the problem: Epidemiological and economic aspects of foot problems in diabetes. In: Boulton, A.J.M., Connor, H. and Cavanagh, P.R. (editors), The foot in diabetes. (Second edition). Chichester, Wiley. 15-24.

Williams, I.M., Picton, A.J. and McCollum, C.N. 1993.
The use of doppler ultrasound 1: Arterial disease. Wound management. 4(1),1-4.

Wilson, J. and Hawkes, J.F.B. 1989. Optoelectronics – an introduction. (Second edition). New York, Prentice Hall International.

World Health Organisation. 1990. Diabetes care and research in Europe: the St Vincent declaration. Diabetic medicine. 7, 554.

Young, M.J., Cavanagh, P.R., Thomas, G., Johnson, M.M., Murray, H. and Boulton, A.J.M. 1992. The effect of callus removal on dynamic plantar foot pressures in diabetic patients. Diabetic Medicine. 9(1), 55-57.

Young, M.J., Coffey, J., Taylor, P.M. and Boulton, A.J.M. 1995. Weight bearing ultrasound in diabetic and rhematoid arthritis patients. The foot. 5, 76-79.

Zhong, J., Seifalian, A.M., Salerud, G.E. and Nilsson, G.E. 1998. A mathematical analysis on the biological zero problem in laser Doppler flowmetry. IEEE Transactions on biomedical engineering. 45(3), 354-64.

Zhou, R. 1991. Bladder pressure sensors. In: Webster, J.G. (editor), Prevention of pressure sores – engineering and clinical aspects. Bristol, Adam Hilger. 109-120.

Zhu, F. and Spronck, J.W. 1992. A capacitive tactile sensor for shear and normal force measurements. Sensors and Actuators. 31, 115-120.